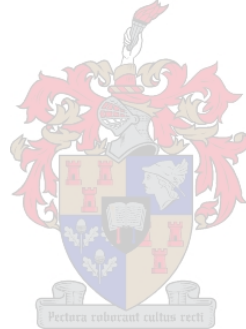


**PETROLOGY, GEOCHRONOLOGY AND PROVENANCE OF THE
LAINGSBURG AND TANQUA KAROO SUBMARINE FAN
SYSTEMS, ECCA GROUP,
SOUTH AFRICA**

by

Oliver Patrice NGUEMA MVE



Thesis presented in partial fulfilment of the requirements for the degree of Master
of Science in the Department of Geology, University of Stellenbosch

DECEMBER 2005

STUDY LEADER: Prof. A. ROZENDAAL

DECLARATION

I, the undersigned, hereby declare that this thesis is my own original work and has not previously in its entirety or in part been submitted at any university for a degree or examination. Where use was made of the work of others it has been acknowledged in the text.


O.P. NGUEMA MVE

18 November 2005

DATE



ABSTRACT

The integration of whole-rock chemistry, heavy mineral chemistry, detrital zircon morphology and age dating has enabled high-resolution characterization of the Permian Laingsburg and Tanqua submarine fan provenance in the Karoo Basin, upper Ecca Group, South Africa.

Geochemically, the Laingsburg and Tanqua sandstones are classified as greywacke and litharenite. The chemical index of alteration values for these sandstones suggest low to moderately weathered sources and a relatively cold climate. Abundant angular clastic grains and lithic fragments as well as the predominance of pristine zircons indicate a near provenance and a first cycle derivation. The investigated sandstones originated from a continental island arc and an active continental margin. The source is dominantly intermediate to felsic and includes tonalites, granodiorites, and adamellites or their volcanic equivalents.

The zircon populations from the Laingsburg and Tanqua submarine fans show a similar age distribution and therefore originated from the same source. Concordia plots and histogram of ages of zircons from these terranes reveal three major age groupings, whose occurrence and distribution has a great significance in terms of regional tectonics and provenance studies. A 260-310 Ma age grouping with a peak in the 270-290 Ma range (58 of the 107 dated grains), supported by their dominant tonalitic and orogenic calc-alkaline rhyolitic source, is correlated with the Choiyoi magmatic arc in the northern Patagonia region. A 460-495 Ma age grouping (14 % of the population) is correlated with the Arroyo Salado granite, Famatinian granite and Deseado Massif of South America. A 545-620 Ma age grouping (11.2 % of the population) is correlated with the Neoproterozoic Pan-African Saldania Belt, Gariiep Belt and equivalents of southern Africa.

Subordinate sources include the Mesoproterozoic Namaqua-Natal Metamorphic Province (1000-1300 Ma; 7.5 % of the population), the Devonian Sierras Pampeanas, Colan Conhué granites and El Laurel tonalites (6.5 % of the total analysed grains) of South America, the Cambrian Cape Granite Suite (5.6 % of the population) and the Cratonic-derived Cape Supergroup in the Cape Fold Belt (0.9%).

The main eruption phase of the Choiyoi transitional arc (270-290 Ma) predates the main tectonic events associated with the development of the Cape Fold Belt. Sedimentation and formation of the subbasins occurred during the first two events of the Cape Orogeny at 278 Ma and 258 Ma and can be correlated with the late stage of the Choiyoi volcanism. The absence of zircons younger than 253 Ma indicates that the post-258 Ma tectonic events caused a considerable development of the Cape Fold Belt and prevented continued transport of sediments into the Tanqua and Laingsburg subbasins from the south and southwest.

The source rock lithologies, age and morphological similarities existing between the investigated zircons and juvenile zircons of tuff horizons of the Dwyka Group suggest a derivation of these successions from the same parental magma. This indicates that the volcanism continued to as late as 253 Ma, after the deposition of the Dwyka tuff, which corresponds to the end of the deposition of the Ecca Group.

UITTREKSEL

Die integrasie van heelrots chemie, swaarmineraal chemie, detritale sirkoon morfologie en ouderdomsdatering maak hoë-resolusie karakterisering van die Permiese Laingsburg en Tanqua submariene-waaier provenans in die boonste Ecce Groep van die Karookom in Suid-Afrika moontlik.

Die Laingsburg en Tanqua sandstene word geochemies geklassifiseer as grouwakke en litareniete. Die chemiese indeks van verandering waardes vir hierdie sandstene dui op lae to gemiddelde verwerking van brongesteentes en 'n relatiewe koue klimaat. Volop hoekige klastiese korrels en litiese fragmente, sowel as die teenwoordigheid van hoofsaaklik ongeskonde sirkone, dui op 'n nabygeleë brongebied en 'n eerste siklus derivasie. Die sandstene het 'n kontinentale eilandboog en aktiewe kontinentale grens oorsprong. Die bron is hoofsaaklik intermediêr tot felsies en sluit tonaliete, granodioriete en adameliëte en hul vulkaniese ekwivalente in.

Die sirkoon populasies van die Laingsburg en Tanqua submariene-waaiers toon dieselfde ouderdomsdistribusie en is dus van dieselfde bron. Konkordia diagramme en histogramme van sirkoon ouderdomme van hierdie terreine dui op drie hoof ouderdomsgroeperings, waarvan die voorkomste en verspreiding van kardinale belang is in terme van regionale tektoniek en brongebied studies. 'n 260–310 Ma ouderdomsgroepering met 'n piek in die 270–290 Ma area (58 van die 107 gedateerde korrels), ondersteun deur hulle dominante tonalitiese en orogeniese kalk-alkaliene riolitiese bronne, word gekorreleer met die Choiyoi magmatiese boog in die noorde van Patagonië. 'n 460–495 Ma ouderdomsgroepering (14% van die populasie) word gekorreleer met die Arroyo Salado graniet, die Famatiniaanse graniet en die Deseado Massif in noordelike Patagonië. 'n 545-620 Ma ouderdomsgroepering (11.2% van die populasie) word gekorreleer met die Neoproterosoïese Pan-Afrika Saldania Gordel, die Gariep Gordel en ekwivalente in suidelike Afrika.

Ondergeskikte bronne sluit die Mesoproterosoïese Namakwa-Natal Metamorfe Provinsie (1000-1300 Ma; 7.5 % van die populasie), die Devoonse Sierras Pampeanas, die Colan Conhué graniete en El Laurel tonaliete van Suid-Amerika (6.5% van die totale geanaliseerde korrels), die Kambriese Kaap Graniet Suite (5.6% van die populasie) en die Kaap Supergroep van kratoniese oorsprong (0.9%) in die Kaapse Plooi Gordel in.

Die hoof erupsie fase van die Choiyoi oorgangsboog (270-290 Ma) is ouer as die hoof tektoniese insidente wat geassosieër is met die vorming van die Kaapse Plooi Gordel. Sedimentasie en vorming van die subkomme het plaasgevind tydens die eerste twee gebeurtenisse van die Kaapse Orogeen teen 278 Ma en 258 Ma, en kan gekorreleer word met die laat stadium van die Choiyoi vulkanisme. Die afwesigheid van sirkone jonger as 253 Ma dui daarop dat die post-258 Ma tektoniese gebeurtenisse 'n belangrike ontwikkeling van die Kaapse Plooi Gordel tot gevolg gehad het, en dat dit die vervoer van sedimente na die Tanqua en Laingsburg subkomme vanuit die suide en suidweste voorkom het.

Die brongesteente litologieë, ouderdom en morfologiese ooreenkomste tussen die bestudeerde sirkone en jong sirkone van tuf lae van die Dwyka Groep dui op dieselfde moedermagma. Dit impliseer dat die vulkanisme voortgeduur het tot so laat as 253 Ma, na die afsetting van die Dwyka tuff, wat ooreenkom met die einde van die afsetting van die Ecce Groep.

ACKNOWLEDGEMENTS

Thank you to God almighty for granting me the chance and ability to successfully complete this study.

I wish to express my deepest gratitude to my supervisor Professor Abraham Rozendaal for assistance and guidance in the technical and scientific preparation of this thesis.

My sincere thanks are due to the Gabonese Government for financing my studies.

I would like to thank the NOMAD project management and the University of Stellenbosch for giving me access to cores and for permission to conduct this study.

I also wish to thank my friends, personnel and fellow students at the Geology Department of the University of Stellenbosch. Special thanks are due to Mr. Johnny Smit for helping me with sample preparation for XRF analyses and to Esmé Spicer for the SEM work. I also wish to thank Belinda Van Lente for providing me with some of her Laingsburg sandstone samples from her Ph.D. study. Thanks and gratitude to Dr. DeVille Wickens for hours of fruitful discussion. His knowledge of the geology of the area greatly benefited my research. I am also grateful to Dr. Andreas Spath (University of Cape Town) for helping me with the ICP-MS geochemical laboratory work. My sincere thanks are also due to Dr. Richard Armstrong and the staff of the SHRIMP laboratory at the Australian National University for the zircon dating.

I am deeply indebted to my fellow Gabonese students for their encouragement and support. I give my heart felt regards to Guy-Modeste Ekwa, Blanche Nyangone, Estelle Nke Assam and my colleague Alain Cedrique Megner for their

encouragement and the very supportive role they have played during my stay in South Africa.

Finally, I am particularly grateful to my parents for their continuous support during all my studies. Special thanks are due to my mother Catherine Ntsame Nguema to whom I dedicate this thesis.

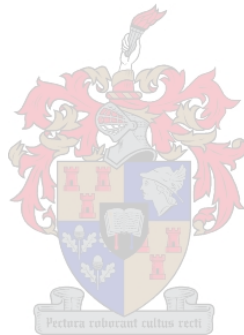


TABLE OF CONTENTS

	PAGES
ABSTRACT	i
ACKNOWLEDGEMENTS	v
TABLE OF CONTENTS	vii
LIST OF FIGURES	x
LIST OF TABLES	xviii
CHAPTER 1: INTRODUCTION	1
1.1 Background	1
1.2 Aims and objectives	13
1.3 Methodology	13
1.3.1 Sampling	13
1.3.2 Analytical techniques	18
CHAPTER 2: REGIONAL GEOLOGICAL SETTING	20
2.1 Introduction	20
2.2 Pre-Karoo geology	20
2.3 Geology of the Karoo Basin	26
CHAPTER 3: LOCAL GEOLOGICAL SETTING	32
3.1 Introduction	32
3.2 The Tanqua Submarine Fan Complex	32
3.3 The Laingsburg Submarine Fan Complex	34
3.4 Correlations between the Laingsburg and Tanqua fans	35
CHAPTER 4: MINERALOGY	38
4.1 Introduction	38
4.2 Petrographic analysis	38

4.2.1	Detrital quartz	39
4.2.2	Chemistry of detrital feldspar	44
4.2.2.1	Methodology	47
4.2.2.2	Results	48
4.3	Climate, relief and transport history	54
4.4	Heavy minerals chemistry	57
4.4.1	Introduction	57
4.4.2	Sphene chemistry	59
4.4.3	Garnet chemistry	61
CHAPTER 5:	BULK ROCK CHEMISTRY	64
5.1	Introduction	64
5.2	Geochemical characteristics of clastic sediments	65
5.2.1	Chemical classification of sandstones	65
5.2.2	Major element concentrations	68
5.3.	Weathering and paleoenvironment conditions during deposition	75
5.3.1	Sediment maturity	75
5.3.2	Weathering	77
5.3.3	Climate	79
5.4	Source rock lithology	82
5.5	Tectonic setting of the source area	86
5.6	Trace element geochemistry	90
CHAPTER 6:	ZIRCON MORPHOLOGY, CHEMISTRY AND GEOCHRONOLOGY	105
6.1	Introduction	105
6.2	Zircon morphology and provenance	106
6.3	Zircon chemistry	115
6.4	Zircon age constraints on provenance	138
6.5	Geochronological results and location of source rocks	146
6.5.1	The Tanqua Karoo subbasin	146

6.5.1.1	The Slope sandstones	146
6.5.1.2	The Skoorsteenberg Formation	149
6.5.2	The Laingsburg subbasin	152
6.6	summary and source rock identification	156
CHAPTER 7:	INTERPRETATION	166
CHAPTER 8:	CONCLUSIONS	179
REFERENCES		185
APPENDIX A:	BOREHOLE LOGS WITH SAMPLE POSITIONS	206
APPENDIX B:	WHOLE ROCK CHEMISTRY (XRF & ICP-MS)	233
APPENDIX C:	ZIRCON CHEMISTRY (LA-ICP-MS)	241
APPENDIX D:	ZIRCON GEOCHRONOLOGY (SHRIMP)	255
APPENDIX E:	CL AND SEM IMAGES OF THE TANQUA AND LAINGSBURG ZIRCONS	(available on CD)

LIST OF FIGURES

	PAGE
CHAPTER ONE	
<p>Fig. 1.1 Location of the study area in the southwest corner of the Karoo Basin of South Africa along the Cape Fold Belt (Bouma and Wickens, 1994).</p>	2
<p>Fig. 1.2 Generalized retro-arc foreland basin model for the Karoo Basin during the early Mesozoic, showing the basin in relation to underlying Archean to Proterozoic crustal terranes, the Cape Fold Belt and the inferred position of a possible arc and subduction zone (Andersson et al., 2003).</p>	4
<p>Fig. 1.3 Block diagram showing the paleogeography of the southwest Karoo Basin during the Cape Orogeny events (Scott et al., 2000).</p>	5
<p>Fig. 1.4 Schematic representations of the three stages in the evolution of the southern part of the Cape-Karoo Basin from early Carboniferous to late Triassic (Johnson, 1991).</p>	9
<p>Fig. 1.5 Transportation from the source (North Patagonian Massif) in part through the actively deforming but not exposed Cape Fold Belt to the depository (first Laingsburg then Tanqua depocentres) of the southwest Karoo Basin (King et al., 2004).</p>	11
<p>Fig. 1.6 Transportation and deposition of sediments from the source terranes (Sierras Pampeanas and North</p>	

- Patagonian Massif) to the Tanqua and Laingsburg depocentres, during the Late Permian (Van Lente et al., 2003). 12
- Fig. 1.7 Outcrop extent of the Tanqua deepwater fans and borehole positions. NB2-NB4 are big-diameter holes whereas NS1-NS4 are slim holes (Andersson et al., 2004). 15
- Fig. 1.8 Geological map of the Laingsburg depocentre, Karoo Basin showing the sample locations (Van Lente, 2004). 17

CHAPTER TWO

- Fig. 2.1 Geographic distribution of the pre-Karoo geology including the Kaapvaal Craton and other cratons and orogenic belts in southern Africa (Frimmel, 2000). 25
- Fig. 2.2 Paleogeography and paleotectonic framework of Gondwanaland during the Late Paleozoic (late Carboniferous-Permian) (López-Gamundí and Rosselo, 1998). 28
- Fig. 2.3 Schematic representation of the Cape and Karoo stratigraphy in the south-western Karoo Basin (Wickens and Bouma, 2000). 31

CHAPTER THREE

- Fig. 3.1 Stratigraphic correlation between the Tanqua and Laingsburg subbasins (King et al., 2004). 37

CHAPTER FOUR

- Fig. 4.1 QmFLt ternary diagram showing the provenance (granitic) of the Tanqua and Laingsburg subbasins sandstones, Eccca Group (King et al., 2004). 40
- Fig. 4.2 QmFLt plot showing the provenance (transitional arc) of the Eccca group sediments (diamonds) including (1, 2 & 3) Waterford Formation sandstones, (4) Ford Brown Formation tuff and (5 & 6) Ripon Formation sandstones (Johnson, 1991). 41
- Fig. 4.3 Undulose quartz, typical of quartz from both igneous and metamorphic sources. 43
- Fig. 4.4 Common (plutonic) quartz grains characterized by straight to slightly undulose extinction, xenomorphic and typical of granites. 43
- Fig. 4.5 Common varieties of K-feldspar and polycrystalline quartz. 45
- Fig. 4.6 Common varieties of albitic plagioclase feldspar. 46
- Fig. 4.7 Compositional range of eight provenance groups of feldspar (Trevena and Nash, 1981) 49
- Fig. 4.8 Expected abundance of sand size detritus as a function of provenance (Lewis, 1984). 52
- Fig. 4.9 Typical example of micaceous sandstones from the Tanqua Karoo. 53

CHAPTER FIVE

- Fig. 5.1 Analysis of alkali content of the Slope (SL1), Laingsburg and Skoorsteenberg (Fans 3, 4 and 5) sandstones based on major element geochemistry (Crook, 1974). 68
- Fig. 5.2 Harker-type major element percentage variation diagrams for Tanqua Karoo (Fans 3, 4 and 5) and Slope (SL1) sandstones. 69
- Fig. 5.3 Classification of terrigenous sandstones using $\log (\text{Na}_2\text{O}/\text{K}_2\text{O})$ versus $\log (\text{SiO}_2/\text{Al}_2\text{O}_3)$ from Pettijohn et al. (1972), with boundaries redrawn by Herron (1988). 76
- Fig. 5.4 Plots of SiO_2 vs. CIA (chemical index of alteration; Nesbitt and Young, 1984)  78
- Fig. 5.5 Molar $\text{CaO}+\text{Na}_2\text{O}-\text{Al}_2\text{O}_3-\text{K}_2\text{O}$ ternary diagram (Nesbitt and Young, 1984) showing the relationship between the studied sedimentary rocks and the calculated weathering trends of some crystalline rocks. 81
- Fig. 5.6 Discriminant function diagram for the provenance signatures of sandstone-mudstone suites using major elements (1) (Roser and Korsch, 1988). 83
- Fig. 5.7 Discriminant function diagram for the provenance signatures of sandstone-mudstone suites using major elements (2) (Roser and Korsch, 1988). 85

Fig. 5.8	Bivariate plots for the discrimination of the plate tectonic setting of sandstones from the Slope, Laingsburg and Skoorsteenberg Formations (Bhatia 1983).	88
Fig. 5.9	Selected trace elements Nb, Y and Zr (in ppm) Versus SiO ₂	92
Fig 5.10	Chondrite-normalized REE abundances in the Tanqua and Slope sandstones (Taylor and McLennan, 1985).	97
Fig. 5.11	Source rock discrimination diagram for the Tanqua turbidites showing Co/Th vs. La/Sc (Condie, 1993).	103
Fig. 5.12	Th/Sc-Zr/Sc plot showing a magmatic arc trend (McLennan et al., 1993).	103
Fig. 5.13	La/Th vs. Hf of the Tanqua and Slope sandstones (Gu et al., 2002).	104



CHAPTER SIX

Fig. 6.1	Zircon morphology classification diagram (Pupin, 1980). (Pupin, 1980).	108
Fig. 6.2	SEM images showing zircon morphologies in various sandstone samples from the Skoorsteenberg (Fans 3, 4 and 5) and Laingsburg (Fans A and F) formations.	112
Fig. 6.3	Morphological classification of detrital zircons from Fans A and F (Laingsburg Formation) and Fans 3, 4 and 5 (Skoorsteenberg Formation), based on SEM image	

	interpretation. Also shown is the distribution of some non-granitic groups of endogenous rocks (Pupin, 1980).	114
Fig. 6.4	Chondrite-normalized rare earth element plots for the Laingsburg sandstones (Taylor and McLennan, 1985).	117
Fig. 6.5	Chondrite-normalized rare-earth element plots for the Tanqua fan sandstones (Taylor and McLennan, 1985).	118
Fig. 6.6	Chondrite-normalized averaged REE patterns of zircons from a range of rock types (Belousova et al., 2002).	119
Fig. 6.7	CART tree for the recognition of zircons from different rock types based on single grain trace element geochemistry (Belousova et al., 2002).	122
Fig. 6.8	Plots of trace and rare earth element data of zircons from the Tanqua Fan 3, superimposed on the fields of zircon compositions used as discriminants for different rock types (Belousova et al., 2002).	126
Fig. 6.9	Plots of trace and rare earth element data of zircons from the Tanqua Fan 4, superimposed on the fields of zircon compositions used as discriminants for different rock types (Belousova et al., 2002).	128
Fig. 6.10	Plots of trace and rare earth element data of zircons from the Tanqua Fan 5, superimposed on the fields of zircon compositions used as discriminants for different rock types (Belousova et al., 2002).	130

Fig. 6.11	Plots of trace and rare earth element data of zircons from the Laingsburg Fan A, superimposed on the fields of zircon compositions used as discriminants for different rock types (Belousova et al., 2002).	132
Fig. 6.12	Plots of trace and rare earth element data of zircons from the Laingsburg Fan F, superimposed on the fields of zircon compositions used as discriminants for different rock types (Belousova et al., 2002).	134
Fig. 6.13	Synoptic diagram showing the source rock lithologies of the Laingsburg (Fans A and F) and Skoorsteenbergr (Fans 3, 4 and 5) Formations (Belousova et al., 2002).	136
Fig. 6.14	CL images, ages and analysis spots for the Slope, Laingsburg (Fans A and F) and Tanqua Karoo (Fans 3, 4 and) submarine fan samples.	142
Fig. 6.15	CL images, ages and analysis spots for inherited zircons from the Laingsburg submarine Fan A and the Skoorsteenbergr fans.	143
Fig. 6.16	U vs. Th diagram based on LA-ICP-MS data	145
Fig. 6.17	U vs. Th diagram based on SHRIMP data	145
Fig. 6.18	Concordia plot and histogram of ages for the Slope sandstones.	148
Fig. 6.19	Concordia plot and histogram of ages for the Skoorsteenbergr sandstones.	151

- Fig. 6.20 Concordia plot and histogram of ages for the Laingsburg sandstones. 155
- Fig. 6.21 Zircon age distributions in the southwestern Eccca Group. 157
- Fig. 6.22 Map of southern Gondwana showing Gondwana granite-rhyolite provinces, including the late Carboniferous to Triassic (290-200 Ma) Choiyoi province and the late Triassic to Jurassic (200-155 Ma) Chon Aike province. Also shown is the boundary separating old cratonic Gondwana from younger accreted terranes (Kay et al., 1989). 160

CHAPTER SEVEN

- Fig. 7.1 Map of the southern South America showing the generalized locations of the Deseado Massif (DM), the North Patagonian Massif (NPM), and the Río de La Plata Craton (RPC). The conjectural extensions of the Dom Feliciano (Bresiliano; B), the Pampean (P) and Famatinian (F) orogenic belts of Neoproterozoic to mid-Ordovician age are also shown (Pankhurst et al., 2003). 174
- Fig. 7.2 Cross section of Southern Gondwana showing the three stages in the evolution of the Cape-Karoo Basin. Also shown, the Choiyoi magmatic arc (Northern Patagonia) and the subduction zone. (Modified from Johnson, 1991). 178

LIST OF TABLES

		PAGE
 CHAPTER ONE		
Table 1.1	Positions of sandstone samples in boreholes drilled in both the Slope and Tanqua deepwater fans	16
 CHAPTER TWO		
Table 2.1	U-Pb chronology of pre-Permian basement rocks of SW Gondwana (Pankhurst et al., 2003).	21
 CHAPTER FOUR		
Table 4.1	Chemical (Ab-An-Or) composition of plagioclase feldspars from Fans 3, 4, and 5 of the Skoorsteenberg Formation.	50
Table 4.2	Microprobe analyses of detrital sphenes from the Skoorsteenberg Fans 3 and 4 of the Tanqua Karoo subbasin.	60
Table 4.3	Representative analyses of detrital garnets from the Tanqua Fans 3 and 4.	63
 CHAPTER FIVE		
Table 5.1	Mean composition of principal sandstone classes and average Laingsburg and Tanqua sandstones.	66

Table 5.2	selected trace element contents of the Slope and Skoorsteenberg fan sandstones.	95
Table 5.3	Range of elemental ratios of Tanqua and Slope sandstones compared to the ratios in similar fractions derived from felsic rocks, mafic rocks, and upper continental crust.	101

CHAPTER SIX

Table 6.1	Provenance determination of the Tanqua and Laingsburg submarine fan sandstones based on the CART tree (Belousova et al. 2002)	123
Table 6.2	Summary of SHRIMP U-Pb zircon data for the Slope sandstone samples.	147
Table 6.3	SHRIMP U-Pb zircon data for the Tanqua Fans 3, 4 and 5 sandstone samples.	150
Table 6.4	Summary of SHRIMP U-Pb zircon data for the Laingsburg Fan sandstone samples.	153
Table 6.5	Inferred provenances of the Permian Laingsburg and Tanqua Karoo sediments, based on 107 U-Pb SHRIMP analyses obtained from 109 detrital zircons.	164

CHAPTER EIGHT

Table 8.1	Recapitulatory table of the main findings of this study.	182
-----------	--	-----

CHAPTER ONE INTRODUCTION

1.1 Background

The Laingsburg and Tanqua fan complexes are located in the south-western corner of the Karoo Basin, South Africa (Fig. 1.1). Since formation, the subbasins have been filled by fine-grained turbidite flows and form well preserved geological outcrops of deepwater sediments. The study area is situated approximately 200 km to the northeast of Cape Town, Western Cape Province. The Tanqua submarine fan complex has a total area of approximately 640 km², while the outcrop area for the submarine fan packages in the Laingsburg subbasin extends east-west for approximately 200 km with a lateral continuity that can be traced for up to 10 km.

Submarine fan systems of turbidite origin have become the most important oil reservoir setting in oil fields of the west coast of Africa, the east coast of South America, the North Sea, the Gulf of Mexico and the South African coast. More recently, one of the world's best geological outcrop analogue for deepwater basin floor sediments, the Tanqua Basin fan complex (Geel et al., 2003), received attention from the regional Novel Modelled Analogue Data (NOMAD) project. The latter is a European-Union/Industry co-funded project involving staff from Statoil, Schlumberger Cambridge Research and the Universities of Liverpool, Delft and Stellenbosch. The NOMAD project was aimed at reducing the development costs of deep-water reservoirs, and increase the success rate of wells drilled through improved reservoir characterization.

An understanding of the origin of sand is critical in the evaluation of clastic depositional systems, placing important constraints on transport, dispersal and depositional patterns that must be taken into consideration in the generation of sedimentological models, on both regional and local scales (Morton, 1991).

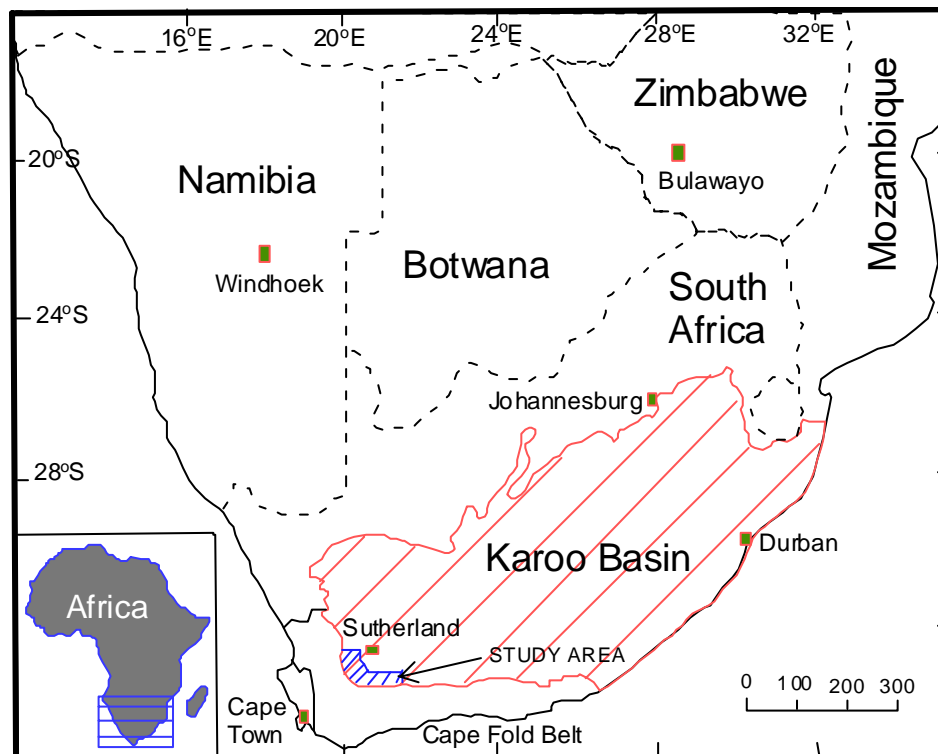


Figure 1.1 Location of the study area in the southwest corner of the Karoo Basin of South Africa along the Cape Fold Belt (Bouma and Wickens, 1994)

Three models have been recently proposed to account for the main provenance area of the Permian Karoo submarine fan systems. The proposed sources included:

(1) The Cape Supergroup in the Cape Fold Belt (Lock, 1980; Kingsley, 1981; Hälbig, 1983; Cole, 1992; Veevers et al., 1994; Adelman and Fiedler, 1998),

(2) A magmatic arc to the south of the present Cape Fold Belt (Elliot and Johnson, 1972; Elliot and Watts, 1974; Martini, 1974; Visser, 1979; Johnson, 1991), and

(3) The North Patagonian Massif (Van Lente et al., 2003; King et al., 2004)

Some interpretations however, combine the aforementioned provenance models.

Andersson et al. (2003) who studied the Sm-Nd isotopic distribution in the five fans of the Skoorsteenberg Formation of the Tanqua depocentre concluded that there is a little or no variation in provenance between the different fans. The investigators believe that the source area of the Skoorsteenberg Formation is probably a late Paleozoic thrust belt and a contemporaneous magmatic arc to the south of the Cape Fold Belt (Fig.1.2).

Scott et al. (2000), studying the chemistry of detrital garnet, tourmaline, and biotite in sandstones from the Skoorsteenberg, Vischkuil and Laingsburg Formations, proposed that the source for these successions includes two rock assemblages: a high-grade metamorphic source and a granitic source. According to investigators, the sandstones in the Laingsburg and Tanqua subbasins originated from an area between the magmatic arc of the subduction zone and the rising, but submerged, fold-thrust belt. This may possibly be an uplifted area of older, metamorphosed sediments in the paleo-Patagonia region toward the southwest, approximately 200-500 km away (Fig.1.3).

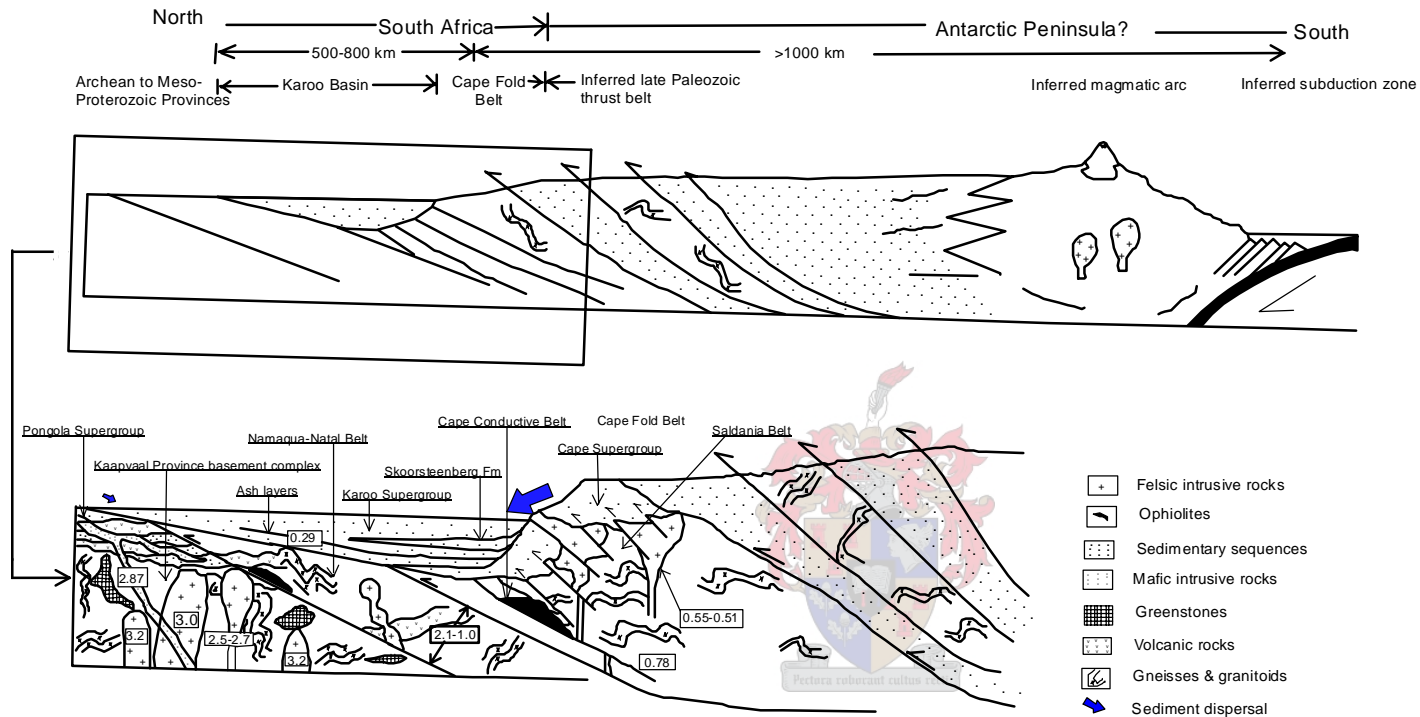


Figure 1.2 Generalized retro-arc foreland basin model for the Karoo Basin during the early Mesozoic, showing the basin in relation to underlying Archean to Proterozoic crustal terranes, the Cape Fold Belt and the inferred position of a possible arc and subduction zone (Andersson et al., 2003).

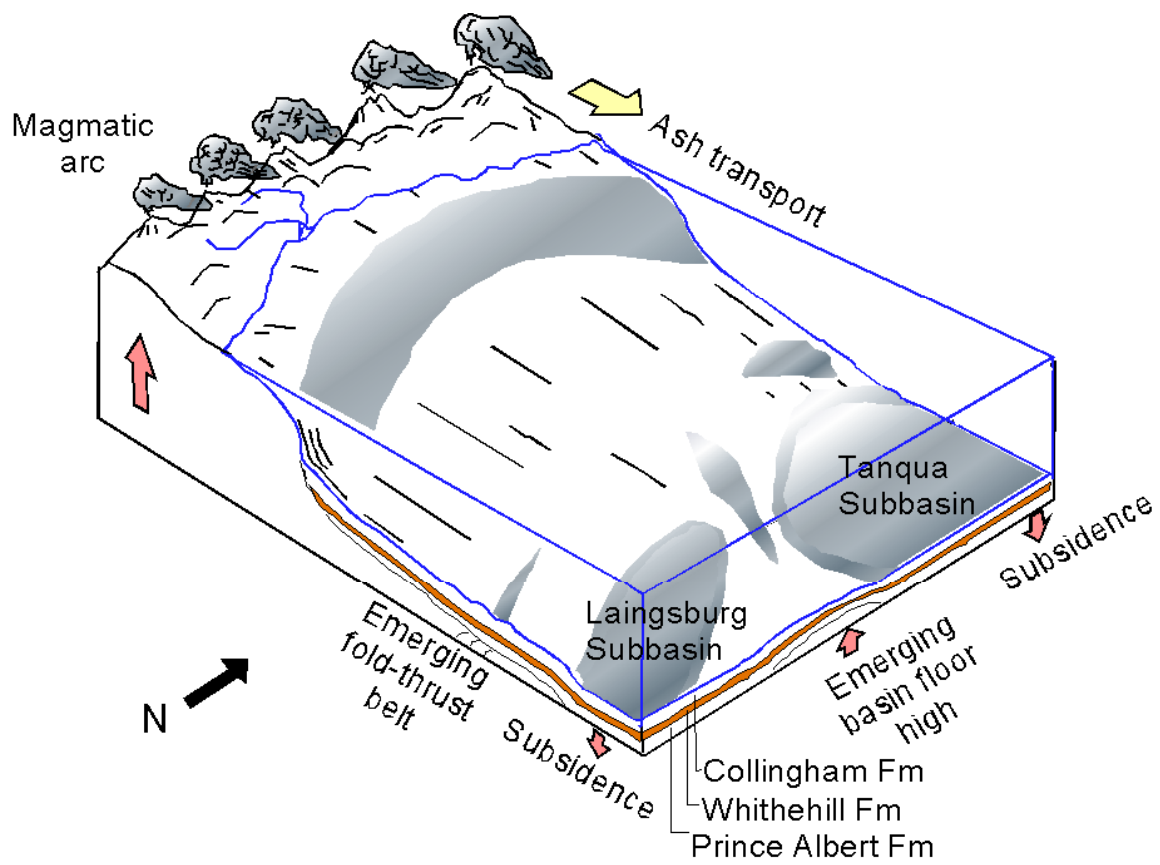


Figure 1.3a Block diagram showing the paleogeography of the southwest Karoo Basin during the first Cape Orogeny event at 278 Ma (Scott et al., 2000).

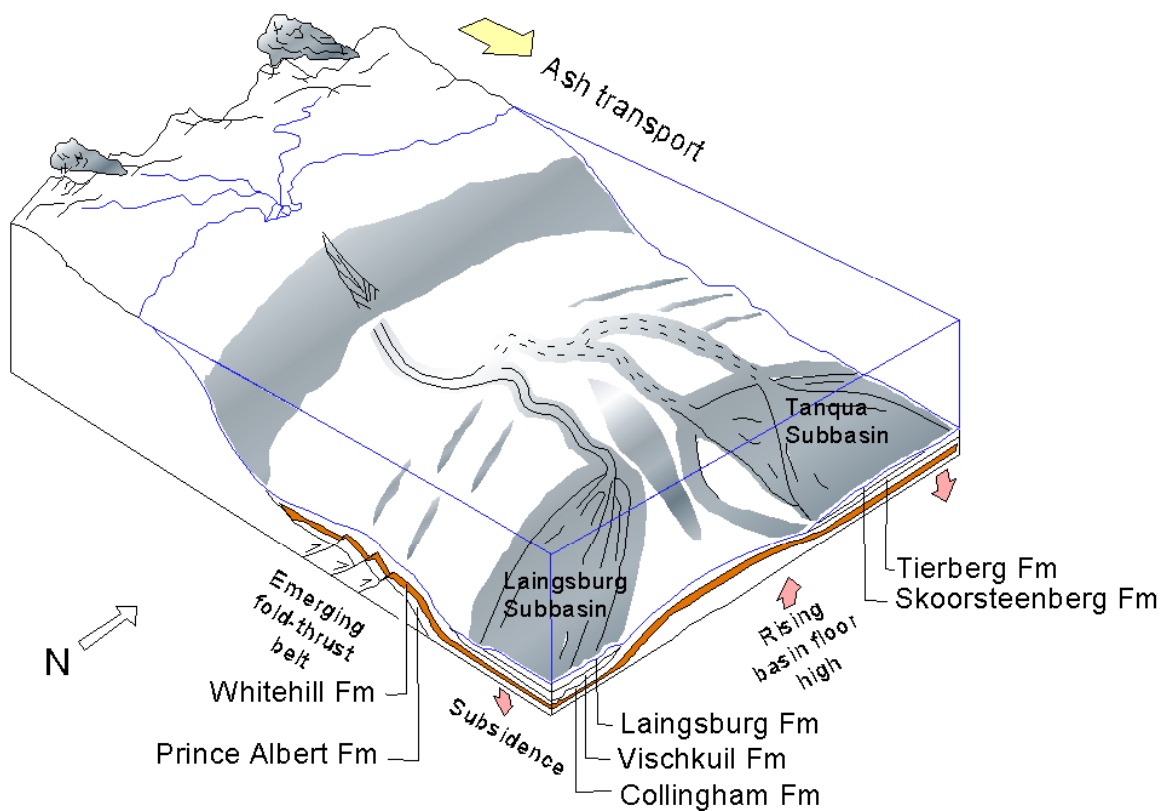


Figure 1.3b Block diagram showing the paleogeography of the southwest Karoo Basin between the first tectonic event of the Cape Orogeny at 278 Ma and the second at 258 Ma (Scott et al., 2000).

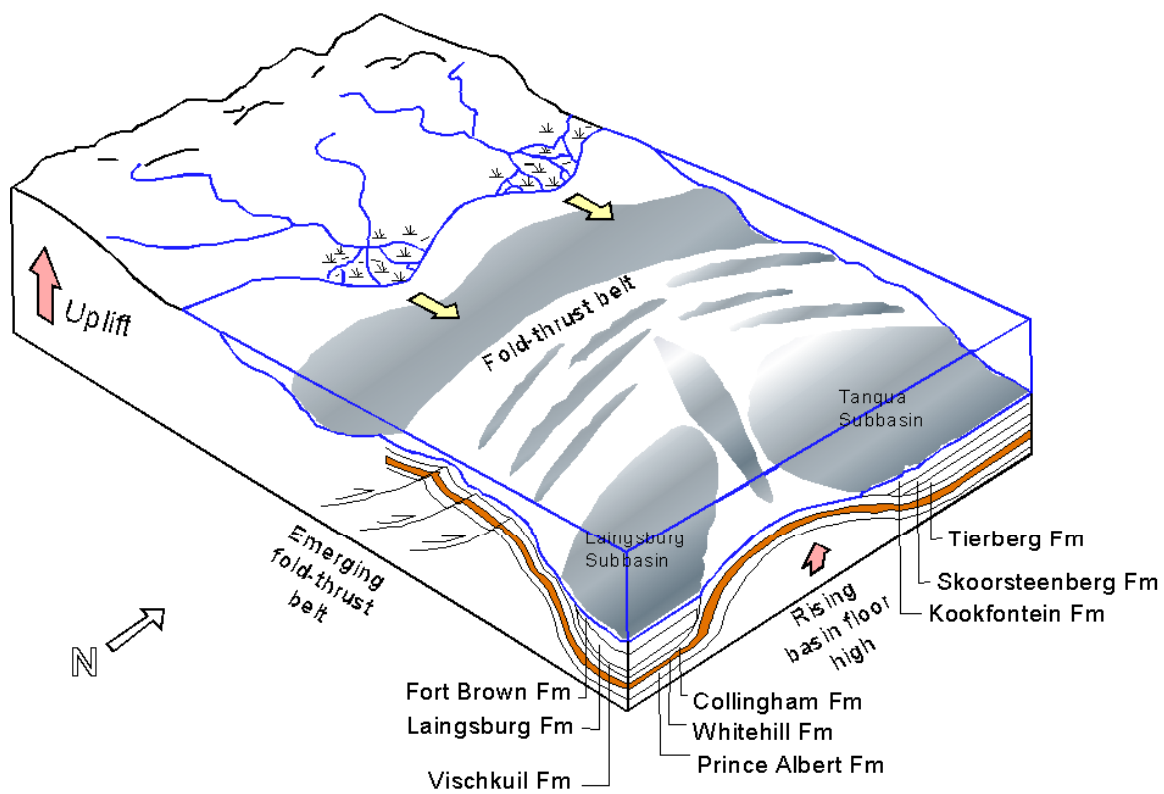


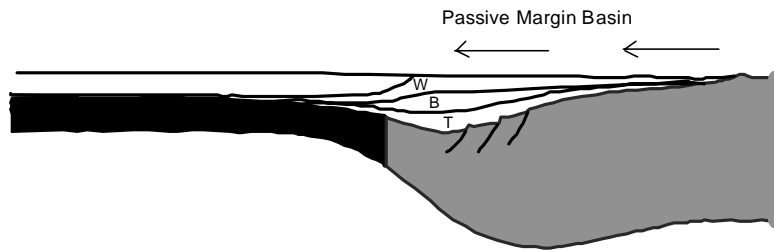
Figure 1.3c Block diagram showing the paleogeography of the southwest Karoo Basin during the Cape Orogeny event at 258 Ma (Scott et al., 2000).

As previously mentioned, the metasedimentary orogenic belt provenance was favoured by Lock (1980), Kingsley (1977, 1981), Hälbich (1983, 1992), Cole (1992), Veevers et al. (1994) and Adelman and Fiedler (1998). The abundance of undulatory quartz together with the predominance of low temperature plagioclase and the rarity of volcanic rocks led Kingsley (1977, 1981) to believe that low-grade metamorphic rocks and sedimentary rocks were the main provenance of the Eccca and lower part of the Beaufort Group. These source rocks were generated during folding and uplift of sediments of the Cape Supergroup south and southeast of the present subcontinent. Presently, these rocks may be located beneath the Falkland Island Plateau (Lock, 1980).

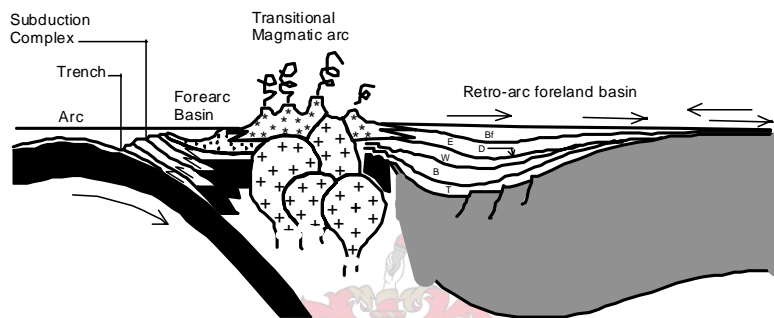
Based on the paleoreconstruction of the Cape Fold Belt, Hälbich (1983, 1992) stated that the orogenic metasedimentary fold belt experienced uplift and erosion during the first Cape Orogeny event at 278 ± 2 Ma. He believed that the Cape Supergroup has played a prominent role during the infill of the Laingsburg and Tanqua Karoo subbasins. However, further investigations are required to precisely find out if the detritus originated from shales and sandstones of the Witteberg and Bokkeveld Groups and the overlying Dwyka Group.

From a traditional quartz-feldspar-lithic fragments (QFL) ternary diagram, Johnson (1991), studying the sandstone petrography of the Eccca Group and the lower Beaufort Group (Adelaide Subgroup) in the south-eastern part of the Karoo Basin, concluded that the sediments were sourced from a provenance outside of the fold-thrust belt and fell in a magmatic arc field (Fig.1.4). Johnson's conclusion is in agreement with the interpretation given by Elliot and Johnson (1972), Martini (1974) and Visser (1979) who proposed a southern magmatic arc beyond, i.e. south of the Cape Fold Belt as source for these successions.

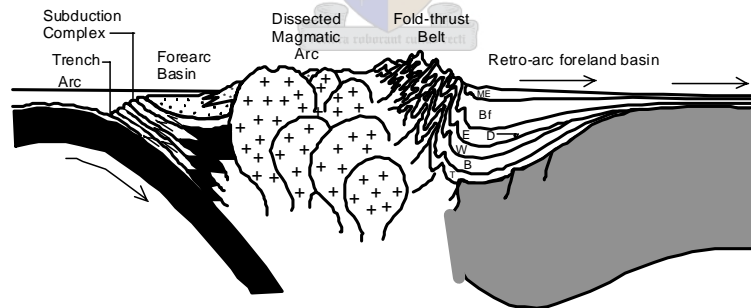
a. Early Carboniferous



b. Late Permian



c. Late Triassic



South

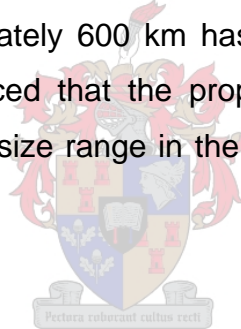
North



Figure 1.4 schematic representations of the three stages in the evolution of the southern part of the Cape-Karoo Basin from early Carboniferous to late Triassic. ME=Molteno+Elliot Formations, Bf=Beaufort Group, E=Ecca Group, D=Dwyka Group, W=Witteberg Group, B=Bokkeveld Group, T=Table Mountain Group (Johnson, 1991).

The existence of a continuous belt of Permian magmatic activity extending from Patagonia past the south of the Cape Fold Belt to Western Australia was suggested by Martini (1974). Visser (1979), Rhodes (1974) and Martini (1974) suggested that the magmatic arc was developed in relation to the late Paleozoic subduction of an oceanic plate underneath it, although Visser's reference to an 'alpine-type orogenic belt' seems inappropriate for a true magmatic arc (Johnson, 1991).

King et al. (Fig. 1.5; 2004) and Van Lente et al. (Fig. 1.6; 2003) demonstrated that sediments from the Laingsburg and Tanqua depocentres are derived from the same source geochemically. Detritus was dominantly first cycle and derived from a granitic source. The North Patagonian Massif is identified as the most suitable source area of the Karoo Basin sediments. A pre-Atlantic Ocean transport pathway of approximately 600 km has been suggested by King et al (2004). The investigators noticed that the proposed source fits the observed good sorting and narrow grain size range in the depository but does not explain the angularity of the grains.



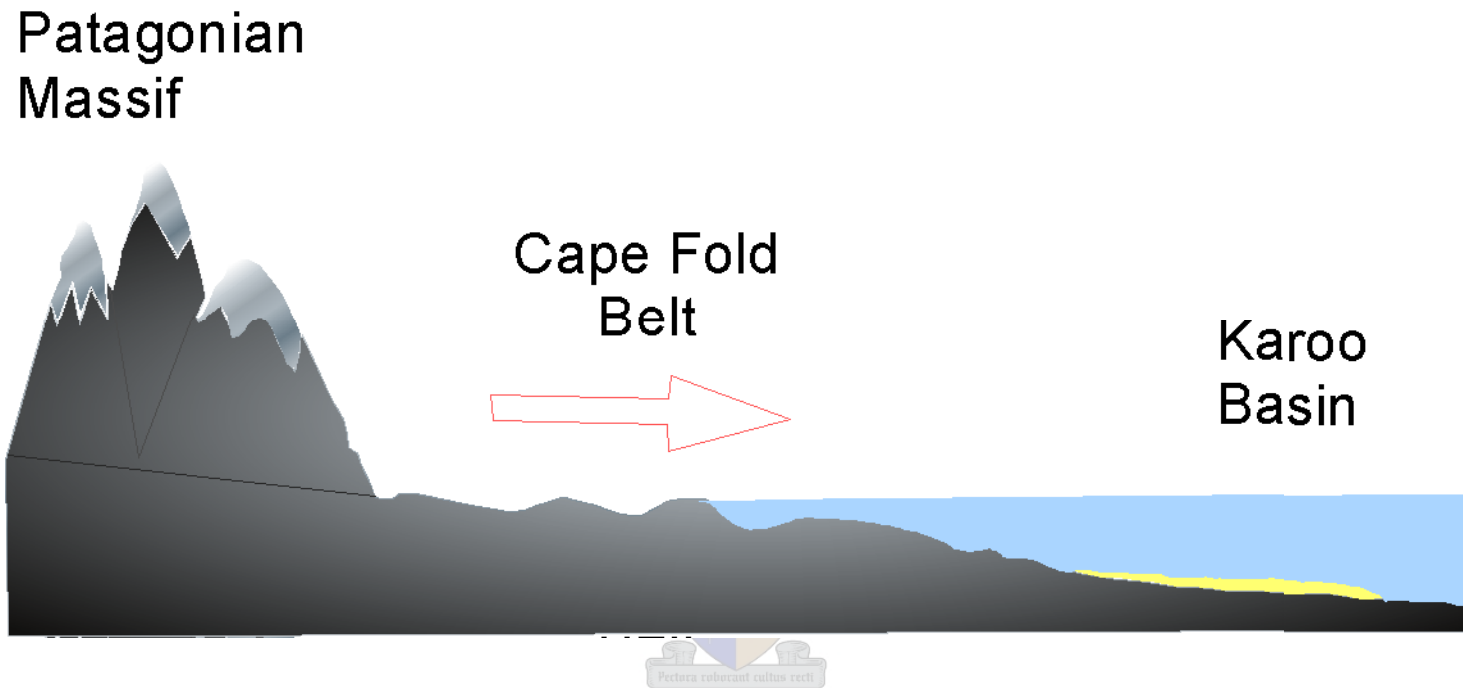


Figure 1.5 Transportation from the source (North Patagonian Massif) in part through the actively deforming but not exposed Cape Fold Belt to the depository (first Laingsburg then Tanqua depocentres) of the southwest Karoo Basin (King et al., 2004).

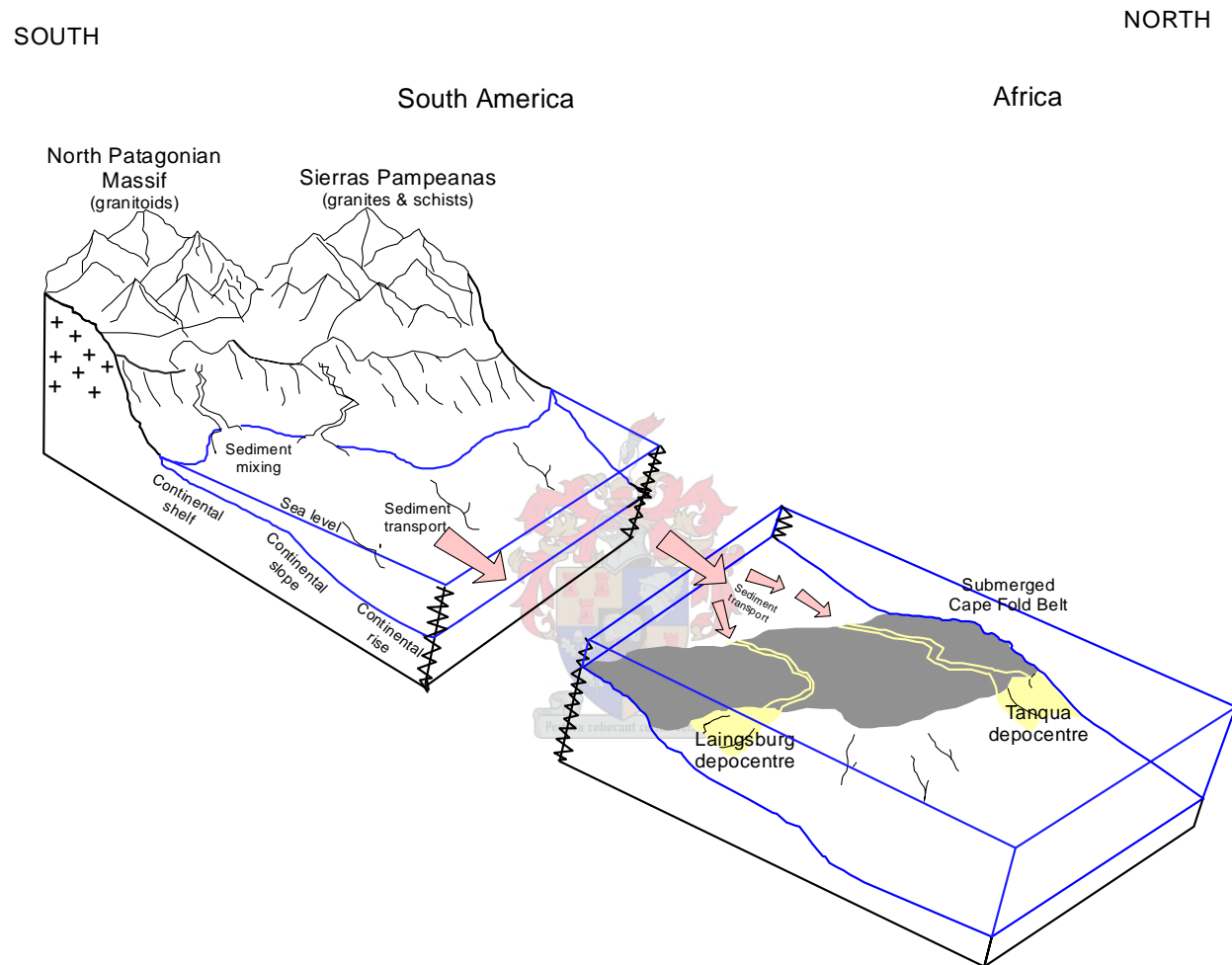


Figure 1.6 Transportation and deposition of sediments from the source terranes (Sierras Pampeanas and North Patagonian Massif) to the Tanqua and Laingsburg depocentres, during the Late Permian (Van Lente et al., 2003).

1.2 Aims and objectives

The principal objective of this investigation is to contribute to the understanding of reservoir rocks in the Laingsburg and Tanqua Karoo subbasins by providing additional information that will assist with the sedimentological model and depositional basin reconstruction. To do so, this study will bring new insight into both the similarities and origin of detritus that filled these basins during the Permian. The related factors investigated in this research include:

- The nature of the source rocks and tectonic setting of the subbasins.
- The effect of chemical weathering on detritus.
- Climate and relief of the source area.
- Transport history of detritus.
- Diagenesis.
- Geochronology of the source rocks.

This study is peripheral to the NOMAD project, therefore initially focused on the Skoorsteenberg Formation of the Tanqua depocentre and later included sandstones of the Laingsburg Formation. The reason for including the Laingsburg samples is to establish the relationship between the two submarine fan complexes. Differences in opinion with regard to the main provenance of the Tanqua and Laingsburg detritus indicate that it is poorly defined and therefore needs to be reconsidered.

1.3 Methodology

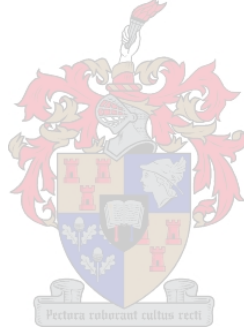
The integration of whole-rock geochemistry, heavy mineral chemistry, detrital zircon morphology and age dating was used to address the aforementioned objectives.

1.3.1 Sampling

Several wells have been drilled in the Tanqua area during the NOMAD project. Core samples (n = 39) used in this study are from four representative wells; SL1,

NS1, NB3 and NB4 (Fig. 1.7). Lithological logs of the wells are presented in Appendix A. Samples were taken in such a manner that the whole fan area from the distal to the proximal parts was represented. The Tanqua samples are from Fans 3, 4 and 5 (Fig. 1.7 and Table 1.1). The SL1 borehole drilled in the Bitterberg area crosses mainly the shoreface sandstones (Waterford Formation) and submarine slope and prodeltaic shale (Kookfontein Formation). Sandstones from the overlying Waterford Formation are informally designated as the Slope sandstones in this study.

The Laingsburg samples are from the lower and upper fans (Fans A and F respectively). The geological map of the Laingsburg depocentre, modified after maps published by the Geological Survey of South Africa, shows the Collingham, Vischkuil, Laingsburg, Fort Brown Formations and sample locations (Fig.1.8).



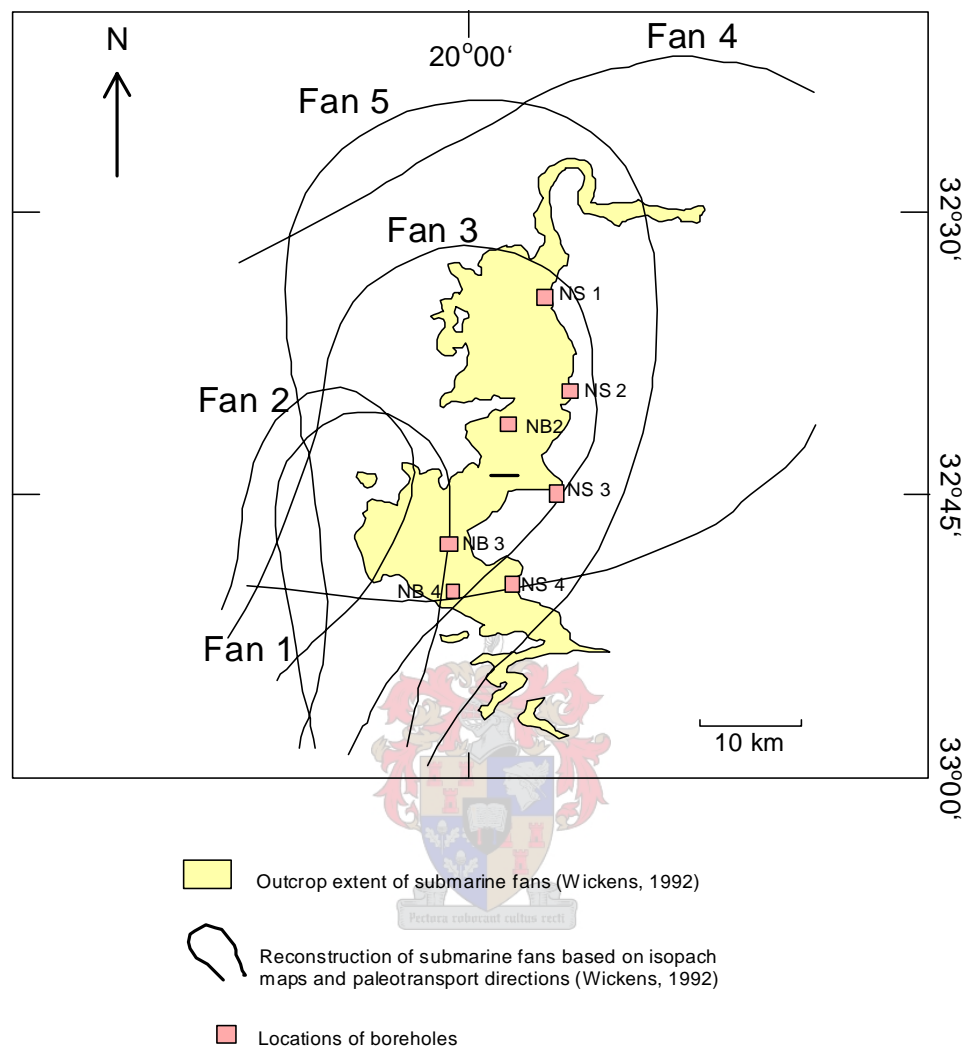


Figure 1.7 Outcrop extent of the Tanqua deepwater fans and borehole positions. NB2-NB4 are big-diameter holes whereas NS1-NS4 are slim holes (Andersson et al., 2004). Note that the present figure does not show the Slope (SL 1) borehole drilled in the Bitterberg area.

Table 1.1 Positions of sandstone samples in boreholes drilled in both the Slope and Tanqua deepwater fans**Slope sediments**

Borehole	Sample nr	Depth (m)	Description
SL	SL1-1	9.78 – 10.01	Fine-gr., grey sst
SL	SL1-2	25.03 – 25.49	Fine-gr., grey sst
SL	SL1-3	63.29 – 63.7	Fine-gr., grey sst
SL	SL1-4	103.2 – 103.65	Fine-gr., grey sst
SL	SL1-5	132.56 – 133.00	Fine-gr., grey sst
SL	SL1-6	170.8 – 171.26	Fine-gr., grey sst
SL	SL1-7	199.8 – 200.20	Fine-gr., grey sst with shale in the top part

Fan 5

Borehole	Sample nr	Depth (m)	Description
SL	SL1-A-F5	256.30 – 256.75	Grey, very fine-gr. sst
SL	SL1-B-F5	259.02 – 259.29	Grey, very fine-gr. sst
NS1	NS1-1-F5	5.70 – 5.77	Grey, fine-gr. sst
NS1	NS1-3-F5	10.04 – 10.31	Grey, fine-gr. sst
NS1	NS1-4-F5	13.91 – 14.17	Grey, fine-gr. sst

Fan 4

Borehole	Sample nr	Depth (m)	Description
NS1	NS1-6-F4	85.34 – 85.50	Massive, fine-gr., grey sst
NS1	NS1-8-F4	94.35 – 94.61	Massive, fine-gr., grey sst
NS1	NS1-10-F4	101.00 – 102.25	Massive, fine-gr., grey sst
NS1	NS1-11-F4	104.24 – 104.8	Massive, fine-gr., grey sst
NB3	NB3-1-F4	12.9 – 13.1	Fine-gr., grey sst
NB3	NB3-2-F4	26.23 – 26.42	Fine-gr., grey sst
NB3	NB3-3-F4	32.52 – 32.85	Fine-gr., grey sst
NB3	NB3-4-F4	40.00 – 40.42	Fine-gr., grey sst

Fan 3

Borehole	Sample nr	Depth (m)	Description
NB3	NB3-A-F3	83.77 – 83.97	Massive, fine-gr., dark grey sst
NB3	NB3-7-F3	99.8 – 100.2	Massive, fine-gr., dark grey sst
NB3	NB3-D-F3	106.22 – 106.39	Massive, fine-gr., dark grey sst
NB3	NB3-E-F3	121.74 – 121.98	Massive, fine-gr., dark grey sst
NB4	NB4-1-F3	4.86 – 5.04	Very fine-gr., grey sst
NB4	NB4-2-F3	6.28 – 6.60	Very fine-gr., grey sst
NB4	NB4-3-F3	9.55 – 9.71	Very fine-gr., grey sst
NB4	NB4-4-F3	14.85 – 15.00	Very fine-gr., grey sst
NB4	NB4-5-F3	19.82 – 20.00	Brown, very fine-gr., sst
NB4	NB4-6-F3	24.22 – 24.41	Massive, very fine-gr., brown sst

NB. This list does not include the 9 Tanqua fan (Fan X) sandstone samples with interstitial calcite cement. gr=grained sst=sandstone. Sample positions are also indicated on detailed borehole logs in Appendix A

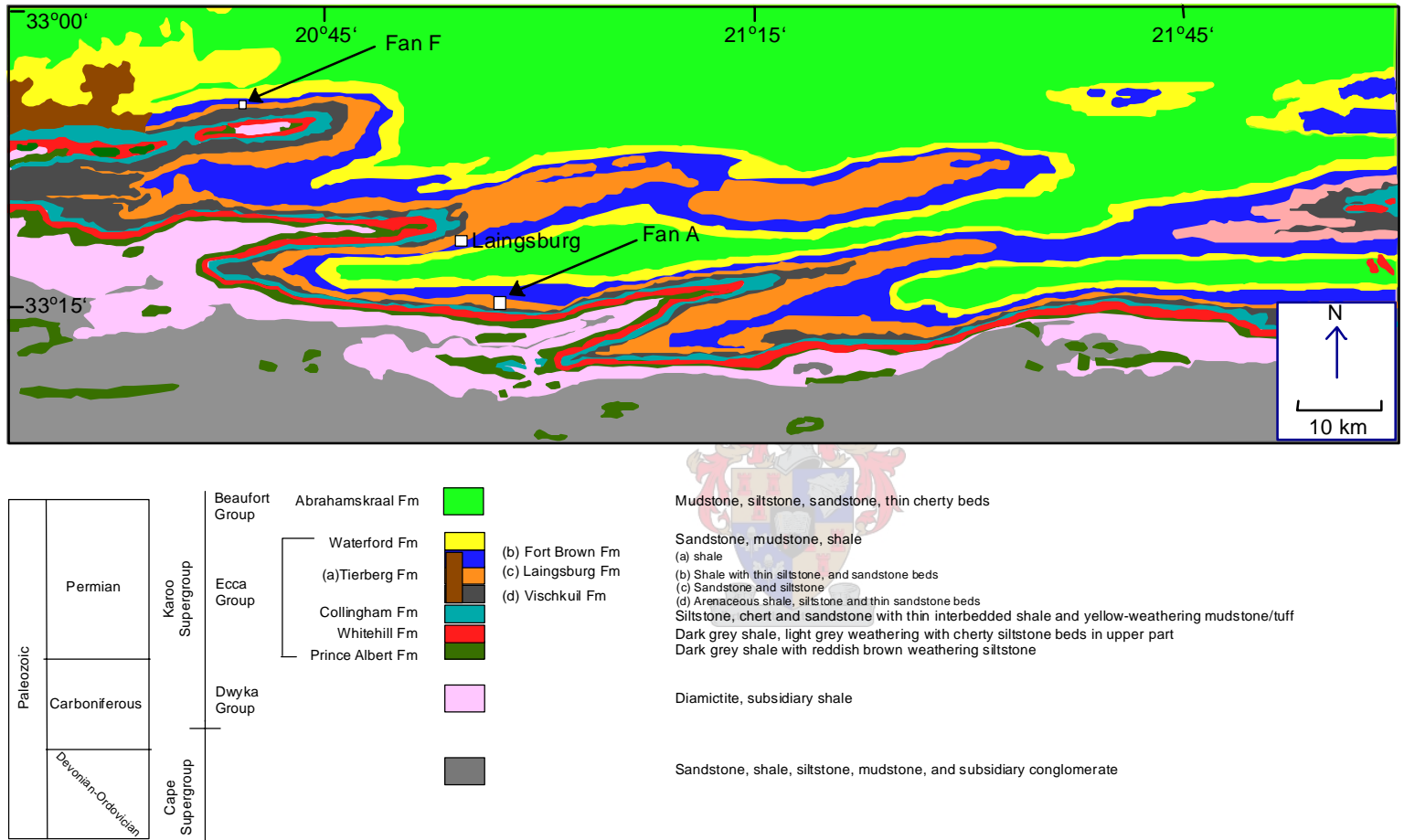


Figure 1.8 Geological map of the Laingsburg depocentre, Karoo Basin showing the sample locations (Van Lente, 2004)

1.3.2 Analytical techniques

The crushed Skoorsteenberg sandstone samples were used to determine the major element concentrations by X-ray fluorescence. The major elements Al_2O_3 , CaO , Cr_2O_3 , Fe_2O_3 , K_2O , MgO , MnO , Na_2O , NiO , P_2O_5 , SiO_2 and TiO_2 were analyzed. Trace elements were measured by inductively coupled plasma emission mass spectrometry (ICP-MS). These elements include Sc, V, Cr, Co, Ni, Cu, Rb, Sr, Y, Zr, Nb, Cs, Ba, La, Ce, Pr, Nd, Sm, Eu, Gd, Tb, Dy, Ho, Er, Tm, Yb, Lu, Hf, Ta, Pb, Th and U. Whole-rock major element geochemical data of Laingsburg fan sandstones used in this study are from Van Lente (2004).

Thin sections were made from the core samples from the Slope sandstones, Skoorsteenberg Formation and from outcrop samples of the Laingsburg Formation for mineralogical analyses by petrographic microscope. Several of these were coated with carbon and used for plagioclase chemistry and mineral identification under the Scanning Electron Microscope (SEM) at the University of Stellenbosch.

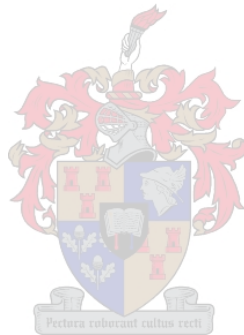
Heavy minerals were separated from light minerals by the method of density separation using bromoform (specific gravity 2.89). Chemical analysis of heavy minerals which included detrital garnet and sphene from the Tanqua area were done by means of the SEM.

Trace element chemistry of the Laingsburg and Skoorsteenberg detrital zircons, mounted on microscope glass slides reported in this study, was acquired by using laser ablation inductively coupled plasma emission mass spectrometry (LA-ICP-MS) at the University of Cape Town.

More than one hundred individual mounted zircons from Fans 3, 4 and 5 of the Skoorsteenberg Formation of the Tanqua subbasin as well as detrital zircons from Fans A and F of the Laingsburg Formation of the Laingsburg subbasin were

evaluated for morphology and inclusions using the polarizing microscope. Numerous scanning electron microscope (SEM) images of single zircon grains were taken (Appendix E). U-Th-Pb geochronological study on these detrital zircons was performed on the Sensitive High Resolution Ion Microprobe (SHRIMP) at the Australian National University (ANU) by Dr. Richard Armstrong.

More information on mineral separation techniques, sample preparation procedure and details of different analytical techniques including XRF, ICP-MS, LA-ICP-MS and SHRIMP are available in the Appendices.

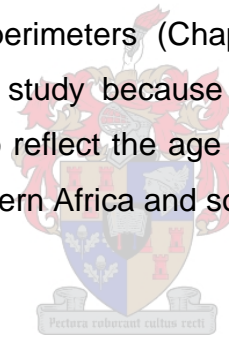


CHAPTER TWO

REGIONAL GEOLOGICAL SETTING

2.1 Introduction

The objective of this section is to give a brief overview of the basement and rocks that indicate Permian metamorphism and magmatic activity, along the magmatic arc back-arc system of the Panthalassan margin. An informative review of pre-Permian basement rocks of southern Patagonia is given by Pankhurst et al. (2003); only a summary is presented in Table 2.1. This study took into consideration the geology of South America because a number of previous investigators have suggested the provenance of the Laingsburg and Tanqua submarine fans in the south and southwest of the Cape Fold Belt to be outside the actual southern African perimeters (Chapter 1). The present chapter is significant in this provenance study because radiometric ages obtained from detrital zircons are expected to reflect the age of the sedimentary, metamorphic and igneous provinces of southern Africa and southern Gondwana.



2.2 Pre-Karoo geology

The sedimentary deposits of the Karoo Basin cover approximately two thirds of the present land area of South Africa (Fig. 1.1). The Karoo strata rest upon the Archean Kaapvaal Province, the Kheis Province, the Kibaran Namaqua-Natal Province and the Pan-African Saldania-Gariep Province (Cole, 1992) (Fig. 2.1).

The Kaapvaal Province comprises a basement complex older than 3 Ga, and a younger supracrustal cover of about 2.9 Ga, including the Witwatersrand and Pongola Supergroup (Beukes and Cairncross, 1991). The basement is composed mainly of granitoids with subordinate orthogneisses and greenstone terranes (~3.2 to 3.5 Ga old), called the Barberton Supergroup and equivalents (Hunter and Wilson, 1988).

Table 2.1 U-Pb chronology of pre-Permian basement rocks of SW Gondwana (Pankhurst et al., 2003).

Orogenic event	Deseado Massif	Northern Patagonia	Argentina North of Patagonia	Antarctic Peninsula
Neoproterozoic-Early Cambrian	Dos Hermanos phyllites with ca. 565 Ma zircons; 540 Ma low grade metamorphism	El Jagüelito Formation with 545 Ma igneous zircons and fossils	Puncoviscana Formation 530-560 Ma zircons and fossils; 535-545 Ma metamorphism	Only known as inherited zircons
Cambrian	523 ± 4; 529 ± 8 Orthogneissic basement of Tierra del Fuego	Only known as inherited zircons	520-530 Pampean belt; 530 ± 3; 527 ± 6 S. de la Ventana granites	Only known as inherited zircons
Mid-Ordovician	476 ± 5; 472 ± 5 cobbles in Permian	476 ± 4 Arroyo Salado granite; 469 ± 4 Gonzalito gneiss	470-490 Famatinian granites	Only known as inherited zircons
Late Ordovician	≥ 450 Dos Hermanos Granite	??	440-470 Famatinian metamorphism	463 ± 5 cobbles in View Point congl.
Silurian	425 ± 4 El Sacrificio Granite	??	??	435 ± 8; 422 ± 18 orthogneiss; 431 ± 12 cobbles in congl.
Devonian	395 ± 4 El Laurel Tonalite, ~ 400 Pb-loss	396 ± 7 Colan Conhué Granite	403 ± 6; 393 ± 5; 382 ± 6 'Achalian'	393 ± 1 Target Hill orthogneiss cores
Carboniferous	344 ± 4 Mina La Leona Granite			327 ± 9 Target Hill overgrowths 347 ± 3 Thurston Island Orthogneiss

Ages reported in this table are in Million years

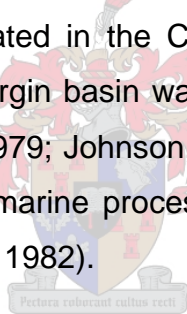
The Kheis Metamorphic Province consists of meta-arenites occurring in what has been described as a thin-skinned fold and thrust belt of Eburnian (~2.0 -1.8 Ga) age (Moen, 1999). The start of the Kheis Orogeny at 1890 Ma was the first accretionary event experienced by the stabilized Kaapvaal-Zimbabwe Craton. The Kheis Province forms part of the Eburnian Orogeny, while the Okwa and Mongodi Metamorphic Provinces also fall within this larger orogenic event (Thomas et al., 1994). This indicates that there was an extensive accretionary event along the western margin of the Kaapvaal-Zimbabwe Craton at 2000 Ma.

The Namaqua-Natal Province (Fig. 2.1) is a 400 km wide high-grade metamorphic belt that occurs to the south and southwest of the Kaapvaal Craton and marks a period of terrane accretion at approximately 1100 Ma (Thomas et al., 1994). Geochronological data demonstrated that the entire evolutionary history of the Namaqua-Natal Belt may be bracketed between about 1200 and 1000 Ma (Thomas and Eglington, 1990; Thomas et al., 1993a; 1993b). The rocks of the Namaqua-Natal Province include calc-alkaline arc-related rocks (i.e. the Richterveld Terrane supracrustal metavolcanics, and orthogneisses). The Namaqua-Natal Province consists of five different terranes and well-preserved immature sedimentary and volcanic rocks known as the Koras Group (Moen, 1987). The Kaaie Terrane located to the west of the Kheis Province consists of metaquartzites, schists and volcanic rocks. West of the Kaaie Terrane is the Areachap Terrane which consists of a narrow belt of amphibolite-grade mafic to intermediate gneisses. Geringer and Ludick (1990) proposed that the Areachap Terrane originated from one or several juvenile volcanic arcs associated with a Mesoproterozoic subduction zone. In the westernmost part of the Province is the volcano-sedimentary Kakamas Terrane, cut by gneisses during the Namaqua event. The Bushmanland Terrane has three main crustal components: remnants of the Paleoproterozoic basement (~1.7-2.0 Ga), Mesoproterozoic supracrustal successions, and various pre-to synorogenic intrusive suites having yielded igneous and metamorphic ages in the 1.2 ± 2 Ga ranges (Thomas et al., 1994). The Bushmanland Terrane deposited on top of the Eburnian Basement is

bounded by the Richterveld Terrane in the north and the Kakamas Terrane to the east (Watkeys, 1986).

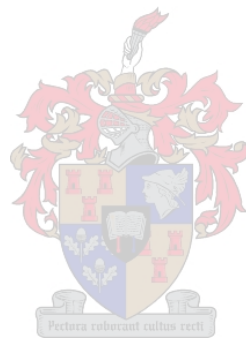
The Saldania Belt and Gariep Group to the south and southwest of the craton (Fig. 2.1) are part of the Neoproterozoic Pan-African Belt and comprise sedimentary and volcanic rocks, the oldest component of which might have been associated with the break-up of Rodinia and opening of the proto-Atlantic in an inferred 780-750 Ma time interval (Dalziel, 1992; Powell et al., 1993). The Cape Granite Suite, regarded as high diapiric plutons, intruded the Saldania Belt between 550 and 510 Ma (Scheepers and Nortjé, 2000; Scheepers and Poujol, 2002).

The Table Mountain, Bokkeveld, and Witteberg Groups together constitute the Cape Supergroup that accumulated in the Cape Basin (Tankard et al., 1982; Broquet, 1992). This passive margin basin was filled by detritus from a cratonic hinterland to the north (Visser, 1979; Johnson, 1991). The sediments underwent extensive reworking by shallow-marine processes on a stable shelf to produce quartz-rich sands (Tankard et al., 1982).



The Saldania Belt rocks and the overlying Cape Supergroup were folded and faulted during the Cape Orogeny (Hälbich, 1992; von Veh, 1992). The early Paleozoic passive continental margin formed an important section of the southern edge of Gondwana, evolving into an active collision margin during the late Paleozoic (Tankard et al., 1982) that led to the development of the Permo-Triassic Cape Fold Belt. The latter consists of two branches (Fig. 2.2c) namely, the Southern Branch trending east-west and the Western Branch that runs northwest-southeast. The Southern Branch experienced greater compressional forces than the Western Branch (De Beer, 1990). Pressure and temperature conditions in the metasedimentary orogenic belt increase from the northern margin of the Orogen southwards with the highest P-T values estimated at 3-4 kb and approximately 350 °C in the south, more specifically in zone 6 of Hälbich and

Swart (1983). $^{40}\text{Ar}/^{39}\text{Ar}$ step-heating analysis of micas from the southern branch of the Fold Belt indicates that the Orogeny was strongly episodic with five individual events at 278 ± 2 Ma, 258 ± 2 Ma, 247 ± 3 , 230 ± 3 Ma, and 215 ± 2 Ma (Hälbich et al., 1983). Further $^{40}\text{Ar}/^{39}\text{Ar}$ dating demonstrated that the Saldania (pre-Cape) rocks were folded and thrust in conformity with the cover during the Cape Orogeny. Dominant age components reflect events at 223 Ma, 239 Ma, 259 Ma, 276 Ma and 294 (Gresse et al., 1992).



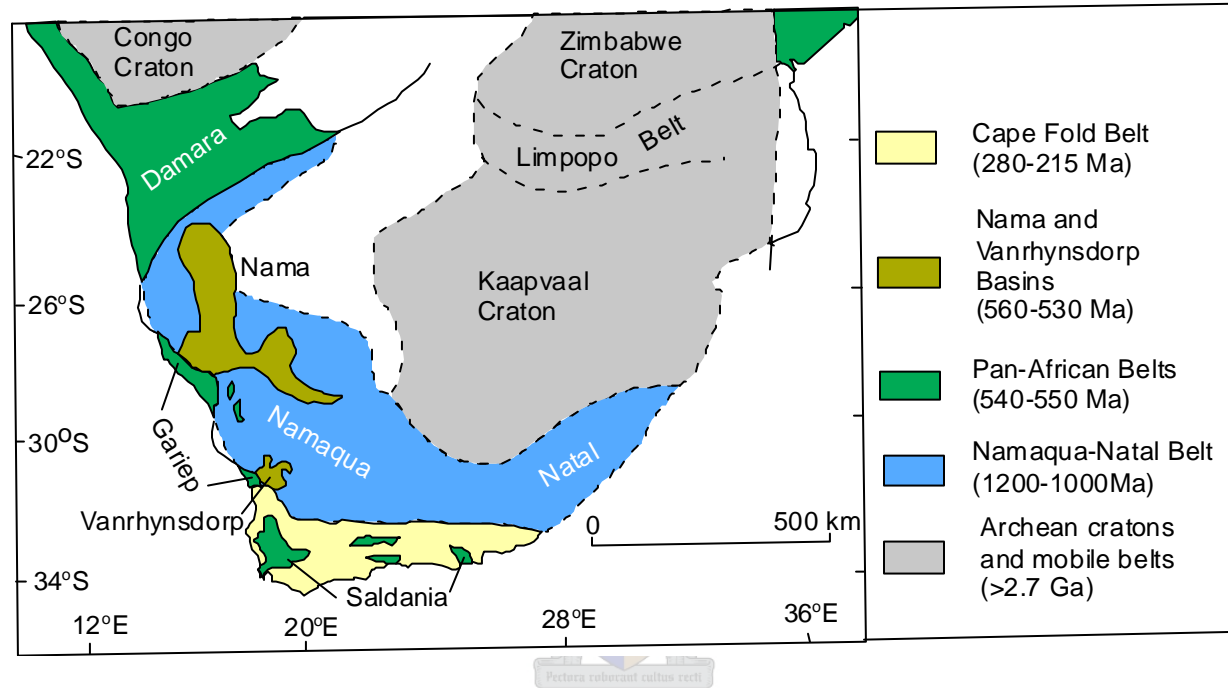


Figure 2.1 Geographic distribution of the pre-Karoo geology including the Kaapvaal Craton and other cratons and orogenic belts in southern Africa (Frimmel, 2000).

2.3. Geology of the Karoo Basin

The Skoorsteenberg and Laingsburg submarine fans were deposited in a typical foreland basin, the latter being simply defined as a sedimentary basin lying between the front of a mountain chain and the adjacent craton (Allen et al., 1986). Like other major southern Gondwana foreland basins (Paraná, Beacon and Bowen Basins), the Karoo Basin developed in response to accretion tectonics along the southern margin of Gondwana during the late Palaeozoic (Fig. 2.2; De Wit and Ransome, 1992, Veevers et al., 1994; López-Gamundí and Rosselo, 1998). Northward subduction of the Panthalassan (Paleo-Pacific Ocean) plate beneath the Gondwana plate led to the formation of a magmatic arc between the Karoo Basin and the southern margin of Gondwana (Johnson, 1991). The Karoo basin formed in front of an advancing thrust and fold belt, the Cape Fold Belt, which wrapped around the south-western margin of South Africa (Hälbich, 1992; Theron, 1969; Fig 2.2c).

The infill of the Karoo Basin started with the Carboniferous glaciogenic Dwyka Group which is overlain by the marine Ecca Group, on top of which was deposited the fluvio-lacustrine Beaufort Group (Johnson et al., 1996; Fig. 2.3).

Continental glaciation covered the area in the late Carboniferous. During glaciation and immediately after the disintegration of ice sheets, diamictites of the Dwyka Group were deposited in the basin (Visser, 1991). The retreat of ice in the early Permian was accompanied by the deposition of the marine Ecca Group which started with the Prince Albert Formation, 180 m of shale and cherty shale beds dated at 288 ± 3 Ma by Bangert et al. (1999).

The Prince Albert Formation is overlain by the Whitehill Formation, a black, carbonaceous shale with pelagic organisms. Deposition of homogeneous black

muds of the Whitehill Formation under starved anoxic conditions reflect a tectonic quiescence and the dormancy of the Cape Orogeny (Wickens, 1994).

The Whitehill Formation is overlain by the Collingham Formation. The latter consists of fine-grained sheet turbidites and intercalated tuffs dated at 270 ± 1 Ma by Turner (1999).

The abrupt lithological change from dark carbonaceous shales (Whitehill Formation) to siliciclastic turbidite deposits associated with abundant tuff beds (Collingham Formation) suggests an important change in tectonic conditions over south-western Gondwana (Wickens, 1994). The Collingham Formation, containing distal turbidites and volcanic ash layers, is the only unit of the Ecca Group that can be related directly to active arc volcanism to the south and southwest. These tuff beds in the Collingham were probably derived from volcanoes located in northern Patagonia, where Permian silicic-andesitic volcanic and plutonic rocks occur (Wickens, 1994). Dating of both these rocks and the late Carboniferous-early Permian to Triassic volcanic events in the Central Andes yielded ages of 290-210 Ma (Breitkreuz et al., 1989). This volcanism correlates with the $^{40}\text{Ar}/^{39}\text{Ar}$ ages of the Cape Orogeny (Wickens, 1994).

In the Tanqua subbasin, mudstones of the Tierberg Formation were deposited on top of the Collingham Formation and are succeeded by the Skoorsteenberg Formation. The latter, also termed the Tanqua basin floor fan complex or Tanqua fans, is one of the formations selected for this study. The Skoorsteenberg Formation is a 400 m succession of five sand-rich submarine fan systems (Bouma and Wickens, 1991; Wickens, 1994), named informally Fan nos. 1-5 from oldest to youngest (Wickens, 1984). More details on the local geology of the Tanqua fans are presented in Chapter 3.

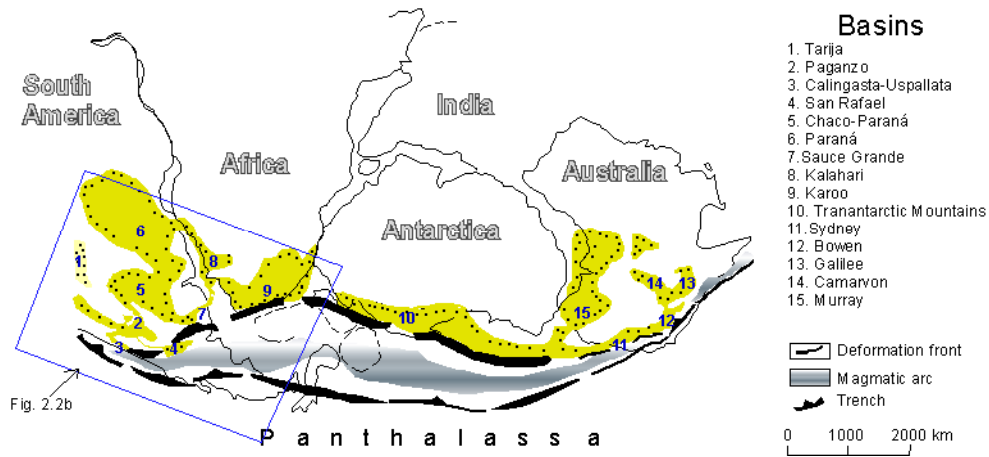


Figure 2.2a Paleogeography and paleotectonic framework of Gondwanaland during the Late Paleozoic (Late Carboniferous-Permian; López-Gamundí and Rosselo, 1998).

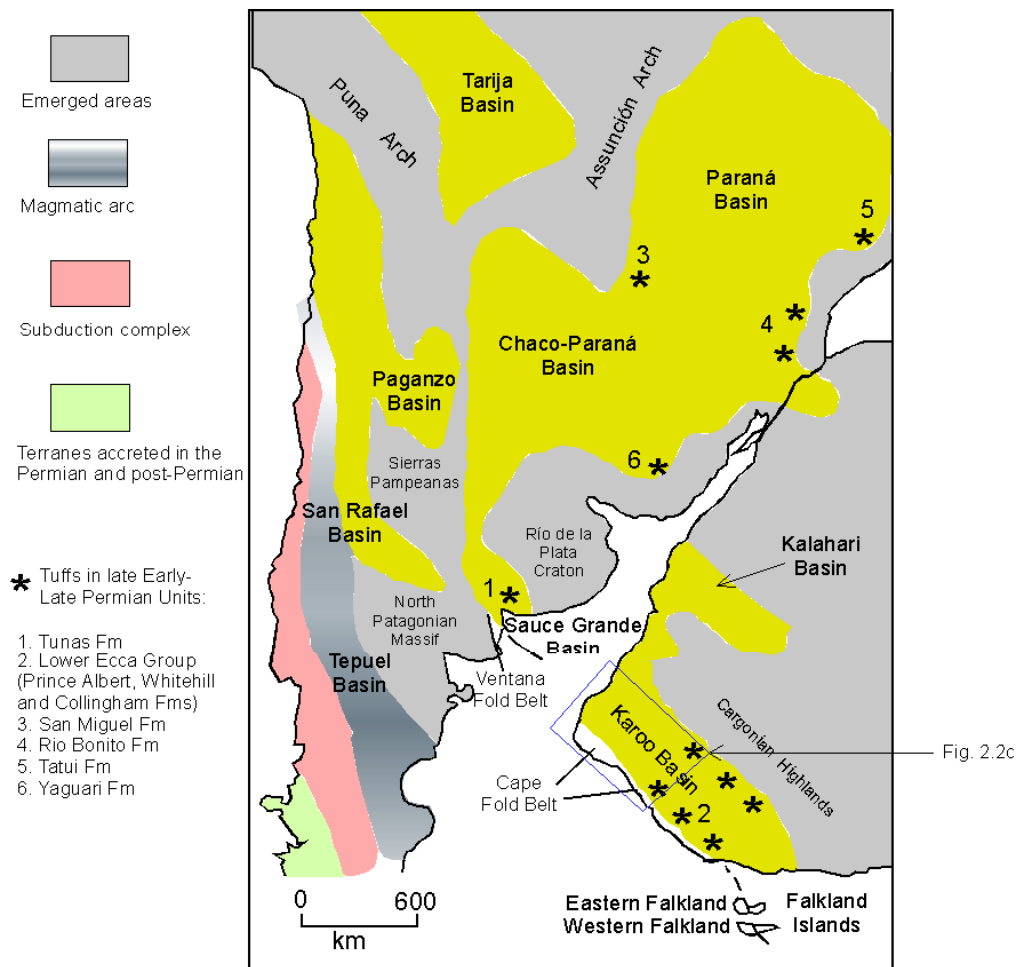


Figure 2.2b Paleogeography and geotectonic setting of western Gondwana (South America and South Africa) during the Late Paleozoic (López-Gamundí and Rosselo, 1998).

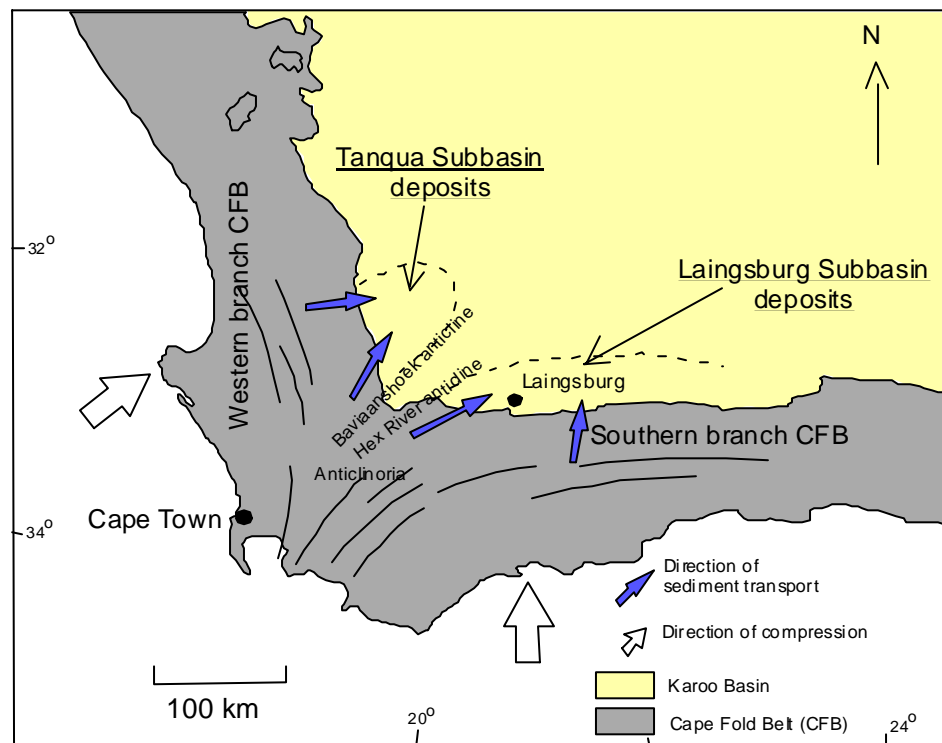
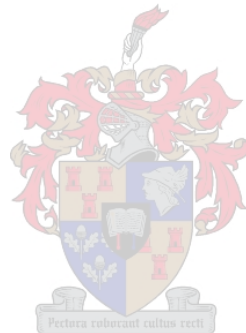


Figure 2.2c Location of the Tanqua and Laingsburg subbasins in the southwest corner of the Karoo Basin shown in relation to the two branches of the Cape Fold Belt and the Baviaanshoek/Hex River anticlinoria (Bouma and Wickens, 1994)

On top of the Skoorsteenberg Formation, the submarine slope and prodeltaic (Kookfontein Formation), shoreface (Waterford Formation) and fluvial (Abrahamskraal Formation, Beaufort Group) successions mark the overall progradation of the sedimentary system to the north and east during mid to late Permian times (Hodgson et al., 2003).

In the Laingsburg subbasin, shale and fine-to very fine-grained sandstones of the Vischkuil Formation were deposited on top of the Collingham Formation. The Vischkuil Formation is overlain by the Laingsburg Formation, a fine-grained turbidite fan complex representing the other investigated formation of this study. Above the submarine fans, basin shales of the Fort Brown Formation and deltaic deposits of the Waterford Formation were deposited.



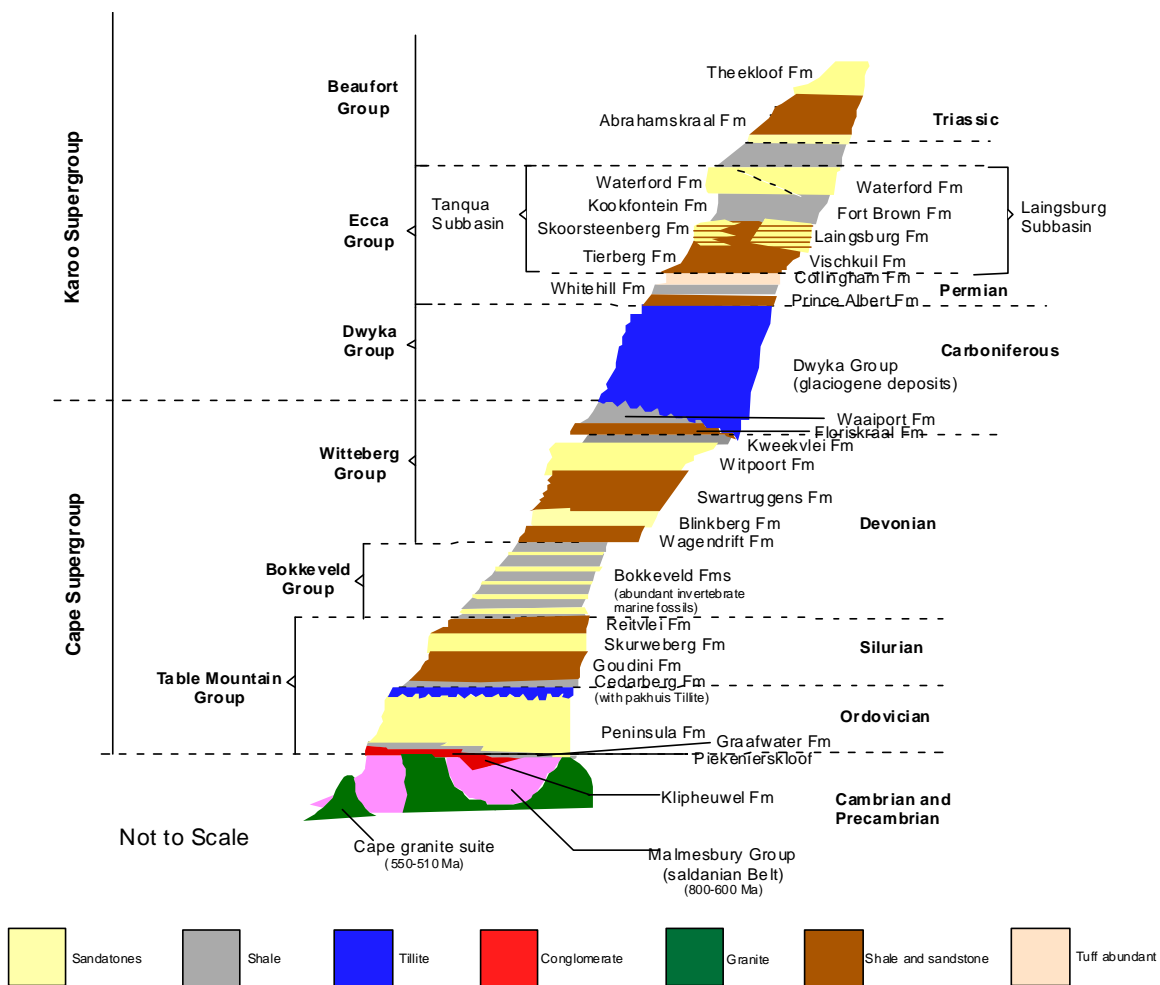


Figure 2.3 Schematic representation of the Cape and Karoo stratigraphy in the south-western Karoo Basin (Wickens and Bouma, 2000).

CHAPTER THREE

LOCAL GEOLOGICAL SETTING

3.1 Introduction

This chapter briefly presents the geology of the study area, placing important constraints on the similarities and correlation between the Laingsburg and Tanqua submarine fan complexes. Detailed study of sedimentary structure features of basin-floor fans are beyond the scope of this investigation. Limited information of the subject is presented here, but more information on these aspects can be found in Wickens (1994), Scott (1997), Sixsmith (2000), Wickens and Bouma (2000), and Hodgson et al. (2003).

3.2 The Tanqua Submarine Fan Complex.

The Skoorsteenberg Formation in the Tanqua subbasin crops out in Ceres/Tanqua east of the Cedarberg mountain range. The formation is a 400 m succession of five sand-rich submarine fan systems (Bouma and Wickens, 1991; Wickens, 1994), named informally Fan nos. 1-5 from oldest to youngest (Wickens, 1984). The fan outcrops are well exposed from south to north over 50 km, providing an opportunity to investigate the development of the five basin floor fans. The five individual arenaceous fan systems are between 20 and 50 m thick and are thought to represent lowstand deposits (Geel et al., in press).

The turbidite fans are separated by basin shale units of comparable thickness and each fan shows abrupt upper and lower boundaries (Wickens, 1994). The Tanqua sandstone samples used in this study are from the Slope and Fans 3, 4 and 5.

Fan 3 is 30 to 50m thick in the southern half of the outcrop and progressively thins northward until it pinches out northeast of the Skoorsteenberg (Wickens and Bouma, 2000). A coarsening and thickening-upward package of siltstone and very fine-grained sandstone turbidites is always present at the base of the fan, although the overlying lithofacies is variable (Hodgson et al., 2003). Fan 3 extends from Ongeluks River in the south to Skoorsteenberg in the north, a distance of approximately 34 km. This fan is separated from Fan 2 by a succession of shale, siltstone and 50 to 80 m thick very thin sandstones. Fan 3 is the best preserved basin-floor fan of the Tanqua fan complex. It therefore shows the most variety of facies and sedimentary structural features of all the fans (Wickens and Bouma, 2000).

According to Wickens and Bouma, Fan 4 is the most widespread and thickest fan, with sedimentary characteristics consistent with deposition in middle to lower fan setting. This fan thins to the south from approximately 60m in the Skoorsteenberg area to about 30 m or less in the Kleine Riet Fontein and Bizansgat area. Fan 5 comprises the last sand-rich turbidites deposited in the Tanqua Karoo subbasin. This fan is similar to Fan 4 in areal extent. The best exposed outcrops are limited to the vicinity of Skoorsteenberg where it has a thickness of 35m.

Geel et al. (in press) identified five lithofacies from the Tanqua subbasin. These include (1) massive shale; (2) laminated shale; (3) siltstones; (4) structured sandstones; and (5) massive sandstones. All lithofacies are highly compacted and show no porosity except for occasional fracturing (Geel et al., in press) due to advanced diagenesis.

Subordinate lithofacies include volcanic ash layers, cherty beds and calcareous layers. These latter are associated mainly with shale horizons (Wickens, 1994).

3.3 The Laingsburg Submarine Fan Complex

As a comprehensive new review of the geology of the Laingsburg area, especially Fan A, is given by Sixsmith (2000), only a very short description of the Laingsburg submarine fan characteristics is presented here.

The Laingsburg Formation in the Laingsburg subbasin is a turbidite fan complex and comprises six turbidite fan systems, each separated by a significant thickness of hemipelagic and turbiditic mudstone. The Laingsburg Formation attains a thickness of 750m in the Laingsburg area along the Buffels River, but thins in a northerly and easterly direction. The Laingsburg Formation consists predominantly of very fine- to fine-grained sandstones, with a maximum grain size of medium sand. Beds commonly exhibit tractional structures, Bouma sequences and sole structures that confirm their origin as turbidites. In outcrop, beds are frequently laterally continuous and parallel-sided.

The six turbidite fans that make up the Laingsburg Formation are informally called fans A-F. Fan A constitutes approximately 40% of the Laingsburg Formation and reaches a thickness of 350 m southeast of Laingsburg. Fan B attains a thickness of between 80 and 150 m, and Fans C-F have thicknesses ranging between 10 to 100 m. The fans represent a basin-fill succession from the basin-floor (Fan A), base of slope (Fan B) and slope (Fans C and F) (Sixsmith, 2000). Investigated sandstone samples are from the lower fan (Fan A) and upper fan (Fan F) of the subbasin.

Sixsmith (2000) identified ten facies for the Laingsburg Formation. These include (1) massive sandstones, (2) structured sandstones, (3) massive siltstones, (4) structured siltstones, (5) silty mudstones, (6) mudstones, (7) mudclast and carbonaceous beds, (8) chaotic deposits, (9) ash deposits and (10) concretionary horizons.

3.4 Correlation between the Laingsburg and Tanqua deepwater fans

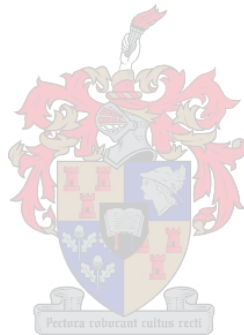
The Skoorsteenberg and Laingsburg deepwater fan complexes occupy similar stratigraphic positions above the Whitehill Formation. The two formations are lithologically alike but do not link with each other. The area between the two turbidite fan complexes is occupied by Tierberg Formation shale (Fig. 2.3). This latter area was interpreted by Wickens (1994) to have been situated over a basin floor high region where no turbidites were deposited.

Wickens (1994) initiated the correlation between the five deepwater fans of the Skoorsteenberg Formation with the fans of the Laingsburg Formation. However, such correlation would assume that the fans were deposited simultaneously in both subbasins. The concurrent deposition of the sand-rich packages in the two adjacent subbasins appears to be unlikely, as indicated by the difference in the subbasin configurations and the number of identified turbidite fans in the two adjacent depocentres. The Laingsburg Formation consists of six fans whereas the Skoorsteenberg Formation consists of five fans. Less tectonic compression resulted in a shallower, open basin in the Tanqua Karoo, whereas more tectonic compression in the Laingsburg area resulted in a deeper, narrow basin (Scott, 1997).

From field and laboratory data, Scott et al. (2000) concluded that the fans were probably deposited in one subbasin at a time, making a very precise correlation of the sand-rich packages from one depocentre to the other virtually impossible. The authors recognized that their data were not conclusive in assessing whether one subbasin filled completely and then the other or if the sedimentation alternated between the two subbasins.

Using a regional basal marker (MC) and overlying shale thickness, the fence diagram illustrating the stratigraphic correlation between the Laingsburg and

Tanqua depocentres of King et al. (2004) indicated that siliciclastic deepwater sedimentation began significantly earlier in the Laingsburg depocentre (Fig. 3.1). Despite the fact that Scott et al. (2000) and King et al. (2004) proposed two different correlations of Laingsburg and Skoorsteenberg submarine fans, the two group of authors demonstrated that the two formations originated from the same general source, though this latter is differently defined. This suggests that the problem of correlations of fans can be dissociated from the problem of provenance, since different correlation models proposed by various authors seems to be due to subbasin configurations rather than the origin of sediments.



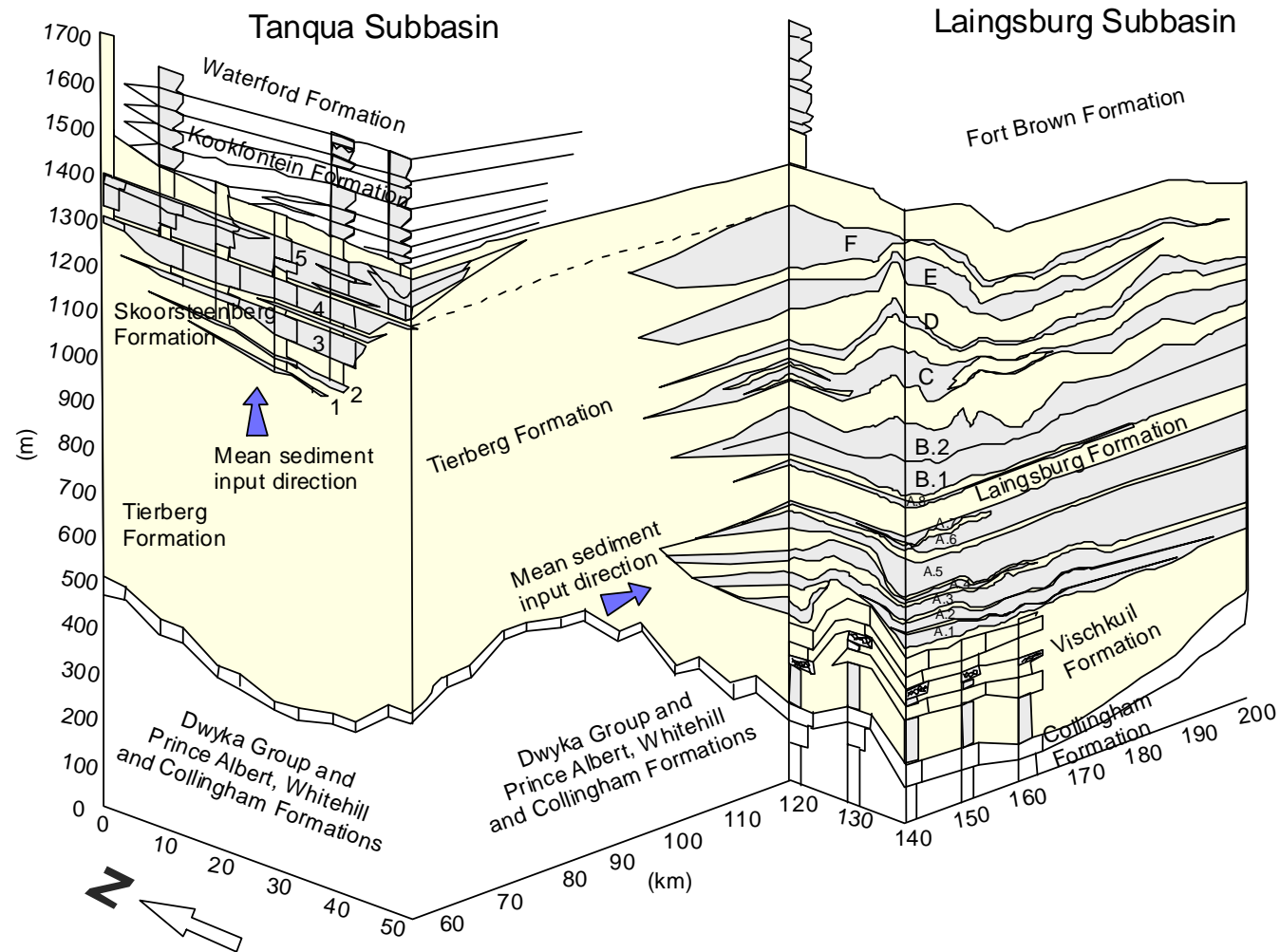


Figure 3.1 Stratigraphic correlation between the Tanqua and Laingsburg subbasins, showing that the Tanqua subbasin deposits are younger than the Laingsburg subbasin deposits (King et al., 2004).

CHAPTER FOUR

MINERALOGY

4.1 Introduction

A standard petrographic microscope was used to investigate the mineralogy and to discover the various factors related to the origin or “birth” of sediments that filled the Permian Tanqua and Laingsburg subbasins in the south-western Karoo Basin. Mineralogical and textural maturity depends on the content of fine-grained material, sorting and roundness of the grains and the basic mineral composition. Petrographical approaches to the identification of source rocks of sandstones included investigations of undulosity and polycrystallinity of quartz grains (Basu et al. 1975), types of feldspar present (Pittman, 1970), and lithic fragments (Pettijohn et al., 1987). Relief and climate of the source area was inferred from grain roundness and average degree of feldspar alteration (Folk, 1980).

Thin sections made from the Laingsburg outcrop sandstones and from core sandstone samples from the Slope and Tanqua submarine Fans 3, 4, 5 were described using a standard petrographic microscope. The study particularly focused on sandstones for heavy mineral extraction, in particular zircons. The results are given below.

4.2 Petrographic analysis

The major rock-forming minerals are quartz, sodic plagioclase (albite), alkali feldspar (mainly orthoclase and microcline), epidote, biotite and muscovite. Diagenetic minerals include illite, chlorite and calcite.

The Laingsburg, Tanqua and Slope sandstones are mineralogically and texturally immature. These sandstones show abundant less stable minerals such as

feldspars and rock fragments not consisting principally of quartz, as well as the predominance of angular grains. The investigated sandstones are fine-to very fine-grained, ranging from 177 to 62 μm with the majority between 125 to 62 μm (Scott, 1997). Based on visual estimation, the feldspar content ranges from 5 to approximately 15 % in most of samples, but can reach up to 35 %.

A traditional quartz-feldspar-lithic fragments (QmFLt) ternary diagram of the Tanqua and Laingsburg sandstones shows a high lithic fragments and feldspar content (Fig. 4.1; King et al., 2004). Similarly, the Waterford Formation sandstones (equivalent of Slope sandstones of this study in the Laingsburg subbasin) show significantly high feldspar and rock fragment (particularly volcanic rock fragment) percentages (Fig. 4.2; Johnson, 1991), confirming the mineralogical immaturity of the investigated sandstones.

In general, investigated sandstones are moderately sorted and comprise angular grains supported by a mud matrix and thin mud laminae (Scott et al., 2000). There was little petrographic evidence for weathering and alteration of minerals in any of the thin sections.



4.2.1 Detrital quartz

Both monocrystalline (single crystal) and polycrystalline (grain comprising a number of crystals with different orientations) quartz varieties are present. Quartz grains present both a uniform and undulose extinction (Fig 4.3). Undulose extinction is a result of strain and is found in quartz grains from both igneous and metamorphic sources (Basu et al., 1975).

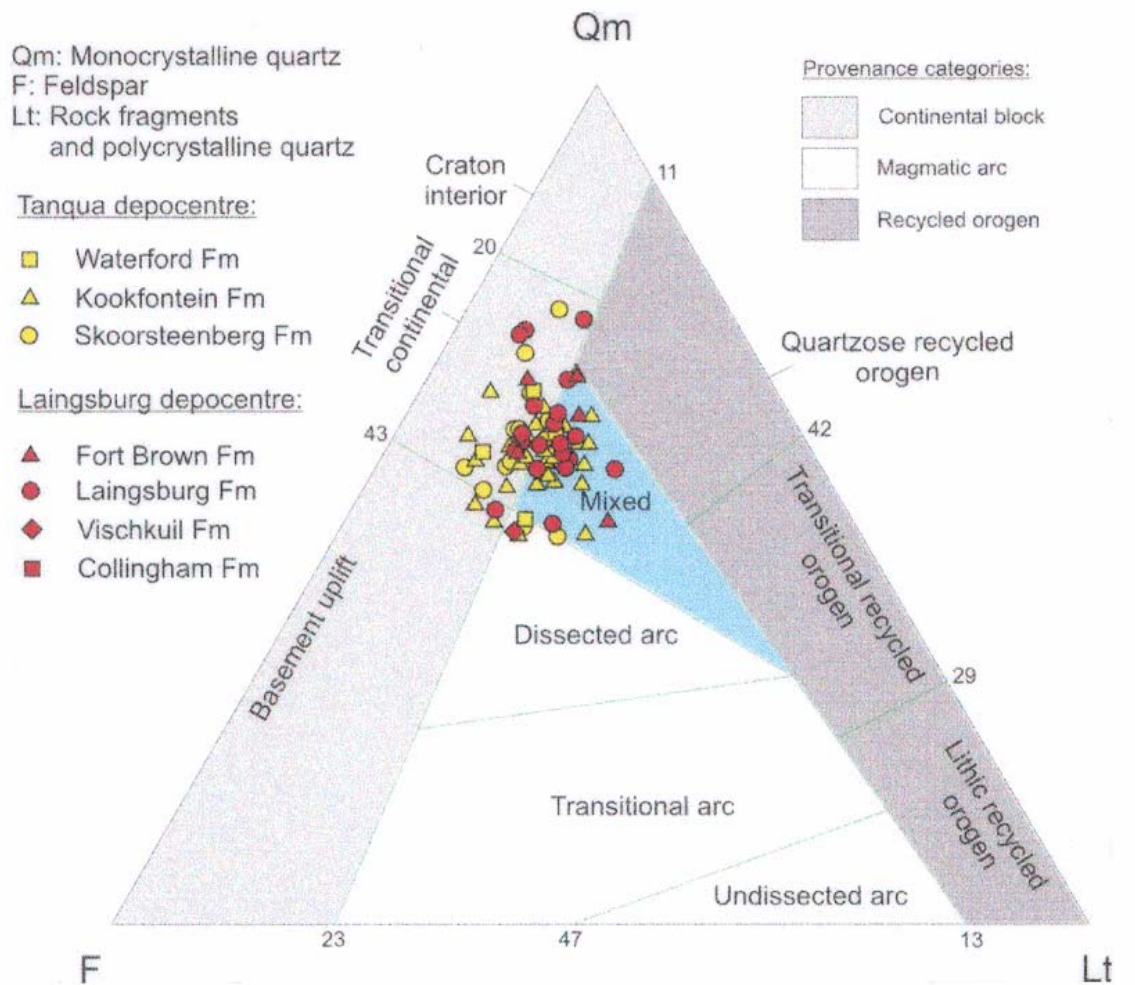


Figure 4.1 QmFLt ternary diagram showing the provenance (granitic) of the Tanqua and Laingsburg subbasins sandstones, Ecca Group (King et al., 2004). Note the near-identical source of the two groups of sandstones. The provenance fields are from Dickinson et al. (1983).

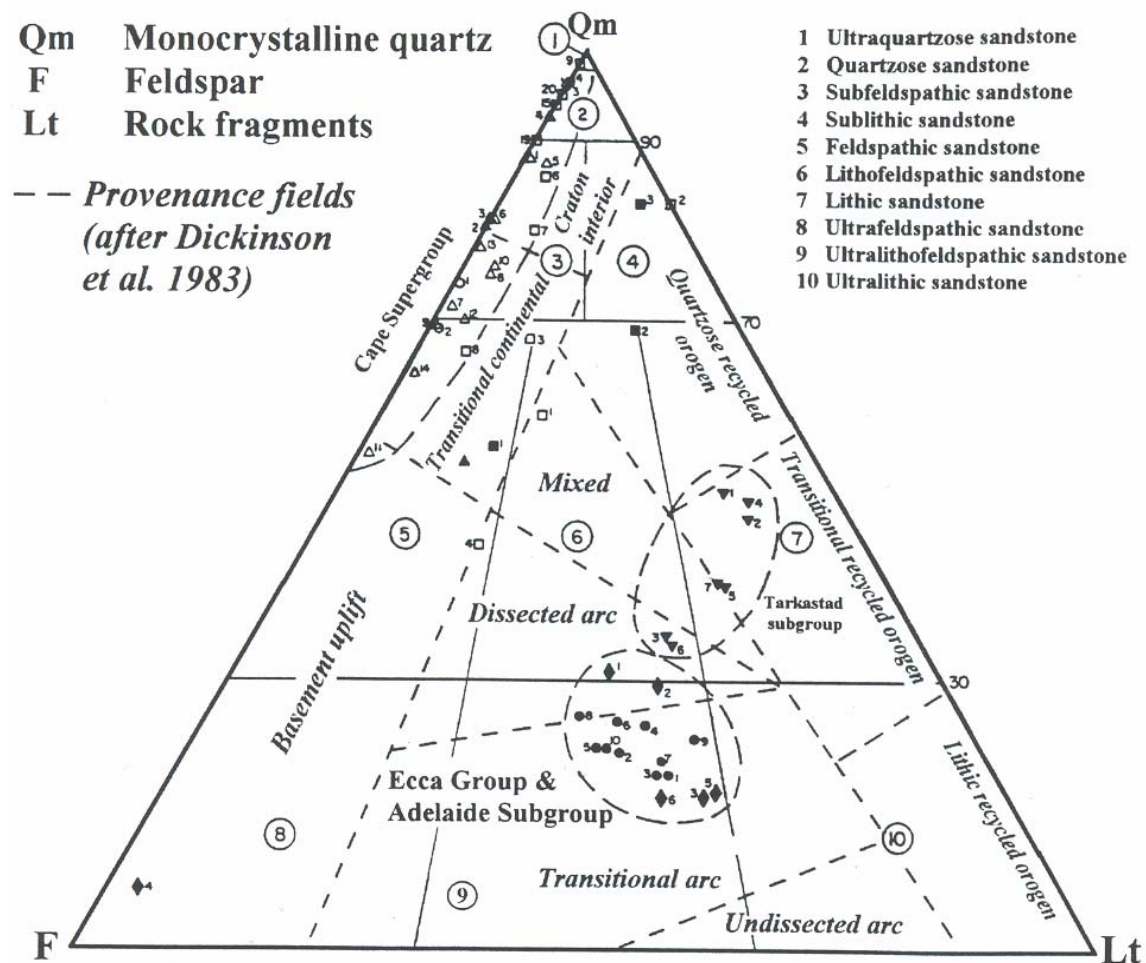


Figure 4.2 QmFLt plot showing the provenance (transitional arc) of the Ecca group sediments (diamonds) including (1, 2 & 3) Waterford Formation sandstones, (4) Ford Brown Formation tuff and (5 & 6) Ripon Formation sandstones (Johnson, 1991). Note the difference between the provenance proposed by King et al. (2004) and Johnson (1991).

Different genetic varieties of quartz grains have been identified. Xenomorphic polycrystalline and monocrystalline quartz grains with straight to slightly undulose extinction containing some inclusions, typical of granite but also furnished by many other sources, have been identified (Fig. 4.4). The occurrence of zircon in quartz grains observed in some thin sections is a common feature of granitoid rocks (Di Giulio et al., 1999).

Metamorphic quartz varieties were also identified in some thin sections. These are often indistinguishable from primary plutonic igneous quartz. Some polycrystalline types have micas (generally parallel remnants of schistosity); these are polymineralic and can be inferred to be metamorphic rock fragments (Lewis, 1984). Added to that, one can identify the presence of elongated and flattened varieties. Some have straight boundaries whereas the others have sutured borders. All present uniform to undulose extinction.

A volcanic quartz variety which is usually monocrystalline and water clear, often euhedral, with rounded corners and resorption embayments is also present. Rounded to subrounded sedimentary quartz with overgrowth are quite rare.

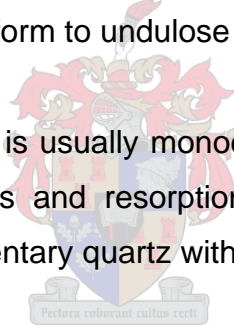
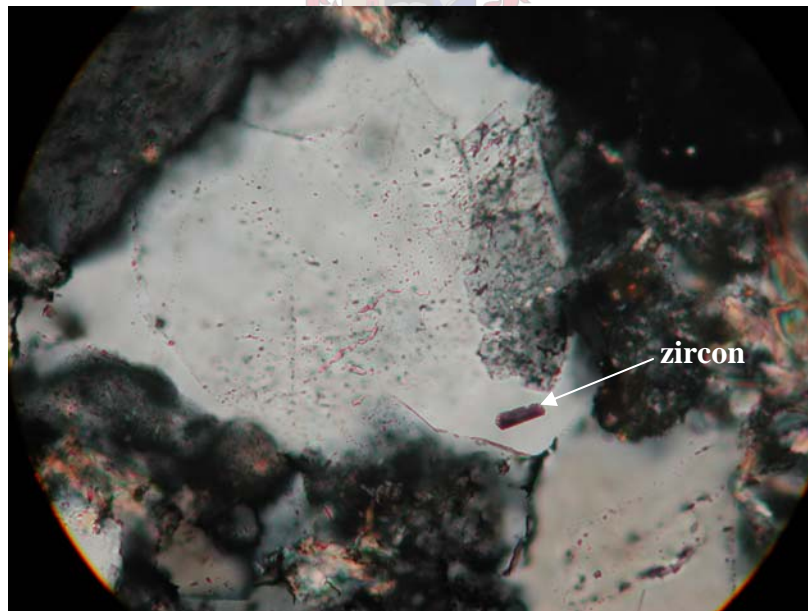




Figure 4.3 The quartz grain in the centre of the field of view shows undulose extinction, typical of quartz from both igneous and metamorphic sources (200 x magnification)



500 x magnification

Figure 4.4 Common (plutonic) quartz grains characterized by straight to slightly undulose extinction, xenomorphic and typical of granites. Note the inclusion of euhedral zircon and some vacuoles (dark dots). The inclusion of zircon in quartz is typical of granitoid sources.

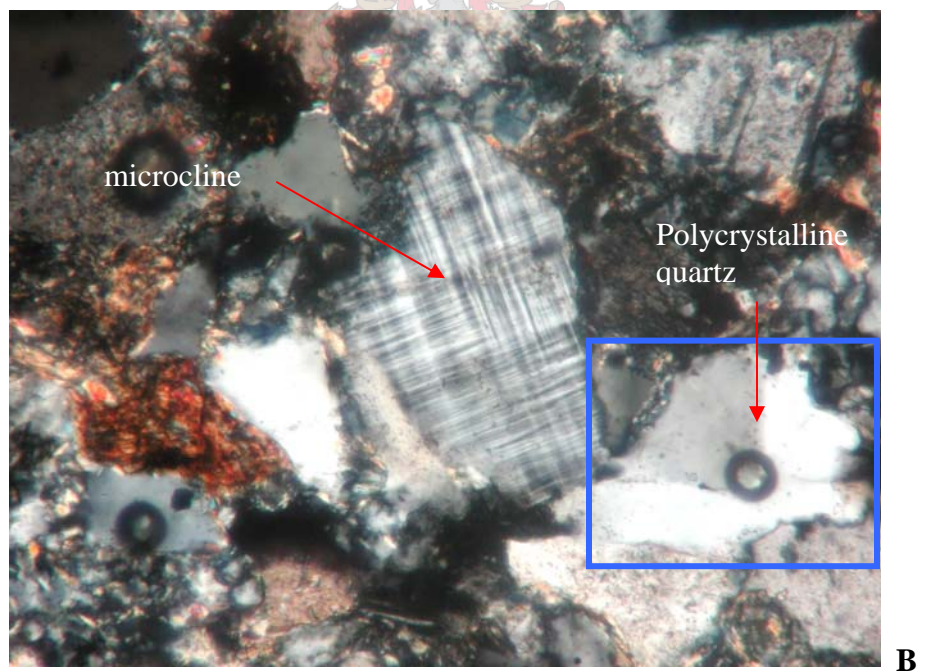
4.2.2 Chemistry of detrital feldspar

Both alkali feldspar and sodic plagioclase are present (Figs. 4.5 and 4.6). The feldspar content is estimated at 5 to 15 % in most of samples, but can reach up to 35 %. Some feldspars are clearly larger than quartz grains. Two varieties of sodic plagioclase were identified. These include the combined Carlsbad-albite (simple) and pericline (polysynthetic) twinned types.

Alkali feldspar grains are mostly orthoclase (fresh, with very few altered grains) but cross-hatched microcline and sanidine are also present. Some of these grains are dissolved and replaced by calcite, clay minerals or sericite.

The presence of albite, K-feldspar (orthoclase, microcline and sanidine) and perthite (intergrowths of Na and K feldspar) infer a multiple origins for the sediments that have filled the Tanqua subbasin. In general, the feldspar of acid volcanics is likely to be sanidine, that of acid plutonic rocks is either microcline or orthoclase and sodic-rich plagioclase (albite) is derived from alkaline volcanic rocks. Perthitic feldspar is indicative of slow cooling and hence characteristic of plutonic source (Pettijohn, 1975).

Feldspars of pyroclastic origin tend to show euhedral forms, commonly broken, and in some cases display a thin envelope of glass, whereas plutonic feldspars are anhedral (Pettijohn, 1975). Feldspars identified in this study are essentially euhedral and exhibit sharp angles suggesting a very short travel distance. Plagioclase feldspars are unstable minerals and cannot resist multiple sedimentation cycles. Therefore, their presence in the investigated sandstones suggests not only a proximal source but that the detritus are first cycle.



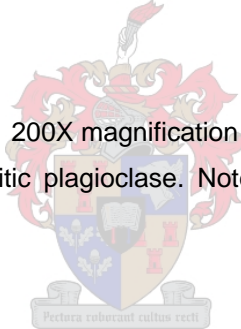
200x magnification

Figure 4.5 Common varieties of K-feldspar. Photograph (A) shows an orthoclase grain with sericitic alteration in a matrix of calcite. Photograph (B) shows a grain of microcline (centre) and polycrystalline quartz (bottom right). Note the angularity of grains.



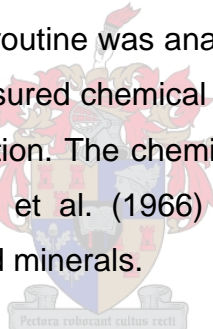
200X magnification

Figure 4.6 Common varieties of albitic plagioclase. Note the angularity of grains and limited alteration.



4.2.2.1 Methodology

Major element chemical analyses of plagioclase, sphene and garnet were performed on a LEO scanning electron microscope coupled to a Link ISIS energy dispersive spectrometry system at the University of Stellenbosch. The microscope operating conditions were set at an accelerating voltage of 20 kV with a beam current of 120 μ A and a probe current of 1.50 nA. Acquisition time was set at 50 seconds and spectra were processed by ZAF corrections and quantified using natural mineral. Mineral compositions were recalculated to mineral stoichiometries and the stoichiometric results were used to evaluate the quality of the analytical data. Mineral standards with a known chemical composition were treated as unknowns and analyzed using the same instrument and calibration set-up employed for unknowns. For instance, a garnet standard not used in the garnet analytical routine was analyzed with the same set-up used for unknown garnet and the measured chemical composition was then compared to the actual, published composition. The chemistry of some plagioclase, garnet and sphene published by Deer et al. (1966) are reported together with the chemical composition of analysed minerals.



Major element chemical analyses of minerals reported in this section represent the average of two repeat analyses of the same mineral generation in a single grain. Only analyses that produced cation totals within 0.05 to 0.17 (depending on the number of cations) of the ideal stoichiometric number for each cation site were used in the calculations. For instance, garnet: Si = 3 ± 0.05 ; Al = $2 \pm 0.05/-0.1$; Fe+Mg+Mn+Ca = $3 \pm 0.1/-0.17$; total cations = $8 + 0.05/-0.1$, for plagioclase feldspar: Al+Si = 4 ± 0.03 and Ca+Na+K = 1 ± 0.06 . Discussion on elemental concentration of detrital sphene and garnet and their provenance implication is presented in the following section.

4.3.2 Results

Trevena and Nash (1981) have demonstrated that electron-probe microanalysis for Ca, K, and Na in detrital alkali feldspar and plagioclase is useful in provenance studies (Fig. 4.7). The authors also found that igneous plagioclase is more likely to be zoned than metamorphic plagioclase and that oscillatory-zoned plagioclase indicate a contribution from volcanic source. This is consistent with the findings of Pitman (1963).

The presence of both unzoned plagioclase crystals and detrital grains of undoubted metamorphic and/or plutonic origin such as microcline-perthite and epidote strongly suggest a metamorphic provenance.

The chemical analysis of 13 plagioclase feldspars from Fans 3, 4 and 5 of the Skoorsteenberg Formation reported in this chapter was undertaken to evaluate their chemical albite-anorthite-orthoclase (Ab-An-Or) composition (Table 4.1). Plagioclase feldspars analyzed in this study are soda-rich. Eleven of the thirteen albite feldspars are nearly pure albite (Ab_{98+}). Plagioclase feldspars with more than 96 % albite (Ab) molecule probably derive from low-grade metamorphic rocks or from silicic plutonic rocks, though that some of this albite could be authigenic as a result of diagenetic albitization (Trevena and Nash, 1981). In this case, the material could also be derived from a volcanic source. Two ($An_{0.7}Or_{5.8}Ab_{93.5}$ and $An_{4.9}Or_{6.4}Ab_{88.7}$) of the thirteen analysed plagioclase feldspars have intermediate composition between pure albite and volcanic plagioclase ($An_{64}Or_{1.5}Ab_{34.5}$ to $An_{13}Or_{11}Ab_{76}$). These two plagioclase feldspars show a chemical composition characteristic of low-temperature rhyolite. It is, therefore, not exclude that some detrital feldspar previously interpreted as plutonic or metamorphic may represent partially albitized volcanic plagioclase. This proposal corresponds to that of many other authors. Based on the abundance of volcanic rock fragments and feldspar, Johnson (1991), for instance, suggested an active magmatic arc as the exclusive source for the

south-eastern Karoo Basin detritus. Plutonic, metamorphic and low-temperature rhyolitic rocks may have all contributed to the infill of the investigated subbasin.

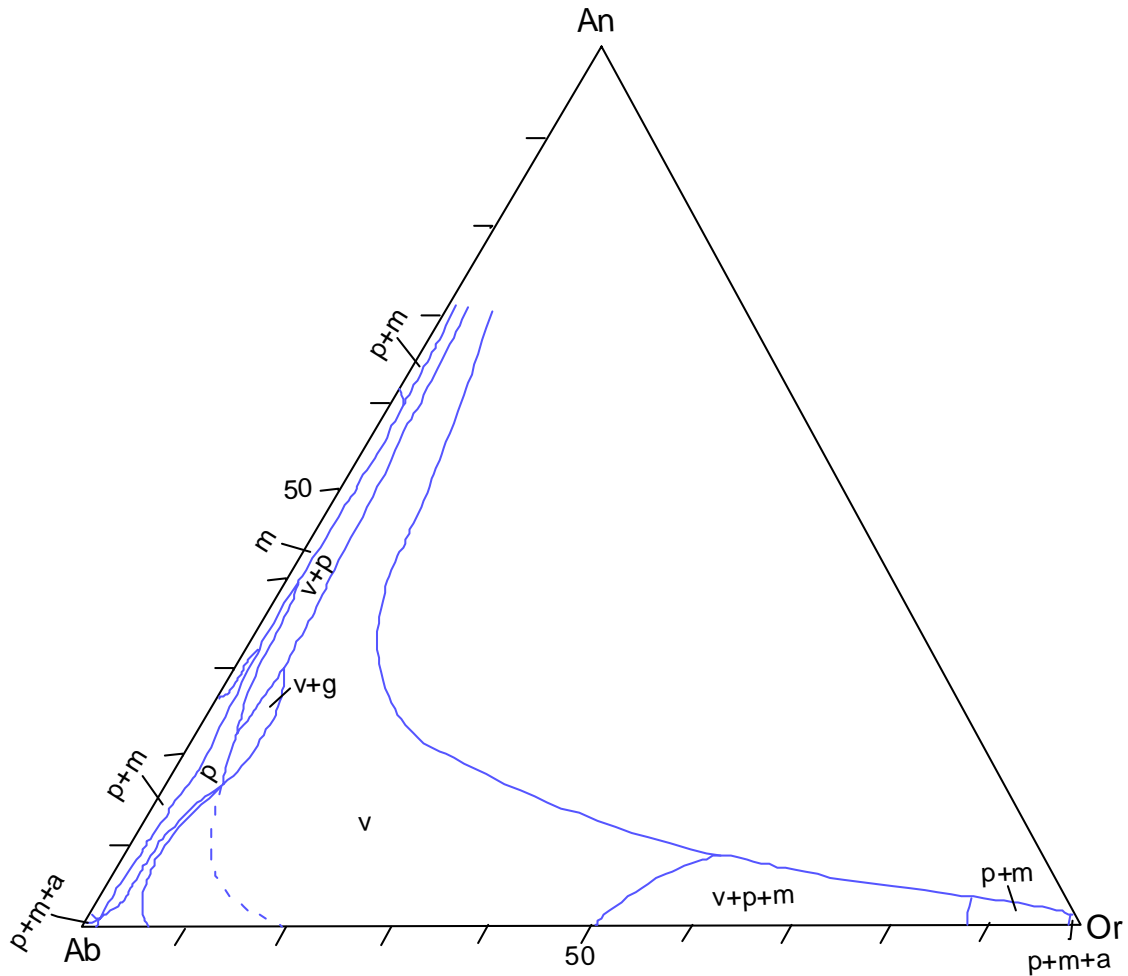


Figure 4.7 Compositional range of eight provenance groups of feldspar (v=volcanic; p=plutonic; m=metamorphic; v+g=volcanic or granophyre; v+p=volcanic or plutonic; p+m=plutonic or metamorphic; v+p+m=volcanic, plutonic or metamorphic; p+m+a=plutonic, metamorphic or authigenic). Analyses to the left of the dashed line are from low temperature rhyolites (Trevena and Nash, 1981)

Table 4.1 Chemical (Ab-An-Or) composition of plagioclase feldspars from Fans 3, 4, and 5 of the Skoorsteenberg Formation

Plagioclase	Fan 3						Fan 4			Fan 5 (NS1-1-F5)				Albite (1).	Albite (2).
	1.	2.	3.	4.	5.	6.	7.	8.	9.	10.	11.	12.	13.		
SiO ₂	67.85	68.20	68.51	67.99	66.84	67.77	65.39	69.15	69.73	70.17	69.15	68.66	67.86	67.84	67.41
TiO ₂	0.00	0.00	0.00	0.00	0.00	0.00	0.00	0.00	0.00	0.00	0.00	0.00	0.00	0.00	0.00
Al ₂ O ₃	19.39	19.31	19.29	19.67	20.58	18.92	21.33	19.58	19.78	19.69	19.53	19.19	19.11	19.55	20.50
CaO	0.22	0.00	0.14	0.00	0.14	0.00	0.97	0.24	0.00	0.00	0.00	0.00	0.16	0.00	0.81
Na ₂ O	11.33	11.40	11.49	11.12	10.54	11.32	9.69	11.13	11.88	11.63	11.59	11.46	11.06	11.17	10.97
K ₂ O	0.00	0.00	0.00	0.34	0.99	0.00	1.06	0.00	0.00	0.00	0.00	0.00	0.00	0.29	0.36
Total	98.79	98.91	99.43	99.11	99.09	98.01	98.44	100.08	101.38	101.50	100.28	99.31	98.18	98.85	100.05
Number of ions on the basis of 8 oxygens															
Si	3.00	3.00	3.00	2.99	2.95	3.01	2.91	3.01	3.00	3.01	3.01	3.01	3.01	2.99	2.95
Ti	0.00	0.00	0.00	0.00	0.00	0.00	0.00	0.00	0.00	0.00	0.00	0.00	0.00	0.00	0.00
Al	1.01	1.00	1.00	1.02	1.07	0.99	1.12	1.00	1.00	1.00	1.00	0.99	1.00	1.02	1.06
Ca	0.01	0.00	0.01	0.00	0.01	0.00	0.05	0.01	0.00	0.00	0.00	0.00	0.01	0.00	0.04
Na	0.97	0.97	0.98	0.95	0.90	0.98	0.84	0.94	0.99	0.97	0.98	0.98	0.95	0.96	0.93
K	0.00	0.00	0.00	0.02	0.06	0.00	0.06	0.00	0.00	0.00	0.00	0.00	0.00	0.02	0.02
Total cations	4.99	4.98	4.99	4.98	4.99	4.98	4.98	4.96	4.99	4.97	4.98	4.98	4.97	4.98	5.00
Mol (%)															
An	1.1	0.0	0.7	0.0	0.7	0.0	4.9	1.2	0.0	0.0	0.0	0.0	0.8	0.0	3.8
Ab	98.9	100.0	99.3	98.1	93.5	100.0	88.7	98.8	100.0	100.0	100.0	100.0	99.2	98.3	94.1
Or	0.0	0.0	0.0	1.9	5.8	0.0	6.4	0.0	0.0	0.0	0.0	0.0	0.0	1.7	2.0

(1) Albite pegmatite, near Court House, Amelia Co., Virginia.

(2) Albite, with quartz and sphene in crevice in amphibolite, Val Devero, Italy.

(1) and (2) are from Deer et al. (1966).

A notable constituent of the investigated sandstones is detrital mica. Like, quartz, feldspar and rock fragments, micas infer the provenance of sandstones (Pettijohn et al., 1987). Micas are derived from schists and gneisses, from plutonic igneous rocks, and from volcanic sources (Fig. 4.7; Lewis, 1984). Mica flakes are preferentially orientated parallel to one another and concentrated in a particular level to form a bedding plane, especially in those sandstones that show advanced diagenesis. Both biotite and muscovite are present. Abundant mica generally suggests a metamorphic provenance for the sand and also a likely proximity to the source (Pettijohn et al., 1987).

Diagenetic minerals identified in this study include illite, calcite and chlorite. Figure 4.8 shows a typical example of the Tanqua fine-grained sandstones, showing abundant biotite, advanced diagenesis and very low grade metamorphism. The observation that the lithofacies in the Tanqua depocentre are highly compacted and show no porosity except for occasional fracturing (Geel et al., in press) is logical since these units are rich in unstable minerals susceptible to diagenesis. Dickinson and Suczek (1979) demonstrated that sandstones of contrasting detrital compositions respond differently to diagenesis and therefore show different trends of porosity reduction with depth of burial. The authors studying the relationship between plate tectonics and various sandstone compositions (quartzose sandstones of the Gulf Coast, arkosic sandstones in California) stated that a reduction of porosity from an initial value of 35 to 40 % to a final value of 10 to 15 % could be expected at burial depths of about 6 to 7 km or more for quartz-rich sands, perhaps 5 km for feldspar-rich arkosic sands, and only 2 to 4 km or less for lithic-rich sandstones. Therefore, the Tanqua and Laingsburg submarine fan sandstone units do not form particularly good hydrocarbon reservoirs because of their low porosity.

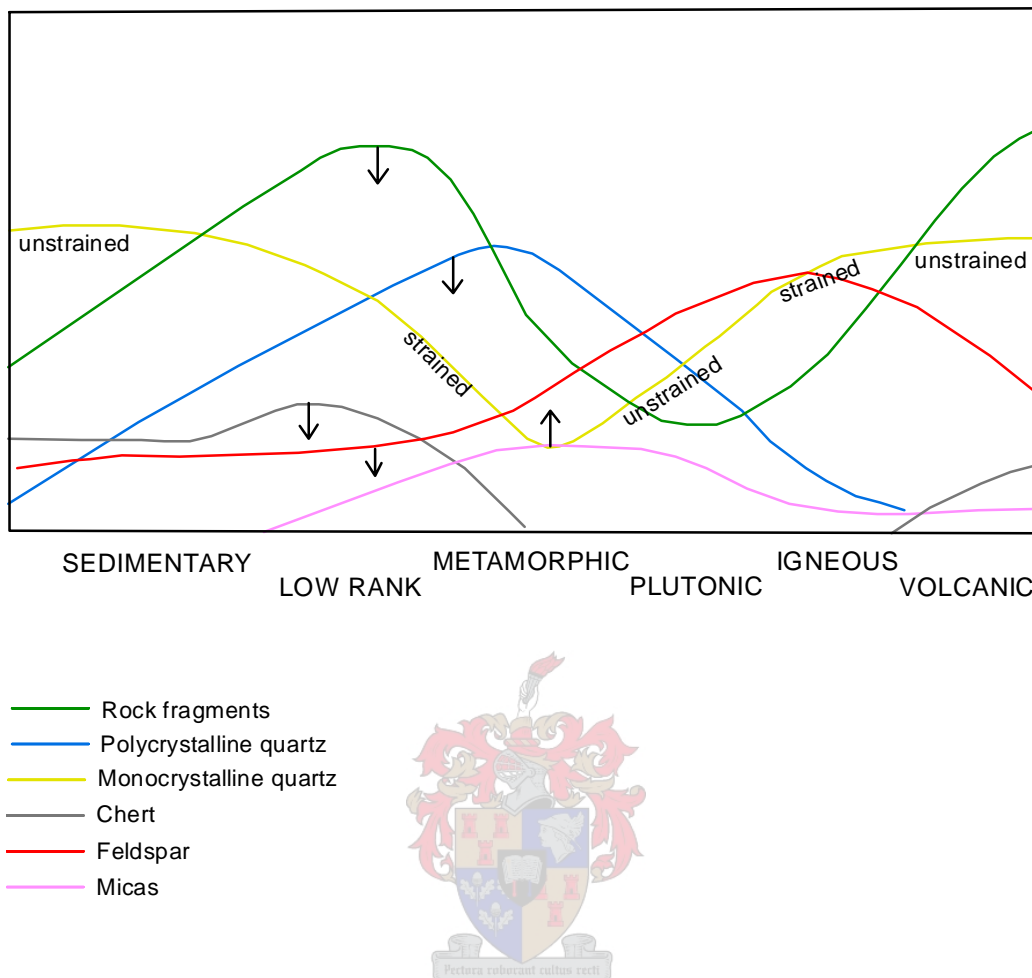
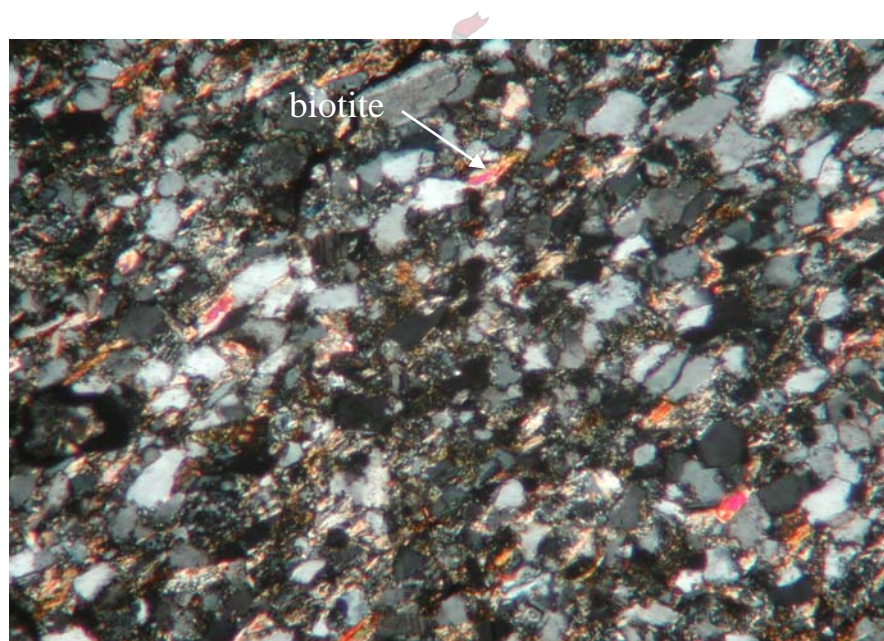
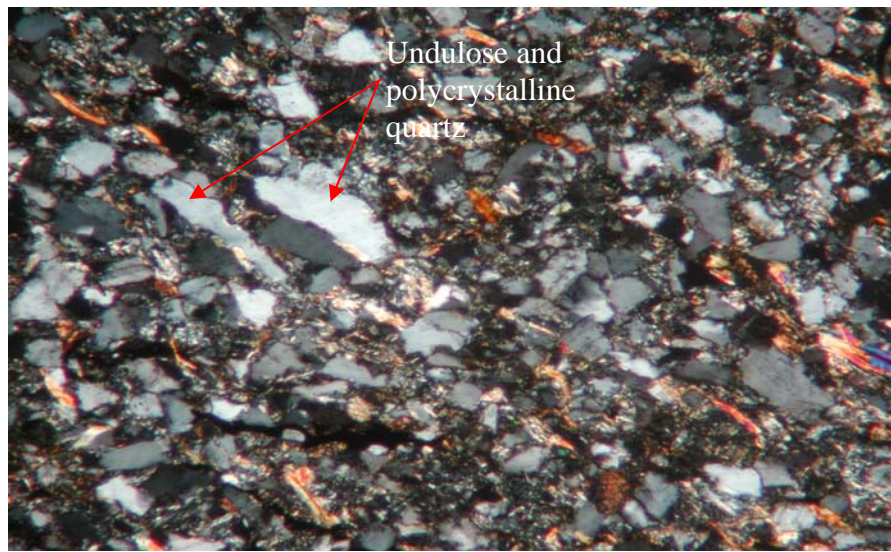


Figure 4.7 Expected abundance of sand size detritus as a function of provenance. Arrows show whether constituent increases or decreases with weathering (Lewis, 1984)



50x magnification

Figure 4.9 Tanqua Karoo fine-grained micaceous sandstones. Crystals are flattened and elongated parallel to bedding. Sandstones are grain-supported with clay and sericite matrix. Note the angularity of the grains and advanced diagenesis.

4.3 Climate, relief and transport history

Mineralogical analyses by petrographic microscope allow discussions and conclusions on the climate, relief and transport history of the Slope, Laingsburg and Skoorsteenberg Fans 3, 4 and 5 sandstones.

Climate, through its influence on weathering processes, can have an effect on the composition of sandstones and thus on provenance interpretation. There is a strong relationship between tectonism, mineralogy and source rock environment. Folk (1980) has used the roundness and average degree of alteration of feldspar to determine the relief and climate of the source area.

According to Folk (1980), feldspar, the essential mineral of arkose, is relatively easily decomposed by chemical weathering. Thus, special conditions are required for the mineral to be abundant in a sediment. Either (1) climatic conditions were too dry (or too cold) to allow much weathering, and the feldspar remained very well-preserved, or (2) uplift and erosion of the source area were so rapid that sufficient time was not available for weathering to be completed. Type (1) is the climatic arkose, because it owes its high feldspar content to a dry or cool climate; type (2) is the tectonic arkose, because it owes its feldspathic constituents to a rapid tectonic uplift. A third type, the volcanic plagioclase-rich arkose, owes its feldspar content to volcanic activity, again a case of rapid deposition short-circuiting weathering.

Limited breakdown of feldspar and the angularity of grains observed in this study are believed to result from the competing influence of rapid tectonic uplift during subduction of the paleo-Pacific plate under the southern edge of Gondwana and associated volcanic activity as indicated by the predominance of albite in the feldspar group, as well as the cold climate that prevailed shortly after the Dwyka ice age.

The Tanqua and Slope sandstones have been identified in this study as mineralogically and texturally immature, reflecting high feldspar and rock fragment content (Fig 4.1; King et al., 2004 and Fig. 4.2; Johnson, 1991), as well as the predominance of angular grains. The high content of unstable rock fragments and the moderately high albitic content of the studied sandstones suggest that they were derived from rugged and high-relief source areas. Detritus was stripped rapidly from elevated areas before weathering processes could destroy unstable clasts and other framework grains (Folk, 1980; Boggs, 1992).

Highly texturally and mineralogically immature sedimentary rock is likely to have formed close to its site of deposition (i.e., limited transport). According to Lewis (1984), deposits from turbidite currents tend to be poorly to moderately sorted and contain abundant matrix because of rapid sedimentation under low energy conditions. Feldspars have smaller mechanical and chemical stability compared to quartz. Therefore, they are destroyed faster than quartz, and their abundance is reduced considerably during successive sedimentation cycles. The observation that feldspars are angular, quite fresh and of similar average grain size (some even larger) as the quartz grains suggests that the Laingsburg and Tanqua Karoo subbasins were dominantly filled by first-cycle materials as previously suggested by King et al. (2004).

In general, it can be noted from this investigation that the Laingsburg, Tanqua and Slope sandstones are moderately to well sorted, with the majority of grains being angular, which according to Scott et al. (2000) indicates shorter overall weathering time. Abundance of feldspars and rock fragments together with the angularity of grains observed here exclude the possibility of the sedimentary Cape Supergroup in the Cape Fold Belt being the main source of the Laingsburg, Skoorsteen and Slope immature sandstones. Sandstones of sedimentary origin are expected to be texturally and mineralogically mature as a result of recycling and breakdown of unstable minerals. Such sandstones are usually

quartz-rich and well sorted with the majority of grains being moderately to very well rounded.

From a quartz-feldspar-rock fragments (QmFLt) plot (Fig. 4 1), King et al. (2004) have suggested the North Patagonian Massif in South America as the most likely source of the Slope, Skoorsteenberg and Laingsburg submarine fan sandstones of the Karoo Supergroup.

However, Johnson (1991), also using a QmFLt diagram (Fig 4.2), argued that the Karoo sandstones, including the ultralithofeldspathic Waterford Formation sandstones (equivalent of the Slope sandstones of this study in the Laingsburg depocentre), originated from a transitional arc.

There are therefore differences in opinion with regard to the main source of the Tanqua and Laingsburg subbasins detritus. King et al. (2004) pointed out the anomaly existing between the North Patagonian Massif located some 600 km away from the depocentre and the angularity of grains. As argued by the investigators, sandstones derived from such a distal source will be well sorted and show narrow grain size range but will not dominantly consist of angular grains and abundant unstable minerals. In addition, the fine-grained nature of the studied sandstones is not consistent with a distal plutonic source rock, especially if this latter is rich in unstable minerals.

Investigated sandstones were certainly derived from a mixed source having metamorphic, granitic and magmatic arc affinity, as indicated by quartz and feldspar grains of metamorphic/plutonic and volcanic origin identified in this study. Sediments are dominantly first cycle and have travelled over very short distance.

The chemical composition analysis of detrital feldspar and a simple petrographic observation done during this investigation does not allow a precise determination

of the relative contribution of each source. The provenance of investigated sandstones will therefore be reconsidered later in this study by using other analytical approaches of provenance determination such as heavy mineral and whole-rock chemistry, morphology and trace element chemistry of detrital zircons combined with U-Th-Pb radiometric zircon ages, in that order.

4.4 Heavy minerals chemistry

4.4.1 Introduction

Heavy minerals are arbitrarily designated as minerals with specific gravity (s.g) greater than 2.85; they sink rather than float in a dense liquid such as bromoform (s.g = 2.89), tetrabromoethane (s.g = 2.966) or methylene iodide (s.g = 3.335) (Lewis, 1984). Despite their lesser volumetric significance in sediments (approximately 1% of the sand-size fraction), heavy minerals are very important in determining the provenance of sediments and factors that operate during the sedimentation cycle, including weathering, transport, deposition and diagenesis (Lewis, 1984; Morton and Hallsworth, 1999).

Mineral separates were prepared from sandstone samples from Fans 3, 4 and 5 of the Skoorsteenberg Formation and from sandstone samples from Fans A and F of the Laingsburg Formation. Heavy minerals were separated from light minerals by the method of density separation using bromoform (Appendix C).

The heavy mineral suite after separation consists of zircon, garnet, pyrite, sphene, apatite, Al-silicate (sillimanite), allanite, chromite, rutile, sphalerite, magnetite and ilmenite.

Trace element concentrations in detrital zircons were used to determine the source rock types of both the Skoorsteenberg and Laingsburg deepwater fans

whereas the chemical properties of Skoorsteenberg garnet and sphene were used to identify the origin of materials that filled the Tanqua subbasin only.

Apart from zircons, no other heavy mineral of the Laingsburg subbasin have been probed during this investigation. Scott et al. (2000) have done extensive work on the chemistry of biotite, garnet and tourmaline in sandstones from the Skoorsteenberg, Vischkuil and Laingsburg Formations, but investigation of the source rock lithology of the upper Ecca Group sediments based on zircon trace element chemistry has not been done before. Therefore, the study deliberately targeted zircons though it also included less stable accessory mineral phases such as garnets and sphenes. Furthermore, the chemical and mechanical durability of zircon suggests that the mineral can survive multiple sedimentation cycles and preserves the igneous signature and age of the source magma (Belousova et al., 2002; Hoskin and Schaltegger, 2003). Thus, the mineral is considered the most reliable provenance indicator for sediments.

Since variations in garnet composition are dependant on paragenesis, the mineral has proved very useful in identifying and characterizing different provenances (Morton, 1985). The chemical composition of sphene can also be used to decipher the lithology of their source rocks (Fleischer and Altsculer, 1969; Deer et al., 1982). Unlike the heavy mineral ratio method commonly used in provenance studies, the microprobe analysis of single heavy mineral avoids, or at least minimizes the problem caused by diagenetic and hydraulic processes (Morton, 1991).

Trace element concentrations of zircons will not be discussed in this chapter, and will be part of Chapter 6 that includes the morphological characteristics, trace element abundances and radiometric ages obtained from detrital zircons of the Tanqua and Laingsburg sandstones.

4.4.2 Sphene chemistry

Sphene is chemically unstable and usually dissolves at an early stage of diagenesis (Mange and Maurer, 1992); it is, therefore, rarely found as detrital grains in sandstones. Possibly for this reason, the chemical composition of sphene has received very little attention in provenance studies. However, the unstableness of sphene may prove to be an advantage insofar as its occurrence in sediments may suggest that their source is monocyclic in origin (Asiedu et al., 2000). The possibility that the subbasin was filled by first cycle materials has been suggested earlier in this chapter.

Sphene is a widespread accessory mineral of undersaturated and intermediate plutonic rocks (Mange and Maurer, 1992). Deer et al. (1982) have demonstrated that there is a link between the chemical composition of sphene and the type of igneous rocks in which the mineral occurs. Sphenes from acidic and intermediate igneous rocks show appreciable Fe, Al and rare earth element contents whereas those from basic to ultrabasic rocks are closest to the theoretical CaTiSiO_2 composition. In metamorphic rocks, sphene occurs predominantly in gneisses and schists rich in ferromagnesian minerals. Sphene with higher Al content (up to 10 wt % Al_2O_3) is typical of metamorphic and skarn sources (Asiedu et al., 2000).

The microprobe analysis results on some sphenes are shown in Table 4.2. The detrital sphene from the Skoorsteenberg fans of the Tanqua Karoo have a chemistry that equates them with an acid to intermediate igneous source based on their low concentration of Al together with an appreciable concentration of Fe.

Table 4.2 Microprobe analyses of detrital sphenes from the Skoorsteenbergs Fans 3 and 4 of the Tanqua Karoo subbasin.

Sample	Fan 3		Fan 4		(1) Sphene	(2) Sphene
	NB4-F3-S1	NB4-F3-S2	NB4-2-F4-S3			
SiO ₂	32.07	32.56	29.67		30.44	29.32
TiO ₂	36.53	36.08	39.92		39.66	35.26
ZrO ₂					0.11	tr
Nb ₂ O ₅					0.34	
Ta ₂ O ₅					0.01	
V ₂ O ₅					0.10	
R.E.					0.37	4.51
Al ₂ O ₃	1.06	1.30	2.96		0.00	1.02
Fe ₂ O ₃ ^T					0.00	1.34
FeO	2.32	2.01	0.64		0.14	1.05
MnO	0.00	0.35	0.03		0.05	0.03
MgO	0.00	0.02	0.26		0.00	0.36
CaO	28.46	27.67	26.27		27.20	25.72
BaO					0.005	0.04
Na ₂ O					0.37	0.14
K ₂ O					0.00	0.07
F					0.61	
H ₂ O ⁺					0.56	0.64
H ₂ O ⁻					0.08	0.18
Total	100.44	99.99	99.75		100.05	99.68

(1) Light reddish brown sphene, nepheline syenite, Kola Peninsula, U.S.S.R. Rare earth (R.E.) elements are La₂O₃ 0.04, Ce₂O₃ 0.12, Pr₂O₃ 0.02, Nd₂O₃ 0.08, Sm₂O₃ 0.02, Gd₂O₃ 0.02, Dy₂O₃ <0.01, Er₂O₃ <0.01, Y₂O₃ 0.05.

(2) Black sphene, pegmatite, Quoscescer, N.E. of Harar, Abyssinia. Rare earth (R.E.) elements include Ce₂O₃ 2.98, Y₂O₃ 1.53.

(1) and (2) are from Deer et al. (1966).

4.4.3 Garnet chemistry

Garnet group minerals are generally interpreted to indicate metamorphic source rocks (Mange and Maurer, 1991). Garnet may also occur in magmatic rocks (Deer et al. 1992). Garnets belong to the solid solution series between pyrope (Mg end-member), almandine (Fe^{2+} end-member), spessartine (Mn end-member) and grossular (Ca end-member). Because of this chemical variability, the chemistry of garnets has proved to be very useful in provenance studies (Morton, 1985, 1987).

Detrital garnets from the Tanqua Karoo subbasin analyzed in this study are rich in FeO (14.48-31.83 wt %, average 27.11 wt %), poor in Cr_2O_3 (less than 0.35 wt %) and TiO_2 (less than 1 wt %). The MgO content ranges from 0.01 to 8.79 wt % with an average of 5.53 weight percent. MnO content is generally low (less than 1 wt %). CaO content is also generally low but can reach up to 24.4 wt %, but is mostly below 5 wt % (Table 4.3).

Analyzed garnets are therefore dominated by almandine-pyrope (up to 35 mol % pyrope) with subsidiary grossular. Spessartine is generally absent.

Almandine garnets are typical of garnetiferous schists and gneisses although they may also occur in some calc-alkali granites and rhyolites (Takeuchi, 1994). Generally, Fe-rich garnet is common in Barrow-type metasediments (e.g. garnet-mica schists). Garnet with higher contents (20 to 30 %) of the Mg end-member and the Ca end-member may originate from amphibolite, blueschist-associated eclogite, or granulite (von Eynatten and Gaupp, 1999). Takeuchi (1994) has shown that almandine garnets with pyrope content from 10 to 40 mol % occur in epidote-amphibolite to granulite facies gneisses.

The predominance of almandine-pyrope garnets in the garnet population indicates a contribution from high-grade metamorphic sources. The present

results confirm the conclusion of Scott et al. (2000) who argued that the Skoorsteenberg and Laingsburg detritus did not originate from the low-grade metasedimentary Cape Fold Belt as proposed by various investigators (Lock, 1980; Kingsley, 1981; Hälbich, 1983; Cole, 1992; Veevers et al., 1994; Adelman and Fiedler, 1998). No available data indeed support the presence of a high-grade orogenic core within the Cape Fold Belt. The highest P-T values obtained in the southern margin of the metasedimentary belt is 3-4 kb and approximately 350°C (Hälbich and Swart, 1983).

The predominance of both first cycle detritus as previously discussed and high-grade metamorphic garnet grains in the garnet population strongly suggest that the main provenance of the Tanqua and Laingsburg deepwater fans is not the metasedimentary Cape Fold Belt.

Almandine-pyrope garnets indicative of a high-grade metamorphic terrane contribution identified in this investigation are believed to have been supplied by the Mesoproterozoic Namaqua-Natal Metamorphic Province basement. The sample contains one garnet with a high Ca content, possibly derived from metamorphosed carbonates.

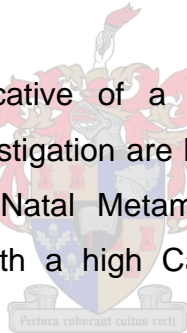


Table 4.3 Representative analyses of detrital garnets from the Tanqua Fans 3 and 4.

sample	NB4-9-F3	NB3-2-F4-G1	NB3-2-F4-G2	NB3-2-F4-G3	NB3-2-F4-G4	NB3-2-F4-G5	NB3-2-F4-G7	(1) garnet	(2) garnet	(3) garnet	(4) garnet
SiO ₂	38.42	38.38	38.67	38.91	38.67	37.85	38.94	38.03	38.69	41.52	35.84
TiO ₂	0.00	0.00	0.00	0.00	0.13	0.03	0.35		0.55	tr	0.03
Al ₂ O ₃	22.68	23.31	22.23	22.78	22.19	21.85	23.32	22.05	18.17	23.01	20.83
Cr ₂ O ₃	0.00	0.00	0.01	0.00	0.00	0.31	0.19			0.22	
Fe ₂ O ₃								0.88	5.70	1.22	0.65
FeO	31.83	14.48	29.10	29.04	29.62	30.41	25.32	29.17	3.78	12.86	1.78
MnO	0.20	0.06	0.08	0.07	0.59	0.11	0.10	1.57	0.64	0.33	33.37
MgO	6.45	0.00	8.00	7.97	2.99	4.54	8.79	6.49	0.76	16.64	2.48
CaO	1.01	24.42	2.10	1.61	5.84	4.90	3.00	1.80	31.76	4.71	5.00
H ₂ O ⁺									0.13		
H ₂ O ⁻									0.06	0.16	
Total	100.59	100.65	100.19	100.38	100.03	100.00	100.01	99.99	100.24	100.67	99.98
Number of ions on the basis of 12 oxygens											
Si	2.99	2.95	2.99	2.99	3.04	2.98	2.97				
Ti	0.00	0.00	0.00	0.00	0.01	0.00	0.02				
Al	2.08	2.11	2.03	2.07	2.06	2.03	2.10				
Cr	0.00	0.00	0.00	0.00	0.00	0.02	0.01				
Fe	2.07	0.93	1.88	1.87	1.95	2.00	1.61				
Mn	0.01	0.00	0.00	0.00	0.03	0.01	0.01				
Mg	0.75	0.00	0.92	0.91	0.35	0.53	1.00				
Ca	0.08	2.01	0.17	0.13	0.49	0.41	0.25				
Total cations	7.97	8.00	8.00	7.98	7.92	7.99	7.96				
End-member composition (%)											
Mg (pyrope)	26	00	31	31	12	18	35				
Fe (almandine)	71	32	63	64	69	68	56				
Mn (spessartine)	00	00	00	00	1	00	00				
Ca (grossular)	3	68	6	5	17	14	9				

Note that for the Tanqua Karoo garnets, FeO represents the total Fe content of the minerals.

(1) Almandine, quartz-biotite gneiss, Adirondack Mts., New York. (2) Brownish red grossular, anorthite-clinozoisite-corundum-garnet schist, Sittampundi complex, Madras. (3) Pyrope, eclogite, Rodhaugen, Sandmore, Norway. (4) Golden yellow spessartine, rhodonite-spessartine-pyrrhotite rock, calc-silicate hornfels, Meldon, Devonshire. (1), (2), (3) and (4) are from Deer et al. (1966).

CHAPTER FIVE

BULK ROCK CHEMISTRY

5.1 Introduction

With the aim of investigating the history, from source to deposition, of the Tanqua Karoo deepwater sediments, a total of 39 sandstone samples were analyzed for their major and trace elements.

The geochemical investigation took into account samples from the Skoorsteenberg submarine Fan 3 (F3), Fan 4 (F4) and Fan 5 (F5), as well as the Slope sediments (SL1), representing the shoreface Waterford Formation. Samples were taken in such manner that the whole fan area from distal to proximal parts was represented. Major element geochemical data of the Laingsburg sandstones reported here and used in some of the diagrams in this chapter are from Van Lente (2004). The sandstones chosen were all fine-to very fine-grained.

Sandstone geochemistry varies systematically with the nature of the source rocks, weathering, diagenesis and metamorphism. In addition, the tectonic setting has been identified as the overall primary control on the composition of sedimentary rocks (Bhatia, 1983; Bhatia and Crook, 1986; Pettijohn et al., 1987). Various studies have shown that the chemical signature of some elements such as Mg, Cr, Ni, Co, Zr, Y, Nb, La, Sc, Th, and Ba is generally preserved in sedimentary rocks through weathering and diagenesis (McLennan et al., 1983; Van de Kamp and Leake, 1985; Cullers et al., 1988). Therefore, the geochemical investigation of the abundance of these relative immobile elements usually provides information about the source material.

5.2 Geochemical characteristics of clastic sediments

5.2.1 Chemical classification of sandstones

The major element composition of the Tanqua Karoo sandstones and the Slope sediments determined in this study are compared to the mean composition of principal sandstone classes (Pettijohn et al., 1987) and presented in Table 5.1. The quartz arenites are nearly pure SiO_2 , the Al_2O_3 coming from clay and the CaO from calcite cement. The litharenites show more Al_2O_3 , Fe-oxides, CaO and K_2O , mostly derived from argillaceous rock fragments. Greywackes have lower SiO_2 than most sandstones, more Al_2O_3 , and dominance of Na_2O over K_2O and MgO over CaO. Arkoses have high Al_2O_3 , K_2O , and Na_2O contents, predictable from the high proportion of feldspars (Pettijohn et al., 1987).

The Tanqua Karoo sedimentary rocks are rich in Al_2O_3 , Fe_2O_3 , MgO, and Na_2O . Fans 3, 4 and 5 are characterized by $\text{Na}_2\text{O}/\text{K}_2\text{O}$ equal to 1.08, 1.37 and 1.07 respectively and MgO/CaO equal to 1.25, 1.27, and 1.52 respectively. However, Slope sandstones have $\text{Na}_2\text{O}/\text{K}_2\text{O}$ equal to 0.78 and MgO/CaO equal to 1.09. $\text{Na}_2\text{O}/\text{K}_2\text{O}$ and MgO/CaO ratios greater than 1 as well as the richness in Al_2O_3 and Fe_2O_3 indicate that the Skoorsteenberg submarine fans belong to the greywacke class of sandstones as expected for most marine turbidites (Pettijohn, 1975).

Table 5.1 Mean composition of principal sandstone classes and average Laingsburg and Tanqua sandstones

W (%)	Average sandstones			Average Laingsburg sandstones		Average Skoorsteenberg sandstones			
	(Pettijohn et al., 1987)			Van Lente (2004)		This study			
	Quartz arenite	Lithic arenite	Greywacke	Arkose	Fan A to Fan F n = 8	Fan 3 n = 10	Fan 4 n = 8	Fan 5 n = 5	Slope n = 7
SiO ₂	95.4	66.1	66.7	77.1	71.43	72.36	74.7	70.94	69.74
Al ₂ O ₃	1.1	8.1	13.5	8.7	12.61	12.52	11.66	13.18	12.99
(Fe ₂ O ₃) _T	0.4	3.8	1.6	1.5	3.43	3.76	3.24	3.86	3.91
FeO	0.2	1.4	3.5	0.7					
MgO	0.1	2.4	2.1	0.5	1.62	1.88	1.47	2.04	1.97
CaO	1.6	6.2	2.5	2.7	2.25	1.15	1.15	1.34	1.8
Na ₂ O	0.1	0.9	2.9	1.5	2.46	2.74	2.67	2.84	2.35
K ₂ O	0.2	1.3	2	2.8	2.34	2.53	1.95	2.64	3.01
H ₂ O ⁺	0.3	3.6	2.4	0.9					
H ₂ O ⁻		0.7	0.6						
TiO ₂	0.2	0.3	0.6	0.3	0.55	0.56	0.5	0.61	0.56
P ₂ O ₅		0.1	0.2	0.1	0.15	0.17	0.13	0.2	0.17
MnO		0.1	0.1	0.2	0.09	0.08	0.07	0.09	0.08
MgO/CaO	0.06	0.38	0.84	0.18	0.72	1.25	1.27	1.52	1.09
Na ₂ O/K ₂ O	0.5	0.69	1.45	0.53	1.05	1.08	1.37	1.07	0.78
CO ₂	1.1	5	1.2	3					
SO ₃			0.3						
S			0.1						
C			0.1						
LOI					1.43	1.89	1.91	1.93	2.03
Total	100.7	100	100.4	100	98.38	99.68	99.54	99.68	98.68

(Fe₂O₃)_T is the total iron.

It is possible to recognize a number of varieties of greywacke. Those rich in rock fragments have been called lithic greywackes; those rich in feldspar are the feldspathic greywackes. The Tanqua submarine sandstones, which are alkali metal-rich immature sandstones characterized by $\text{Na}_2\text{O} > \text{K}_2\text{O}$, may be classified as feldspathic greywackes, whereas the Slope sediments, characterized by high alkali ($\text{Na}_2\text{O} + \text{K}_2\text{O}$) content, low $\text{SiO}_2/\text{Al}_2\text{O}_3$ and $\text{Na}_2\text{O} < \text{K}_2\text{O}$, are closer to lithic greywackes (Pettijohn et al., 1987).

Crook (1974) subdivided greywackes on the basis of SiO_2 content and the relative $\text{K}_2\text{O}/\text{Na}_2\text{O}$ ratio into three classes and assigned each to a plate tectonic setting and provenance. The quartz-poor variety, characterized by low SiO_2 content is typical of volcanic provenance. The quartz-rich (average 89 % SiO_2 , $\text{K}_2\text{O}/\text{Na}_2\text{O} > 1$) indicates a sedimentary provenance and the quartz-intermediate (average 68-74 % SiO_2 , $\text{K}_2\text{O}/\text{Na}_2\text{O} < 1$) being of mixed provenance. Crook (1974) attributed the quartz-poor types to the island arc environment, the quartz-rich class to tectonically inactive continental margins, and the intermediate type to tectonically active margins of continents or microcontinents.

The majority of the Tanqua sandstones have a SiO_2 range of 66.28-76.04 and $\text{K}_2\text{O}/\text{Na}_2\text{O}$ less than 1, whereas the majority of the Slope sediments have $\text{K}_2\text{O}/\text{Na}_2\text{O}$ greater than 1, and a SiO_2 content which varies between 66.75 and 73.42 (Appendix B). Both the Slope and the Tanqua Karoo submarine sandstones may be classified as quartz-intermediate (Figure 5.1) and are therefore derived from a mixed source in an active continental margin region.

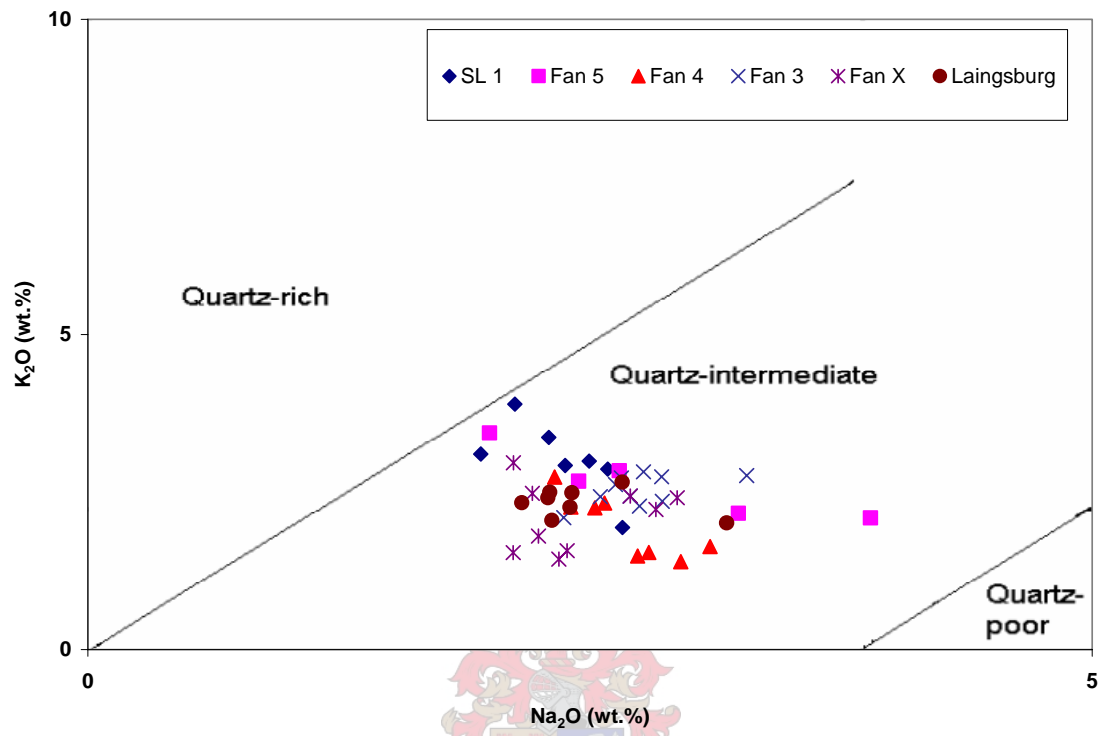


Figure 5.1 Analysis of alkali content of the Slope (SL1), Laingsburg and Skoorsteenberg (Fans 3, 4 and 5) sandstones based on major element geochemistry (Crook, 1974). Note that the Laingsburg data are from Van Lente (2004).

5.2.2 Major element concentrations

Variations in the major element geochemistry of the studied sedimentary rocks are shown on Harker diagrams (Figs. 5.2a and 5.2b).

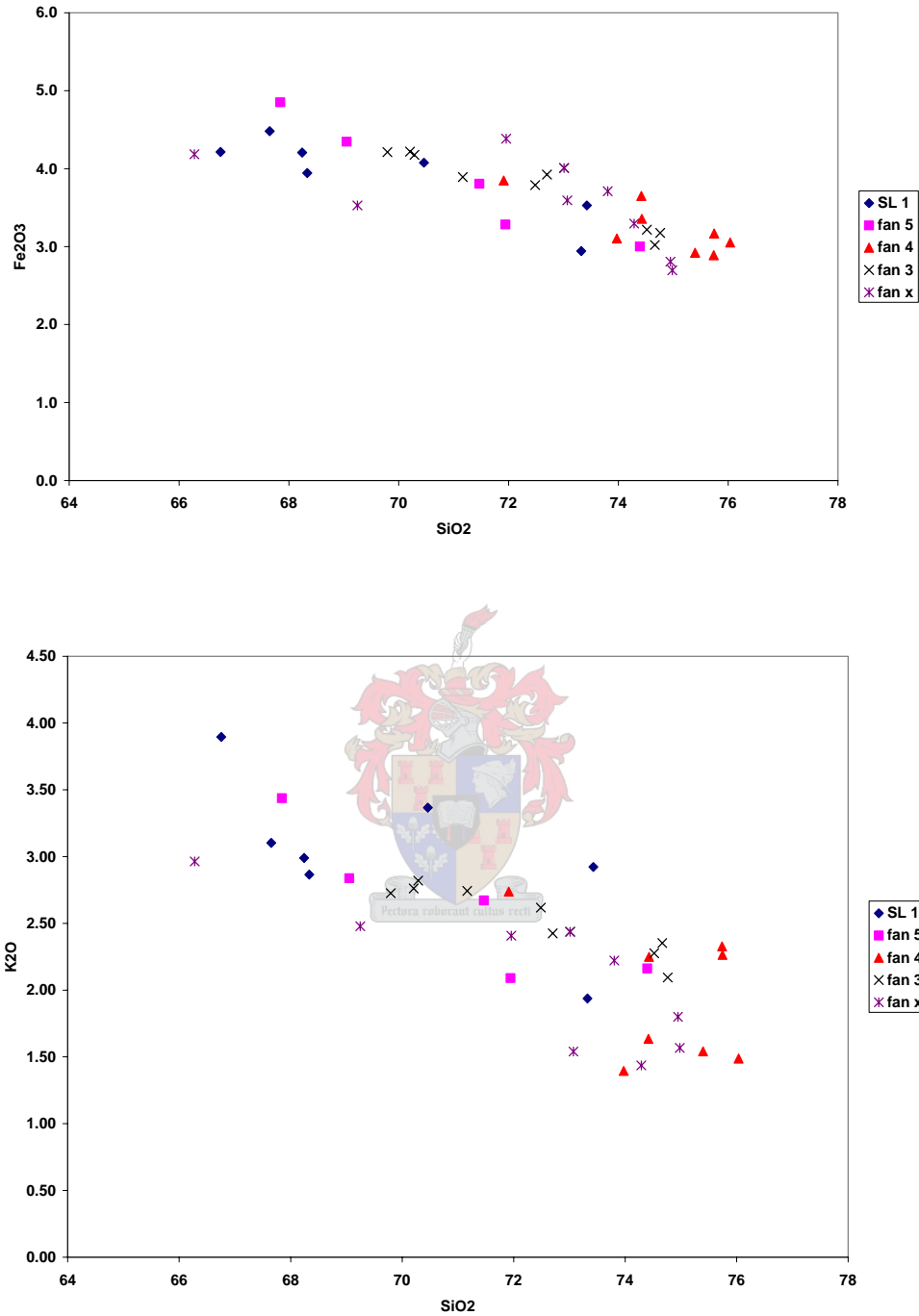


Figure 5.2a Harker-type major element percentage variation diagrams for Tanqua Karoo (Fans 3, 4 and 5) and Slope (SL1) sandstones. Note the negative correlation of SiO₂ and remaining major oxides. Fan 4 sandstones are certainly more mature than sandstones from other fans, therefore show higher SiO₂ content and lower remaining major element abundances. (SL=slope sandstone, Fan x = Tanqua fan sandstone samples with interstitial calcite cement).

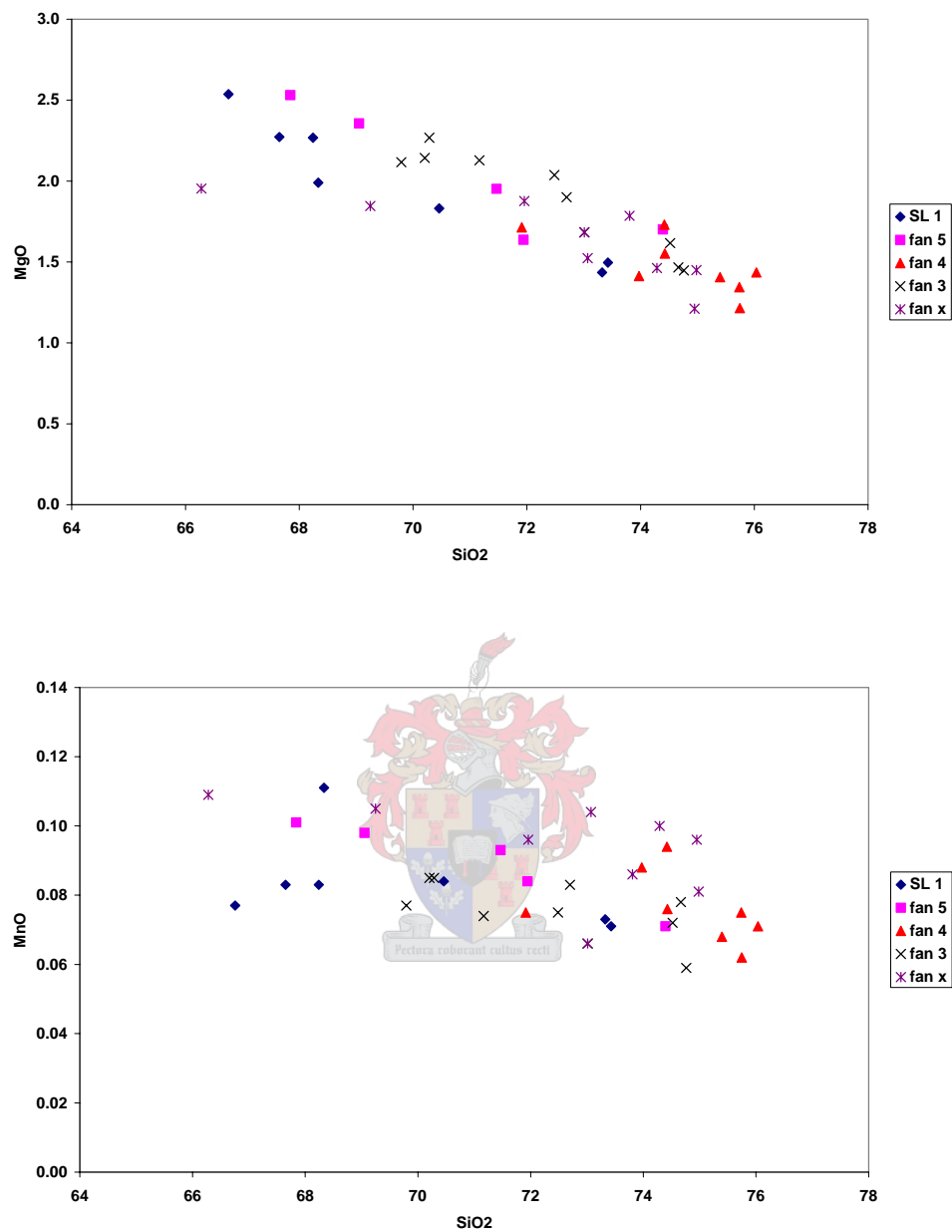


Figure 5.2a (continued) Harker-type major element percentage variation diagrams for Tanqua Karoo and Slope sandstones

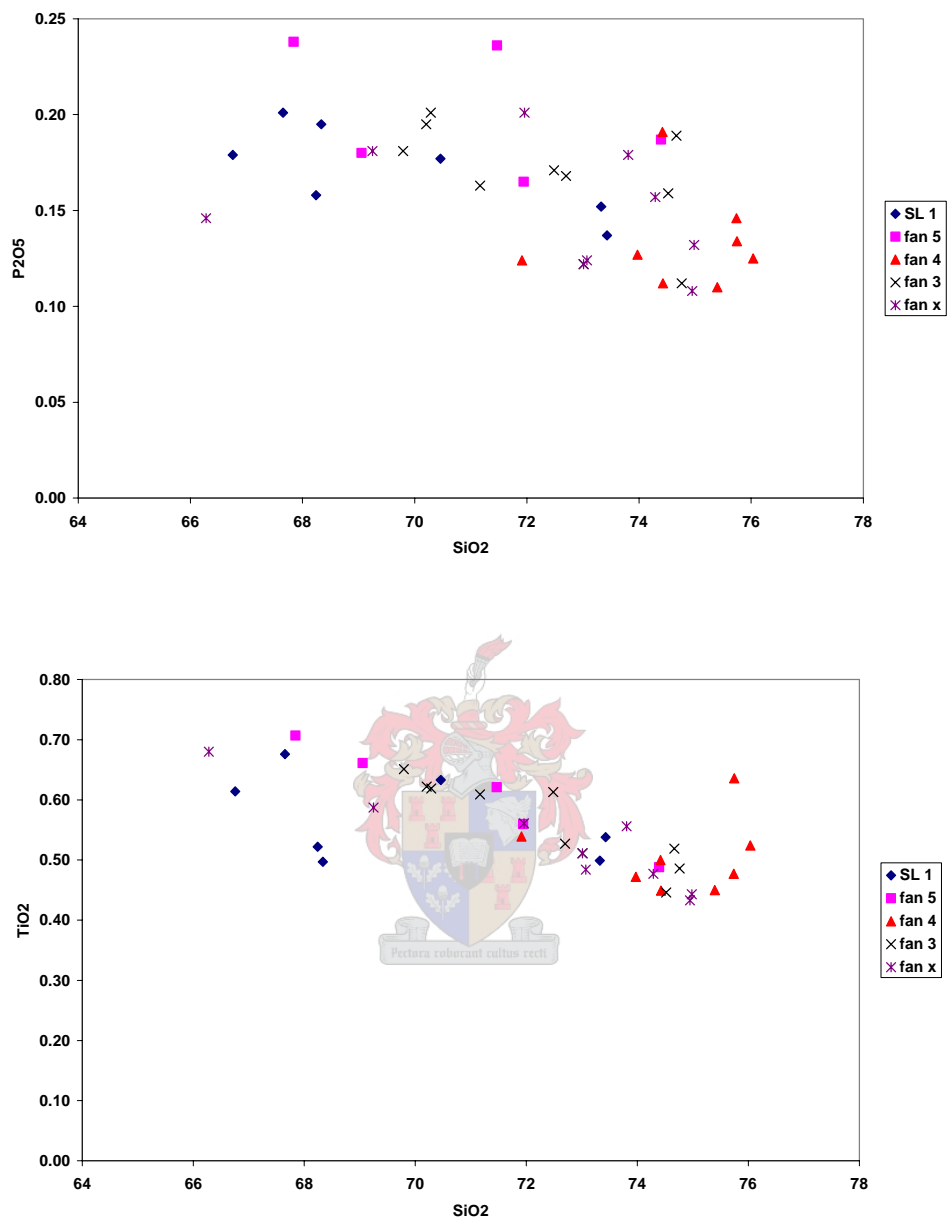


Figure 5.2a (continued) Harker-type major element percentage variation diagrams for Tanqua Karoo and Slope sandstones

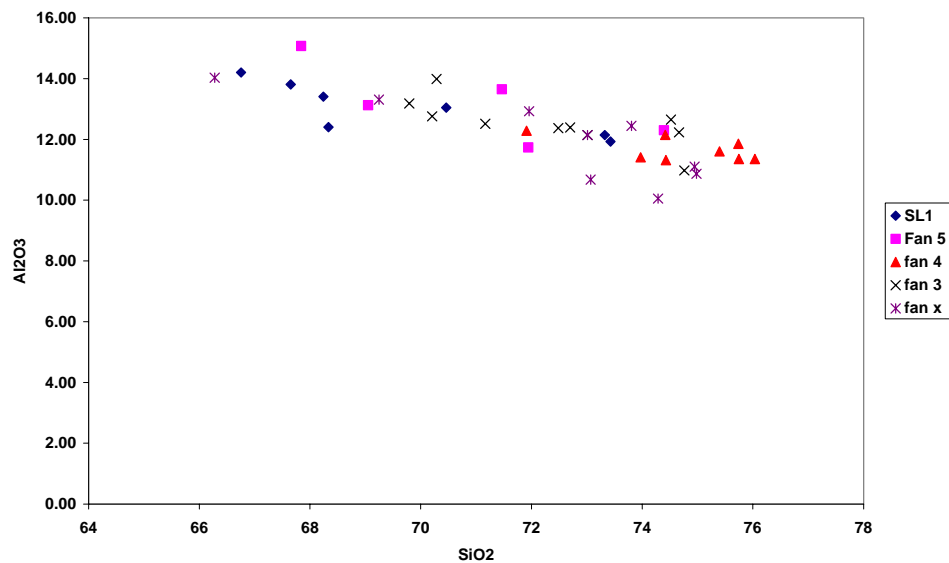
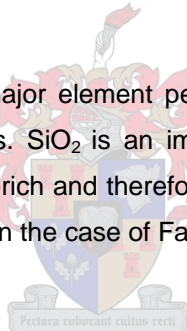


Figure 5.2a (continued) Harker-type major element percentage variation diagrams for Tanqua Karoo and Slope sandstones. Al₂O₃ vs. SiO₂ is an important maturity index. Note that Slope sediments are dominantly clay-to shale-rich and therefore plot at relatively higher Al₂O₃ for lower SiO₂, with the opposite being observed in the case of Fan 4.



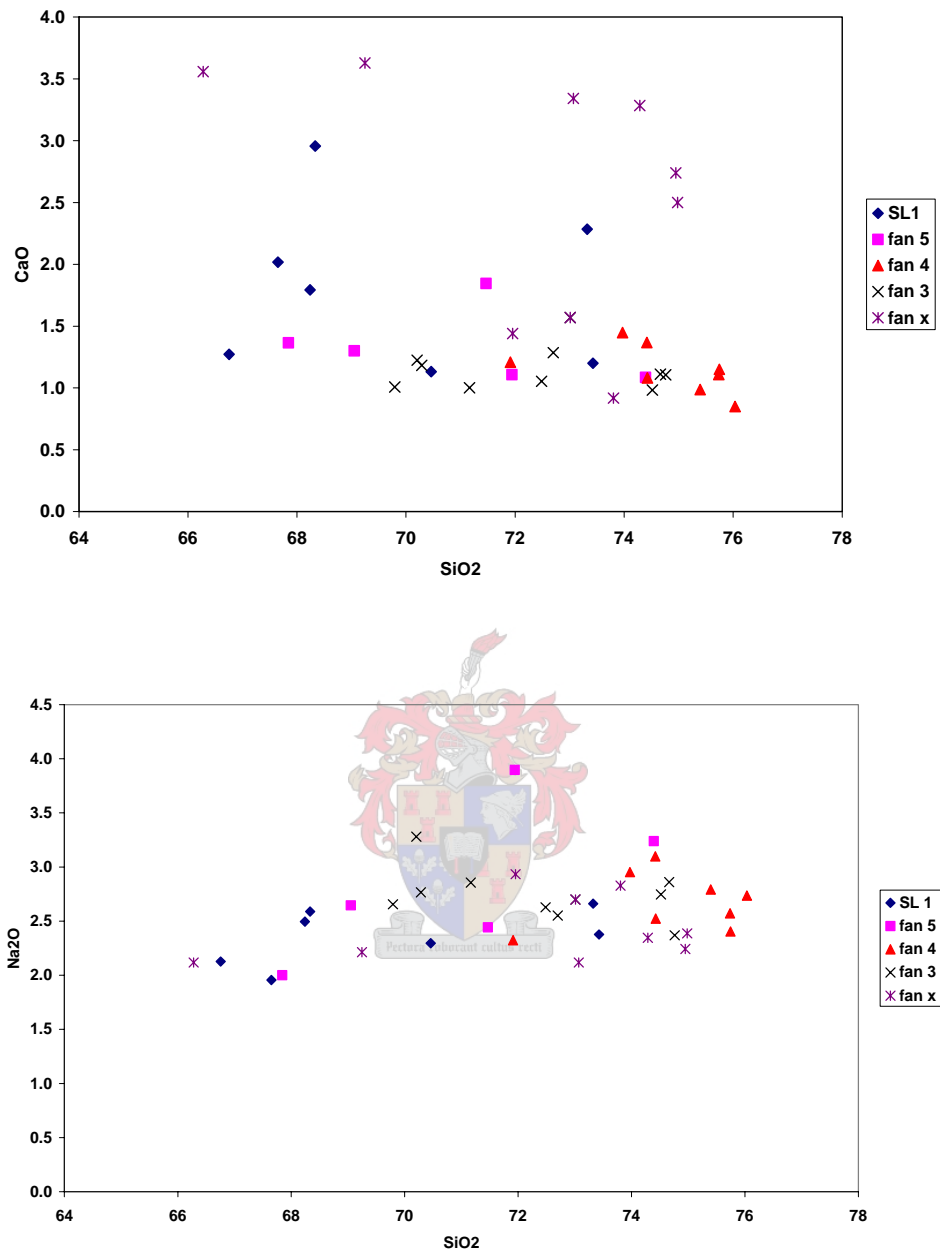


Figure 5.2b Harker-type major element percentage variation diagrams for Tanqua Karoo and Slope sandstones. Note the weak positive correlation of SiO₂ versus Na₂O. Non-correlation of SiO₂ versus CaO is presumably due to secondary carbonate veins.

Investigated sand units show homogeneous composition in terms of their major element concentrations. Standard deviations for all the major elements in the analyzed samples are relatively low (below 1) and equal to 1.92, 1.36 and 2.56 for SiO_2 for Fans 3, 4 and 5.

Fan 4 is more mature than other fans and therefore shows relatively higher SiO_2 and lower remaining major element concentrations.

There are pronounced negative correlations between SiO_2 and most of the other major oxides. Na_2O is the only major oxide which positively correlated with silica. In the case of Al_2O_3 , Fe_2O_3 , TiO_2 , K_2O , MgO , MnO and P_2O_5 (though very weak), diagrams denote both an increase in the quartz content and a decrease in the chemically unstable grains such as plagioclase and volcanic rock fragments.

It is worth noting that several samples (Fan X) with high CaO and LOI contents were excluded because they have interstitial calcite cement that can lead to errors.

Weak correlations between SiO_2 and CaO and Na_2O may be due the greater mobility of these elements during weathering, diagenesis and metamorphism. The problem of excess Na_2O in greywackes is a general one (Pettijohn, 1975; Pettijohn et al., 1987) and includes samples in this study that have high bulk $\text{Na}_2\text{O}/\text{K}_2\text{O}$ (Appendix B). During chemical weathering, K is preferably incorporated in clay minerals, whereas Na is leached.

Various explanations have been offered to account for the high Na_2O content of the greywackes. Engel and Engel (1953) suggested that the high Na_2O content is due to the high content of albitic feldspar in the source rock. Also, it may be due to post-depositional albitization (Turner and Verhoogen, 1960), probably as a result of interaction with (1) Na^+ ions in sea water or (2) interstitial water with an

originally Ca-plagioclase (Nesbitt and Young, 1989; Feng and Kerrich, 1990; Holail and Moghazi, 1998).

The textural and chemical immaturity of the Slope and Skoorsteenberg sandstones indicate that their bulk chemistry, including Na-enrichment, are inherited from the source areas. The excess of Na_2O is definitely due to the presence of abundant albite in the source rocks.

5.3 Weathering and paleo-environment conditions during deposition.

5.3.1 Sediments maturity

Sediment maturity may be measured in terms of the SiO_2 content and the $\text{SiO}_2/\text{Al}_2\text{O}_3$ ratio (Potter, 1978), which reflect the relative abundance of quartz, feldspar and clay. Feldspar content can also be determined from whole-rock chemistry using the alkali content ($\text{Na}_2\text{O} + \text{K}_2\text{O}$). Using the index of chemical maturity $\text{SiO}_2/\text{Al}_2\text{O}_3$ and the $\text{Na}_2\text{O}/\text{K}_2\text{O}$ ratio, Pettijohn et al. (1972) proposed a classification for terrigenous sands based upon a plot of $\log(\text{Na}_2\text{O}/\text{K}_2\text{O})$ versus $\log(\text{SiO}_2/\text{Al}_2\text{O}_3)$. This classification diagram, which has been redrawn by Herron (1988), shows the relationship between elemental composition, mineralogy and rock type. These may be applied to Tanqua Karoo and Slope sediments since there has been no major loss of K and Na during diagenesis.

Fan 4 shows markedly higher $\text{SiO}_2/\text{Al}_2\text{O}_3$ ratios and consequently lower $\text{Na}_2\text{O} + \text{K}_2\text{O}$ contents than other fans, reflecting its more quartz-rich, clay-poor nature. On average, Slope sediments have a $\text{SiO}_2/\text{Al}_2\text{O}_3$ ratio equal to 5.37 and $\text{Na}_2\text{O} + \text{K}_2\text{O}$ equal to 5.36 wt % (Table 5.1), indicating also its immature nature because typical greywackes have $\text{SiO}_2/\text{Al}_2\text{O}_3$ equal to 5 and $\text{Na}_2\text{O} + \text{K}_2\text{O}$ equal to 4.9 (Pettijohn, et al., 1987).

On the Pettijohn et al. (1972) and Herron (1988) sandstone classification diagram, the Skoorsteenberg, Laingsburg and Slope sandstones plot on the boundary between greywackes and litharenites, with the majority of samples falling within the litharenite field. Both greywackes and litharenites are chemically immature sandstones. This may argue for minimum amount of weathering during erosion and deposition and limited transport.

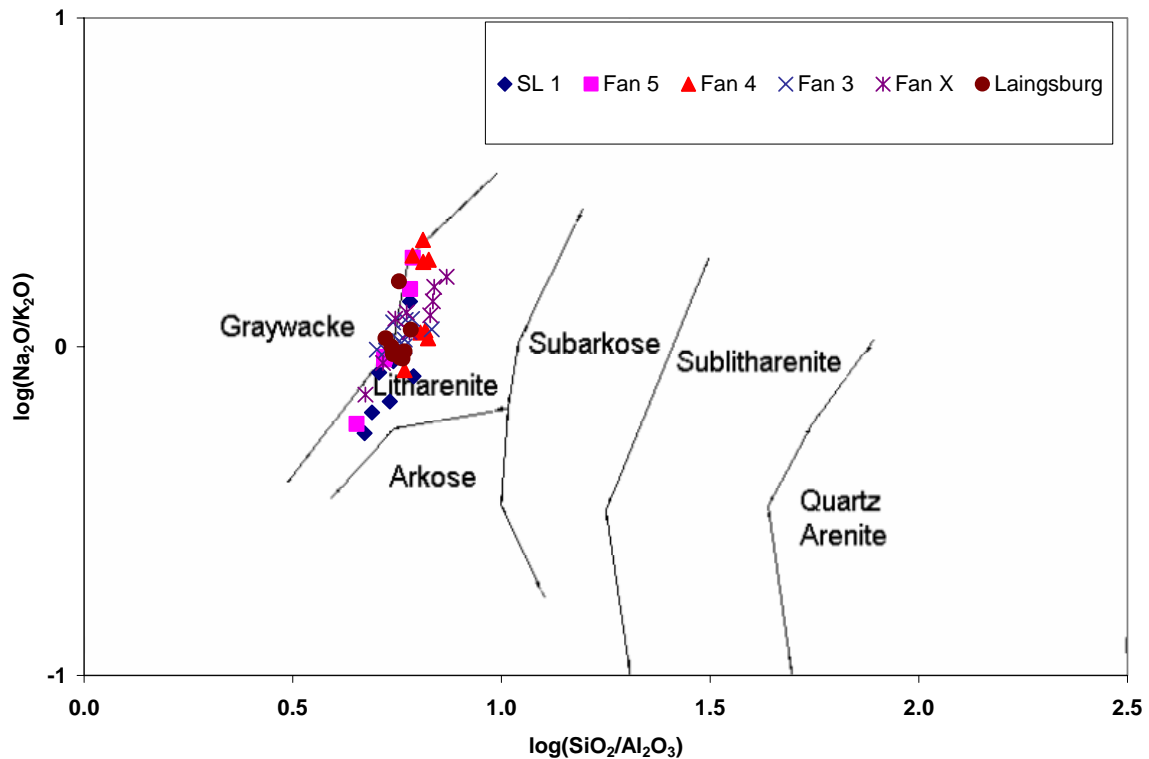


Figure 5.3 Classification of terrigenous sandstones using $\log(\text{Na}_2\text{O}/\text{K}_2\text{O})$ versus $\log(\text{SiO}_2/\text{Al}_2\text{O}_3)$ from Pettijohn et al. (1972), with boundaries redrawn by Herron (1988). Note that major element data of Laingsburg sandstones is from Van Lente (2004).

5.3.2 Weathering

Alteration of igneous rocks during weathering results in depletion of alkali and alkaline earths and preferential enrichment of Al_2O_3 in sediments. Various authors have utilized the so-called chemical index of alteration (or CIA) of Nesbitt & Young (1982) to evaluate the intensity of weathering in the source area of greywackes (Floyd et al., 1991; Camiré et al., 1993; Toulkeridis et al., 1999). The CIA can also be used as an estimate of the climatic conditions that existed during the formation of clastic sedimentary rocks. The chemical index of alteration is calculated as:

$$\text{CIA} = [\text{Al}_2\text{O}_3 / (\text{Al}_2\text{O}_3 + \text{CaO}^* + \text{Na}_2\text{O} + \text{K}_2\text{O})] \times 100 \text{ (in molecular proportion).}$$

CaO^* represents CaO associated with the silicate fraction of the sample. Samples with high CaO and LOI content are excluded since they may contain interstitial calcite cement. Advanced diagenesis shown by some sandstone is not expected to change the CIA value significantly.

Fresh granites and granodiorites have CIA values between 45 and 55 whereas more intense weathering, which results in residual clays such as kaolinite and gibbsite-rich shale, produces CIA values close to 100. CIA values of average shales range between 70 and 75 (Taylor and McLennan, 1985).

Glacial tills and clays are formed primarily by mechanical processes at low temperature and have low CIA values similar to their source materials. Therefore, low CIA values indicate cold climates whereas high CIA values suggest hot and humid ones (Nesbitt & Young, 1982).

The CIA values of the Skoorsteenberg samples vary from 63.72 to 67.81, from 65.95 to 69.12 and from 62.33 to 68.91 for Fans 3, 4 and 5 respectively. Slope sandstones have CIA values between 59.59 and 66.12 while sandstones of the

Laingsburg Formation have CIA values ranging from 53.27 to 69.29. These data suggest low to moderately weathered sources for the Laingsburg, Skoorsteenberg and Slope sandstones.

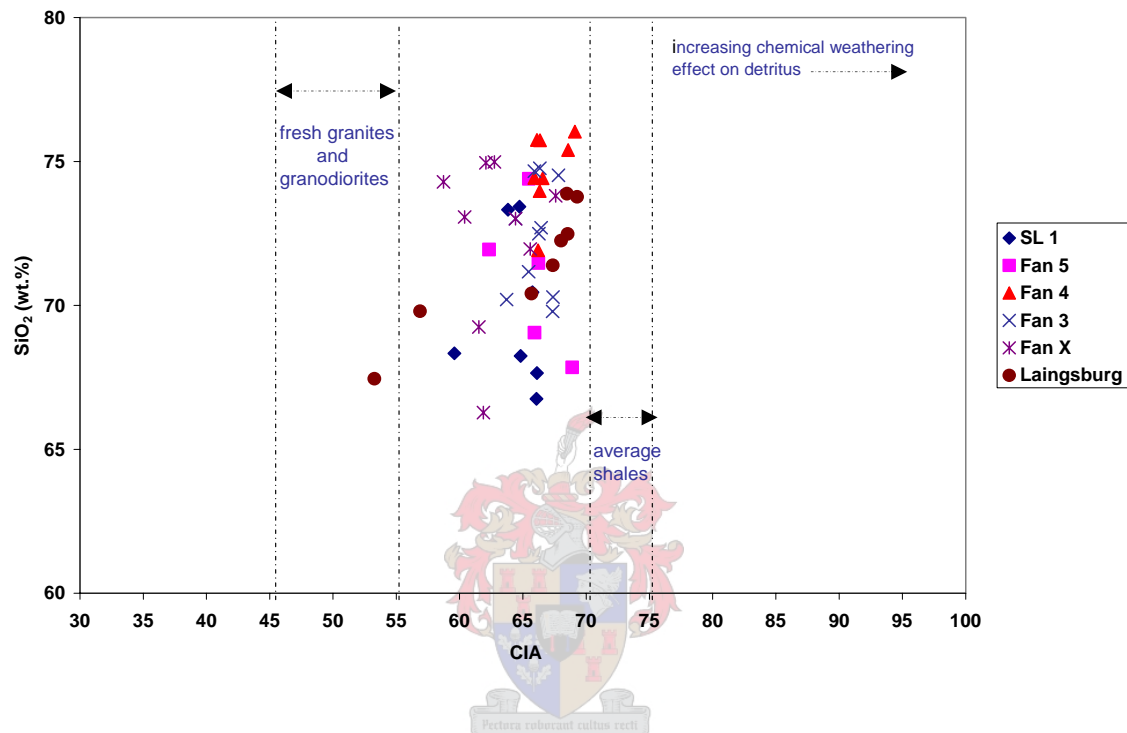


Figure 5.4 SiO₂ vs. CIA (Chemical index of alteration) of the Slope, Laingsburg and Tanqua deepwater sandstones. Note the low to moderate weathering degree of the investigated sandstones. CIA values of igneous rocks are from Nesbitt and Young (1982) and those of average shale are from Taylor and McLennan (1985).

5.3.3 Climate

Pleistocene tills having CIA values of around 52, Pleistocene glacial clays having average values of around 65 or Pleistocene varved clays with average CIA values of around 62 were formed in extreme cold conditions, whereas residual clays with CIA values greater than 90 and Amazon cone muds that have average CIA values between 82 and 86 are likely to have been formed in hot, humid climates (Nesbitt & Young, 1982).

The Skoorsteenberg, Laingsburg and Slope sandstones with CIA values varying between 53.27 and 69.29 are likely to have been formed in a relatively cold environment, which is to be expected shortly after the Dwyka ice age. A large abundance of angular quartz and feldspar grains, as well as abundant lithic fragments in the Tanqua and Laingsburg sandstones is typical of tectonic arkose (Folk, 1980), a characteristic sediment near uplifted basement. The source area was uplifted and eroded so rapidly that sufficient time was not available for weathering to be completed. Another possibility is the probable existence of plagioclase-rich arkose, owing its feldspathic constituents to volcanic activity, again a case of rapid deposition short-circuiting weathering.

The terms climatic and tectonic arkoses have been introduced to sedimentology to characterize sediments owing their high feldspar contents to climate (too cold or too dry) and rapid basement uplift respectively.

Weak chemical weathering and limited breakdown of feldspar observed here resulted from the competing influence of three main factors:

1. Rapid basement uplift due to plate convergence and subduction along the paleo-Pacific margin in the south-western part of Gondwana,
2. Intermediate to felsic volcanism associated to that subduction, and
3. A relatively cold climate which prevailed shortly after the Dwyka glaciation age.

The ternary plot $(\text{CaO}^* + \text{Na}_2\text{O})\text{—Al}_2\text{O}_3\text{—K}_2\text{O}$ (Fig. 5.5) is a graphic representation of the chemical index of alteration where the initial stages of weathering form a trend parallel to the $(\text{CaO}^* + \text{Na}_2\text{O})\text{—Al}_2\text{O}_3$ side of the diagram (i.e. unweathered rocks plot along the left-hand side of the plagioclase—K-feldspar line) whereas advanced weathering shows a marked loss in K_2O as compositions move towards to the Al_2O_3 apex. The trends follow mixing lines representing the removal of alkalis and Ca in solution during the breakdown of first plagioclase and then potassium feldspar and ferromagnesian silicates. The Skoorsteenberg of the Tanqua Karoo, Laingsburg and Slope sandstones plot at relatively high alkali values (~5 wt %) and relatively lower Al_2O_3 contents, suggesting low to moderate weathering. The ternary plot $(\text{CaO}^* + \text{Na}_2\text{O})\text{—Al}_2\text{O}_3\text{—K}_2\text{O}$ (Fig. 5.5) can also be used for provenance investigation. The Skoorsteenberg and Laingsburg submarine fan and Slope sandstones form a relatively homogeneous group around the weathering trend of granodiorite and adamellite suggesting these rocks as their most obvious precursors. Adamellite is a granite in which one third to two-thirds of the total feldspar is plagioclase. The term is often used as a synonym for quartz monzonite. Many samples from Fan 4 plot between the weathering trend of tonalite and granodiorite, suggesting that the Fan 4 sediments were dominantly derived from intermediate igneous (tonalite-granodiorite) sources, whereas other investigated fans are mainly derived from more felsic (granodiorite-adamellite) sources.

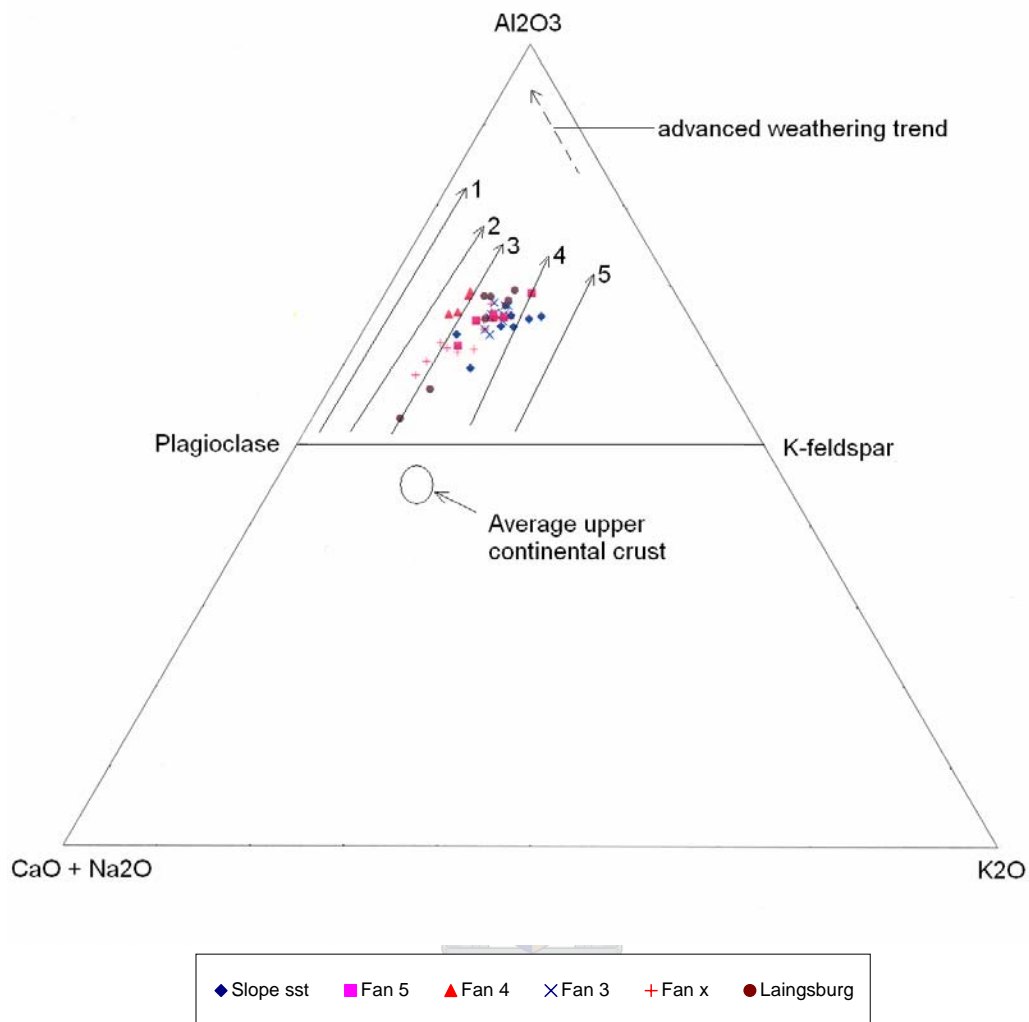


Figure 5.5 Molar $CaO+Na_2O—Al_2O_3—K_2O$ ternary diagram (Nesbitt and Young, 1984) showing the relationship between the studied sedimentary rocks and the calculated weathering trends of some crystalline rocks. The arrows 1-5 represent the weathering trends of (1) gabbro, (2) tonalite, (3) granodiorite, (4) adamellite and (5) granite respectively (Nesbitt and Young, 1984). Noteworthy is the more intermediate igneous composition of Fan 4. The Skoorsteenberg, Laingsburg and Slope sandstones have undergone low to moderate weathering, and therefore plot between the advanced weathering zone and the average upper continental crust of Taylor and McLennan (1985).

5.4 Source rock lithology

The Slope, Laingsburg and Tanqua fan sediments are immature litharenites and greywackes (Figure 5.3). According to Pettijohn et al. (1987), in the same way that the arkoses denote a plutonic provenance (granite and gneisses), litharenites denote a supracrustal provenance (volcanic, low grade metamorphic and sedimentary rocks).

Two discriminant functions, using major oxides, were calculated, and the results are plotted in Figure 5.6. The discriminant functions D1 and D2 were developed by Roser and Korsch (1988), who distinguished between sediments whose provenance is primarily mafic, intermediate or felsic igneous and quartzose sedimentary. A plot of the two discriminant functions based upon the oxides of Ti, Al, Fe, Mg, Ca, Na and K proved to be effective in differentiating between the four provenances. It is noteworthy that this discrimination diagram does not take into consideration biogenic phases (CaO in CaCO_3 or biogenic SiO_2)

Plotting D1 versus D2 indicates that the Permian Tanqua and Laingsburg subbasins in the south-western Karoo basin were filled by both quartzose sedimentary and felsic igneous rocks since samples plot astride the border between them. It is worth noting that the majority of points fall within the sedimentary field suggesting a dominantly sedimentary provenance. Samples are not scattered in the aforementioned fields, but form a homogeneous group. This remarkable homogeneous geochemical nature of the analyzed samples, representing each of the investigated submarine fans, suggests little or no variation in their source.

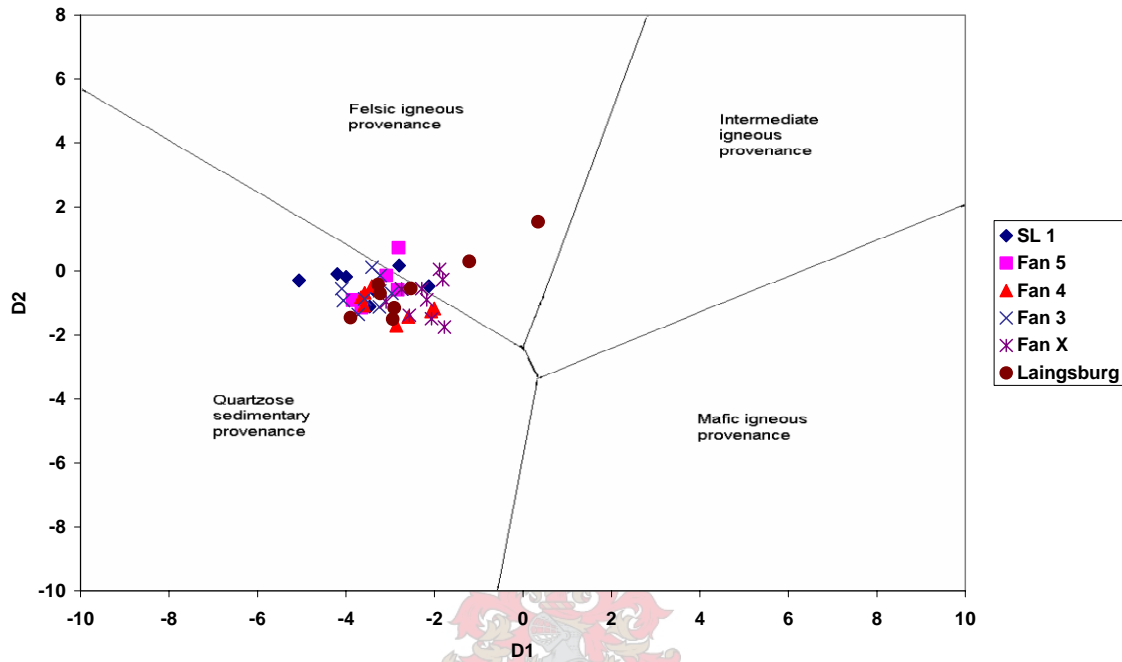


Figure 5.6 Discriminant function diagram for the provenance signatures of sandstone-mudstone suites using major elements (Roser and Korsch, 1988).

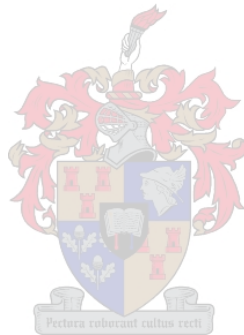
$$D1 = -1.773TiO_2 + 0.607Al_2O_3 + 0.76 Fe_2O_{3(total)} - 1.5MgO + 0.616CaO + 0.509Na_2O - 1.224K_2O - 9.09$$

$$D2 = 0.445TiO_2 + 0.07Al_2O_3 - 0.25Fe_2O_{3(total)} - 1.142MgO + 0.438CaO + 1.475 Na_2O + 1.426 K_2O - 6.861$$

(in molecular weight).

Because of the presence of minor isolated calcite veins in the fans, we deliberately used the second diagram of Roser and Korch (1988) to circumvent any possible problem of biogenic phases in sediments and optimize the current results.

Plotting D3 against D4 (Fig. 5.7) shows quite similar results, but produces a distribution which indicates a more mixed provenance. The diagram reveals that the Tanqua and Laingsburg subbasins were filled by felsic, intermediate igneous and sedimentary source materials. Again Fan 4 shows a more intermediate igneous provenance.



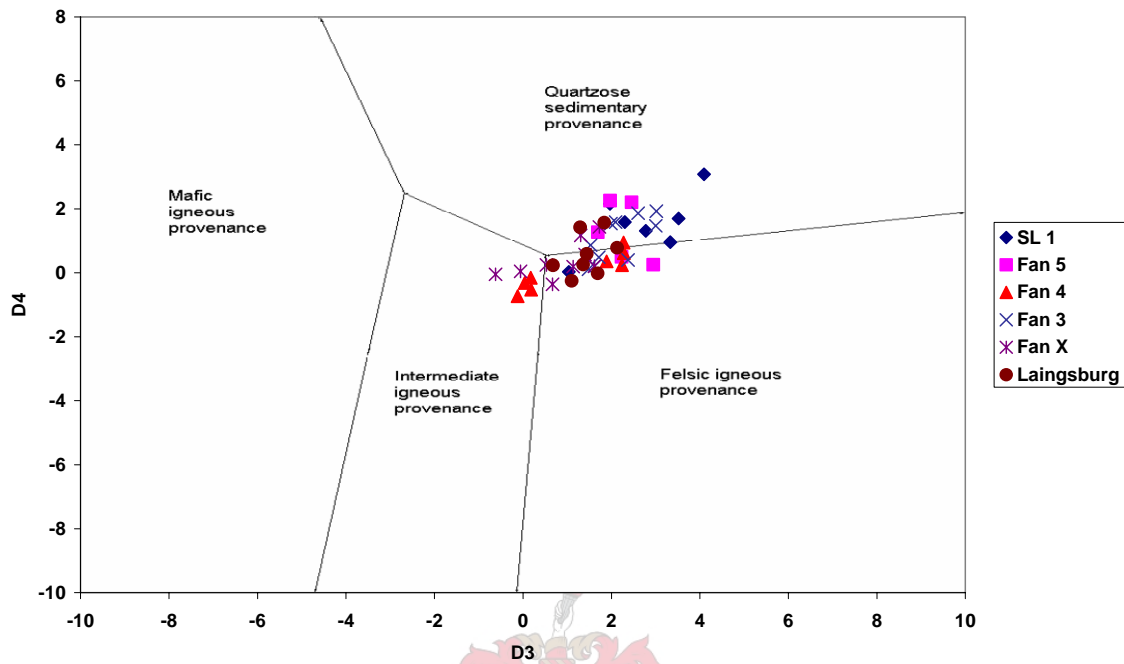


Figure 5.7 Discriminant function diagram for the provenance signatures of sandstone-mudstone suites using major elements (Roser and Korsch, 1988).

$$D3 = 30.638\text{TiO}_2/\text{Al}_2\text{O}_3 - 2.541\text{Fe}_2\text{O}_3\text{ (total)}/\text{Al}_2\text{O}_3 + 7.329\text{MgO}/\text{Al}_2\text{O}_3 + 12.031\text{Na}_2\text{O}/\text{Al}_2\text{O}_3 + 35.402\text{K}_2\text{O}/\text{Al}_2\text{O}_3 - 6.328$$

$$D4 = 56.500\text{TiO}_2/\text{Al}_2\text{O}_3 - 10.879 \text{Fe}_2\text{O}_3\text{ (total)}/\text{Al}_2\text{O}_3 + 30.875\text{MgO}/\text{Al}_2\text{O}_3 - 5.404 \text{Na}_2\text{O}/\text{Al}_2\text{O}_3 + 11.112 \text{K}_2\text{O}/\text{Al}_2\text{O}_3 - 3.89 \text{ (in molecular weight).}$$

5.5 Tectonic setting of the source area

On the sandstone subdivision diagram of Crook (1974), all the Slope, Laingsburg and Tanqua sandstone samples may be classified as quartz intermediate (Fig. 5.1; Crook, 1974). Quartz-intermediate sediments are indicative of an Andean-type active continental margin. This convergence type takes place when a surface of one plate is continental and the other oceanic. It is maintained by subduction of the oceanic plate beneath the continental plate; the oceanic lithosphere is consumed deep in the mantle below the continental margin (Pettijohn et al., 1987).

Various authors have utilized bivariate plots, based on major element geochemistry, developed by Bhatia (1983), to investigate the tectonic setting of greywackes (McCann, 1991; Holail and Moghazi, 1998). Bhatia (1983) divided a series of plots to differentiate four main tectonic settings. The four tectonic settings defined by Bhatia (1983) are the oceanic island arc (OIA), continental island arc (CIA), active continental margin (ACM) and passive margin (PM). The discriminant parameters are TiO_2 wt% vs. $(\text{Fe}_2\text{O}_3 + \text{MgO})$ wt%, $\text{Al}_2\text{O}_3/\text{SiO}_2$ vs. $(\text{Fe}_2\text{O}_3 + \text{MgO})$ wt%, $\text{K}_2\text{O}/\text{Na}_2\text{O}$ vs. $(\text{Fe}_2\text{O}_3 + \text{MgO})$ wt% and $\text{Al}_2\text{O}_3/(\text{CaO} + \text{Na}_2\text{O})$ vs. $(\text{Fe}_2\text{O}_3 + \text{MgO})$ wt%.

The oceanic island arc (OIA) sandstones, dominantly derived from calc-alkaline andesites, are characterized by the high abundance of $\text{Fe}_2\text{O}_3 + \text{MgO}$ (8-14%), TiO_2 (0.8-1.4%), and low $\text{Al}_2\text{O}_3/\text{SiO}_2$ (0.24-0.33%) and $\text{K}_2\text{O}/\text{Na}_2\text{O}$ (0.2-0.4) ratios.

The continental island arc (CIA) sandstones, dominantly derived from felsic rocks, have lower $\text{Fe}_2\text{O}_3 + \text{MgO}$ (5-8%) and TiO_2 (0.5-0.7%), and higher $\text{Al}_2\text{O}_3/\text{SiO}_2$ (0.15-22%) and $\text{K}_2\text{O}/\text{Na}_2\text{O}$ (0.4-0.8%).

The active continental margins (ACM; Andean type and strike-slip basins) sandstones are dominantly derived from the uplifted basement and reflect the composition of the upper continental crust (UCC). They are characterized by low

$\text{Fe}_2\text{O}_3 + \text{MgO}$ (2-5%), TiO_2 (0.25-0.45%) and $\text{K}_2\text{O}/\text{Na}_2\text{O}$ ratio more or less equal to 1.

Passive margins (PM) are significantly enriched in SiO_2 and depleted in Al_2O_3 , TiO_2 , Na_2O , and CaO and have a $\text{K}_2\text{O}/\text{Na}_2\text{O}$ ratio of more than 1, suggesting their highly recycled and matured nature.

Using major elements for discrimination of the tectonic setting of the Tanqua Karoo and Slope sandstones, leads to the conclusions that these sediments originated from a continental island arc (CIA) and an active continental margin (ACM) (Fig. 5.8).

The distribution of the points in the active continental margin (ACM) and continental island arc (CIA) fields of Bhatia (1983) suggests that:

1. For the CIA; the sediments could have been derived from a wide range of sources but have a dominant contribution from felsic volcanics.
2. For the ACM; The Tanqua subbasin was developed on or adjacent to a thick continental crust composed of rocks of older fold belts. Igneous metamorphic materials and sediments related to these terranes are dominantly derived from granite-gneisses and siliceous volcanics of the uplifted basement.

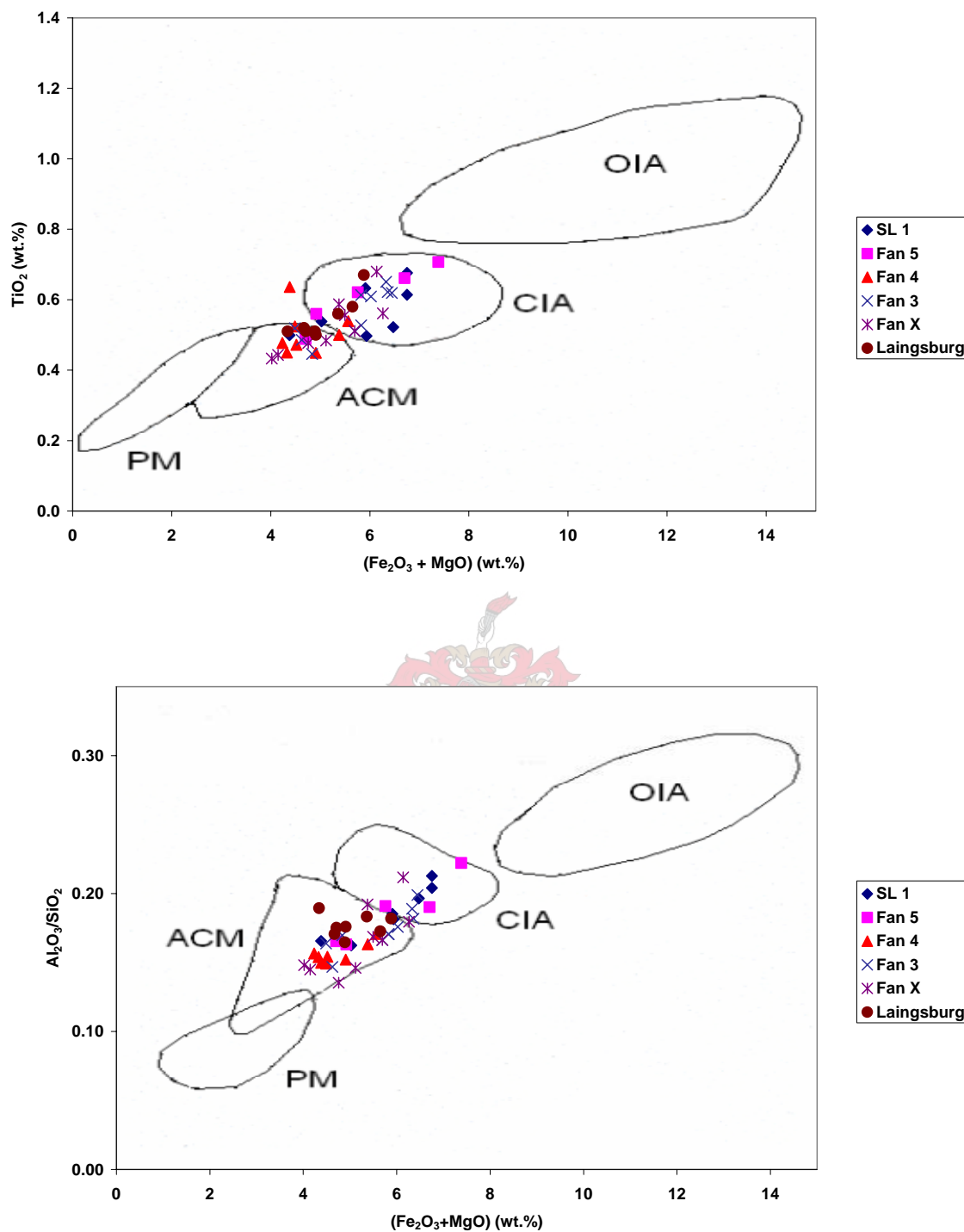


Figure 5.8 Bivariate plots for the discrimination of the plate tectonic setting of sandstones from the Slope, Laingsburg and Skoorsteenberg Formations: OIA—oceanic island arc; CIA—continental island arc; ACM—active continental margins; PM—passive margins (Bhatia, 1983). Laingsburg data is from Van Lente (2004).

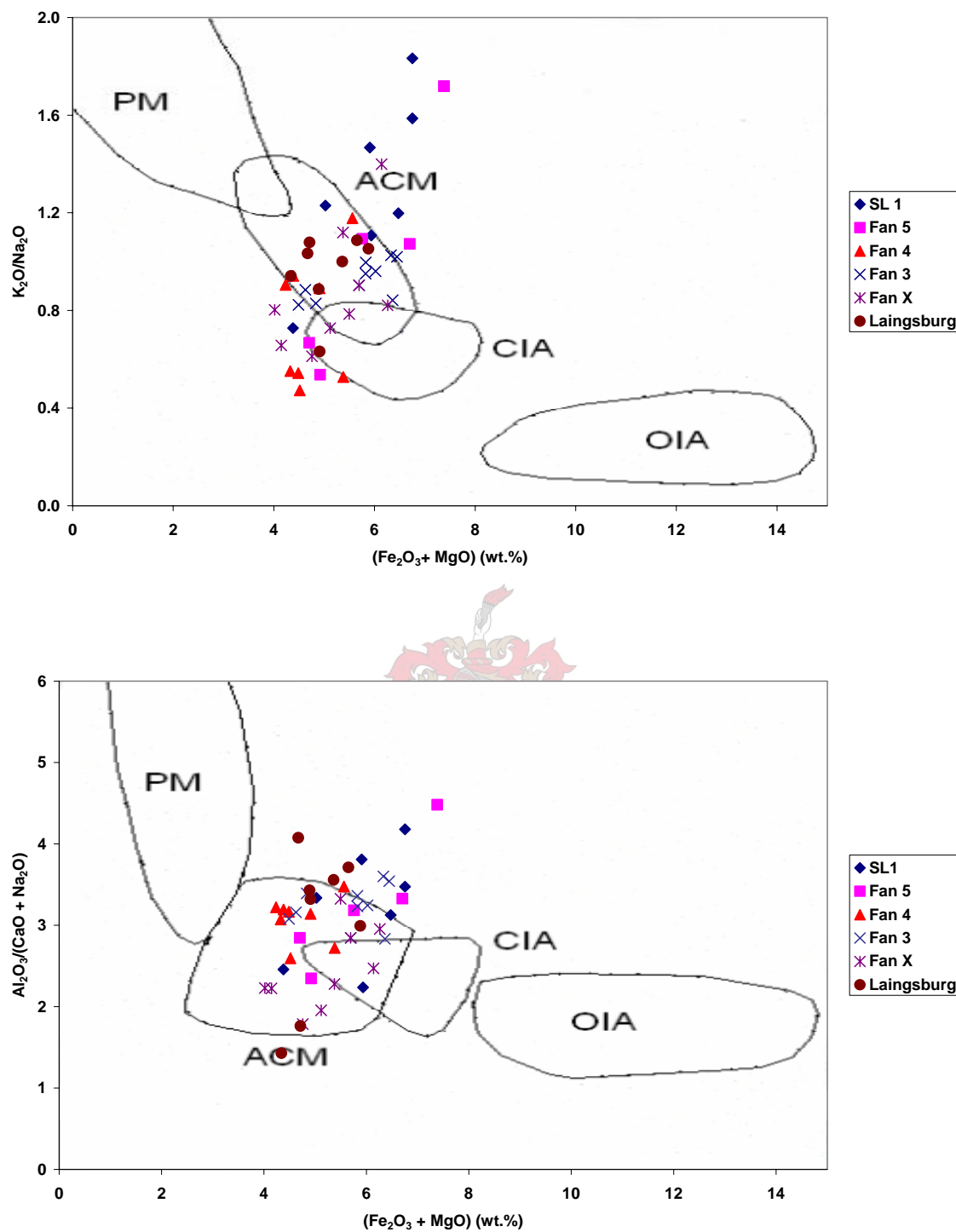


Figure 5.8 (continued) Bivariate plots for the discrimination of the plate tectonic setting of sandstones from the Slope, Laingsburg and Skoorsteenberg Formations: OIA—oceanic island arc; CIA—continental island arc; ACM—active continental margins; PM—passive margins (Bhatia, 1983). Laingsburg data is from Van Lente (2004).

5.6 Trace Element Geochemistry

Trace element concentrations of the Slope and Skoorsteenberg sandstones reported in this study were determined by ICP-MS.

As previously mentioned, the chemical record of clastic sedimentary rocks results from the competing influence of various factors such as source rock lithology, intensity of weathering, hydraulic sorting during transport and sedimentation, diagenesis and post-depositional reactions (McLennan, 1989).

Selected trace elements may be used to identify the above-mentioned geological processes. The most important elements in this respect are REE, Th, Sc and to less extent Cr and Co. REE are potentially very powerful tools for reconstructing provenance compositions because they are transferred unfractionated into the sediment (Taylor and McLennan, 1985). Original source signatures are unaffected by diagenesis and metamorphism (Awwiller, 1994; Taylor et al., 1986). Despite the fact that REE and selected trace elements are known to be relatively immobile, it is always advisable to evaluate the effect of post-depositional reactions as well as the extent to which these key trace elements survived sedimentary processes in order to be transported unfractionated within the sediment (Rollinson, 1993).

Zircon, sphene, garnet, apatite and rutile have been identified within the Tanqua Karoo sandstones. The presence of such weathering-resistant phases can significantly influence the chemical composition of sandstones, by controlling the distribution of major elements (P_2O_5 and TiO_2) and some trace elements (REE, Th, U, Zr, Hf and Nb) and therefore these conservative elements may not be representative of provenance (Cullers et al., 1987). Sandstones are more likely to be affected by mineral sorting than fine-grained sedimentary rocks like shales. This would be reflected in the REE patterns of sandstones and the abundance of some key trace elements relative to SiO_2 . Hydraulic fractionation of zircon for

instance will lead to fractionation because the mineral is commonly enriched in HREE (Camiré et al. 1993). The Zr, Nb, Y, TiO_2 , and P_2O_5 abundance in the investigated sandstones is constant (Appendix B) and very weakly correlated with SiO_2 suggesting a minimal effect of hydraulic sorting. There is no a defined relationship between heavy mineral accumulation and quartz-rich fraction. It can be noted from the above that weathering-resistant phases did not affect the trace element chemical composition of investigated sandstones and are therefore representative of the provenance of the Skoorsteenberg and Slope sandstones. Zr, Nb and Y of Fan 4 sandstones show a negative correlation with SiO_2 while major elements P_2O_5 and TiO_2 show very weak to no correlation when plotted against SiO_2 (Fig. 5.2a). The two major elements, however, indicate that Fan 4 is more mature than other fans as these sandstones are generally plotted at high quartz content and relatively low remaining major oxides. Zr, Nb and Y tend to concentrate in the quartz-poor fraction, indicating a considerable decrease in the minerals bearing these elements with an increase of quartz content (Fig. 5.9).



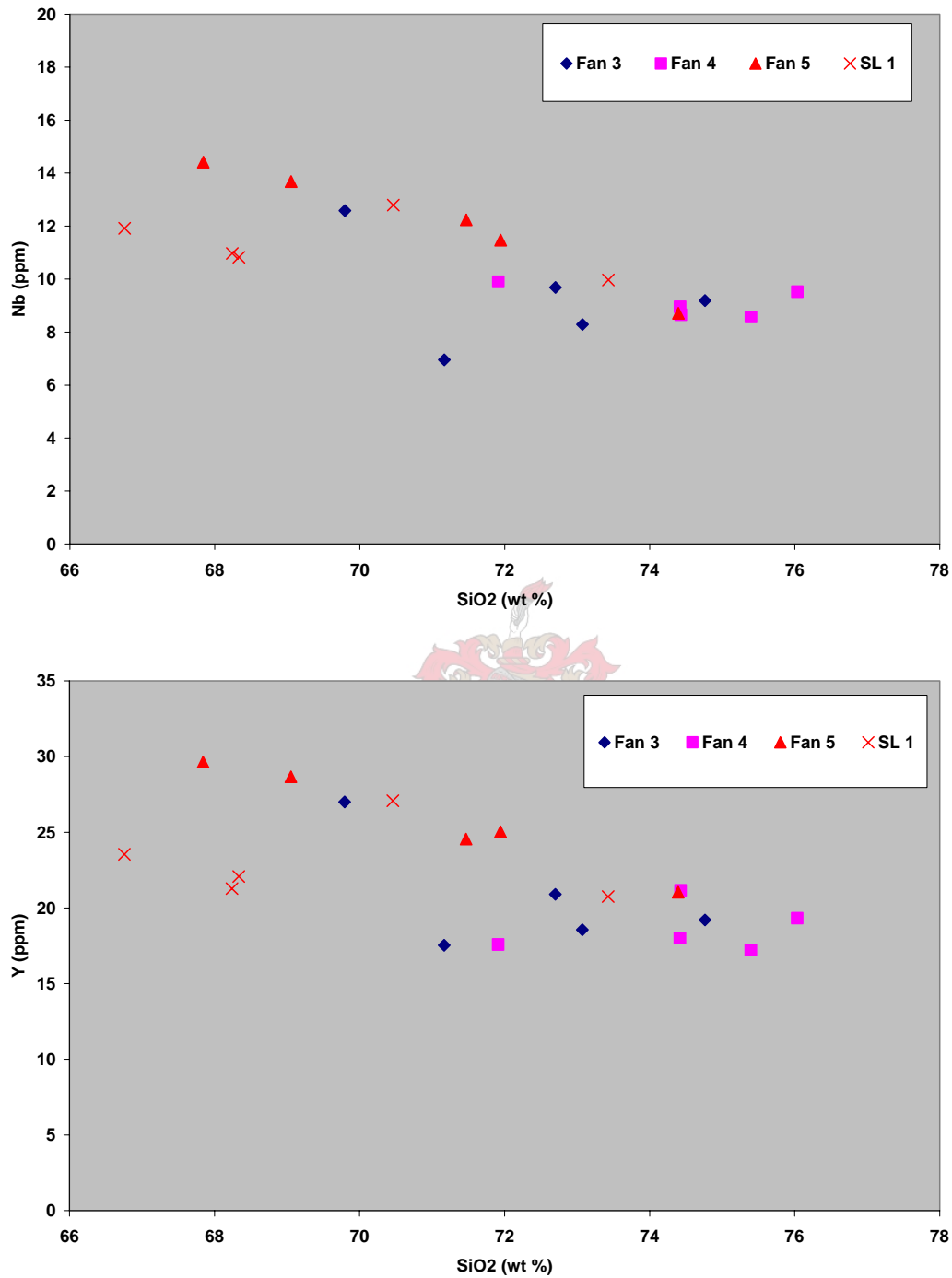


Figure 5.9. Selected trace element concentrations (in ppm) vs. SiO₂. Note that trace element abundance in analyzed Slope and Tanqua sandstones are not correlated with SiO₂, suggesting a minimal effect of hydraulic sorting, especially in the case of the Slope, Fan 3 and Fan 5. However, Nb and Y in Fan 4 are negatively correlated with SiO₂.

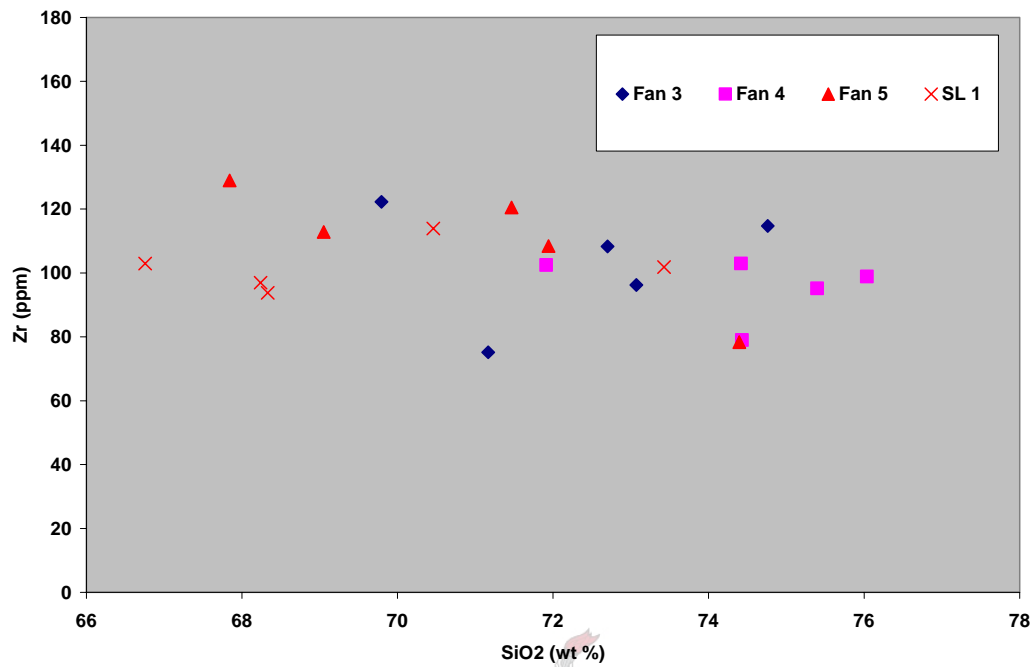
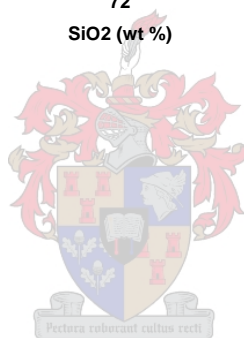


Figure 5.9 (continued) Zr vs. SiO₂



U is preferentially leached during diagenesis and metamorphic dehydration processes. The Th/U ratios may reach 8 to 10 in upper amphibolite and granulite facies (Weaver and Tarney, 1984; Wedepohl, 1991). The Th/U ratios, in the investigated samples, are constant and relatively low (Table 5.2). Diagenesis and metamorphism are also expected to affect the large ions lithophile elements (Cs, Sr, K, Rb, Ba) (Hower et al. 1976), since LILE are very mobile. The general constancy of ratios K/Rb, K/Ba, Ce/Sm and Th/U (Floyd et al., 1991) within the Tanqua and Slope sandstones suggests that they have not systematically changed. However, small differences in these ratios are probably related to advanced diagenesis as expected for most mineralogically immature sandstones.

Th/U ratios of sedimentary rocks are expected to increase with increasing weathering due to the oxidation and loss of uranium (Taylor and McLennan, 1985; McLennan et al. 1990, 1995). Th/U ratios above 4 are related to weathering history (McLennan et al., 1995). Investigated samples show relatively constant and low Th/U ratios very close to the upper continental crust value of 3.8, suggestive of low to moderate weathering as previously indicated by major element abundance.



Table 5.2 selected trace element contents of the Slope and Skoorsteenberg fan sandstones

Sample	Rb	Sr	Ba	Ce	Sm	Th	U	Th/U	Ce/Sm	K/Rb	K/Ba
Slope											
SL1-1	86.1	168	512	67.3	5.44	9.92	2.45	4.06	12.4	282	47.4
SL1-2	92.7	276	651	66.0	5.58	10.8	3.88	2.78	11.8	268	38.1
SL1-4	110	208	590	73.1	6.36	12.0	3.04	3.93	11.5	254	47.3
SL1-6	131	271	786	65.8	5.87	11.9	3.56	3.34	11.2	246	41.2
SL1-7	104	331	707	75.0	5.66	12.1	3.49	3.46	13.3	229	33.7
Fan 5											
SL1-A-F5	129	168	542	81.2	6.83	13.5	3.42	3.95	11.9	222	52.7
SL1-B-F5	96.0	158	376	72.1	6.03	11.6	3.24	3.58	12.0	231	59.0
NS1-1-F5	73.1	125	487	48.2	4.64	9.14	2.32	3.93	10.4	246	36.9
NS1-3-F5	77.0	125	481	65.1	5.80	10.7	2.89	3.69	11.2	225	36.1
NS1-4-F5	102	116	584	75.6	6.68	12.5	3.29	3.80	11.3	232	40.3
Fan 4											
NB3-1-F4	74.5	143	480	49.8	4.09	7.83	2.59	3.02	12.2	305	47.4
NB3-4-F4	80.4	159	526	56.2	5.39	8.95	2.55	3.51	10.4	232	35.5
NS1-6-F4	51.8	154	281	56.0	4.43	8.50	2.18	3.90	12.6	247	45.6
NS1-8-F4	51.2	152	321	65.2	5.22	9.78	2.29	4.28	12.5	241	38.5
NS1-10-F4	45.4	165	230	61.0	5.00	9.25	2.20	4.20	12.2	299	58.9
Fan 3											
NB3-7-F3	91.2	166	689	72.7	6.33	12.1	3.21	3.76	11.5	248	32.9
NB3-E-F3	76.4	152	661	61.3	5.08	10.1	2.55	3.98	12.1	263	30.4
NB4-1-F3	67.0	133	565	54.3	4.43	9.06	2.40	3.78	12.2	259	30.8
NB4-5-F3	68.4	136	647	49.9	4.25	8.59	1.98	4.34	11.7	333	35.2
NB4-10-F3	53.5	215	231	56.7	4.81	8.90	2.27	3.93	11.8	223	51.7

The REE data was normalized to chondritic meteorites (Taylor and McLennan, 1985). The chondritic meteorites were chosen because they are thought to be relatively unfractionated samples of the solar system dating from the original nucleosynthesis (Rollinson, 1993). Chondrite-normalized REE patterns for the Tanqua fans and Slope sandstones are shown in Figure 5.10. The REE concentrations are approximately 100 times chondrite for the light rare earth element (LREE) La, while the heavy rare earth elements (HREE) Gd to Lu are approximately 10 times the chondritic abundance. Compared to other fans, Fan 4 shows a general depletion of both light and heavy rare earth elements, indicating its higher quartz content (average 74.70 wt %, Table 5.1). Although absolute concentrations in REE are variable, the chondrite-normalized patterns are similar for different samples and different fans, having steep patterns typical of North American Shale Composite (NASC). Relative to chondritic meteorites, NASC has about 100 times the light REE and about 10 times the heavy REE content and a small negative Eu anomaly (Rollinson, 1993). Because the NASC is considered to represent the “average crustal material”, it can be therefore assumed that the Tanqua sandstones were partially, if not totally, derived from crustal materials.

The REE patterns of the investigated samples are parallel, reflecting the similar $(La/Sm)_N$, Eu/Eu^* and $(Gd/Yb)_N$ ratios in all the group of rocks. These features suggest the absence of heavy mineral fractionation in the sandstones during sedimentary processes (Taylor and McLennan, 1985; McLennan, 1989; Wronkiewicz and Condie, 1989) and are consistent with similar combinations of REE-bearing minerals in all the investigated sandstones (Ugidos et al., 1997). The general uniformity of the REE signatures suggests that heavy mineral fractionation or alteration did not seriously affect the REE characteristics of these rocks but that they are original from the source (Ugidos et al., 1997). In addition, similar REE patterns of investigated sandstones indicate that these sediments have a similar source and that they have been exposed to the same depositional environment.

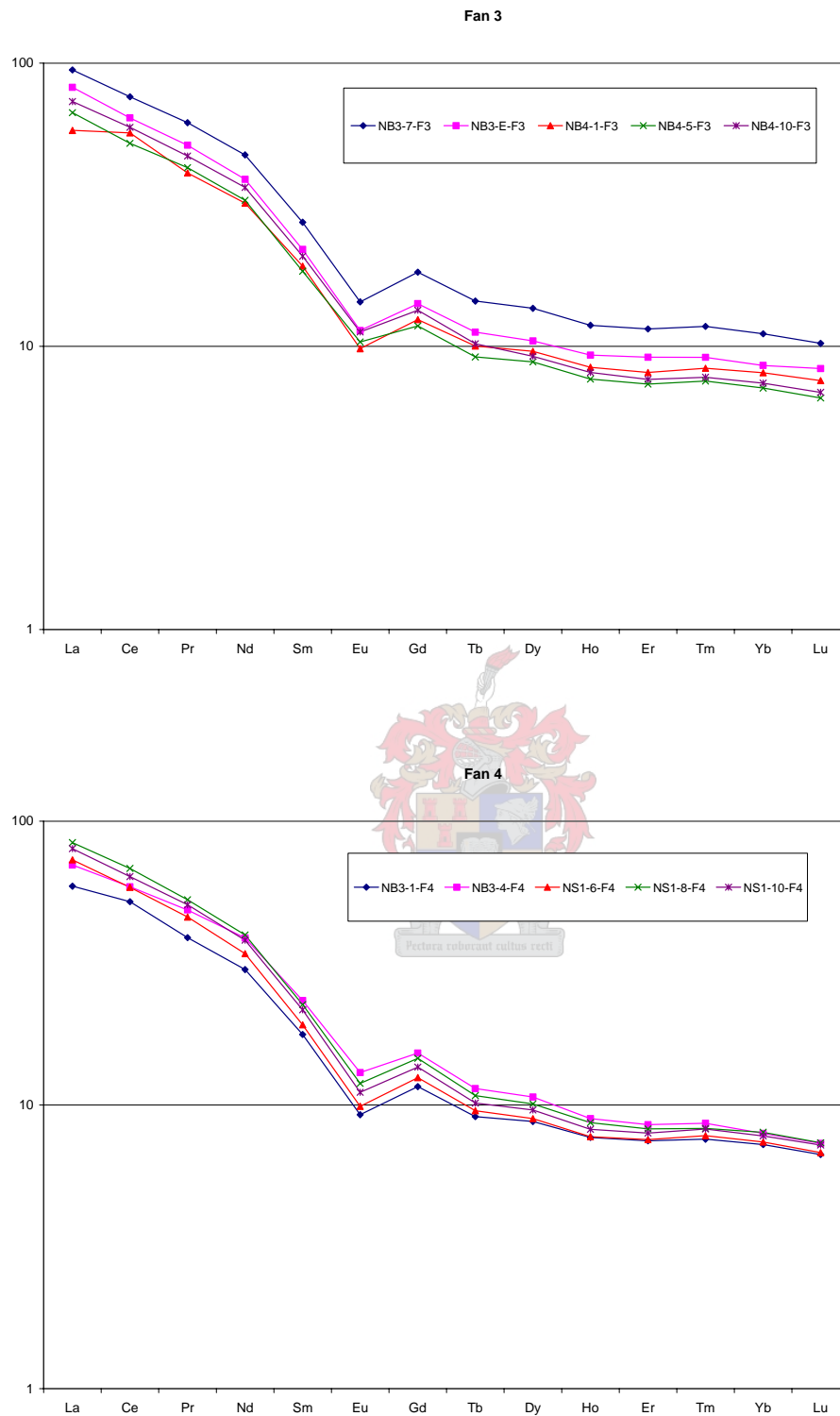


Figure 5.10 Chondrite-normalized REE abundances in the Tanqua and Slope sandstones. REE data of chondritic meteorites are from Taylor and McLennan (1985).

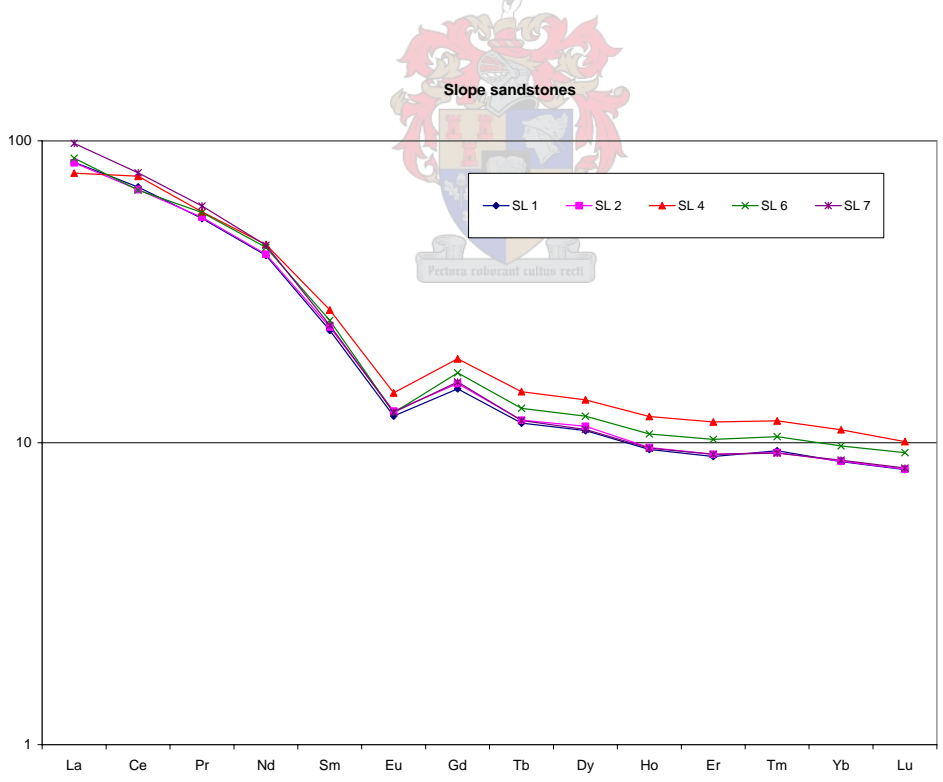
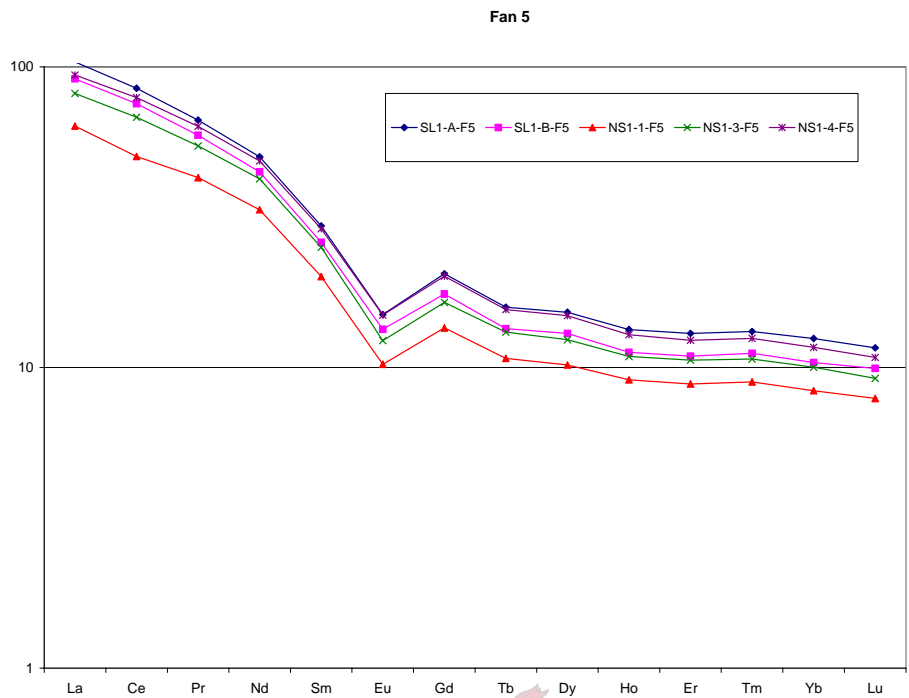


Figure 5.10 (continued)

The analyzed sandstones exhibit overall REE fractionation; the La_N/Yb_N varies from 7.08 to 11.20, 7.59-8.79, 8.13-10.49, and 7.18-9.87 in Slope sandstones, Fan 5, Fan 4 and Fan 3 respectively. The light REEs are fractionated; La_N/Sm_N ratio varies from 2.84 to 4.01, 3.17-3.51, 3.00-3.81, and 3.01-3.74 for slope sandstones, Fan 5, Fan 4 and Fan 3 respectively. The heavy REEs are slightly fractionated and therefore show flat patterns; Gd_N/Yb_N value ranges from 1.72 to 1.82, 1.62-1.73, 1.60-1.92, 1.54-1.81 for the slope sandstones, for Fan 5, Fan 4, and Fan 3. All the investigated sandstones show a negative Eu anomaly (Fig. 5.10).

The relative REE patterns and the size of the Eu anomaly have been extensively used to infer sources of sedimentary rocks (Taylor and McLennan, 1985; Wronkiewicz and Condie, 1989). Felsic igneous rocks usually contain higher LREE/HREE ratios and negative Eu anomalies, and mafic igneous rocks contain lower LREE/HREE ratios with little or no Eu anomalies (Cullers, 1994; 2000). Some tonalites and granodiorites derived from eclogite melting may contain very large LREE/HREE ratios with little or no Eu anomalies (Cullers and Graf, 1984). The significant enrichment of LREEs, the distinctive Eu anomalies, and the flat HREE patterns of the Permian turbidites in the Tanqua area (Fig. 5.10) suggest a derivation from the upper continental crust composed chiefly of intermediate to felsic components.

High field strength elements (HFSE) Zr, Nb, Hf, Y, Th and U are preferentially partitioned into melt during crystallization and anatexis (Feng and Kerrich, 1990), and as a result these elements are enriched in felsic rather than mafic sources. In addition, because of their immobile behaviour, there are thought to reflect provenance composition (Taylor and McLennan, 1985).

Th, Sc and REEs are good indicators of crustal compositions, because their distribution is not considerably affected by diagenesis and metamorphism and is

less affected by heavy mineral phases than that for elements such as Sn, Zr and Hf (Cullers et al., 1979; Bhatia and Crook, 1986; Wronkiewicz and Condie, 1987). Co, Sc and Cr abundances are higher in mafic than in felsic igneous rocks, whereas rare-earth elements and Th are more concentrated in felsic igneous rocks. Ratios such as Eu/Eu^* , $(\text{La}/\text{Lu})_{\text{N}}$, La/Sc , Th/Sc , La/Co , Th/Co and Cr/Th are significantly different in felsic and mafic source rocks and can therefore provide information about the origin of sedimentary rocks (Cullers et al., 1988; Wronkiewicz and Condie, 1989; Condie and Wronkiewicz, 1990; Cullers, 1994). Table 5.3 shows values of the ratios Eu/Eu^* , $(\text{La}/\text{Lu})_{\text{N}}$, La/Sc , Th/Sc , La/Co , Th/Co and Cr/Th for the Tanqua and Slope sandstones.

Four ratios (Eu/Eu^* , $(\text{La}/\text{Lu})_{\text{N}}$, La/Sc and Th/Sc) out of the seven used in this investigation strongly support felsic igneous rocks as a possible source (Table 5.3). However, Th/Co suggests a mafic provenance whereas Cr/Th and La/Co point to a mixed felsic/mafic origin. The current situation indicates that the choice of a specific elemental ratio is very important in the provenance study since all the selected trace element ratios are not necessarily perfect provenance indicators. The more elemental ratios one will consider the more realistic a provenance model will be. For that reason, this study will focus on bivariate plots. Nevertheless, it can be noted from the above ratios that the Tanqua Basin was mainly filled by intermediate to felsic rocks, with a small contribution from mafic rocks as previously suggested by major element concentrations.

Table 5.3. Range of elemental ratios of Tanqua and Slope sandstones in this study compared to the ratios in similar fractions derived from felsic rocks, mafic rocks, and upper continental crust.

Elemental ratio	Tanqua Karoo and Slope sandstones ¹ (n = 20)				Sediment from felsic sources ²	Sediment from mafic sources ²	Upper Continental Crust ³
	Fan 3	Fan 4	Fan 5	Slope			
La/Sc	3.45 – 4.58	3.28 – 4.64	3.08 – 4.32	2.82 – 4.27	2.50 – 16.3	0.43 – 0.86	2.21
Th/Sc	1.20 – 1.55	1.19 – 1.61	1.09 – 1.54	1.16 – 1.43	0.84 – 20.5	0.05 – 0.22	0.79
La/Co	0.21 – 0.68	0.26 – 0.40	0.26 – 1.37	0.42 – 0.83	1.80 – 13.8	0.14 – 0.38	1.76
Th/Co	0.09 – 0.24	0.09 – 0.13	0.10 – 0.49	0.13 – 0.31	0.67 – 19.4	0.04 – 1.40	0.63
Cr/Th	4.76 – 40.3	7.31 – 60.8	3.24 – 7.99	3.01 – 25.0	4.00 – 15.0	25.0 – 500	7.76
Eu/Eu*	0.64 – 0.70	0.64 – 0.69	0.60 – 0.63	0.60 – 0.65	0.40 – 0.94	0.71 – 0.95	0.63
(La/Lu)_N	7.65 – 10.6	8.82 – 11.4	8.05 – 9.19	7.74 – 11.9	3.00 – 27.0	1.10 – 7.00	9.73

¹This study.

²Cullers (1994, 2000); Cullers and Podkovyrov (2000); Cullers et al. (1988).

³Taylor and McLennan (1985).

Various bivariate plots have been used in this study in order to decipher the source rocks of the Tanqua turbidites.

On La/Th vs. Hf and Th/Sc vs. Zr/Sc plots, samples form relatively homogeneous groups, indicating that all the turbidites fans originated from the same source. On the plot Co/Th versus La/Sc (Fig. 5.11), the data display relatively constant and low to moderate La/Sc ratios for a relatively moderate to high Co/Th, indicating a more felsic source relative to the average composition of andesite. The Th/Sc versus Zr/Sc (Fig. 5.12) plot showing a magmatic-arc trend of McLennan et al. (1993) points to rhyodacitic provenance and a La/Th versus Hf diagram (Fig. 5.13) suggests that the investigated fans were derived from a mixed felsic/intermediate source.

In general, major, trace and rare-earth element characteristics in the Tanqua Karoo sandstones reveal that the south-western corner of the Permian Karoo Basin was filled by a wide range of plagioclase-rich intermediate igneous rocks. Possible provenances include tonalite, granodiorite and adamellite or their volcanic equivalents (dacites) as suggested by molar $(\text{CaO}+\text{Na}_2\text{O})-\text{Al}_2\text{O}_3-\text{K}_2\text{O}$ ternary diagram developed by Nesbitt and Young (1984) (Fig. 5.5) used in this study to investigate the effect of chemical weathering. On the basis of discriminant function diagrams for provenance signature of sedimentary rocks of Roser and Korsch (1988) (Figs. 5.6 and 5.7), the Slope, Laingsburg and Tanqua Karoo submarine fan sandstones show a dominant sedimentary provenance. The mobility of major elements makes a dominant sedimentary source as determined by Roser and Korsch (1988) less probable. The morphology and trace element abundances of detrital zircons from investigated deepwater fans are expected to confirm the present result since they are also characteristic of the source magma.

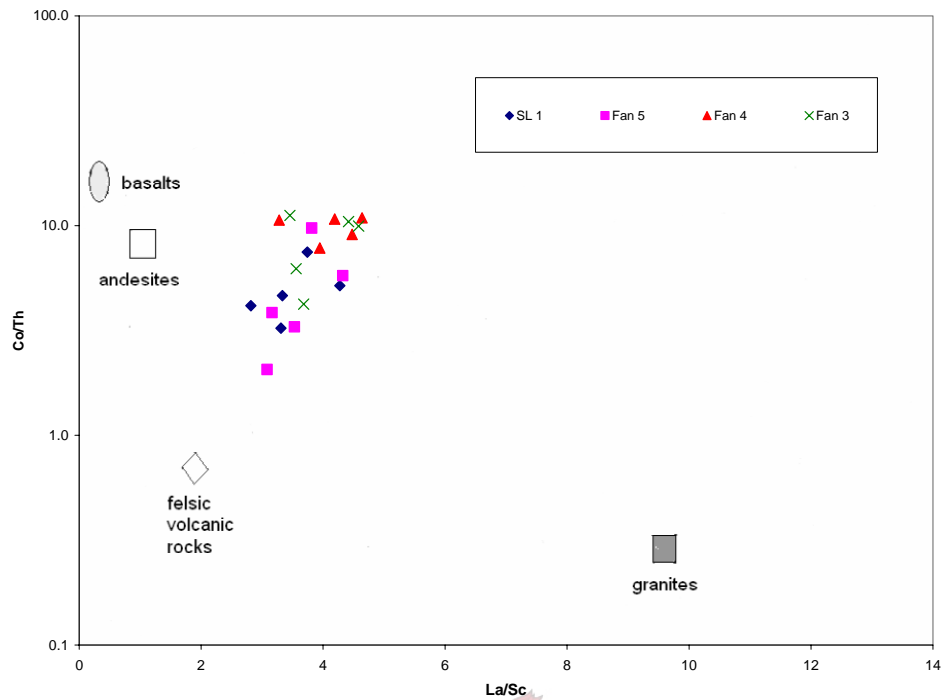


Figure 5.11 Source rock discrimination diagram for the Tanqua turbidites showing Co/Th vs. La/Sc (Condie, 1993).

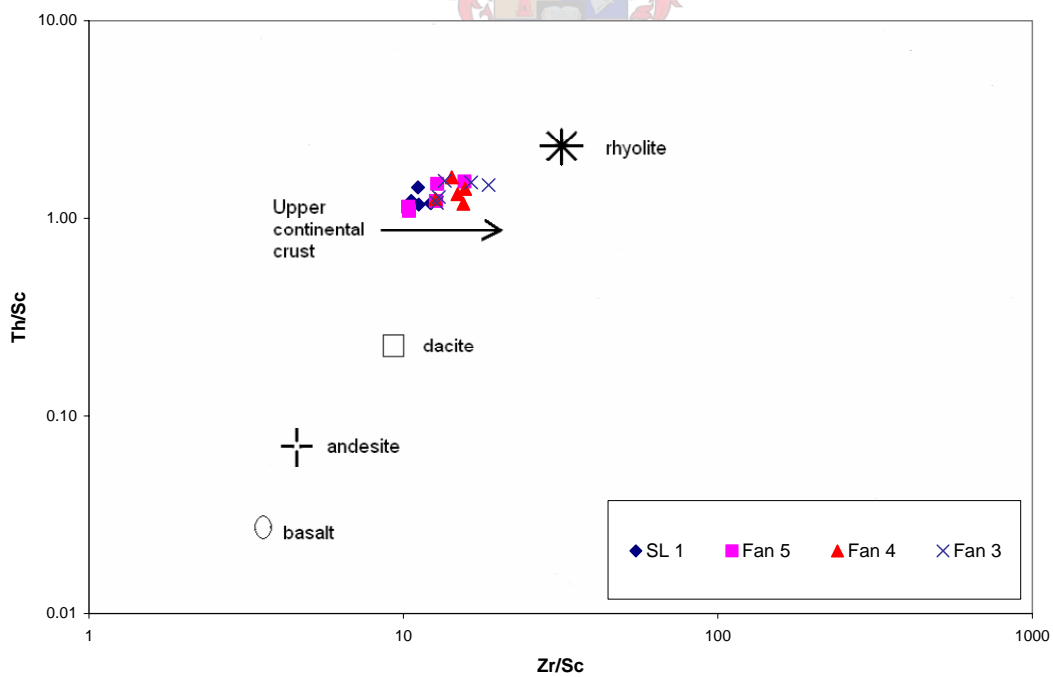


Figure 5.12 Th/Sc-Zr/Sc plot showing a magmatic arc trend (McLennan et al., 1993). Plutonic equivalents plot in similar positions.

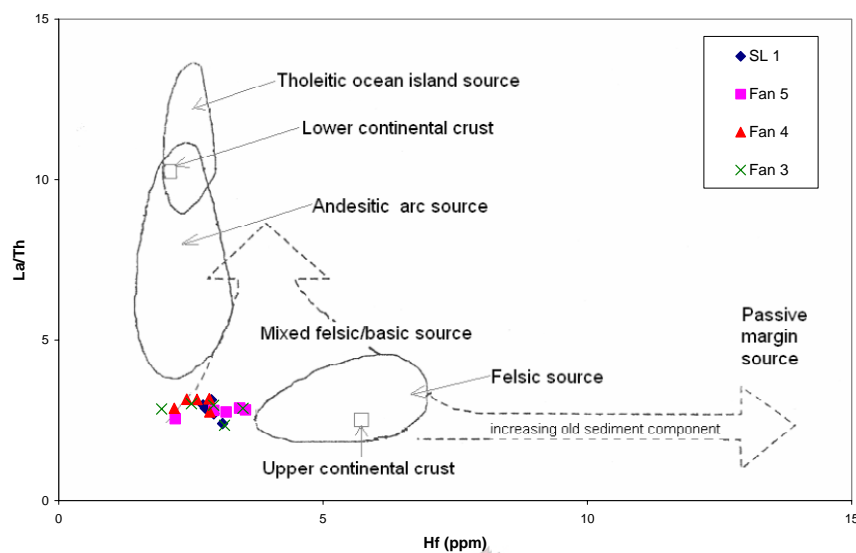


Figure 5.13 La/Th vs. Hf of the Tanqua and Slope sandstones (Gu et al., 2002).

The discrimination diagram La/Th versus Hf also excludes passive margins and ocean island arcs as possible tectonic settings of both the Tanqua Karoo submarine fans and Slope sandstones, which have characteristics intermediate between these two types.

CHAPTER SIX

ZIRCON MORPHOLOGY, CHEMISTRY AND GEOCHRONOLOGY

6.1 Introduction

Zircon is a remarkable mineral because of its ubiquitous occurrence, ranging from crustal rocks to mantle xenoliths, lunar rocks, meteorites and tektites (Speer, 1980). The chemical and mechanical durability of zircon suggests that the mineral can survive multiple sedimentation cycles and preserves the igneous signature of the source magma, as well as providing the age of their crystallization (Hoskin and Schaltegger, 2003).

The present section combines morphology, trace element abundances and SHRIMP U-Pb radiometric ages obtained from detrital zircons to provide information on the provenance and the similarities of the Skoorsteenberg and Laingsburg Formations in the Tanqua and Laingsburg depocentres respectively.

The typological study of zircon is based on Pupin's (1980) classification scheme, which ranks the zircons according to the importance of T and A indices (Fig. 6.1). The index A indicates the morphological development of pyramidal faces (101) and (211) of each type or subtype whereas the index T indicates the development of prismatic faces (100) and (110). The index A is strongly influenced by the nature of the host rock whereas the index T is controlled by the crystallization temperature. This method is extremely valuable, since zircons exhibit a morphology controlled by the physical and chemical conditions under which they crystallized. Here, we examined the similarities of the zircon populations within the investigated fans. This may facilitate the provenance interpretation since sandstone units of the same origin are expected to show remarkably similar zircon populations of the same ages.

The age given by the U-Pb conventional single zircon techniques is the age of the metamorphic or igneous rock that the target mineral originally formed in, regardless of the nature and the location of the source rocks. The potential source rock is deduced by comparing grain ages with those of potential protosources (Sircombe, 1999).

6.2 Zircon morphology and provenance

The morphological classification diagram of zircon was initially developed for metamorphic and igneous rocks by Pupin (1980). This approach has been subsequently applied to low-grade metamorphic and sedimentary rocks (Dabard et al., 1996).

Pupin's (1980) morphological study of zircon populations from granitic rocks led to the proposition of a genetic classification with three main divisions including (1) Granites of crustal or mainly crustal origin (orogenic granites); (2) Granites of crustal + mantle origin, i.e., hybrid granites (orogenic granites); and (3) Granites of mantle or mainly mantle origin (anorogenic granites). In this classification, the crustal origin granites are characterized by low (A) and (T) indices and the mantle origin granites with high (A) and (T). In between, the hybrid granites are essentially represented by the calc-alkaline rocks.

Granites of crustal or mainly crustal origin (orogenic granites) include:

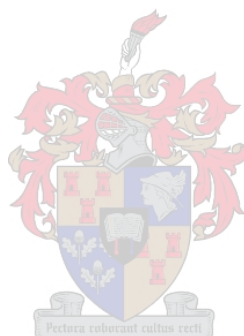
- a.** Autochthonous and intrusive aluminous leucogranite;
- b.** (Sub) autochthonous monzogranites and granodiorites;
- c.** Intrusive aluminous monzogranites and granodiorites.

Granites of crustal + mantle origin i.e. hybrid granites (orogenic granites) comprise:

- a. Calc-alkaline series granites;
- b. Sub-alkaline series granites.

Granites of mantle or mainly mantle origin (anorogenic granites) include:

- a. Alkaline series granites
- b. Tholeiitic series granites.



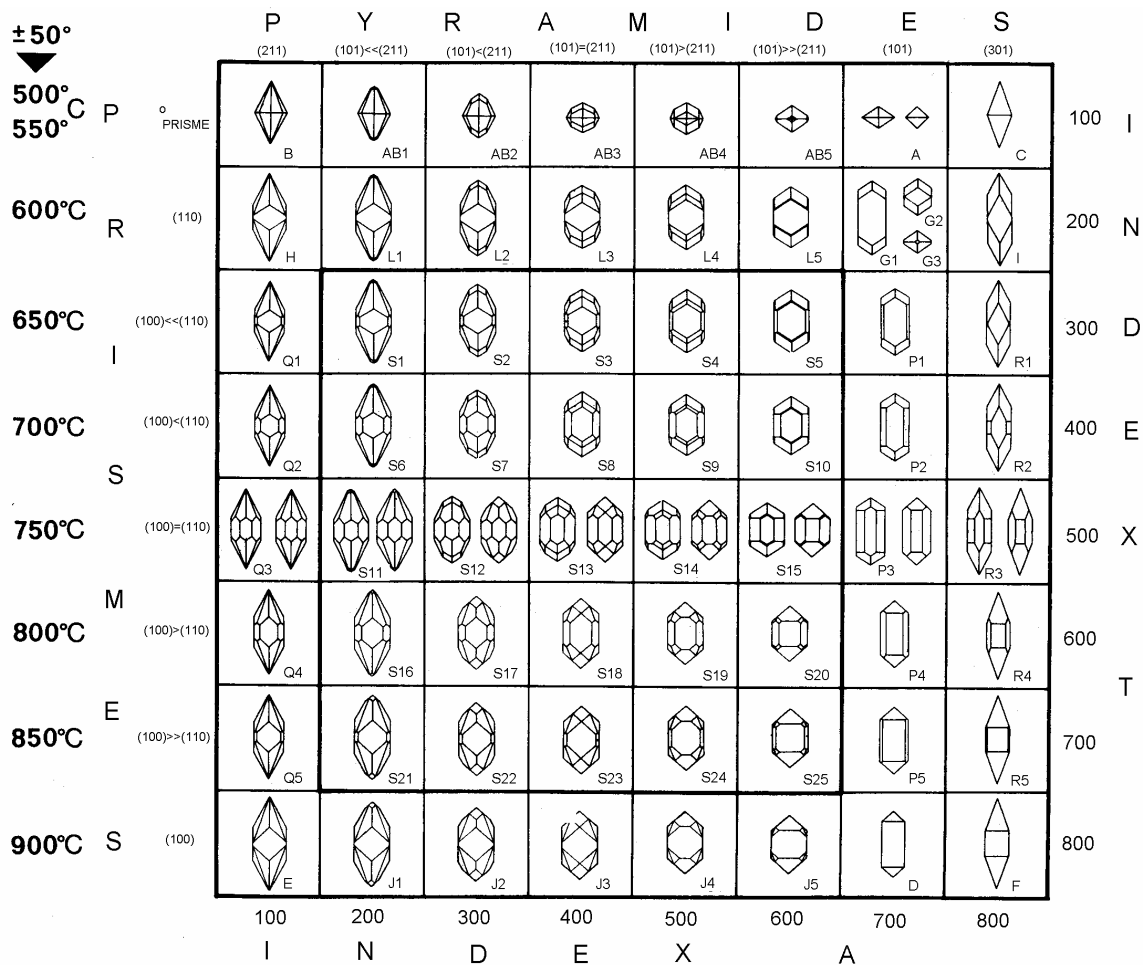


Figure 6.1 Zircon morphology classification diagram (Pupin, 1980). The classification is based upon the development of both the prismatic (T) and pyramidal (A) faces of individual minerals. Also shown is the temperature at which each subtype forms.

The majority of the zircons within the investigated fans are quite small; their size ranges from 80 to 150 μm , with very few grains exceeding 150 μm . A detailed study of the Tanqua zircon sizes reveals that the zircon population averages 125.72 μm ($n = 68$), 126.48 μm ($n = 75$), and 131.37 μm ($n = 43$) within Fans 3, 5 and 4 respectively. This suggests that the zircon groups of the investigated sand units are very similar especially for Fan 3 and Fan 5. In Fan A and Fan F of the Laingsburg Formation, the zircon size averages 124.83 μm ($n = 35$) and 127.15 μm ($n = 48$) respectively. The narrow zircon grain size range observed here is indicative of a strong similarity existing between the two submarine fan complexes.

Most of zircons are perfectly euhedral, with well developed and very well preserved crystal faces (Fig. 6.2). The investigated populations show no or an extremely minimal degree of rounding, implying a very short travel distance of the sediments and a nearby source area. Subrounded and overgrowth species are not abundant, but are present in all samples. This may imply subordinate sedimentary and/or metamorphic sources.

Samples from the investigated fans are all very similar, having a dominance of subpopulation around type S with a secondary occurrence of type P (Fig. 6.3). Abundant in all the fans are subtypes S18, S13 and S19, in decreasing order. Although not abundant, P1, P2, P3, P4 and P5 subtypes are also present. This classifies the investigated zircon groups with an A index of 200 to 700 and a T index of 400 to 700. The temperature of formation of those subtypes ranges from 700 to 850°C.

The Skoorsteenberg and Laingsburg deepwater fan sandstones contain an important number of detrital zircons with growth discontinuities, vitreous inclusions and sharp edges, suggesting a volcanic origin (Pupin, 1980; Dabard et al., 1996).

A similar distribution of zircons from the Skoorsteenberg and Laingsburg submarine fans in the morphological diagram suggests that the two deepwater

fan complexes certainly originated from the same source. Furthermore, the dominance of subpopulation (S) over other subgroups indicates that the fans derived mainly from a hybrid (mantle + crust) source (Pupin 1980). The Tanqua and Laingsburg subbasins were filled from an intermediate source consisting mainly of tonalites (T) and orogenic calc-alkaline rhyolites (CAR) as indicated by the predominance of S18, S13 and S19 subtype zircons (Fig. 6.3).

The mixed nature (crust + mantle) of the main source results in a complex genetic model. The variation of one component of the sum (crust + mantle) did affect the distribution of the zircon population within the investigated fans. The sum (crust + mantle) did not remain constant during the infill of the basin. This resulted in a slight change in the nature of Fan 4 of the Skoorsteenberg Formation.

Fan 4 indeed shows a slightly different origin. This fan resulted from the same source slightly enriched in alkaline rocks. In fact, zircons from Fan 4 are inclusion-rich compare to the populations of other fans. Generally, zircons from sialic crust are inclusion-poor and are similar to those found in migmatites. Inclusions become more numerous and diversified as the mantle component of the sum (crust + mantle) increases (Pupin, 1980).

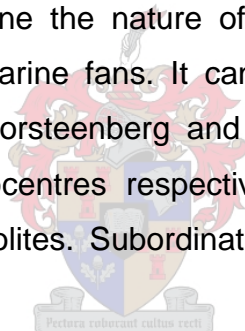
A small group of type P zircons (generally less than 10 % of the total classified grains) identified in this investigation indicates a minor contribution of alkaline basalt rocks.

The paucity of overgrowths and rounded zircons excludes the possibility of the metasedimentary Cape Fold Belt being the main supplier of the sediments that filled the Permian Laingsburg and Tanqua Karoo subbasins as proposed by various investigators (Lock, 1980; Kingsley, 1981; Hälbig, 1983; Cole, 1992; Veevers et al., 1994; Adelman and Fiedler, 1998).

The assumption that the Skoorsteenberg and Laingsburg submarine fans originated mainly from the Cape Fold Belt suggests that the heavy mineral group,

within the investigated sandstone samples, includes abundant subrounded to rounded zircons due to recycling from the cratonic hinterland to the Cape Supergroup and then transported into the Eccca Group. So far, no evidence supports such a source. The angularity of quartz and feldspar grains and the abundance of rock fragments exclude the possibility of a main sedimentary source. Also, the predominance of high-grade metamorphic garnet as discussed earlier in this thesis is not consistent with a dominantly low-grade metamorphic provenance such as the Cape Fold Belt.

Sedimentary and plutonic/metamorphic materials can be considered as subordinate sources. The latter certainly resulted from progressive unroofing of the basement and older sediments during the infill of the subbasins. Trace and rare earth element chemistry obtained from the same investigated zircons will also help to precisely determine the nature of the main source rocks of the Tanqua and Laingsburg submarine fans. It can be noted, however, from this typological study that the Skoorsteenbergr and Laingsburg Formations, in the Tanqua and Laingsburg depocentres respectively were derived mainly from tonalites and calc-alkaline rhyolites. Subordinate source rocks included alkali basalts.



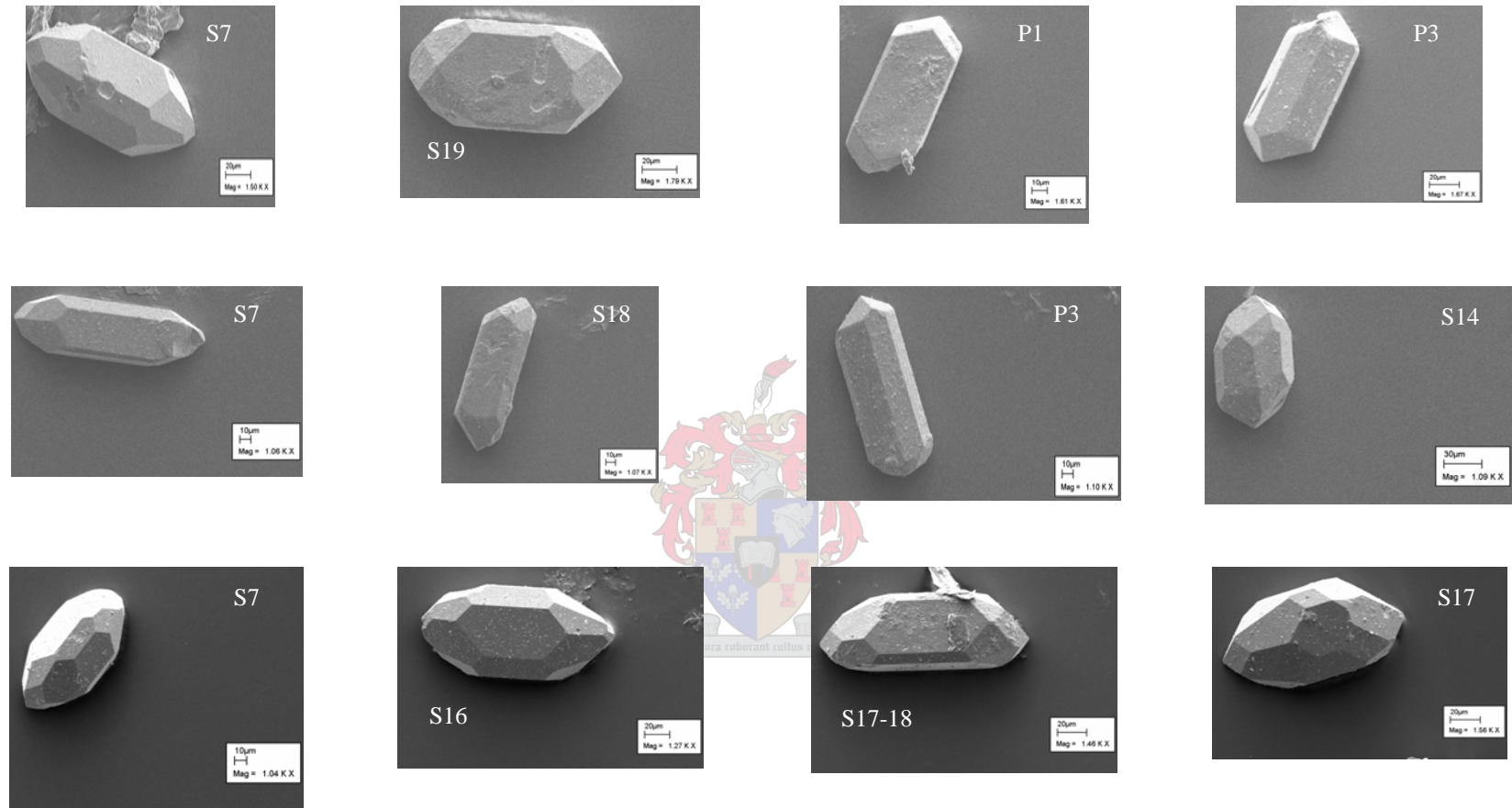


Figure 6.2 SEM images showing zircon morphologies in various sandstone samples from the Skoorsteenberg Formation. Fan 3 (first row), Fan 4 (second row), and Fan 5 (third row). Note that zircons show very well preserved crystal faces due to no or limited mechanical transport and abrasion

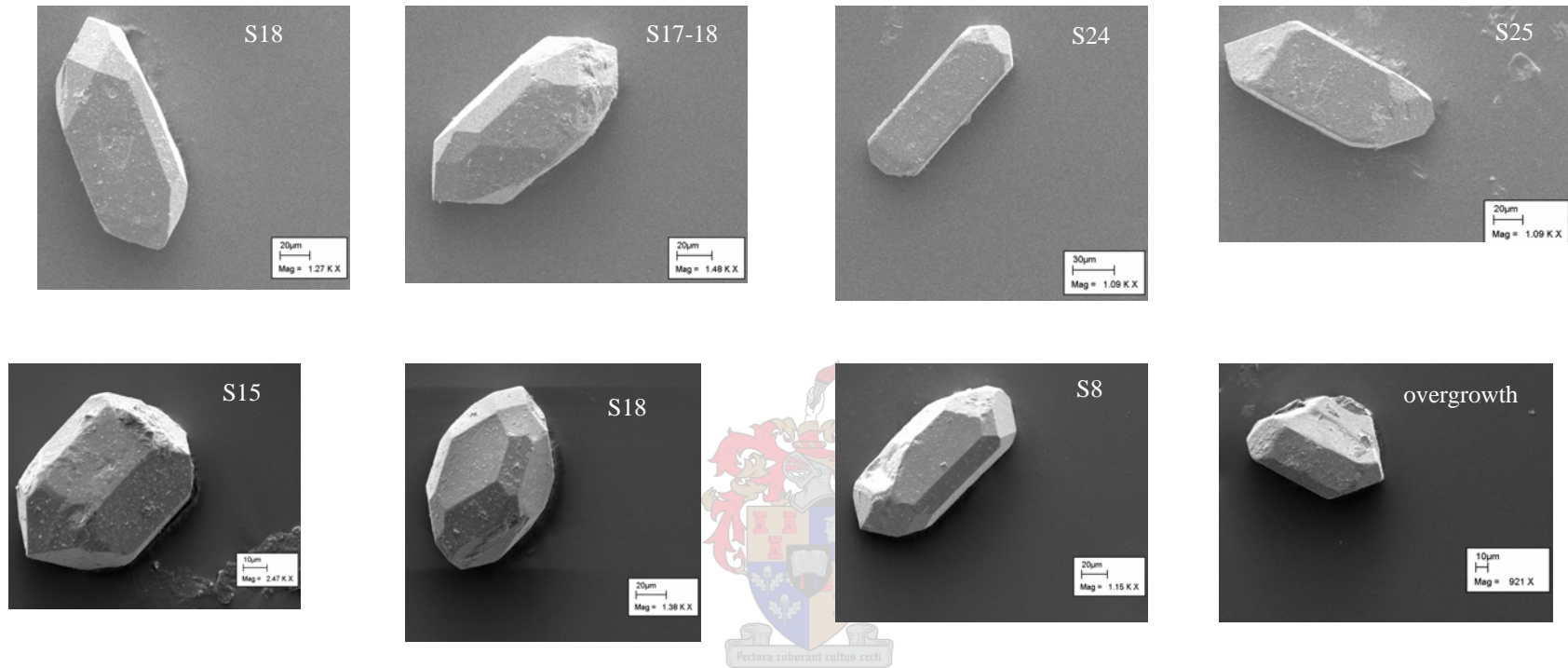


Figure 6.2 (continued) SEM images showing zircon morphologies in various sandstone samples from Laingsburg fans. Fan A (first row) and Fan F (second row). Grains show very well preserved crystal faces due to no or limited mechanical transport and abrasion.

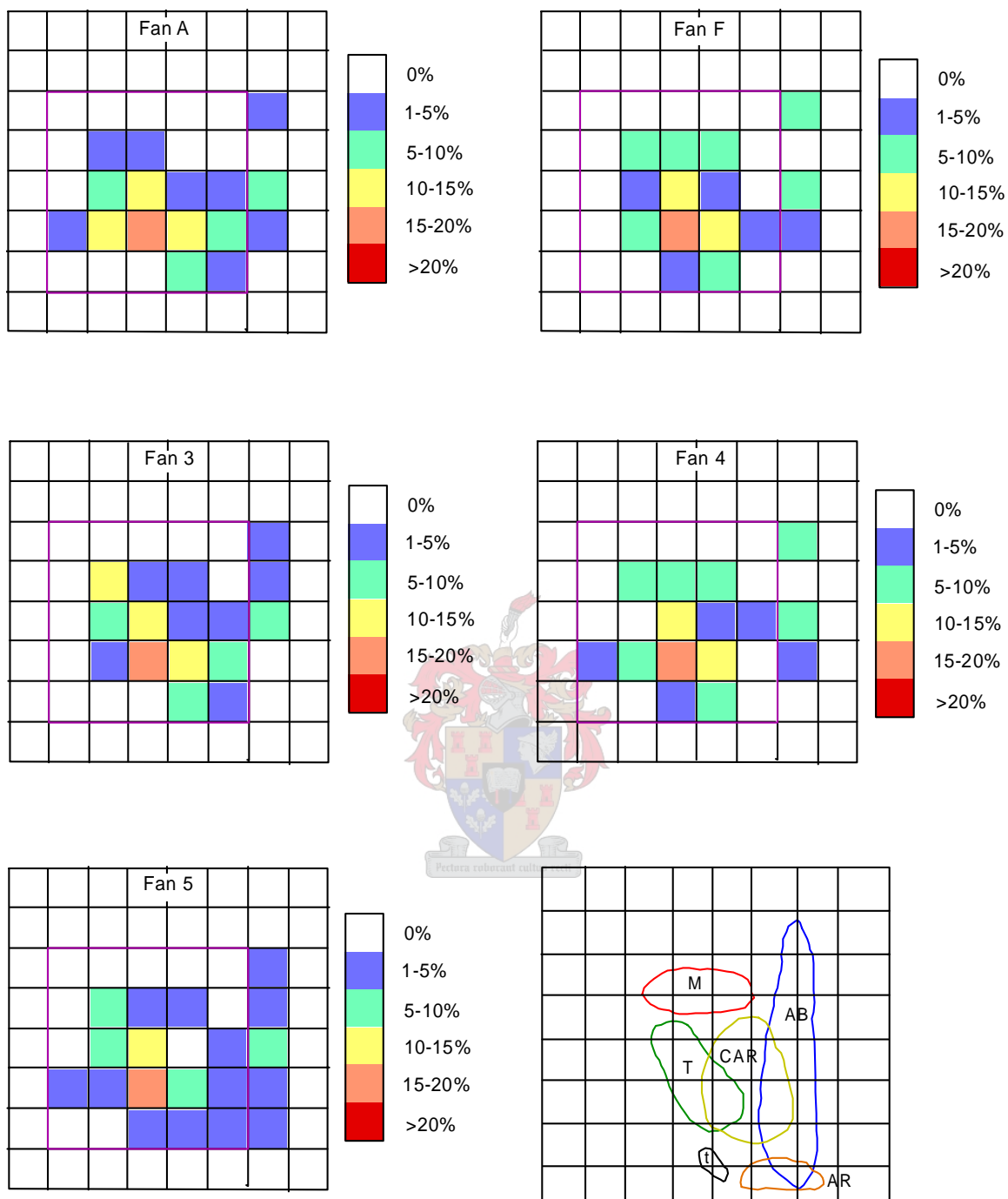


Figure 6.3 Morphological classification of detrital zircons from Fans A and F (Laingsburg Formation) and Fans 3, 4 and 5 (Skorsteenbergr Formation), based on SEM image interpretation. Also shown is the distribution of some non-granitic groups of endogenous rocks including (AB) alkaline basalts; (AR) alkaline series rhyolites from anorogenic complexes; (CAR) calc-alkaline series rhyolites (orogenic); (M) migmatites; (*t*) trachyandesites series; (T) tonalites (Pupin, 1980).

6.3 Zircon chemistry

Chondrite normalized rare earth element patterns of the Skoorsteenberg and Laingsburg deepwater basin floor fan detrital zircons analyzed in this study are very similar. These normalized patterns are characterized by a steeply-rising slope from the light rare earth elements (LREE) to the heavy rare earth elements (HREE) with a positive Ce-anomaly and a negative Eu-anomaly (Fig. 6.4 and Fig. 6.5). This pattern is characteristic for unaltered zircon (Hoskin and Schaltegger, 2003). In general, REE patterns of investigated zircons from Fans 3, 4 and 5 of the Skoorsteenberg Formation in the Tanqua subbasin and analyzed zircons from Fans A and F of the Laingsburg Formation in the Laingsburg subbasin rise rapidly from Gd to Lu (Fig. 6.4 and Fig. 6.5). Because the ionic radii of the REE decrease from La^{3+} to Lu^{3+} (Shannon, 1976), the substitution into the zircon lattice becomes progressively easier for the REE of higher atomic number (Nagasawa, 1970; Hancher et al., 2001). Therefore, the typical chondrite-normalized REE zircon patterns increase rapidly from Sm to Lu (Fig. 6.6).

The large range of REE concentrations, from tens of ppm to several per cent, distinguishes zircons of different origin. Zircons from pegmatites and granitoids show the highest concentration of rare earth elements (ΣREE up to 1.5-2 wt %), lower amounts of REE (ΣREE up to 90 to 480 ppm) are typical for zircons from mafic rocks and kimberlitic zircons contain the lowest concentrations of REE (typically less than 50 ppm) (Belousova et al., 2002).

Analyzed zircons show variable abundances of ΣREE (Appendix C). Fan A and Fan F in the Laingsburg area show ΣREE concentrations ranging from 504 to 4133 ppm and 575 to 2265 ppm respectively. The Tanqua Fans 3, 4 and 5 show REE abundances which range from 613 to 3462, 695 to 3433 and 1298 to 4742 ppm respectively. These highest REE abundances obtained from analyzed

zircons suggest that both the Laingsburg and Tanqua Karoo sediments were mainly derived from granitoids and/or syenite pegmatites.

The size of Eu anomalies ($\text{Eu}/\text{Eu}^* = \text{Eu}_N/(\text{Sm}_N \cdot \text{Gd}_N)^{1/2}$) of analyzed zircons was measured. Belousova et al. (2002) have shown that the kimberlitic and carbonatic zircons show little or no Eu anomaly. In addition, the Eu anomaly becomes significant in zircons from more felsic, fractionated rock types. Eu^{2+} is less compatible in zircon than Eu^{3+} , but the absence of a negative Eu anomaly in some zircons, and its ubiquitous appearance in zircons from fractionated and relatively oxidized rocks such as granitoids, where most Eu would be expected to be divalent, suggests that these anomalies largely reflect partitioning of Eu^{2+} into plagioclase during magmatic evolution. All the zircons analyzed in this study show a high negative Eu anomalies (Fig. 6.4 and Fig. 6.5) suggesting that those zircons crystallized from felsic magmas (Belousova et al., 2002).

Identical to the Eu/Eu^* ratio, the Ce/Ce^* ratio describes the enrichment of Ce relative to a smooth REE pattern. Most of zircons analyzed in this study show a positive Ce anomaly (Fig. 6.4 and Fig. 6.5). The size of the Ce anomaly is given by Ce/Ce^* (with the Ce/Ce^* ratio being equal to $\text{Ce}_N/(\text{La}_N \cdot \text{Pr}_N)^{1/2}$). According to Belousova et al. (2002), zircons from syenitic pegmatites show the most pronounced Ce anomalies (Ce/Ce^* from 2 to over 300), whereas weak Ce anomalies (Ce/Ce^* from 1 to 10) are typical of zircons from kimberlites, carbonatites and granitoids. In addition, most zircons from granitoids have Ce/Ce^* within a restricted range from 1 to 3. The majority of zircons analyzed in this study show a Ce positive anomaly value below or almost equal to 3 (Appendix C), suggesting granitoids or equivalents as the main sources of the Laingsburg and Tanqua Karoo submarine fans. Contrary to zircons found in pegmatites, carbonatic and kimberlitic zircons show almost no Ce anomalies, indicating a low oxidation state of the source magma (Shnukov et al., 1989).

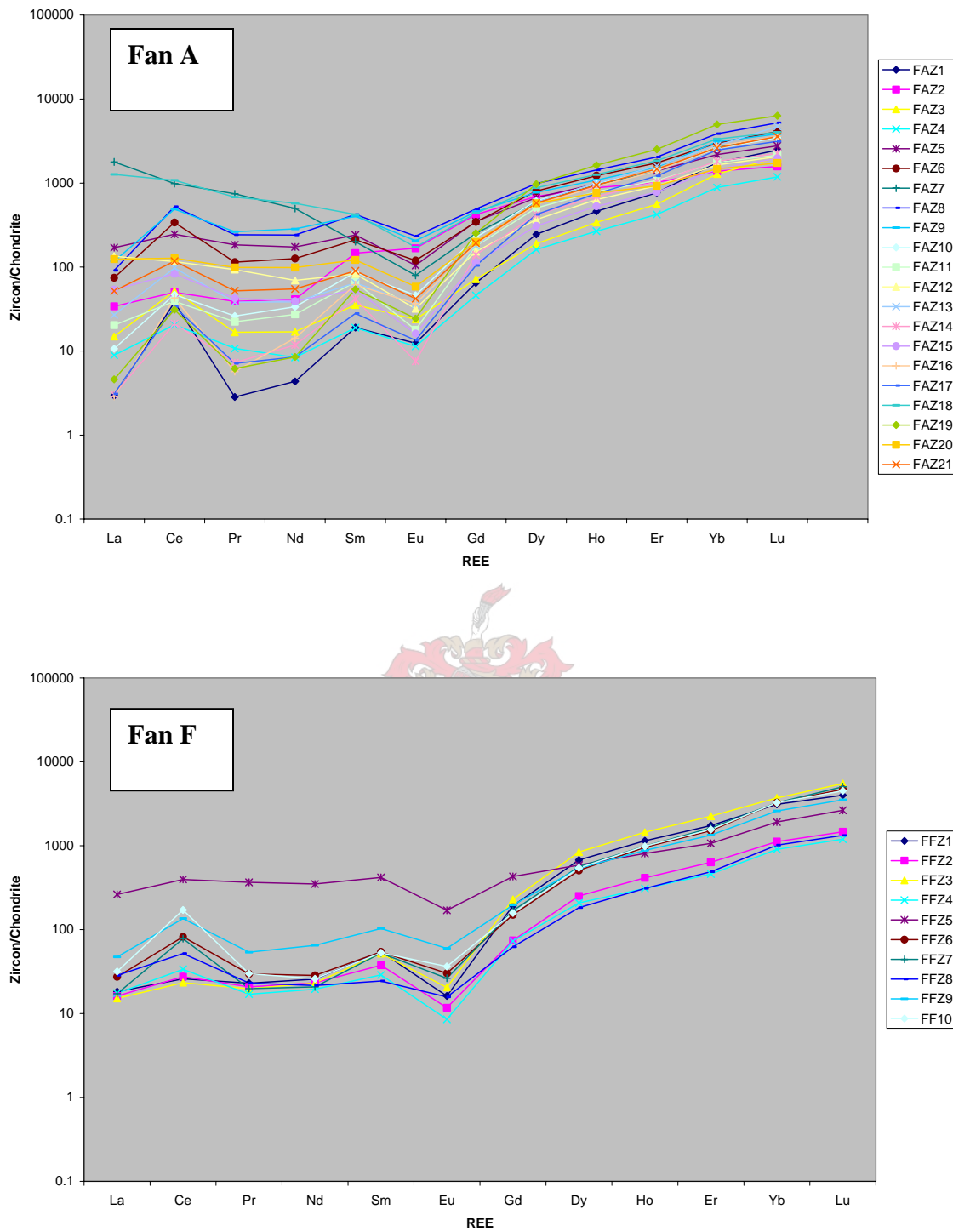


Figure 6.4 Chondrite-normalized rare-earth element plots for the Laingsburg fans. Chondrite-normalized values are from Taylor and McLennan (1985).

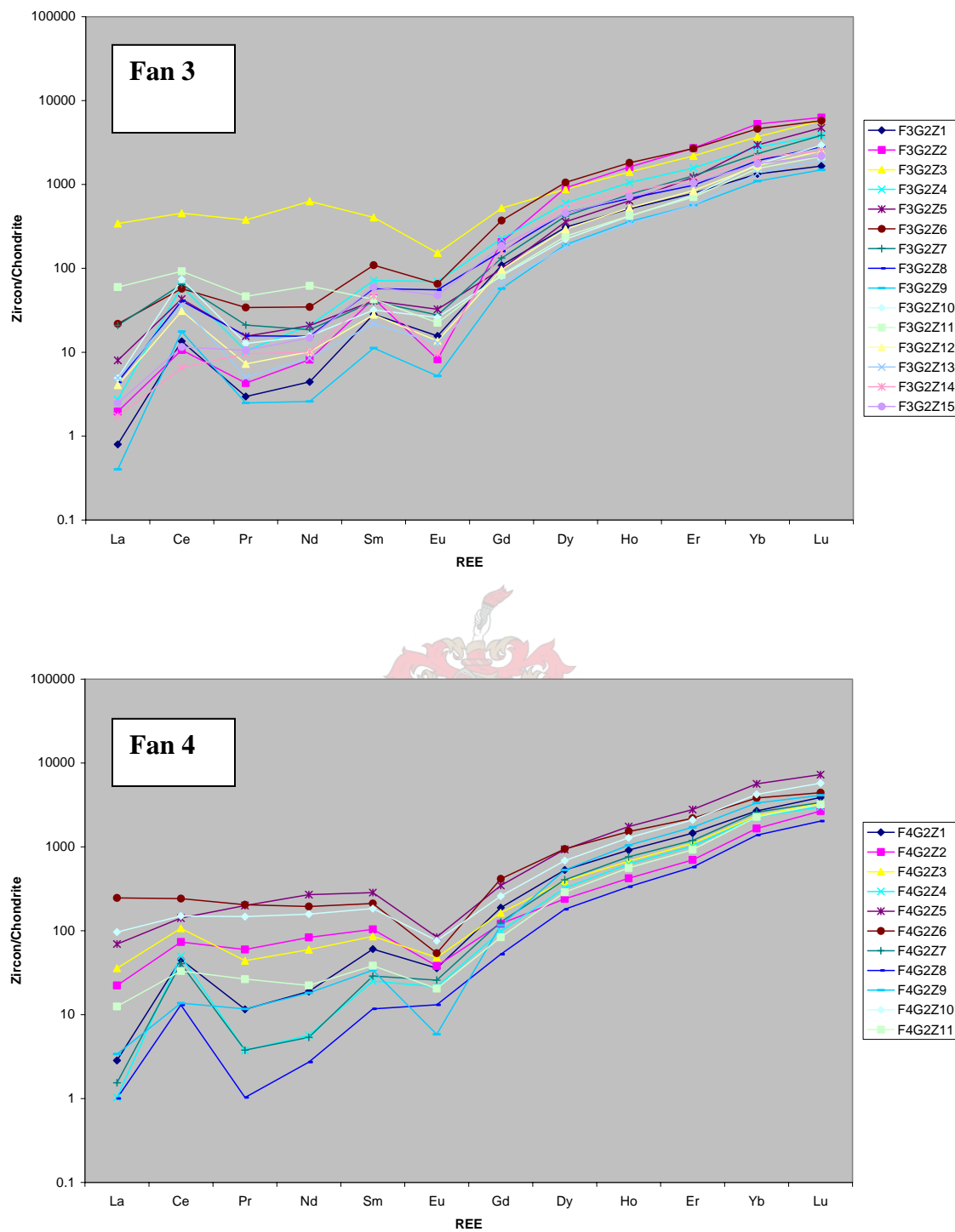


Figure 6.5 Chondrite-normalized rare-earth element plots for the Tanqua fans. Chondrite-normalized values are from Taylor and McLennan (1985).

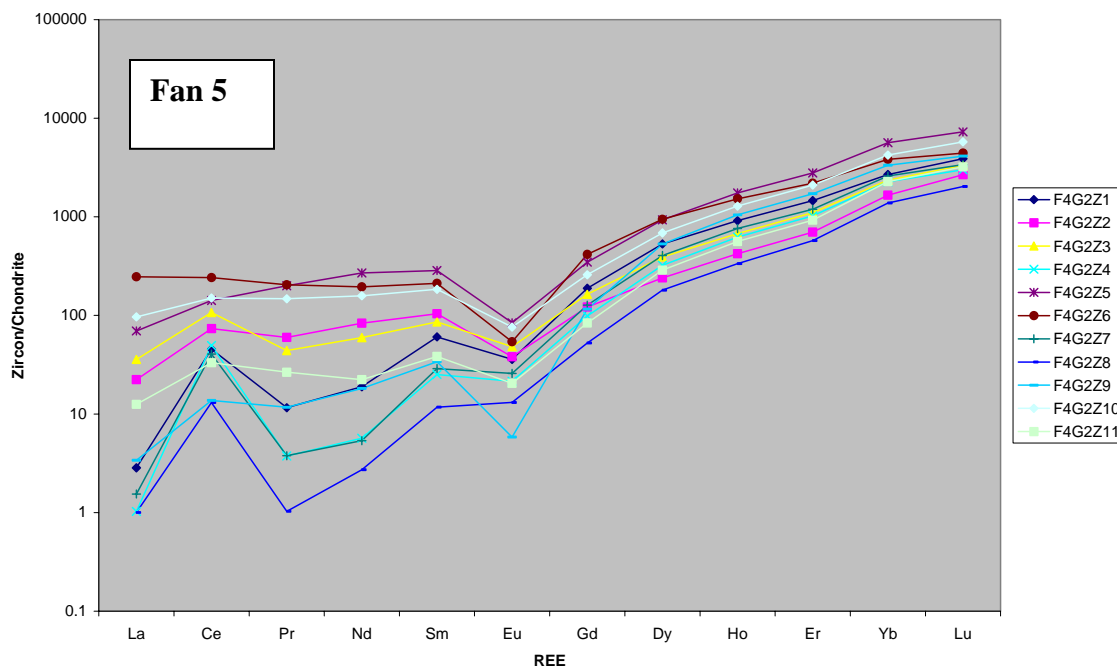


Figure 6.5 (continued).

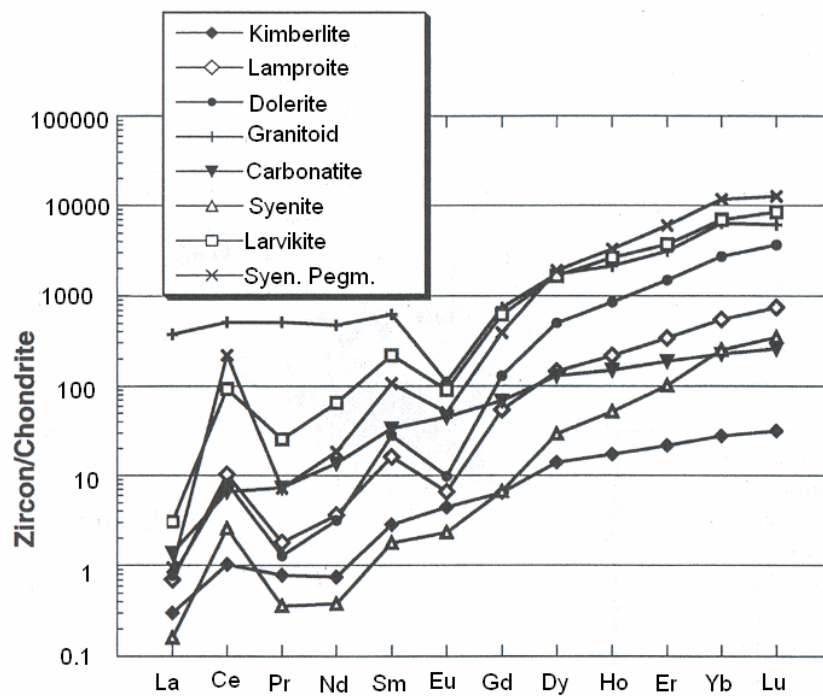


Figure 6.6 Chondrite-normalized averaged REE patterns of zircons from a range of rock types (Belousova et al. 2002).

Belousova et al. (2002) recently defined a classification and regression tree (CART) to recognize zircons from different rock types (Fig. 6.7). Data sets of elements of the “tree” includes Hf, Lu, Y, U and Yb. Zircons from kimberlites, carbonatites, mafic rocks (diabase + basalt), syenitic rocks (syenites and larvikites) and Ne-syenite pegmatites are recognized with a probability of correct classification of more than 80%. Zircons from granitoids (as a group) are identified with a probability exceeding 75%, whereas the classification of these into groups of different SiO₂ content is more ambiguous. Zircons from granitoids with 65-70% SiO₂ generally classify as crystallising within rocks with either higher (40%) or lower (30%) SiO₂ contents. The probability of correct classification by SiO₂ group for zircons from other granite classes ranges from 49% for those with 70-75% SiO₂, to 63 % for those with >75% SiO₂ (Belousova et al., 2002).

The CART tree is similar to a botanical key, with binary switches defined by element concentrations. A zircon grain is run through the tree and ends up in a terminal node that corresponds to rock type (Belousova et al., 2002). The possible source rock in which a given zircon occurs was deduced by comparing the value of a specific element proposed by the CART with the value of the same element obtained by LA-ICP-MS analysis. Every single zircon grain was then classified.

This study optimizes the result of this classification by integrating various analytical approaches of provenance discrimination. These include the fields of zircon composition defined by the same authors (Fig. 6.8-6.13), the morphological classification diagram of Pupin (1980), the chemical composition of detrital sphenes, and major and trace element characteristics of the whole rock reported in the foregoing part of this thesis.

A summary of the result of the provenance determination of the Tanqua and Laingsburg submarine fans based on the CART tree is presented in Table 6.1. A

complete classification showing the origin of each analysed zircon is available in Appendix C.

The 114 single grains of zircon from different Tanqua fans analyzed in this study show a similar and dominant granitoids origin with subsidiary syenite/monzonite provenance. Of the 42 analyzed zircons from Fan 3, 40 show a granitoid derivation while 2 show a syenite/monzonite origin. A total of 36 zircons from Fan 4 were analyzed, 30 of them derived from granitoids and 6 showing a syenite/monzonite provenance. Of the 36 analyzed grains from Fan 5, 34 show a granitoid affinity and only 2 crystallized within syenites/monzonites.

Similar results were obtained from trace element chemistry of the 31 probed zircons from Fan A and Fan F of the Laingsburg subbasin. Of the 21 analyzed zircons from Fan A, 20 showed a crystallization within granitoids and only 1 showed chemical composition of basalt zircons. Zircon chemistry also shows that 90 % of the sediments in Fan 5 were derived from granitoids and 10 % from basalts.

Analyzed zircons from the Laingsburg and Tanqua Karoo subbasins therefore show a remarkably similar provenance. Detritus was mainly supplied by granitoids with less than 65 % SiO₂ (rhyodacite, granodiorite and tonalities) and granitoids with 70-75 % SiO₂ (granite) (Table 6.1). The granitoid source represents more than 90 % of the 145 analysed zircons. In general, syenite/monzonite and basalt represent subordinate sources of both the Tanqua and Laingsburg fans.

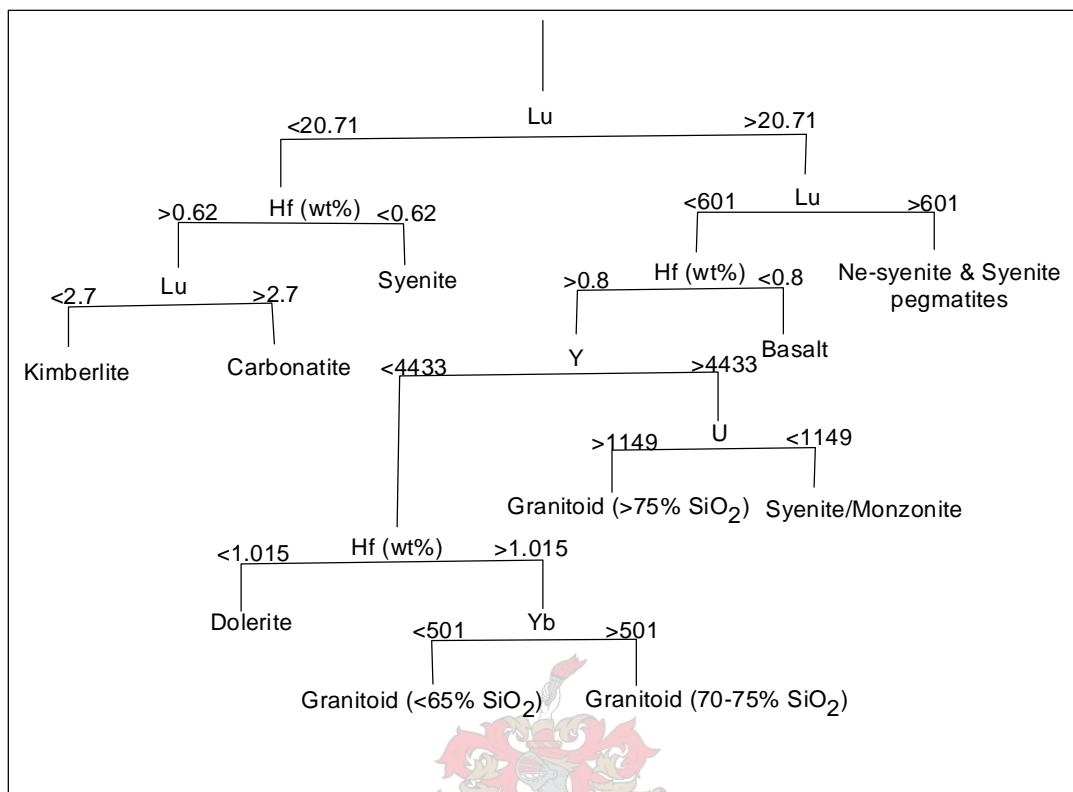


Figure 6.7 CART tree for the recognition of zircons from different rock types based on single grain trace element geochemistry (Belousova et al., 2002).

Table 6.1 Provenance determination of the Tanqua and Laingsburg submarine fan sandstones based on the CART tree (Belousova et al., 2002)

Skoorsteenberg sandstones	Total (no. grains)	Granitoids (%)			Syenite/ Monzonite (%)
		⁽¹⁾ granitoid with <65 % SiO ₂	⁽²⁾ granitoid with 70-75% SiO ₂	⁽³⁾ granitoid with >75% SiO ₂	
Fan 3	42	14 (~ 33 %)	25 (~ 60 %)	1 (~ 2 %)	2 (~ 5 %)
Fan 4	36	4 (~ 11 %)	25 (~ 69 %)	1 (~ 3 %)	6 (~ 17 %)
Fan 5	36	10 (~ 28 %)	23 (~ 64 %)	1 (~ 3 %)	2 (~ 5 %)

Laingsburg sandstones	Total (no.grains)	Granitoids (%)			Basalt (%)
		⁽¹⁾ granitoid with <65 % SiO ₂	⁽²⁾ granitoid with 70-75% SiO ₂	⁽³⁾ granitoid with >75% SiO ₂	
Fan A	21	8 (~ 38 %)	12 (~ 57)	0	1 (~ 5 %)
Fan F	10	3 (30 %)	6 (60 %)	0	1 (10 %)

(1) Rhyodacites, tonalities and granodiorite

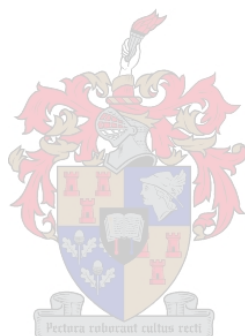
(2) Granites

(3) Leucogranite and aplite granite

Belousova et al. (2002) also proposed various discrimination frameworks based on zircon trace elemental signatures to recognize zircons from specific rock types. The provenance diagrams developed by Belousova et al. (2002) used in this investigation are Y versus U, Nb/Ta and Yb/Sm, as well as Nb versus Ta (Figs. 6.8 – 6.13). These latter suggest that the submarine Fans 3, 4 and 5 of the Skoorsteenberg Formation in the Tanqua depocentre as well as the submarine Fans A and F of the Laingsburg Formation in the Laingsburg subbasin were all predominantly derived from granitoids or their volcanic equivalents. The granitoid group of the provenance diagrams includes (1) aplites and leucogranites, (2) granites and (3) granodiorites and tonalites. It is noteworthy that although granitoid sources can be generally accepted, a complete discrimination between the aforementioned granitoids is obtained when plotting Nb versus Ta. This diagram clearly indicates that the investigated deepwater basin floor fans were mainly derived from granodiorites and tonalites or their volcanic equivalents (dacites). Syenitic rocks (syenite pegmatites and larvikites) can be considered as the Tanqua subordinate sources. Larvikites are alkalic syenites containing phenocrysts of two often intimately intergrown feldspars, especially oligoclase and alkali feldspar. An insignificant number of zircons from the Laingsburg Fan F show a basaltic derivation (Fig. 6.12).

As previously mentioned, the morphological classification diagram developed by Pupin (1980) reveals that zircon populations of the Skoorsteenberg and Laingsburg Formations are very similar and dominated by the subpopulation (S), suggesting that these formations originated mainly from tonalites and orogenic calc-alkaline rhyolites. This result is confirmed in this section by trace element abundances obtained from the same detrital zircon grains. Trace element abundance plotted on various provenance diagrams of Belousova et al. (2002) also points to tonalitic and granodioritic (or their volcanic equivalents) main sources. This confirms that the morphology of zircon reflects the physical and chemical conditions under which the mineral crystallizes (Pupin, 1980).

The Skoorsteenberg and Laingsburg provenance results obtained from both zircon morphology and zircon trace element concentrations are in perfect accordance with whole-rock major and trace element chemistry which previously indicated that the Skoorsteenberg and Laingsburg deepwater fans predominantly originated from tonalites, granodiorites and adamellite or/and their volcanic equivalents, with minor alkali-basalts.



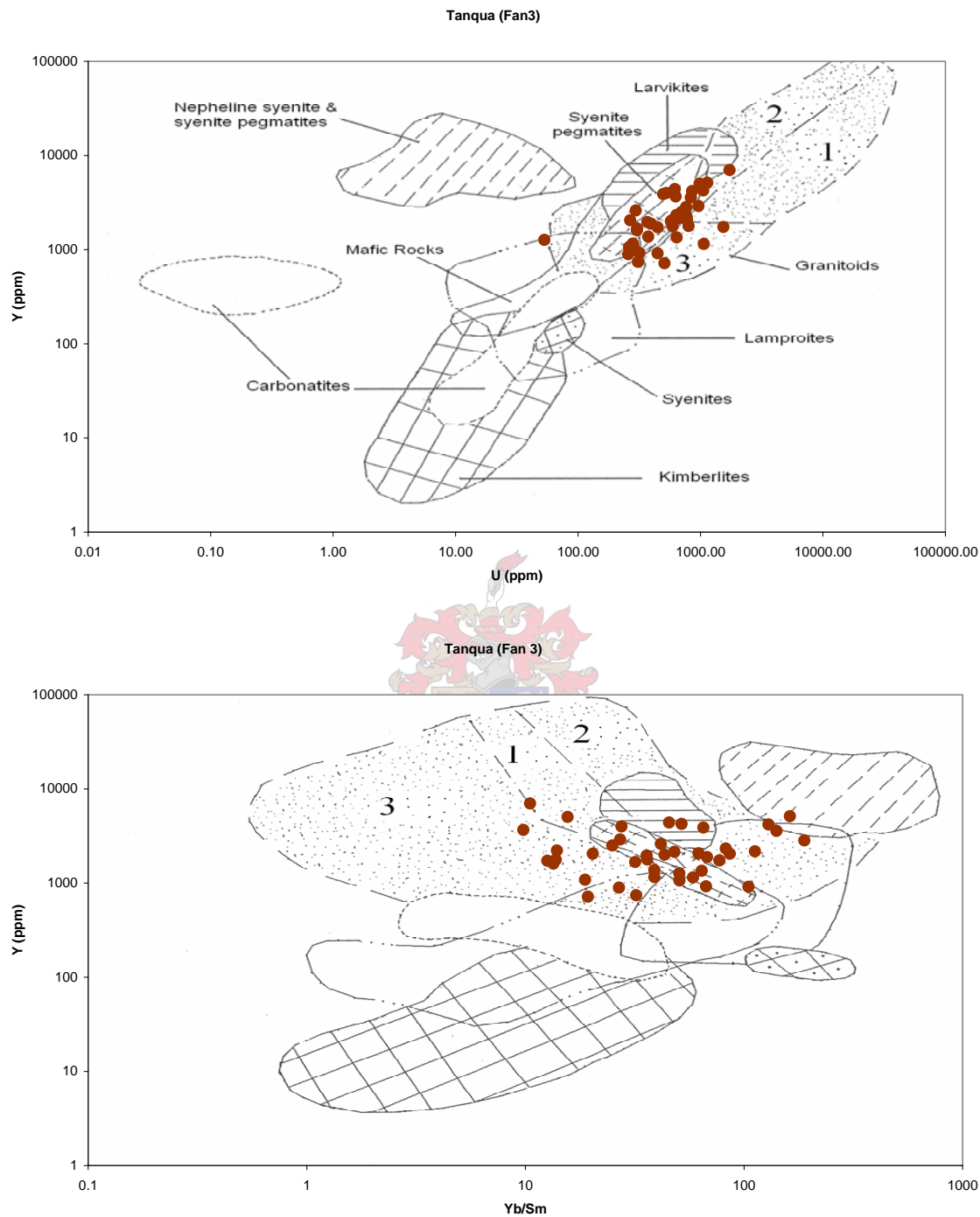


Figure 6.8 Plots of trace and rare earth element data of zircons from the Tanqua Fan 3, superimposed on the fields of zircon compositions used as discriminants for different rock types (Belousova et al., 2002). Granitoid subfields are: (1) aplites and leucogranites; (2) granites; (3) granodiorites and tonalites.

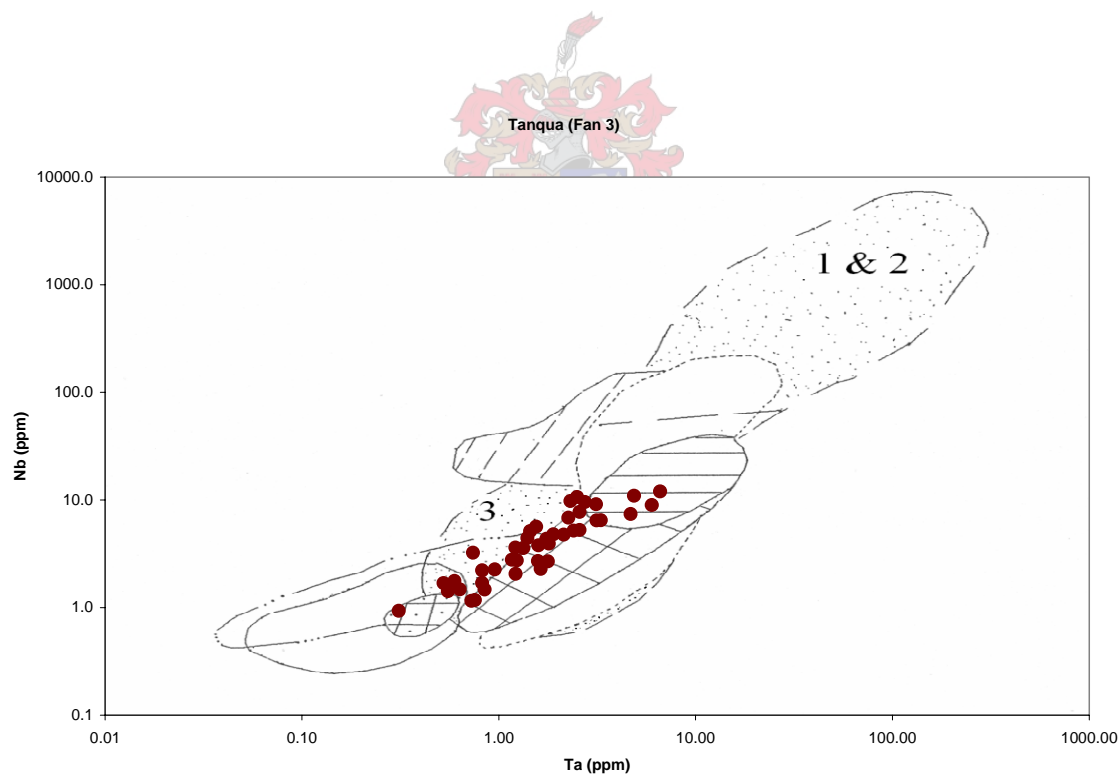
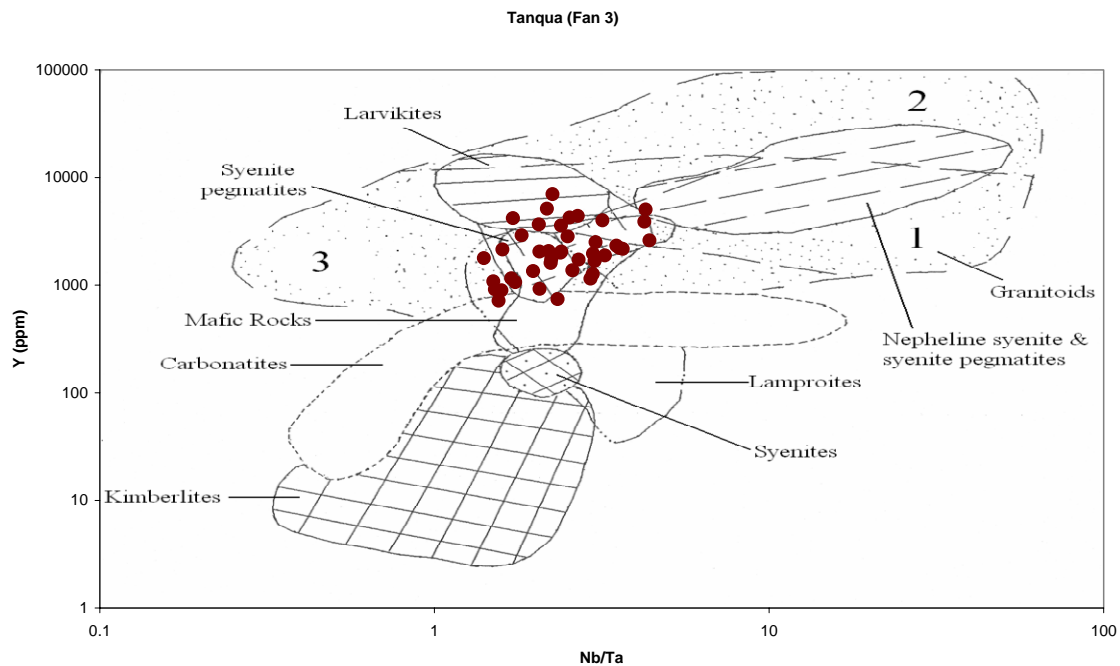


Figure 6.8 (continued). Note that compared to other diagrams that generally suggest a granitoid derivation, Nb vs. Ta points to granodioritic and tonalitic provenances precisely.

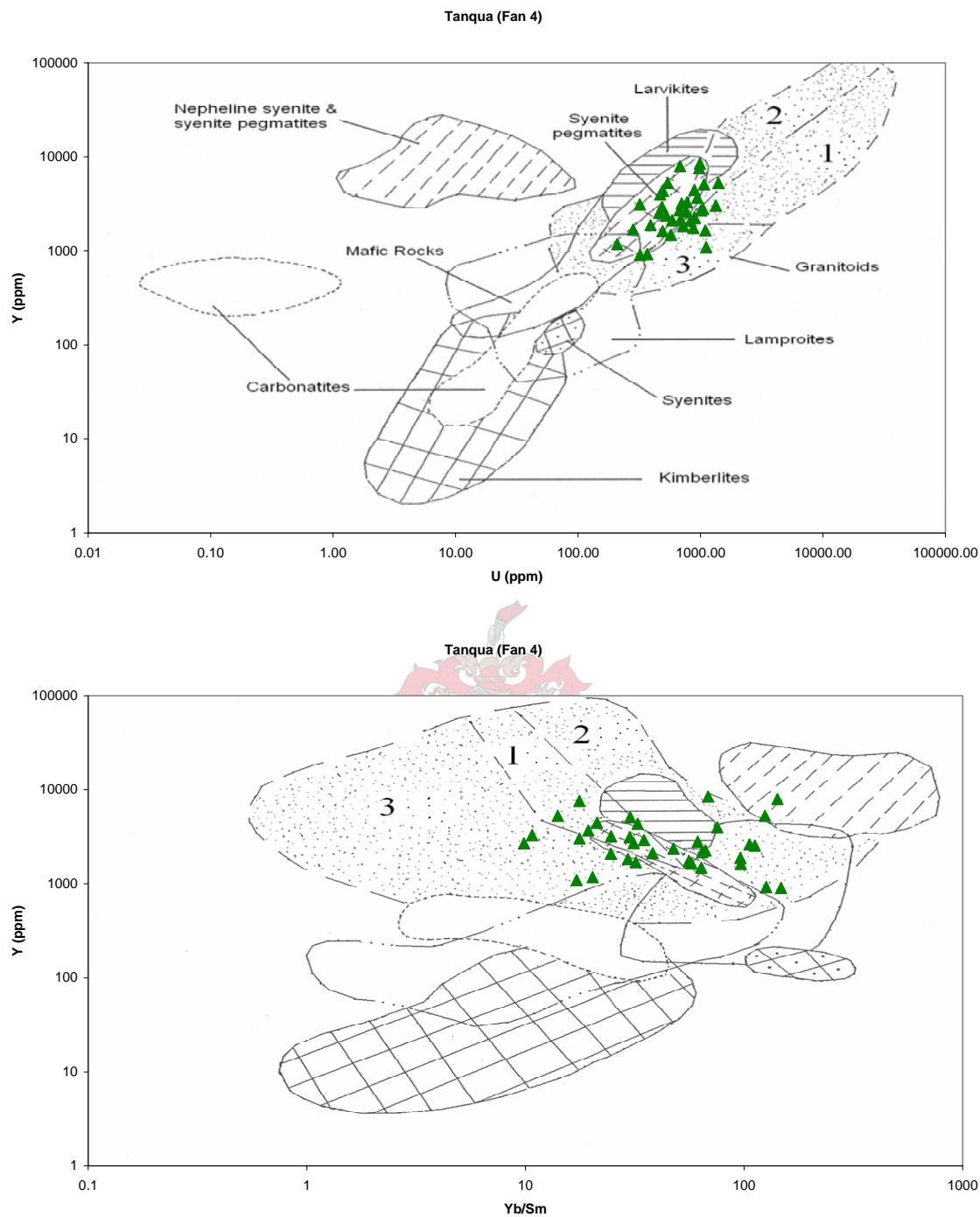


Figure 6.9 Plots of trace and rare earth element data of zircons from the Tanqua Fan 4, superimposed on the fields of zircon compositions used as discriminants for different rock types (Belousova et al., 2002). Granitoid subfields are: (1) aplites and leucogranites; (2) granites; (3) granodiorites and tonalites.

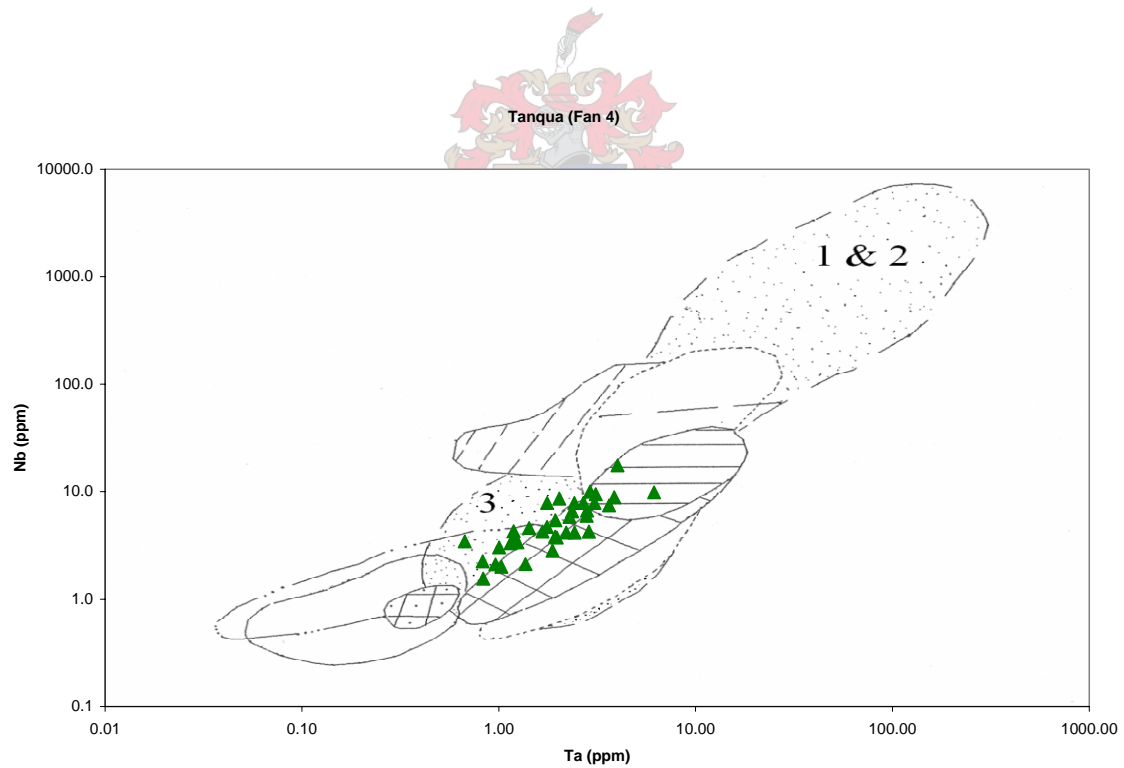
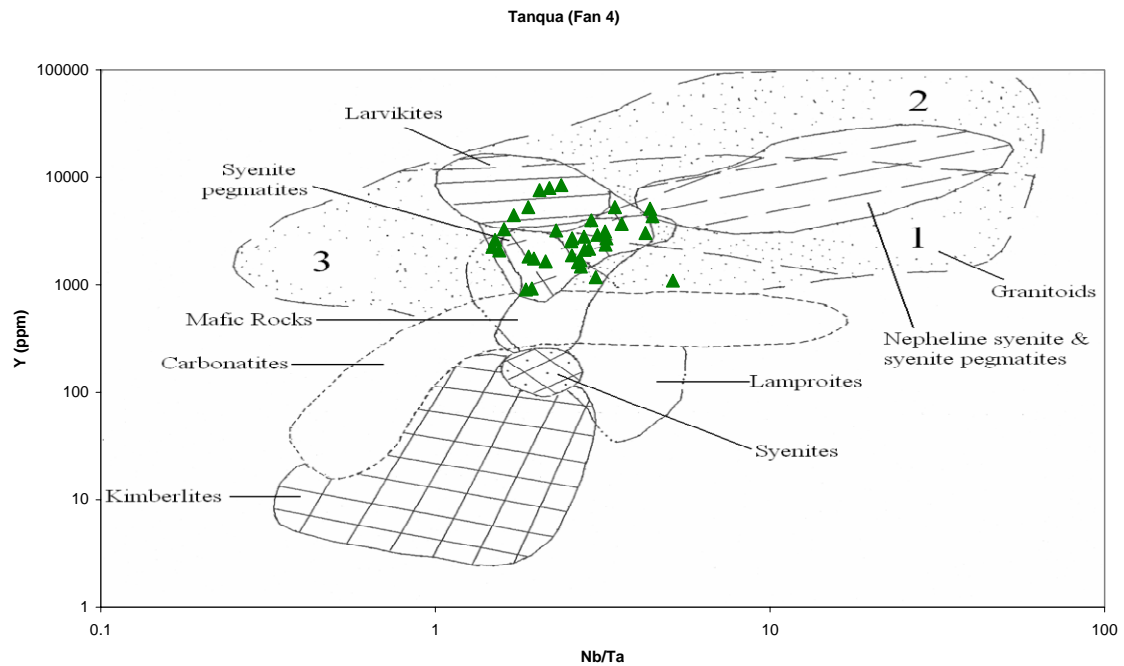


Figure 6.9 (continued).

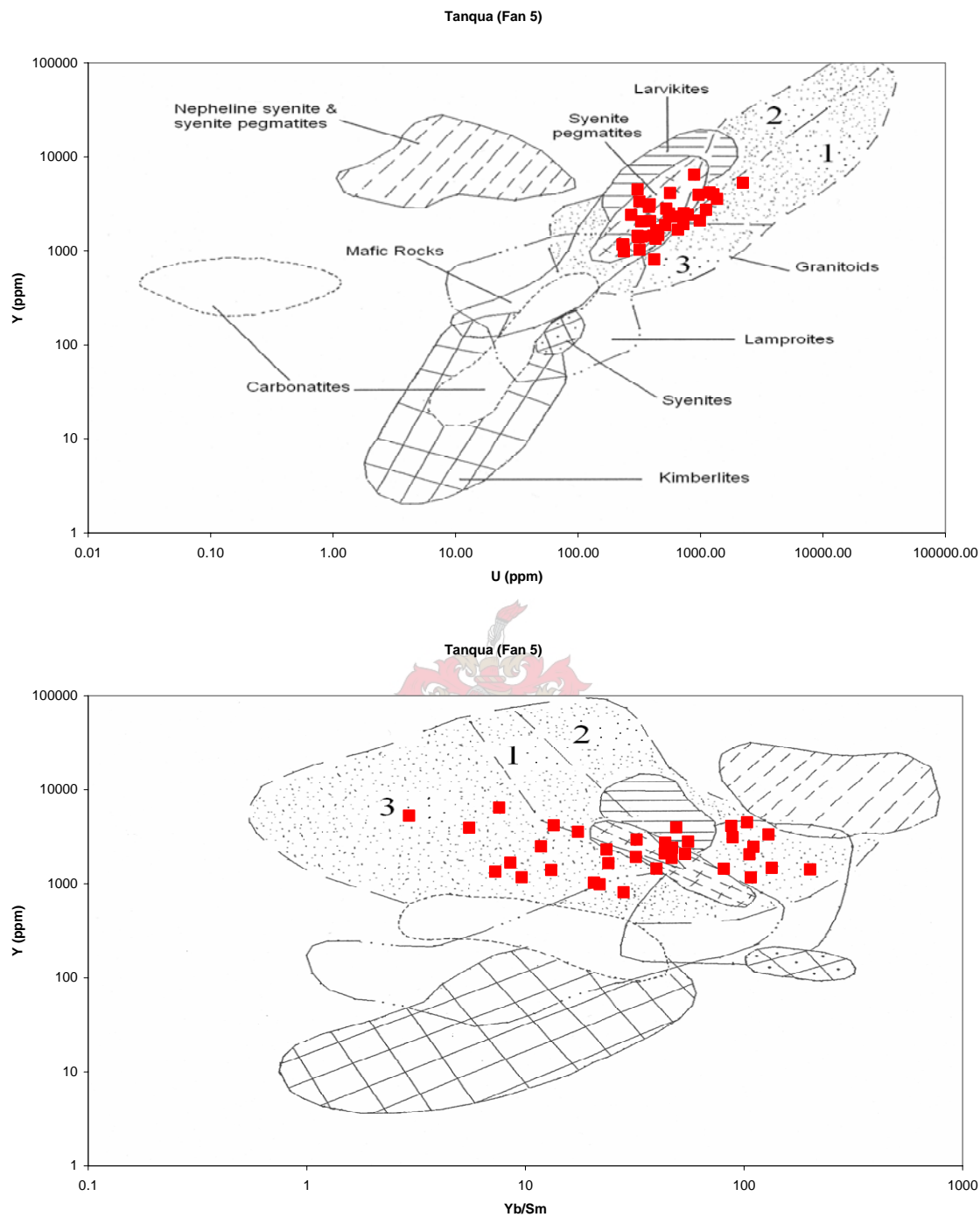


Figure 6.10 Plots of trace and rare earth element data of zircons from the Tanqua Fan 5, superimposed on the fields of zircon compositions used as discriminants for different rock types (Belousova et al., 2002). Granitoid subfields are: (1) aplites and leucogranites; (2) granites; (3) granodiorites and tonalites.

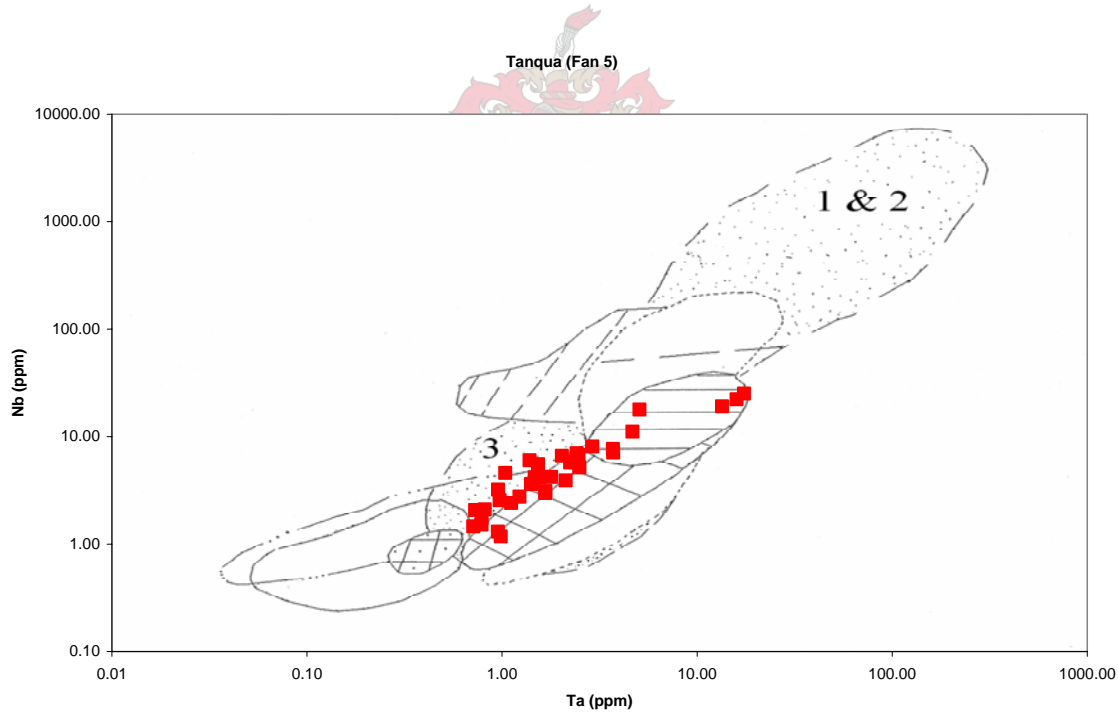
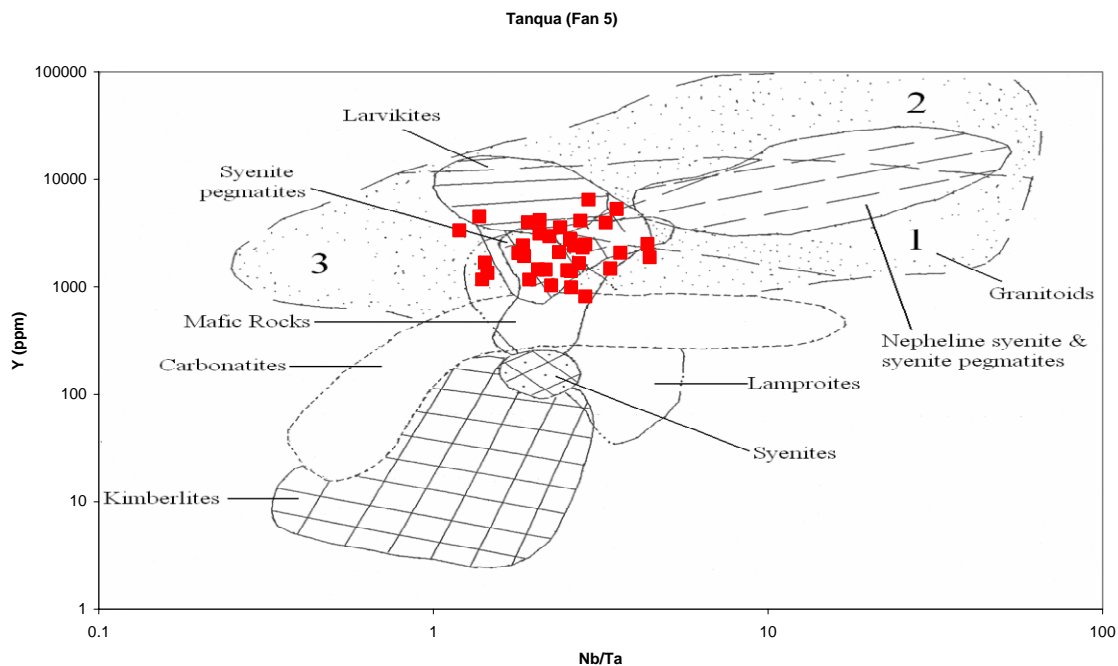


Figure 6.10 (continued).

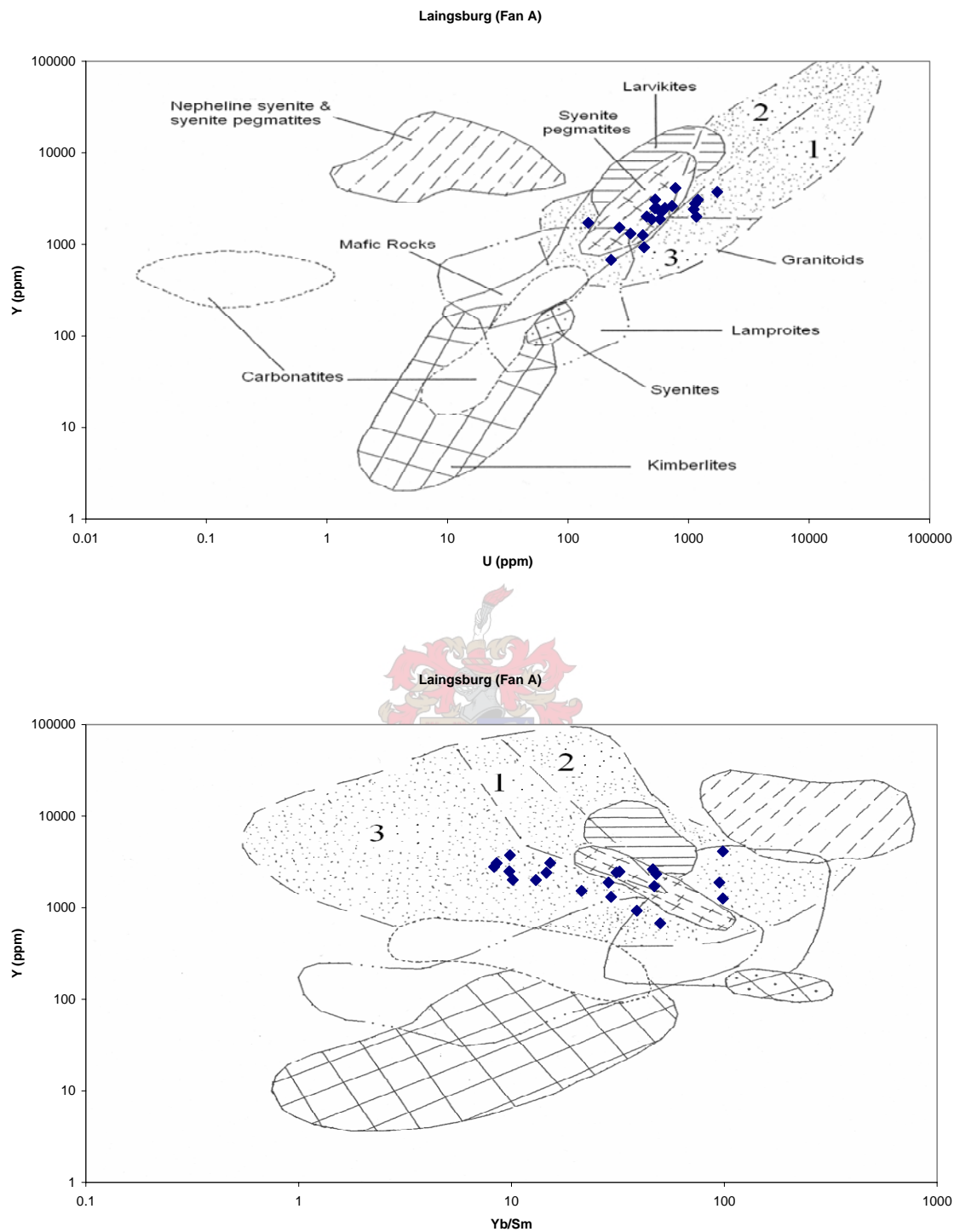


Figure 6.11 Plots of trace and rare earth element data of zircons from the Laingsburg Fan A, superimposed on the fields of zircon compositions used as discriminants for different rock types (Belousova et al., 2002). Granitoid subfields are: (1) aplites and leucogranites; (2) granites; (3) granodiorites and tonalites.

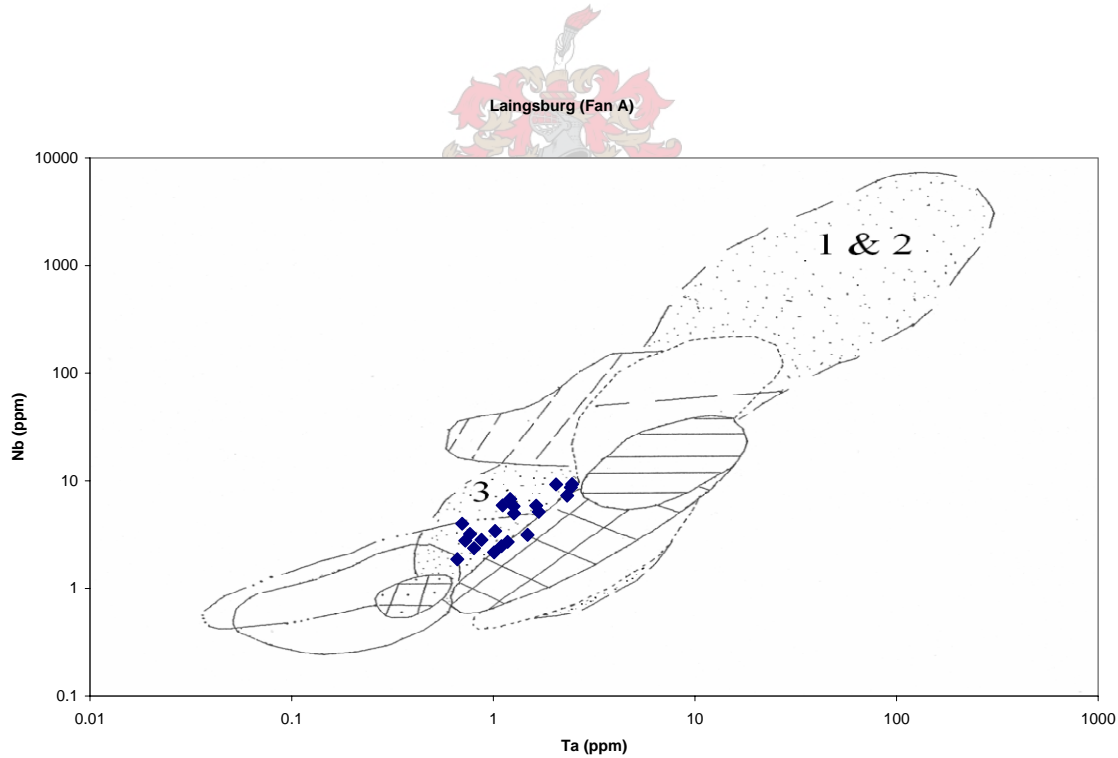
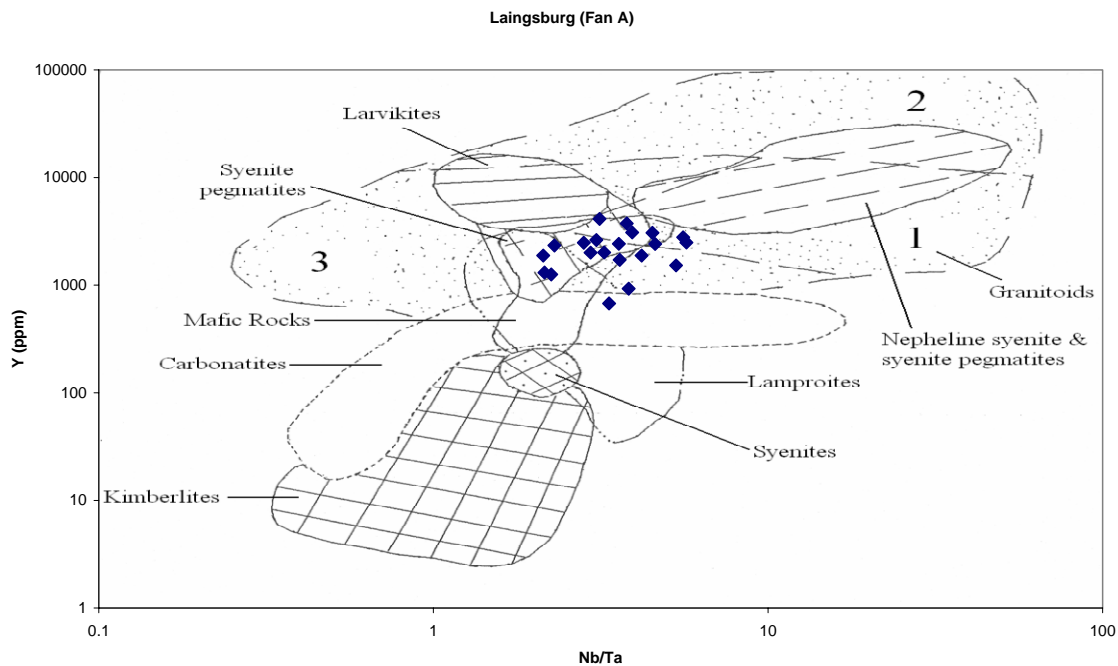


Figure 6.11 (continued).

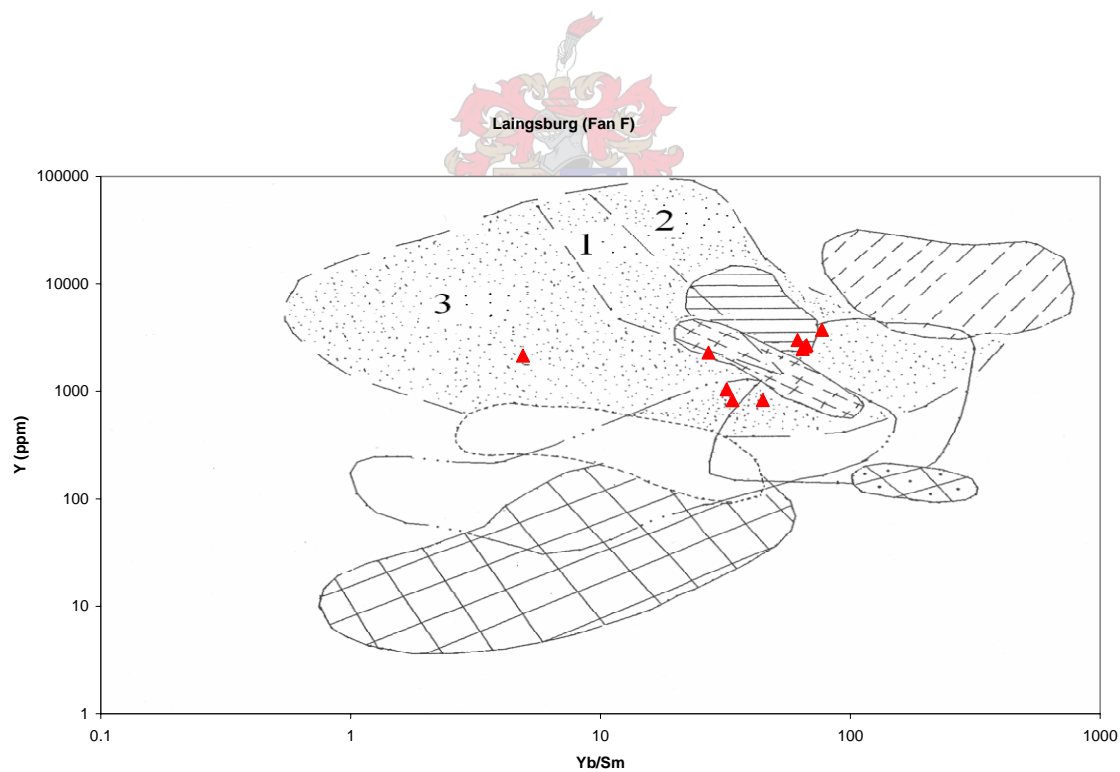
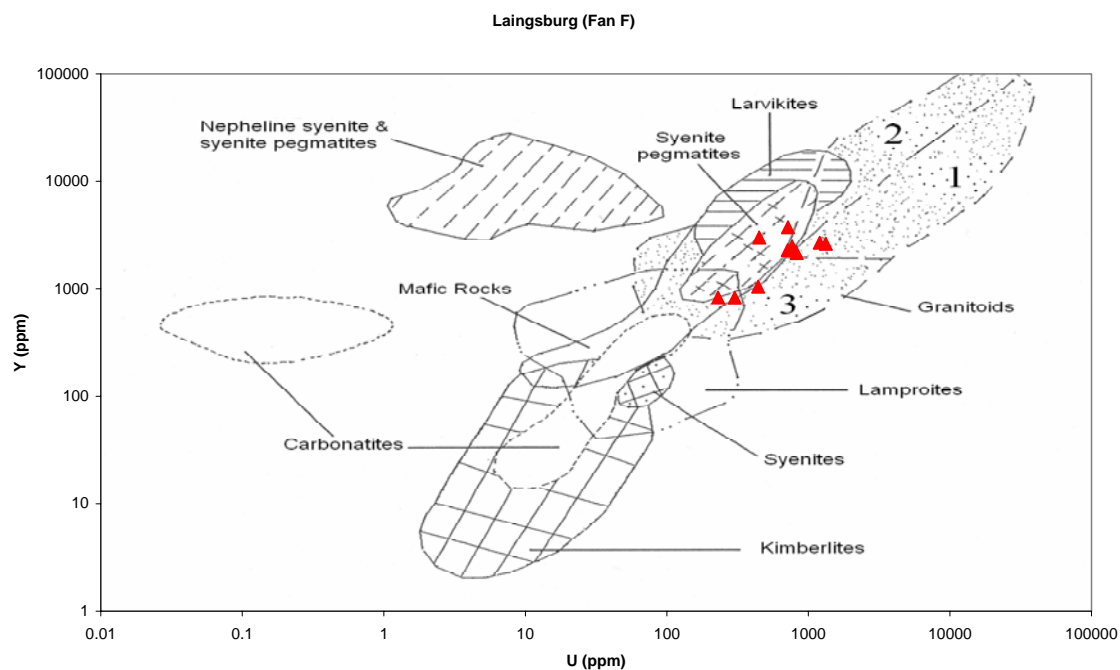


Figure 6.12 Plots of trace and rare earth element data of zircons from the Laingsburg Fan F, superimposed on the fields of zircon compositions used as discriminants for different rock types (Belousova et al., 2002). Granitoid subfields are: (1) aplites and leucogranites; (2) granites; (3) granodiorites and tonalites.

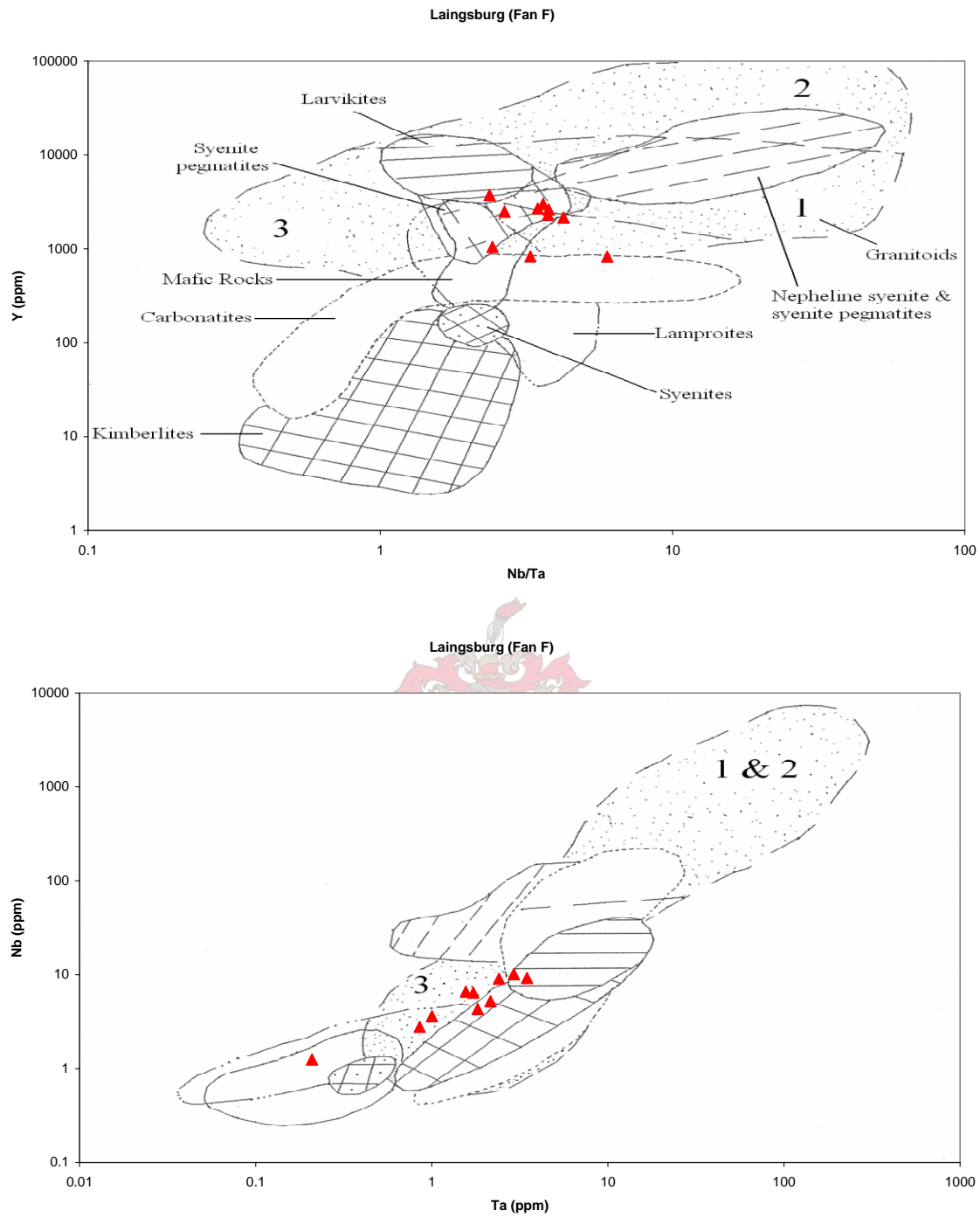


Figure 6.12 (continued). Note that one grain shows a mafic derivation.

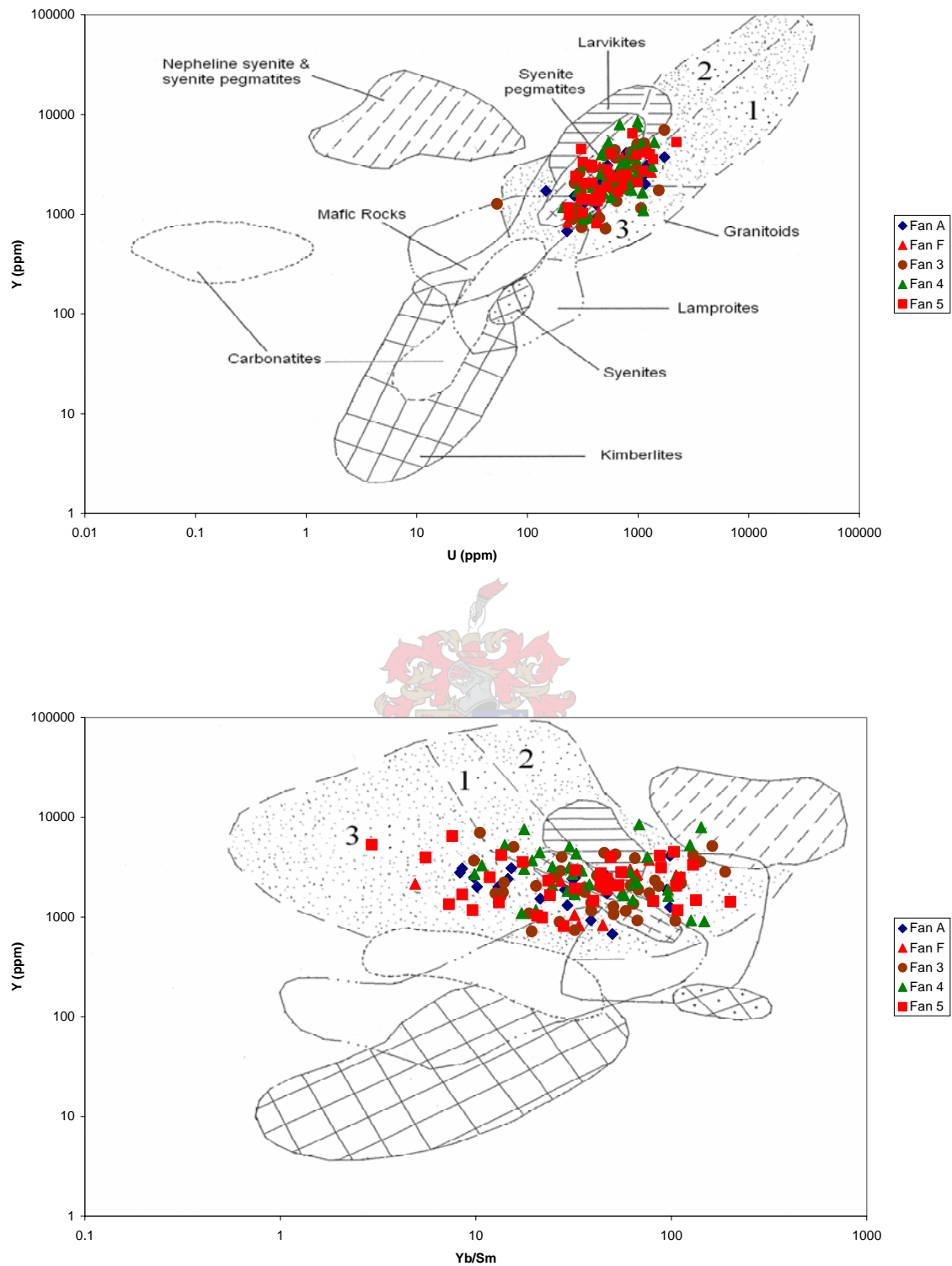


Figure 6.13 Synoptic diagrams showing the source rock lithologies of the Laingsburg (Fans A and F) and Skoorsteenberg (Fans 3, 4 and 5) Formations (Belousova et al., 2002). Note the identical source of the two datasets.

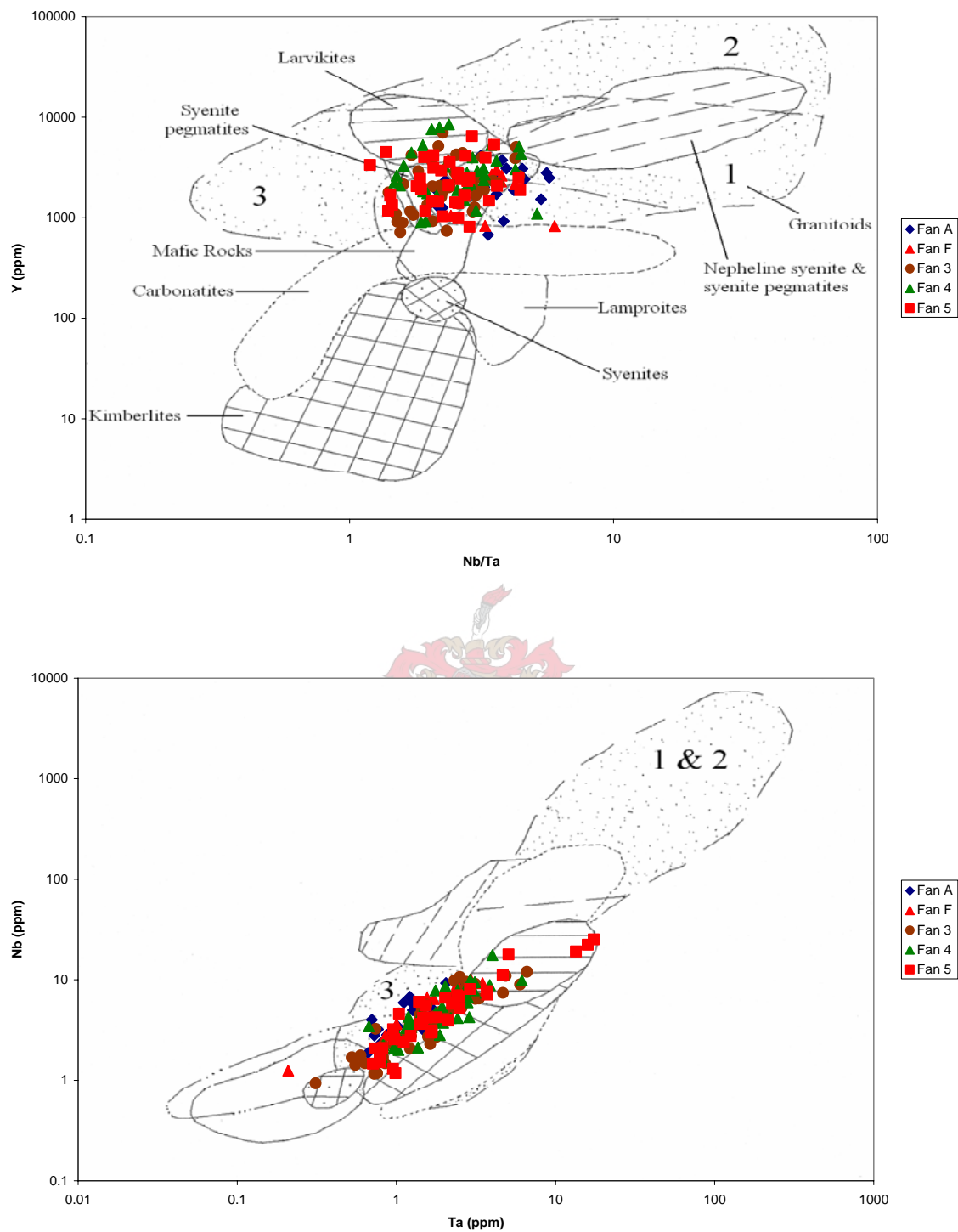


Figure 6.13 (continued) Provenance of the Laingsburg (Fans A and F) and Skoorsteenberg (Fans 3, 4 and 5) Formations (Belousova et al., 2002). It is noteworthy that the two datasets show an identical source. Samples are mostly plotted in the granitoid subfield (3) of the Nb vs. Ta diagram suggesting a tonalitic and granodioritic main provenance

6.4 Zircon age constraints on provenance

The provenance of the Permian Tanqua and Laingsburg submarine fan systems of the south-western corner of the Karoo Basin was investigated using the SHRIMP ion probe to determine the age of a large and representative number of separated zircon grains. To enhance the interpretation of the U-Pb radiometric data obtained, a short summary of the geology, mainly focused on lithologies and ages of pre-Karoo formations in southern Africa and southern Gondwana is given below. The paleogeography and paleotectonic framework of Gondwana during the late Paleozoic is presented in Figure 2.2.

Including information on the geology of south-western Gondwana is of great importance in this study as previous authors argued that the sediments in the investigated deepwater fans were derived from an area outside southern Africa, more precisely in adjacent regions (during the Permian) of southern Gondwana. Recently, López Gamundí and Rosselo (1998) have also demonstrated that as integral parts of Du Toit's 'Samfrau geosyncline', the Sauce Grande Basin-Ventana Fold Belt (Argentina) and Karoo Basin-Cape Fold Belt (South Africa) share similar paleoclimatic, paleogeographic, and paleotectonic aspects related to the late Paleozoic tectono-magmatic activity along the Panthalassan continental margin of Gondwana.

The geology of southern Africa comprises the Archaean Kaapvaal Craton fringed by four main orogenic belts including the Kheis Belt (2000 – 1800 Ma), Namaqua-Natal Belt (1200 – 1000 Ma), Pan-African Saldania Belt (550 – 540 Ma) and Cape Fold Belt (278 – 215 Ma) (Fig.2.1).

The Kaapvaal Province consists of a basement complex older than 3 Ga, and a younger supracrustal cover of about 2.9 Ga, including the Witwatersrand and Pongola Supergroups (Beukes and Cairncross, 1991). The basement is composed mainly of granitoids with subordinate orthogneisses and volcano-

sedimentary greenstone belts (~3.5 to 3.2 Ga old), including the Barberton Supergroup and equivalents (Hunter and Wilson, 1988).

The Kheis Province consists predominantly of meta-arenites located in what has been described as a thin-skinned fold and thrust belt of Eburnian (~2.0 -1.8 Ga) age (Moen, 1999). Geochronological data has demonstrated that the entire evolutionary history of the Namaqua-Natal Belt may be bracketed between about 1200 and 1000 Ma (Thomas and Eglington, 1990; Thomas et al., 1993 a, b).

The Saldania Belt is part of the Neoproterozoic Pan-African Belt and comprises sedimentary and volcanic rocks. The metavolcanic and metasedimentary rocks of the Bridgetown Formation were dated at approximately 600 Ma by Rozendaal et al. (1999). Deposition of the Gariep group lasted from approximately 750 to 580 Ma (Frimmel, 2000). The Cape Granite Suite intruded the Saldania Belt between 550 and 510 Ma (Scheepers and Nortjé, 2000; Scheepers and Poujol, 2002).

The Saldania rocks are overlain by the Cape Supergroup. The Table Mountain, Bokkeveld, and Witteberg Groups together constitute the Cape Supergroup that accumulated in the Cape Basin (Tankard et al., 1982; Broquet, 1992). This passive margin basin was filled by detritus from a cratonic hinterland to the North (Visser, 1979; Johnson, 1991).

The choice of appropriate discriminant criteria used to identify the source materials contributing to clastic deposits is the key to correct provenance identification.

Andersson et al. (2003), King et al. (2004) and Van Lente (2004) investigated the provenance of the Skoorsteenberg and Laingsburg Formations on the basis of Sm-Nd isotopic data obtained from sandstones.

In fact, Sm-Nd isotopes can provide some indication of the presence of mantle-derived constituents in sedimentary rocks. However, Sm-Nd isotopic analysis and whole-rock geochemistry provide averaged composition of different source materials involved but do not enable an identification of specific source rock types. Therefore, a sediment that originated from two source rocks, one of crustal and the other of juvenile affinity, could have the same intermediate isotopic signature as sediment derived from the reworking of a single rock type of hybrid composition. However, the first sediment presents two zircon populations whereas the second contains a single zircon population (Dabard et al., 1996). This can yield significant misinterpretation of the provenance, especially when dealing with sediments of mixed provenance such as the Laingsburg and Tanqua Karoo fan sandstones.

Detrital zircons from the Tanqua subbasin used in this study are from Fans 3, 4 and 5 (sample #63). The samples #66 and #64 comprise detrital zircons from the Laingsburg lower and upper fans respectively. Slope sandstones are represented by zircon grains of the sample #65. Considering the fact that the age of a single detrital zircon grain is the age of the igneous or metamorphic rock that it originally formed in, this technique is in effect directly measuring the ages of a sediment's protosources, regardless of their nature and location. Sediment provenance is deduced by comparing grain ages with known geochronological data from potential sources (Sircombe, 1999).

U-Pb analyses were performed on both the SHRIMP I and the SHRIMP RG instruments at the Research School for Earth Sciences (RSES) at the Australian National University, Canberra. Data reduction was done using the SQUID Excel Macro of Ludwig (2000). For the zircon calibration the Pb/U ratios have been normalised relative to a value of 0.1859 for the $^{206}\text{Pb}/^{238}\text{U}$ ratio of the FC1 reference zircons, equivalent to an age of 1099 Ma (Paces and Miller, 1993). Uranium and thorium concentrations were determined relative to the SL13 standard. Uncertainties given for individual U-Pb zircon analyses (ratios and

ages) are at the 1σ level. Concordia plots and weighted mean age calculations were carried out using Isoplot/Ex (Ludwig, 1999).

A minimum of 58 analyses is considered the optimum number of analyses in order to have a 95% probability of finding a component that would be present in a proportion of 5% (Dodson et al., 1988). A total of 67 and 40 zircons from the Tanqua and Laingsburg subbasin respectively were analysed in this study, giving a 95 % probability of finding a component present in a proportion of 4 to 8 % (Appendix D) and indicating a high probability of dating a representative population with most of the components being represented. More information on analytical procedures and philosophy, including selection of zircon grains, Pb-loss, mixed analysis and “preferred age” are presented in Appendix D.

Cathodoluminescent (CL) images of the zircons indicates that a significant proportion of the Tanqua and Laingsburg zircon populations are dominated by euhedral zircons characterized by primary, well developed, undisturbed magmatic zoning, with no growth lines or cores (Fig. 6.14) and are therefore considered to represent a juvenile component of the investigated submarine fans. This young zircon population shows no sign of a detrital origin, such as percussion markings or rounding of grains.

A second group of zircons comprises grains that show highly complex patterns with no distinct zoning, irregular embayments and/or overgrowths (Fig. 6.15), while others contain a core of an earlier zircon generation. These cores are interpreted as inherited zircons and often reflect an earlier magmatic or metamorphic event.

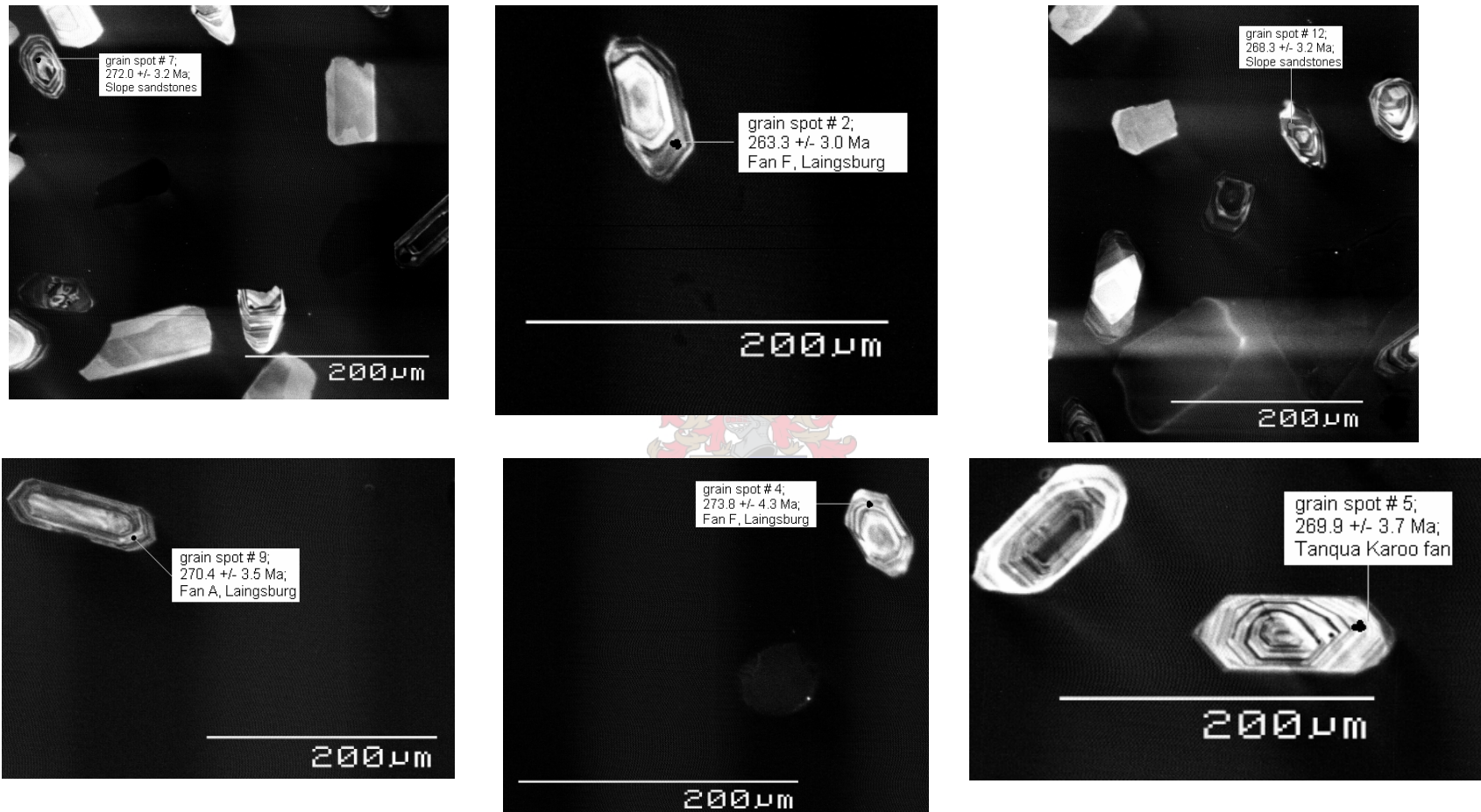


Figure 6.14 CL images, ages and analysis spots for the Slope, Laingsburg (Fans A and F) and Tanqua Karoo (Fans 3, 4 and 5) submarine fan samples.

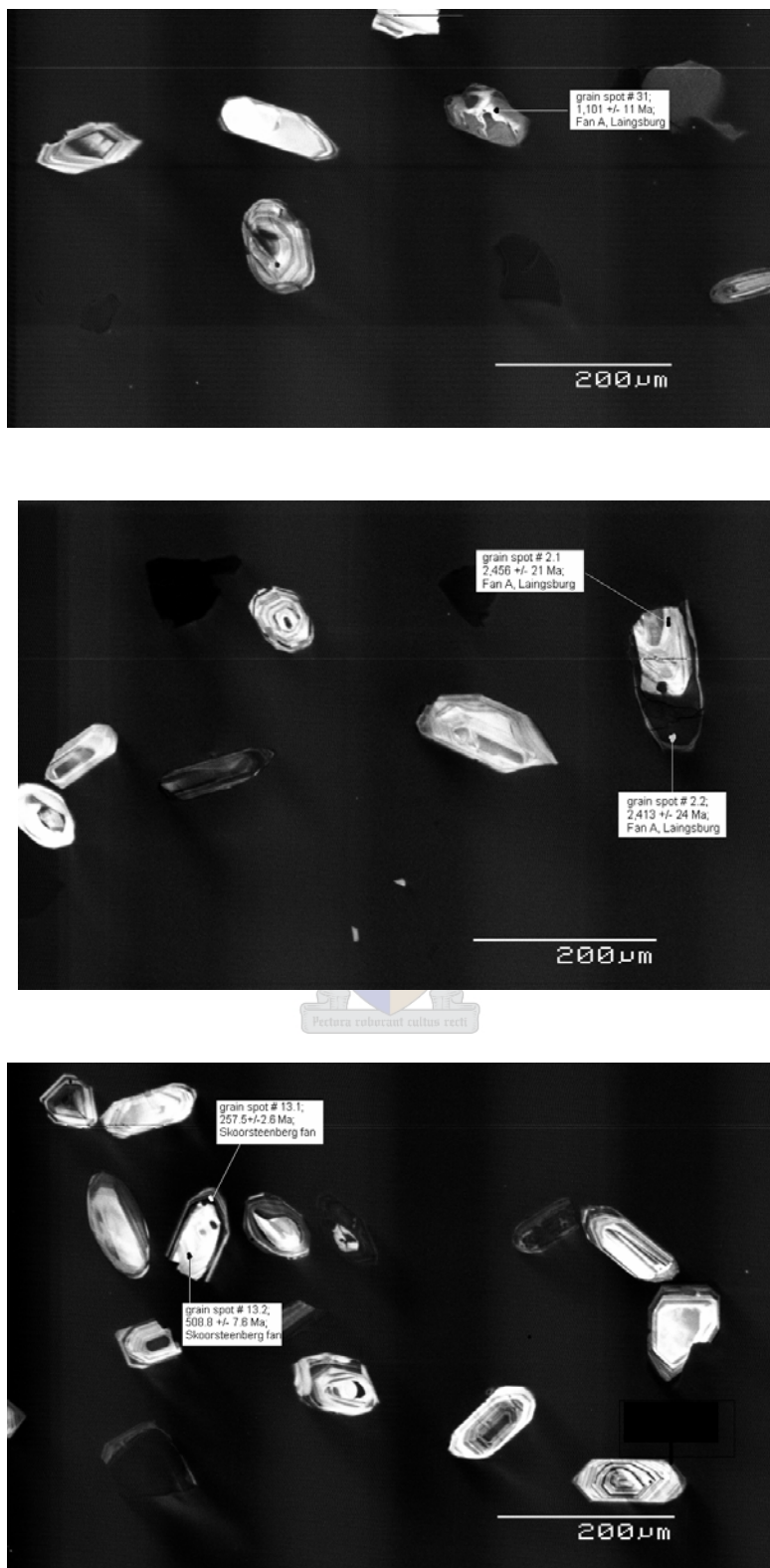


Figure 6.15 CL images, ages and analysis spots for inherited zircons from the Laingsburg submarine Fan A and the Skoorsteenberg fans.

U and Th contents give a measure of radiation damage (metamictisation) of zircons, because the radiation dose experienced is a function of U and Th content and time since crystallization. Unlike damaged zircons, zircons in pristine condition at the time of sedimentary transport are mechanically and chemically robust and can survive weathering, transport and high-temperature metamorphism and anatexis. The U content is the dominant control on metamictisation, although age also plays a role because very old zircons of average U content will have experienced a greater dose than younger grains of similar U content because dose is time-related. Zircon populations with uniformly low U and Th contents are likely to be polycyclic and to be associated with relatively mature sandstone compositions, whereas populations that include high-U grains are likely to include first-cycle material and are associated with more immature sediments (Hallsworth et al., 2000).

The presence of high-U detrital zircons of all ages (Figs 6.16 and 6.17; Table 6.2-6.4) suggests that the Slope, Tanqua and Laingsburg detritus are dominantly first-cycle and the sedimentary transport was relatively short, as previously indicated by the abundance of angular quartz and feldspar and the predominance of zircons with very well preserved crystal faces. This also excludes the Cape Supergroup clastic sedimentary sequence as the dominant source for the investigated submarine fan sandstones. The difference observed between the LA-ICP-MS and SHRIMP technique (Figs 6.16 and 6.17) comes from the fact that LA-ICP-MS measures the total U and Th while SHRIMP is based only on radiogenic U and Th (^{238}U and ^{232}Th). In addition, SHRIMP data was obtained only from pristine zircons (close system) whereas LA-ICP-MS data include both data obtained from pristine and metamict zircons

Radiometric ages obtained from each spot in different grains are plotted in Figures 6.18-6.20. Most of the grains analyzed are concordant, indicating that the Uranium loss was not important.

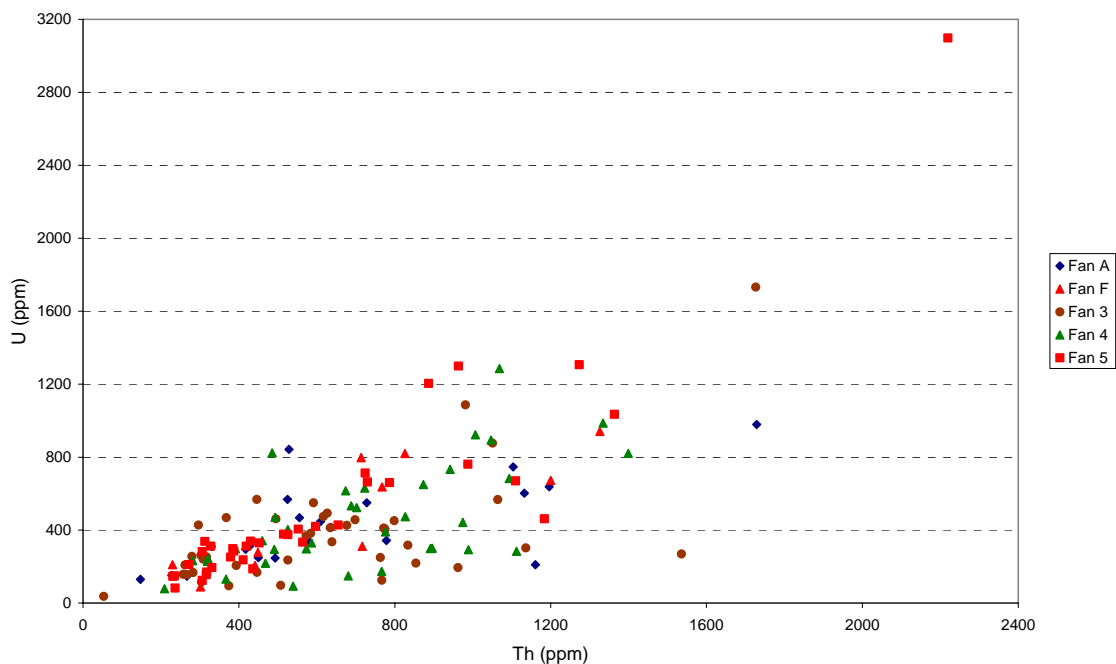


Figure 6.16 U vs. Th diagram based on LA-ICP-MS data. Note the high U content (> 400 ppm) of some zircons, implying a first-cycle derivation of the investigated submarine fans.

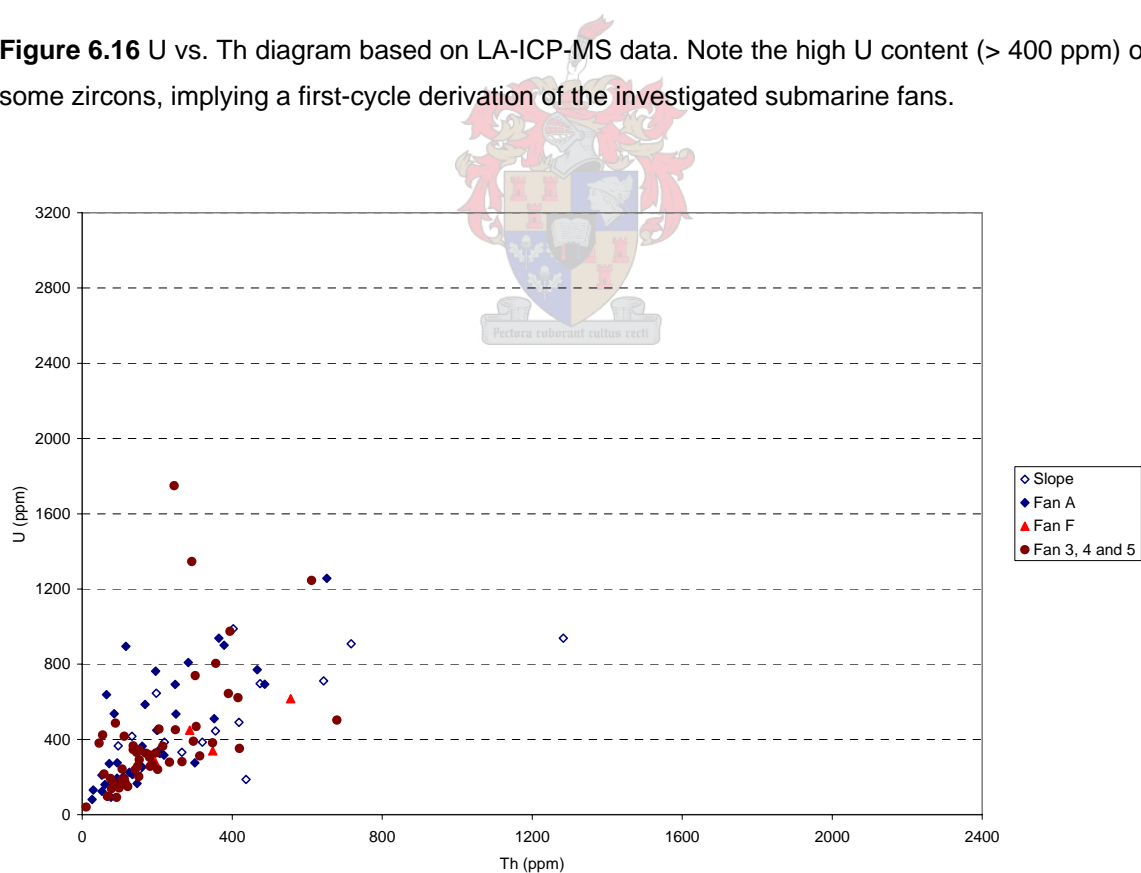


Figure 6.17 U vs. Th diagram based on SHRIMP data. The presence of high-U and Th detrital zircons confirms a short transport history and a first-cycle derivation of the investigated sandstones.

6.5 Geochronological results and location of source rocks

Conclusions on the source rock identification presented in this section are based on the best 107 $^{206}\text{Pb}/^{238}\text{U}$ ages obtained from 109 zircons. The age of both the xenocrystic cores (grain spot # 2.1 Laingsburg and grain spot # 13.2 Skoorsteenberg) and the two contaminated grains (grain spots # 30.1 and # 31.1 Skoorsteenberg) were not taken into consideration. In complex, multi-age zircons (e.g. grain spots # 13.1 and # 13.2 of the Skoorsteenberg samples and grain spots # 2.1 and # 2.2 of the Laingsburg) the youngest identified zone was analysed with the view to obtaining the age of the source rock (rather than the age of the xenocrystic cores).

Most of the geochronological information for younger zircons ($\sim < 800$ Ma) is contained in the $^{206}\text{Pb}/^{238}\text{U}$ geochronometer, as the ^{207}Pb peak is very small. For this investigation, a "Preferred Age" refers to the way in which individual ages for grains are calculated. If the zircon is younger than 700 Ma (based on the $^{206}\text{Pb}/^{238}\text{U}$ date) then the $^{206}\text{Pb}/^{238}\text{U}$ age is used. For older zircons the $^{207}\text{Pb}/^{206}\text{Pb}$ date is used. Major age groupings were determined on the basis on $^{206}\text{Pb}/^{238}\text{U}$ ratio because of a relatively low error associated with this ratio, also because of a significant presence of zircon grains younger than 800 Ma in all the investigated populations.

6.5.1 The Tanqua Karoo subbasin

6.5.1.1 The Slope sandstones

Concordia plot and histogram of ages of zircons from the Slope (Waterford Formation) sandstones show three major age groupings (Fig. 6.18). The late Carboniferous-Permian rocks (260-310 Ma) are by far the most important sources of the Slope sandstones. This population represents 67 % (12 zircons) of the 18 analyzed zircons. The Ordovician (450-495 Ma) age grouping (4 zircons, i.e. 22%) is the second most important provenance. Cambrian (495-545

Ma) and Neoproterozoic (545-1000) groups are thinly represented, with only 1 out of 18 analyzed zircons falling into each of these age ranges (Fig. 6.18 and Table 6.2).

Table 6.2 Summary of SHRIMP U-Pb zircon data for the Slope sandstone samples.

Grain. Spot	% $^{206}\text{Pb}_c$	ppm U	ppm Th	$^{232}\text{Th}/^{238}\text{U}$	ppm $^{206}\text{Pb}^*$	(1) $^{206}\text{Pb}/^{238}\text{U}$ Age	(1) $^{207}\text{Pb}/^{206}\text{Pb}$ Age	% Discordant	(1) $^{207}\text{Pb}^*/^{206}\text{Pb}^*$ $\pm\%$	(1) $^{207}\text{Pb}^*/^{235}\text{U}$ $\pm\%$	(1) $^{206}\text{Pb}^*/^{238}\text{U}$ $\pm\%$	err corr			
1.1	1.49	491	418	0.88	53.2	755.5 \pm 8.0	778 \pm 80	3	0.0651	3.8	1.116	4.0	0.1243	1.1	.281
2.1	0.43	366	96	0.27	13.1	262.7 \pm 3.1	266 \pm 71	1	0.0516	3.1	0.2957	3.3	0.04159	1.2	.364
3.1	0.21	188	437	2.40	12.1	463.3 \pm 6.0	458 \pm 56	-1	0.0561	2.5	0.577	2.9	0.07451	1.3	.468
4.1	1.96	938	1283	1.41	60.7	459.3 \pm 4.7	493 \pm 110	7	0.0570	5.0	0.581	5.1	0.07385	1.1	.207
6.1	0.10	989	403	0.42	64.5	471.5 \pm 4.6	445 \pm 30	-6	0.05581	1.4	0.5839	1.7	0.07588	1.0	.597
7.1	0.07	385	321	0.86	14.3	272.0 \pm 3.2	295 \pm 87	8	0.0522	3.8	0.310	4.0	0.04310	1.2	.302
8.1	0.77	336	162	0.50	23.3	497.4 \pm 5.6	579 \pm 87	14	0.0593	4.0	0.656	4.2	0.08021	1.2	.283
9.1	11.30	155	105	0.70	6.71	281.6 \pm 6.4	563 \pm 790	50	0.059	36	0.36	36	0.0446	2.3	.064
10.1	0.78	386	219	0.59	15.2	286.8 \pm 3.5	441 \pm 130	35	0.0557	6.0	0.349	6.2	0.04549	1.2	.201
11.1	0.21	331	266	0.83	12.8	282.2 \pm 3.4	358 \pm 67	21	0.0537	3.0	0.331	3.2	0.04475	1.2	.382
12.1	1.77	446	355	0.82	16.6	268.3 \pm 3.2	268 \pm 170	0	0.0516	7.4	0.302	7.5	0.04250	1.2	.164
13.1	0.98	909	717	0.82	34.2	273.4 \pm 2.9	182 \pm 91	-50	0.0497	3.9	0.297	4.0	0.04332	1.1	.266
14.1	0.30	417	133	0.33	27.2	471.3 \pm 5.1	440 \pm 42	-7	0.0557	1.9	0.582	2.2	0.07586	1.1	.510
15.1	0.12	696	475	0.70	25.7	270.4 \pm 2.9	276 \pm 41	2	0.05179	1.8	0.3059	2.1	0.04283	1.1	.519
16.1	0.68	167	79	0.49	6.14	268.4 \pm 3.9	395 \pm 150	32	0.0546	6.6	0.320	6.7	0.04252	1.5	.222
17.1	0.08	646	198	0.32	26.0	295.1 \pm 3.2	1,031 \pm 24	71	0.07362	1.2	0.4754	1.6	0.04684	1.1	.686
18.1	0.04	711	644	0.94	26.5	273.4 \pm 2.9	315 \pm 30	13	0.05268	1.3	0.3146	1.7	0.04332	1.1	.626
19.1	0.13	235	150	0.66	8.40	263.0 \pm 3.4	313 \pm 75	16	0.0526	3.3	0.302	3.6	0.04164	1.3	.369

Errors are 1-sigma; Pb_c and Pb* indicate the common and radiogenic portions, respectively.

Error in standard calibration was 0.28 % (not included in above errors but required when comparing data from different mounts).

(1) Common Pb corrected using measured ^{204}Pb .

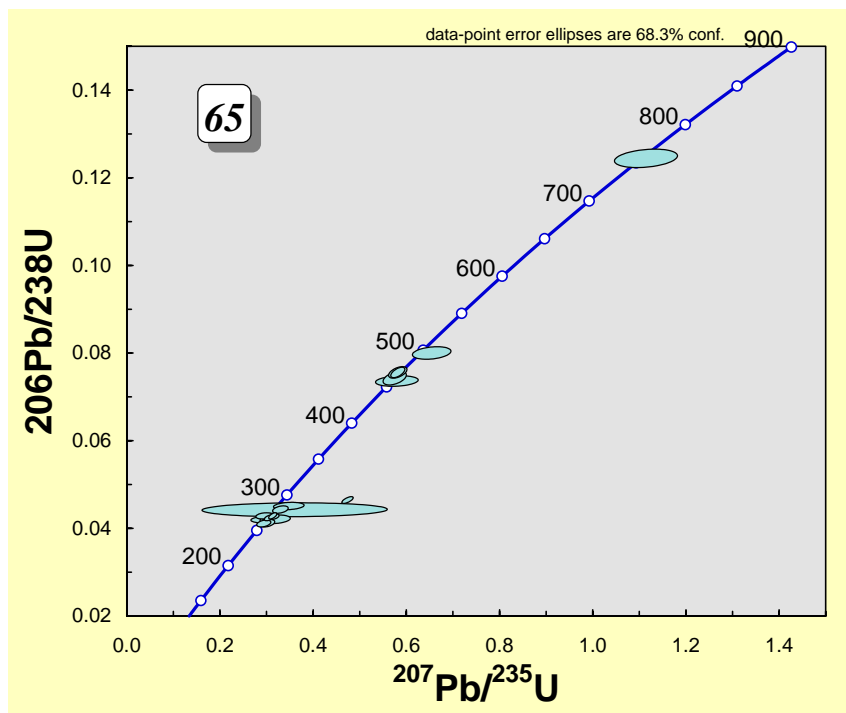


Figure 6.18a $^{206}\text{Pb}/^{238}\text{U}$ vs. $^{207}\text{Pb}/^{235}\text{U}$ concordia plot for detrital zircons within the Slope sandstones.

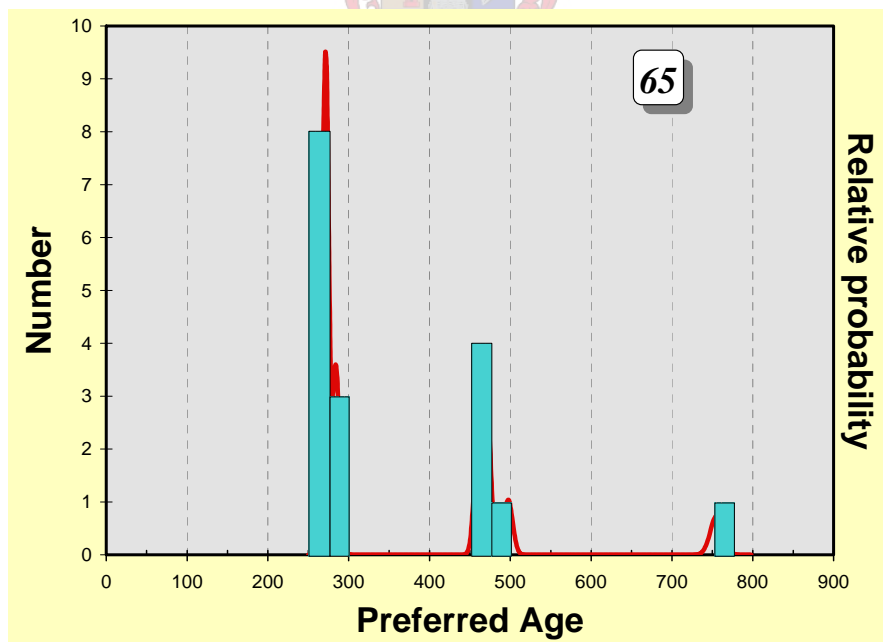


Figure 6.18b Histogram of ages for the Slope sandstones. Note the three major age groupings (i.e. the late Carboniferous-Permian, Ordovician and Neoproterozoic group).

6.5.1.2 The Skoorsteenberg Formation (Tanqua submarine fans)

Fifty-two analyses were obtained from 51 zircons. The results are shown on a concordia plot and histogram of ages (Fig. 6.19). The zircon population in Fans 3, 4 and 5 of the Tanqua subbasin shows a very similar age distribution to the Slope zircons. All analyses are concordant and many may also be assigned to three major groups on the basis of their $^{206}\text{Pb}/^{238}\text{U}$ ratios since most of the analysed zircons are younger than 800 Ma (see Appendix D for discussion of preferred age). The zircon population in the Skoorsteenberg Formation is also dominated by a late Carboniferous to Permian age zircons (260-310 Ma; 55.0 % of the total analyzed grains) together with an Ordovician group (470-495 Ma; 16.3 % of the population) and a significant Proterozoic presence (545-1105 Ma; 14.2 %). It is noteworthy that zircons from Neoproterozoic provinces (545-1000 Ma; 10.2 %) are better represented than those of Mesoproterozoic age (1000-1105 Ma; 4.0 %). Some other Paleozoic zircons namely the early Devonian (370-415; 10.2 %), and Cambrian (495-542 Ma; 4.0 %) grains have been also identified. The Triassic and early Jurassic grains (218.0 ± 2.9 Ma and 194.8 ± 3.8 Ma, respectively) are considered to be unreliable because of a major discrepancy between U/Pb and Pb/Pb ages, probably as a result of contamination. The ages given by these two youngest grains were not considered during the identification of major age groupings of zircons from the Skoorsteenberg fans. As previously mentioned, the age of the source rock, in complex, multi-age zircons (e.g. grain spots # 13.1 and # 13.2 of the Skoorsteenberg samples and grain spots # 2.1 and # 2.2 of the Laingsburg) was obtained from the youngest identified zone and not from xenocrystic cores.

Table 6.3 SHRIMP U-Pb zircon age for the Tanqua Fans 3, 4 and 5 sandstone samples.

Grain. Spot	% $^{206}\text{Pb}_c$	ppm U	ppm Th	$^{232}\text{Th}/^{238}\text{U}$	ppm $^{206}\text{Pb}^*$	(1) $^{206}\text{Pb}/^{238}\text{U}$ Age	(1) $^{207}\text{Pb}/^{206}\text{Pb}$ Age	% Discordant	(1) $^{207}\text{Pb}^*/^{206}\text{Pb}^*$ ±%	(1) $^{207}\text{Pb}^*/^{235}\text{U}$ ±%	(1) $^{206}\text{Pb}^*/^{238}\text{U}$ ±%	err corr			
1.1	0.14	366	136	0.39	20.9	415.0 ± 4.5	439 ± 47	5	0.0557	2.1	0.510	2.4	0.06649	1.1	.464
2.1	0.21	240	201	0.87	12.4	376.3 ± 4.5	346 ± 69	-9	0.0534	3.1	0.443	3.3	0.06011	1.2	.376
3.1	0.00	41	11	0.27	5.78	985 ± 17	1,093 ± 44	10	0.0759	2.2	1.728	2.9	0.1651	1.8	.642
4.1	0.17	279	233	0.86	11.6	304.2 ± 3.6	305 ± 67	0	0.0525	3.0	0.350	3.2	0.04832	1.2	.383
5.1	0.36	203	151	0.77	7.47	269.9 ± 3.7	255 ± 110	-6	0.0513	4.9	0.302	5.1	0.04275	1.4	.272
6.1	--	216	59	0.28	34.6	1,102 ± 11	1,119 ± 19	2	0.07693	0.95	1.978	1.5	0.1865	1.1	.765
7.1	0.06	1246	612	0.51	103	594.7 ± 5.4	669 ± 14	11	0.06185	0.66	0.8241	1.2	0.09665	0.95	.821
8.1	0.13	346	136	0.41	12.8	272.2 ± 3.1	278 ± 55	2	0.0518	2.4	0.3083	2.7	0.04313	1.2	.440
9.1	0.07	456	205	0.46	31.0	491.7 ± 4.9	521 ± 28	6	0.05777	1.3	0.631	1.7	0.07925	1.0	.625
10.1	0.21	271	187	0.72	22.3	589.2 ± 6.5	592 ± 57	0	0.0597	2.6	0.788	2.9	0.0957	1.1	.403
11.1	0.03	1749	246	0.15	63.0	264.9 ± 2.5	293 ± 20	10	0.05217	0.88	0.3018	1.3	0.04195	0.97	.740
12.1	0.00	423	55	0.13	30.4	516.8 ± 5.3	550 ± 26	6	0.05854	1.2	0.674	1.6	0.08346	1.1	.673
13.1	0.85	740	302	0.42	26.1	257.5 ± 2.6	277 ± 80	7	0.0518	3.5	0.291	3.7	0.04075	1.0	.285
13.2	0.15	98	67	0.71	6.91	508.8 ± 7.6	550 ± 62	7	0.0585	2.9	0.663	3.2	0.0821	1.6	.478
14.1	--	380	45	0.12	57.0	1,037.8 ± 9.8	1,054 ± 16	2	0.07447	0.81	1.793	1.3	0.1747	1.0	.785
15.1	0.10	452	249	0.57	24.7	397.8 ± 4.1	417 ± 33	5	0.05512	1.5	0.4838	1.8	0.06366	1.1	.581
16.1	0.09	1346	292	0.22	117	618.6 ± 5.5	593 ± 24	-4	0.05970	1.1	0.829	1.4	0.10072	0.93	.648
17.1	1.75	150	122	0.84	6.42	307.9 ± 4.8	410 ± 200	25	0.0549	9.1	0.371	9.3	0.04892	1.6	.173
18.1	0.00	316	182	0.59	21.4	489.0 ± 5.4	471 ± 32	-4	0.05647	1.4	0.614	1.8	0.07881	1.1	.623
19.1	0.63	191	113	0.61	7.79	297.0 ± 4.4	301 ± 130	1	0.0524	5.7	0.340	5.9	0.04715	1.5	.256
20.1	0.23	805	356	0.46	53.5	479.7 ± 4.6	480 ± 35	0	0.05669	1.6	0.604	1.8	0.07726	0.99	.535
21.1	0.00	193	76	0.40	12.8	479.4 ± 5.9	473 ± 40	-1	0.0565	1.8	0.602	2.2	0.07721	1.3	.576
22.1	0.22	257	181	0.73	9.78	279.2 ± 3.6	265 ± 74	-5	0.0515	3.2	0.314	3.5	0.04426	1.3	.375
23.1	0.00	258	148	0.59	19.7	548.7 ± 6.2	560 ± 32	2	0.05882	1.5	0.720	1.9	0.0888	1.2	.625
24.1	0.00	621	415	0.69	23.0	271.6 ± 2.9	256 ± 33	-6	0.05134	1.5	0.3046	1.8	0.04303	1.1	.595
25.1	0.00	644	390	0.63	42.2	473.7 ± 4.6	474 ± 23	0	0.05656	1.0	0.5946	1.5	0.07626	1.0	.701
26.1	0.10	328	197	0.62	12.6	280.7 ± 3.4	315 ± 51	11	0.0527	2.3	0.3233	2.6	0.04450	1.2	.484
27.1	0.23	171	115	0.70	8.78	374.2 ± 5.2	389 ± 82	4	0.0544	3.7	0.449	3.9	0.05976	1.4	.364
28.1	0.92	138	79	0.59	9.29	481.3 ± 6.7	494 ± 87	3	0.0571	3.9	0.610	4.2	0.0775	1.4	.345
29.1	0.25	487	89	0.19	33.0	488.3 ± 5.3	563 ± 45	13	0.0589	2.1	0.639	2.4	0.07870	1.1	.479
30.1	0.14	383	348	0.94	11.3	218.0 ± 2.9	320 ± 63	32	0.0528	2.8	0.2504	3.1	0.03440	1.3	.436
31.1	0.42	163	84	0.54	4.30	194.8 ± 3.8	278 ± 140	30	0.0518	6.1	0.219	6.5	0.03067	2.0	.308
32.1	0.80	92	92	1.03	7.00	542.1 ± 8.6	527 ± 130	-3	0.0579	5.9	0.701	6.1	0.0877	1.7	.270
33.1	0.19	417	112	0.28	16.4	288.6 ± 3.3	290 ± 49	0	0.0521	2.1	0.3289	2.4	0.04578	1.2	.475
34.1	0.32	243	107	0.46	8.93	269.4 ± 3.6	316 ± 75	15	0.0527	3.3	0.310	3.6	0.04268	1.4	.381
35.1	0.11	330	145	0.45	13.8	306.6 ± 3.6	328 ± 51	7	0.0530	2.2	0.3559	2.5	0.04871	1.2	.476
36.1	0.33	313	314	1.04	10.8	253.0 ± 3.2	294 ± 77	14	0.0522	3.4	0.288	3.6	0.04002	1.3	.357
37.1	0.00	364	215	0.61	23.9	474.2 ± 5.2	477 ± 31	1	0.05661	1.4	0.596	1.8	0.07633	1.1	.630
38.1	0.22	142	99	0.72	5.54	285.2 ± 4.5	323 ± 85	12	0.0529	3.7	0.330	4.1	0.04524	1.6	.394
39.1	0.15	282	266	0.98	11.0	286.7 ± 3.6	301 ± 62	5	0.0524	2.7	0.3284	3.0	0.04548	1.3	.428
40.1	0.00	346	151	0.45	12.9	272.9 ± 3.3	275 ± 57	1	0.0518	2.5	0.3087	2.8	0.04325	1.2	.444
41.1	0.25	503	680	1.40	20.6	299.5 ± 3.3	290 ± 55	-3	0.0521	2.4	0.3416	2.6	0.04755	1.1	.423
42.1	0.71	390	296	0.79	15.1	282.0 ± 3.3	280 ± 85	-1	0.0519	3.7	0.320	3.9	0.04471	1.2	.308
43.1	0.22	145	98	0.70	5.55	280.9 ± 4.4	277 ± 87	-1	0.0518	3.8	0.318	4.1	0.04454	1.6	.388
44.1	9.37	305	180	0.61	13.5	295.2 ± 4.8	616 ± 490	52	0.060	23	0.390	23	0.04685	1.7	.072
45.1	0.18	975	394	0.42	38.2	286.9 ± 2.8	292 ± 43	2	0.05214	1.9	0.3272	2.1	0.04551	1.0	.477
46.1	0.26	184	106	0.59	7.81	309.8 ± 4.4	321 ± 94	3	0.0528	4.1	0.358	4.4	0.04923	1.4	.332
47.1	0.83	468	304	0.67	18.3	283.9 ± 3.8	349 ± 94	19	0.0535	4.2	0.332	4.4	0.04503	1.4	.316
48.1	0.04	292	152	0.54	11.7	293.4 ± 3.7	300 ± 82	2	0.0523	3.6	0.336	3.8	0.04657	1.3	.339
49.1	0.42	352	419	1.23	19.1	394.4 ± 4.6	393 ± 79	0	0.0545	3.5	0.474	3.7	0.06309	1.2	.322
50.1	0.00	239	142	0.61	8.56	263.1 ± 3.7	342 ± 58	23	0.0533	2.5	0.3062	2.9	0.04166	1.4	.488
51.1	0.40	325	172	0.55	12.7	285.2 ± 3.6	260 ± 140	-10	0.0514	6.0	0.321	6.2	0.04524	1.3	.209

Errors are 1-sigma; Pb_c and Pb* indicate the common and radiogenic portions, respectively.

Error in standard calibration was 0.28 % (not included in above errors but required when comparing data from different mounts).

(1) Common Pb corrected using measured ^{204}Pb .

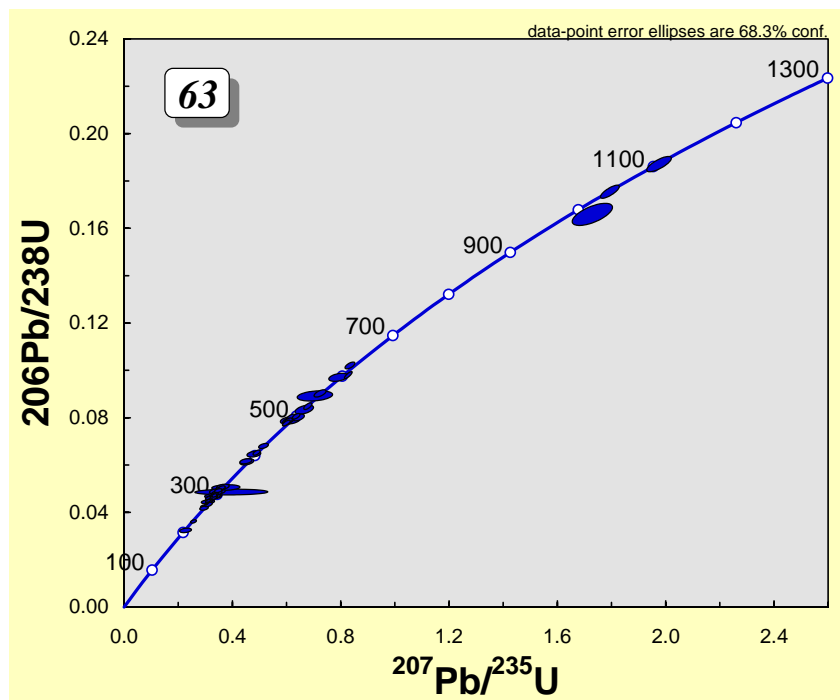


Figure 6.19a $^{206}\text{Pb}/^{238}\text{U}$ vs. $^{207}\text{Pb}/^{235}\text{U}$ concordia plot for detrital zircons within the Tanqua Karoo submarine Fans 3, 4 and 5 sandstones, indicating a predominance of late Carboniferous-Permian (310-260 Ma) ages.

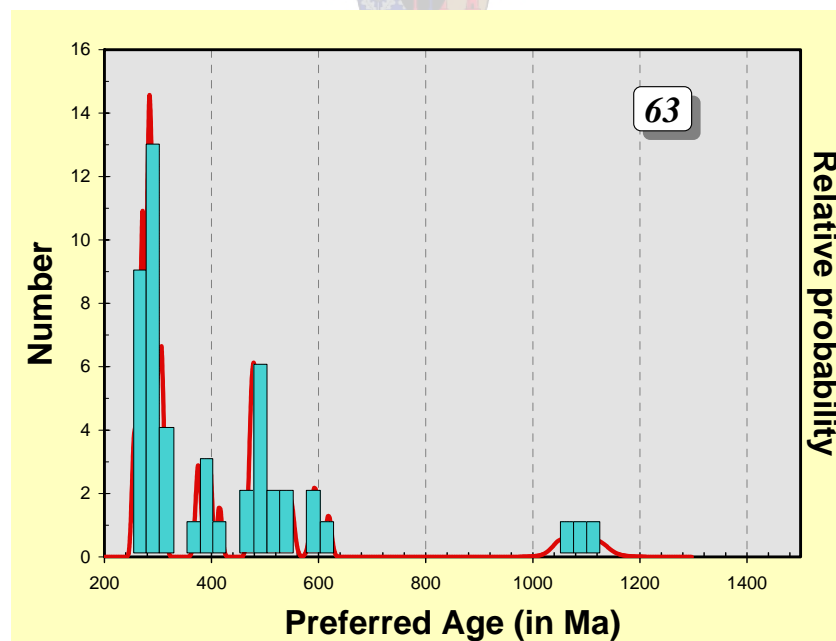


Figure 6.19b Histogram of ages for the Tanqua Karoo submarine Fans 3, 4 and 5 sandstones.

6.5.2 The Laingsburg Formation in the Laingsburg subbasin

Thirty-seven analyses were obtained from 36 zircons from sandstone samples of the lower fan (Fan A) of the Laingsburg Formation and four analyses were obtained from four detrital zircons from sandstone samples of the upper fan (Fan F). Only the results of the lower fan are shown on a concordia plot and histogram of ages (Fig. 6.20). A concordia plot could not be obtained from the analyses of zircons from Fan F because of their small number. The problem here was the difficulty of obtaining zircons from the collected samples. However, for the identification of the “age groupings”, zircons from Fan A and Fan F were not considered separately but as a single mineral population from the Laingsburg Formation. Similar to the Tanqua zircons, many analyses of the Laingsburg zircons may be assigned to three main groups on the basis of their $^{206}\text{Pb}/^{238}\text{U}$ ratio. Group 1, which represents the main provenance terrane with 47.5 % of the total analysed grains, comprises late Carboniferous to Permian (260-319 Ma) detrital zircons. Group 2 comprises zircons of Mesoproterozoic and Neoproterozoic age (15 % each). Group 3, which comprises zircons of Ordovician and Cambrian age (7.5 % each), is the third most important source of the Laingsburg detritus. Two Devonian zircons (363.9 ± 4.2 and 386.2 ± 4.7 Ma; 5%) were also identified. The only Eoproterozoic zircon (2456 ± 21 Ma) analyzed in this study is near concordant, almost certainly due to U-loss.

Table 6.4 Summary of SHRIMP U-Pb zircon data for the Laingsburg Fan A sandstone samples.

Grain. Spot	% $^{206}\text{Pb}_c$	ppm U	ppm Th	$^{232}\text{Th}/^{238}\text{U}$	ppm $^{206}\text{Pb}^*$	(1) $^{206}\text{Pb}/^{238}\text{U}$ Age	(1) $^{207}\text{Pb}/^{206}\text{Pb}$ Age	% Discordant	(1) $^{207}\text{Pb}^*/^{206}\text{Pb}^*$ $\pm\%$	(1) $^{207}\text{Pb}^*/^{235}\text{U}$ $\pm\%$	(1) $^{206}\text{Pb}^*/^{238}\text{U}$ $\pm\%$	err corr
1.1	0.49	210	52	0.26	13.3	457.7 \pm 5.5	472 \pm 94	3	0.0565 4.2	0.573 4.4	0.07359 1.2	.283
2.1	0.85	810	283	0.36	325	2,456 \pm 21	2,671 \pm 11	8	0.1820 0.66	11.64 1.2	0.4636 1.0	.843
2.2	0.04	160	60	0.39	62.6	2,413 \pm 24	2,667 \pm 11	10	0.1815 0.67	11.36 1.4	0.4541 1.2	.871
3.1	0.33	254	160	0.65	9.64	278.0 \pm 3.6	340 \pm 99	18	0.0533 4.4	0.324 4.6	0.04406 1.3	.290
4.1	9.11	901	378	0.43	115	817.1 \pm 9.2	976 \pm 340	16	0.072 17	1.34 17	0.1351 1.2	.071
5.1	0.00	93	77	0.85	7.30	564 \pm 12	597 \pm 60	6	0.0598 2.8	0.754 3.5	0.0914 2.2	.628
6.1	0.00	131	29	0.23	25.3	1,306 \pm 15	1,250 \pm 30	-4	0.0822 1.5	2.544 2.0	0.2245 1.2	.634
7.1	0.42	202	110	0.56	7.69	278.6 \pm 3.8	283 \pm 130	2	0.0519 5.8	0.316 5.9	0.04417 1.4	.232
8.1	0.00	536	86	0.16	52.4	694.1 \pm 7.1	694 \pm 18	0	0.06258 0.83	0.981 1.4	0.1137 1.1	.793
9.1	4.86	693	487	0.73	26.8	270.4 \pm 3.5	467 \pm 260	42	0.0564 12	0.333 12	0.04284 1.3	.111
10.1	0.34	938	364	0.40	35.8	279.2 \pm 2.9	282 \pm 82	1	0.0519 3.6	0.317 3.7	0.04426 1.1	.281
11.1	16.80	267	188	0.73	12.4	283.0 \pm 7.2	350 \pm 1200	19	0.054 51	0.33 51	0.0449 2.6	.051
12.1	0.25	365	160	0.45	14.2	284.3 \pm 3.3	275 \pm 75	-3	0.0518 3.3	0.322 3.5	0.04510 1.2	.336
13.1	0.03	770	467	0.63	131	1,161 \pm 11	1,216.3 \pm 9.9	5	0.08079 0.50	2.198 1.1	0.1973 10	.892
14.1	0.30	325	207	0.66	12.3	276.8 \pm 3.2	238 \pm 73	-16	0.0509 3.2	0.308 3.4	0.04388 1.2	.352
15.1	0.19	895	117	0.13	70.4	563.7 \pm 5.5	546 \pm 27	-3	0.05842 1.2	0.736 1.6	0.09138 1.0	.644
16.1	5.47	693	248	0.37	36.6	363.9 \pm 4.2	391 \pm 300	7	0.0545 14	0.436 14	0.05807 1.2	.087
17.1	0.10	510	352	0.71	19.3	277.3 \pm 3.0	264 \pm 37	-5	0.05152 1.6	0.3122 1.9	0.04395 1.1	.567
18.1	0.17	449	199	0.46	30.4	488.4 \pm 5.2	523 \pm 35	7	0.05782 1.6	0.628 1.9	0.07871 1.1	.571
19.1	--	586	168	0.30	43.2	531.2 \pm 5.5	547 \pm 23	3	0.05846 1.1	0.692 1.5	0.08589 1.1	.707
20.1	10.66	1257	652	0.54	74.6	386.2 \pm 4.7	440 \pm 540	12	0.056 24	0.47 24	0.06174 1.3	.052
21.1	0.39	450	201	0.46	16.6	270.3 \pm 3.1	340 \pm 68	21	0.0533 3.0	0.314 3.2	0.04282 1.2	.365
22.1	0.15	272	72	0.27	18.1	480.3 \pm 5.3	493 \pm 40	3	0.0570 1.8	0.608 2.2	0.07735 1.1	.529
23.1	2.59	317	218	0.71	13.7	309.3 \pm 3.8	421 \pm 220	27	0.0552 9.6	0.374 9.7	0.04915 1.3	.130
24.1	0.31	81	26	0.33	12.3	1,046 \pm 13	1,058 \pm 63	1	0.0746 3.1	1.811 3.4	0.1761 1.3	.392
25.1	0.14	536	250	0.48	21.3	291.2 \pm 3.1	285 \pm 47	-2	0.0520 2.0	0.3312 2.3	0.04621 1.1	.473
26.1	0.24	214	134	0.65	8.30	284.5 \pm 3.5	252 \pm 79	-13	0.0513 3.4	0.319 3.7	0.04513 1.3	.346
27.1	2.09	276	93	0.35	9.96	260.3 \pm 3.3	274 \pm 190	5	0.0517 8.3	0.294 8.4	0.04120 1.3	.152
28.1	0.38	351	209	0.61	13.3	277.0 \pm 3.3	296 \pm 51	6	0.0522 2.2	0.3162 2.6	0.04390 1.2	.478
29.1	0.05	638	65	0.11	43.9	496.1 \pm 4.9	495 \pm 27	0	0.05709 1.2	0.630 1.6	0.08000 1.0	.646
30.1	0.08	762	196	0.27	102	932.8 \pm 8.6	985 \pm 13	5	0.07196 0.64	1.545 1.2	0.1557 10	.842
31.1	1.20	276	300	1.12	44.8	1,101 \pm 11	1,061 \pm 53	-4	0.0747 2.6	1.919 2.8	0.1863 1.1	.382
32.1	0.04	125	53	0.44	18.3	1,016 \pm 12	1,039 \pm 29	2	0.0739 1.4	1.741 1.9	0.1708 1.2	.656
33.1	0.20	166	147	0.91	7.27	319.1 \pm 4.4	273 \pm 110	-17	0.0517 4.6	0.362 4.8	0.05075 1.4	.295
34.1	0.13	194	93	0.50	23.1	833.5 \pm 9.0	822 \pm 32	-1	0.0665 1.5	1.266 1.9	0.1380 1.2	.602
35.1	0.94	275	190	0.71	11.7	307.8 \pm 3.9	270 \pm 150	-14	0.0517 6.6	0.348 6.7	0.04891 1.3	.196
36.1	2.12	225	126	0.58	9.61	306.6 \pm 4.3	315 \pm 200	3	0.0527 9.0	0.354 9.1	0.04872 1.4	.157

Errors are 1-sigma; Pb_c and Pb^* indicate the common and radiogenic portions, respectively.

Error in standard calibration was 0.28 % (not included in above errors but required when comparing data from different mounts).

(1) Common Pb corrected using measured ^{204}Pb .

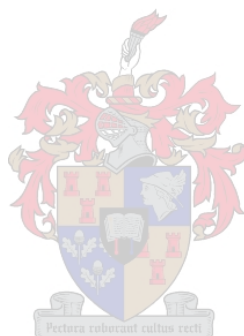
Table 6.4 (continued) Summary of SHRIMP U-Pb zircon data for the Laingsburg Fan F sandstone samples.

Grain. Spot	% $^{206}\text{Pb}_c$	ppm U	ppm Th	^{232}Th ^{238}U	ppm $^{206}\text{Pb}^*$	(1) ^{206}Pb ^{238}U Age	(1) ^{207}Pb ^{206}Pb Age	% Dis- cor- dant	(1) $^{207}\text{Pb}^*$ $^{206}\text{Pb}^*$ $\pm\%$	(1) $^{207}\text{Pb}^*$ ^{235}U $\pm\%$	(1) $^{206}\text{Pb}^*$ ^{238}U $\pm\%$	err corr
1.1	0.19	449	287	0.66	32.4	518.3 ± 5.4	551 ± 36	6	0.05856 1.6	0.676 2.0	0.08373 1.1	.552
2.1	1.56	616	556	0.93	22.4	263.3 ± 3.0	452 ± 140	42	0.0560 6.4	0.322 6.5	0.04169 1.2	.177
3.1	0.75	340	348	1.06	68.8	$1,356 \pm 13$	$1,331 \pm 39$	-2	0.0857 2.0	2.766 2.3	0.2341 1.1	.471
4.1	5.96	283	194	0.71	11.2	273.8 ± 4.3	452 ± 400	39	0.0560 18	0.335 18	0.04339 1.6	.090

Errors are 1-sigma; Pb_c and Pb^* indicate the common and radiogenic portions, respectively.

Error in standard calibration was 0.28 % (not included in above errors but required when comparing data from different mounts).

(1) Common Pb corrected using measured ^{204}Pb .



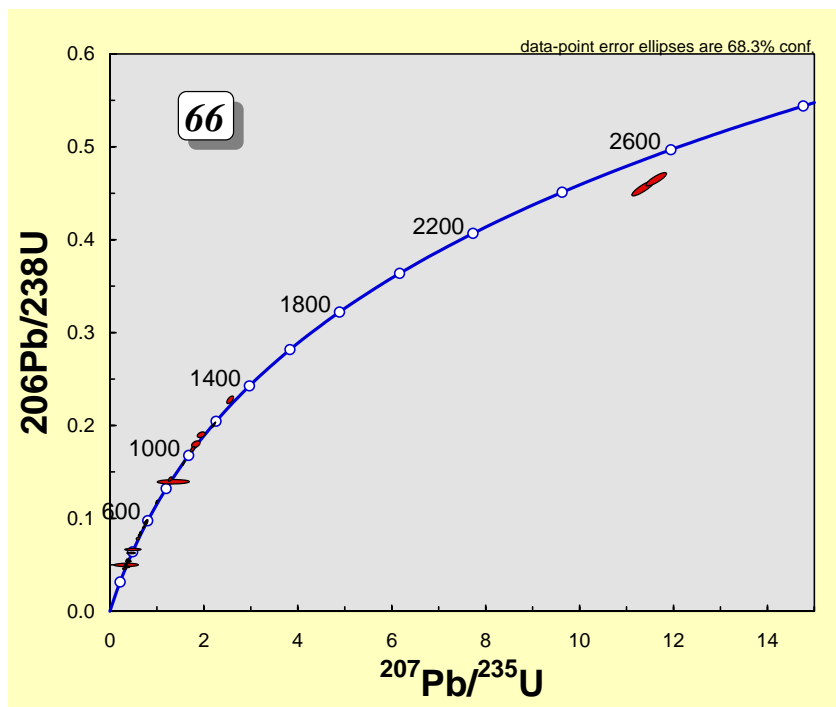


Figure 6.20a $^{206}\text{Pb}/^{238}\text{U}$ vs. $^{207}\text{Pb}/^{235}\text{U}$ concordia plot for detrital zircons within the Laingsburg submarine Fan A sandstones.

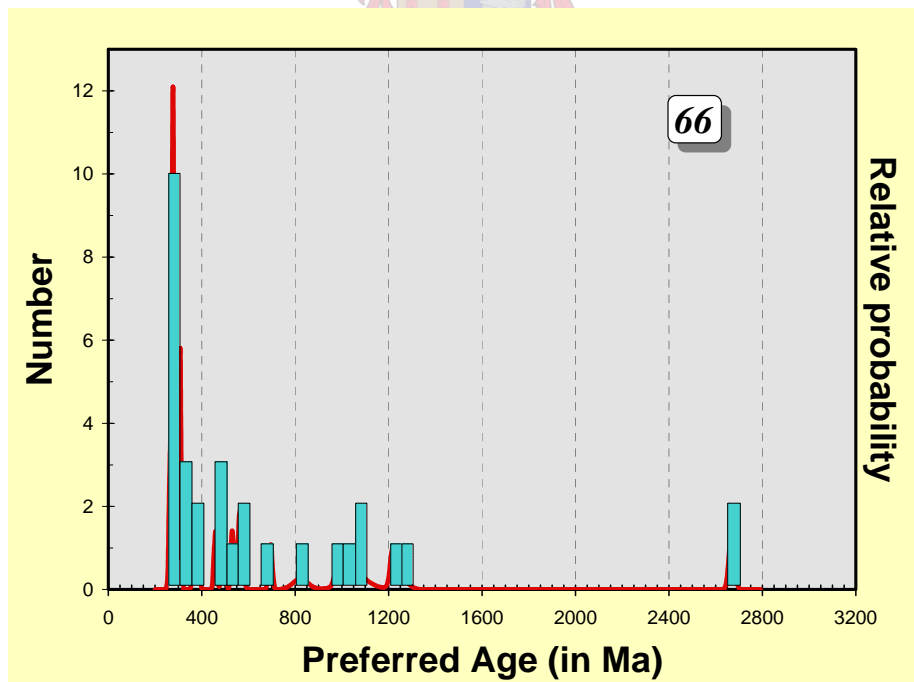


Figure 6.20b Histogram of ages for the Laingsburg submarine Fan A sandstones. Note the predominance of late Carboniferous-Permian (310-260 Ma) ages.

6.6 Summary and source rock identification

The zircon populations from the Tanqua and Laingsburg subbasins show similar age distributions and therefore originated from the same source.

Taken together, detrital zircons (107 analyses of 109 zircons) from the investigated formations suggest a dominant late Carboniferous-Permian provenance (260-310 Ma; 54.2 % of the total analyzed zircons) with a peak in the 270-290 Ma range. It is followed by Ordovician (460-495 Ma; 14.0 %) and Neoproterozoic (545-620 Ma; 11.2 %) sources. In decreasing order of abundance, Mesoproterozoic (1000-1300 Ma; 7.5 %), Devonian (6.5 %), Cambrian (5.6 %), and Eoproterozoic (1 %) populations represent subordinate sources with less than 7.5 % of the total analyzed grains each.

In general, the zircon age distribution is similar within the Slope, Skoorsteenberg and Laingsburg Formations, showing the predominance of late Carboniferous-Permian, Ordovician and Neoproterozoic provenances, though the second and third main sources vary. Indeed, the Ordovician zircons represent the second most important source in both the Tanqua and Slope sandstones, while the same population occupies the third position in the Laingsburg area. This similarity suggests that investigated subbasins shared a similar provenance history. This age pattern confirms evidence obtained from zircon chemistry and supports a similarity in provenance between the Laingsburg and Tanqua Karoo deepwater sediments. Several authors have indeed suggested that the Tanqua and Laingsburg fans originated from the same source (Scott, 1997; King et al. 2004).

A clustered bar chart displaying the contribution of each source or age grouping based on all 107 analyses obtained from 109 zircons from the southwestern Ecca Group (Laingsburg, Skoorsteenberg and Waterford zircons) is shown in Figure 6.21.

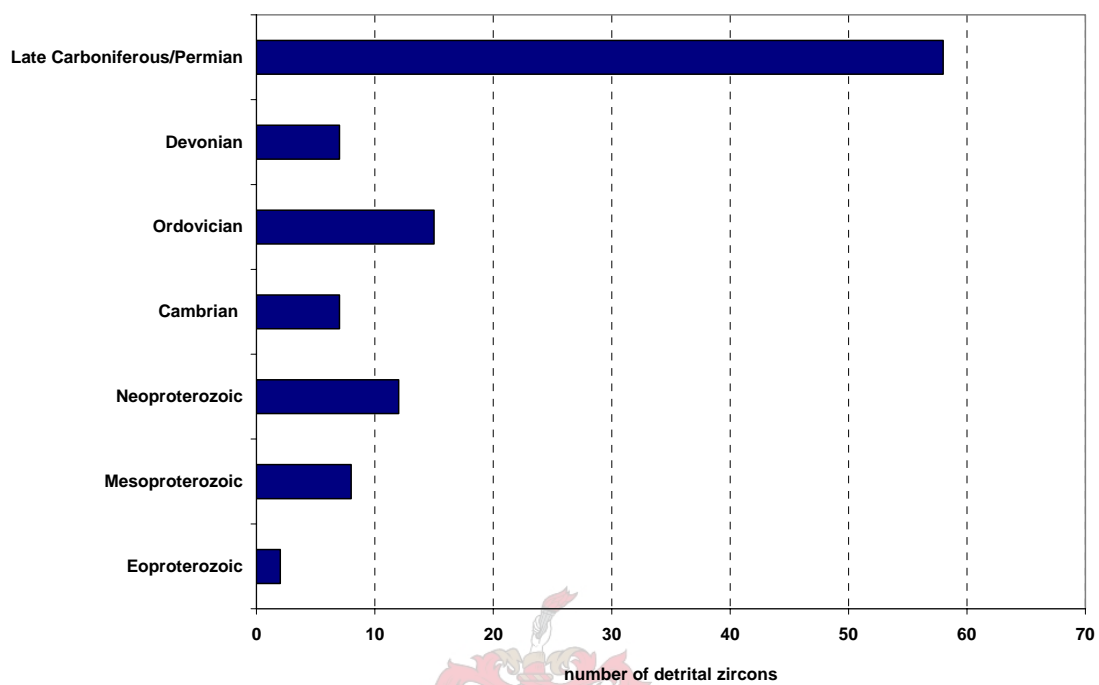


Figure 6.21 Zircon age distributions in the southwestern Ecca Group. Note that the contribution of each source rock is evaluated on the basis of $^{206}\text{Pb}/^{238}\text{U}$ ratios for 107 analyses from 109 detrital zircons.

There are difficulties in reconciling the mineralogical and isotopic evidence with a source located within South Africa. However, a 260-310 Ma age grouping coupled with indications of tonalitic and orogenic calc-alkaline rhyolitic rocks correlate with volcanic activity in the northern Patagonian region (Fig. 6.22). These extensive rhyolitic ignimbrite and consanguineous airborne tuffaceous material form part of the Choiyoi volcanics that erupted during the late Carboniferous-early Permian to Triassic (Kay et al., 1989). Granites and rhyolites of the Choiyoi province crop out in northern and central Chile and Argentina (Kay et al., 1989). Indeed, the inception of the foreland phase was accompanied by juvenile volcanogenic material derived from the magmatic arc established along the Gondwanan continental margin. Evidence of that volcanism was identified in the Sauce Grande (Argentina), Karoo (South Africa) and Paraná Basin as discussed by López Gamundí and Rossello (Fig.2.2a, b; 1998) and is summarized below.

In southern America, radiometric data from ignimbrites exposed approximately 250 km west of the Ventana Fold Belt range from Early Permian (270 Ma) to Early Triassic (230 Ma) (Sruoga and Llambías, 1992). Additional Rb-Sr (whole rock) determinations for plutonic rocks of the North Patagonian Massif indicate early to late Permian ages (258 ± 15 , 259 ± 16 Ma; Pankhurst et al., 1992). Horizons rich in rhyolitic glass shards were also identified in sequences contemporaneous with the Tunas Formation along the eastern margin of the Paraná Basin in Brazil (López Gamundí and Rossello, 1998). The oldest occurrence of tuffaceous material has been identified in sediments of the Rio Bonito Formation (late Early Permian, 275-265 Ma) and, less abundantly, in deposits of its time equivalent in the northern margin of the basin (Tatui Formation; López Gamundí and Rossello, 1998). Along the southern margin of the basin, tuffaceous material has also been identified in the Yaguary Formation (Kazanian –Tatarian; 260-250 Ma).

In southern Africa, the first juvenile volcanogenic material in the form of tuffs appeared in the upper Dwyka Group of the Karoo Basin (López Gamundí and Rosselo, 1998). Abundant tuffaceous horizons are common as interbeds in the siliciclastic deposits of the Ecca and Beaufort Groups. Rhyodacitic and rhyolitic tuff beds are particularly abundant in the Prince Albert, Whitehill and Collingham Formations of the late Early Permian (260 Ma) lower Ecca Group (Elliot and Watts, 1974; Martini, 1974; McLachlan and Jonker, 1990). Juvenile zircons from two tuff horizons of the basal Prince Albert Formation of the Ecca Group sampled in the Western Cape were dated at 288 ± 3.0 and 289 ± 3.8 Ma by Bangert et al. (1999).



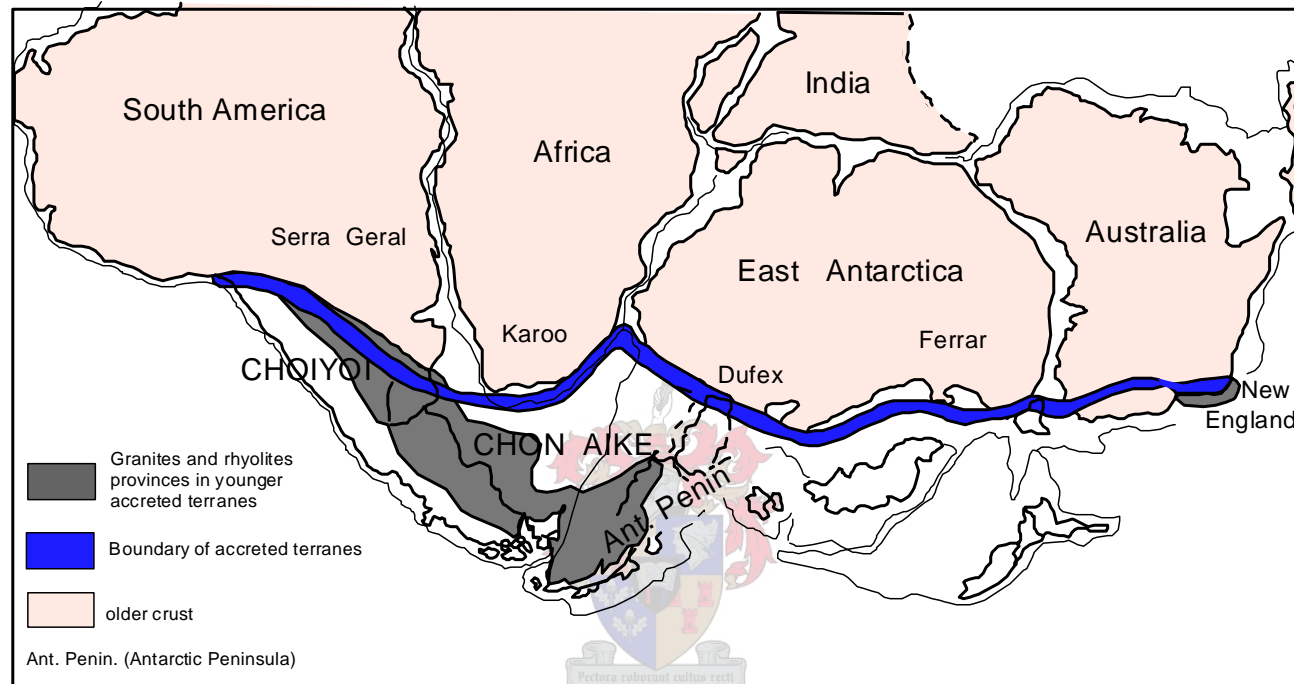


Figure 6.22 Map of southern Gondwana showing Gondwana granite-rhyolite provinces, including the late Carboniferous to Triassic (290-200 Ma) Choiyoi and the late Triassic to Jurassic (200-155 Ma) Chon Aike provinces. Also shown is the boundary separating old cratonic Gondwana from younger accreted terranes (Kay et al., 1989).

The second most important source of the investigated submarine fans and Slope sandstones is of Ordovician age (460-495 Ma). This age grouping represents 7.5 %, 16.3 %, and 22.2 % of the total analyzed detrital zircons from the Laingsburg, Skoorsteenberg and Slope sandstones respectively. This age grouping shows no correlation with any metamorphic or igneous province in southern Africa. However, these provenance ages of detrital zircons are also correlated with materials available in the adjacent region (southern South America) of the Gondwana margin. A 460-495 Ma age grouping is closely correlated with the mid-Ordovician intrusive activity reported in northern Patagonia. The Arroyo Salado granite (northern Patagonia), Famatinian granite (Argentina, north of Patagonia), and Deseado Massif (Argentina) (Table 2.1) can be regarded as the most likely suppliers of Ordovician age materials of the Waterford (Slope deposits), Skoorsteenberg and Laingsburg Formations. A summary of the igneous history of Patagonia and U-Pb chronology of Paleozoic magmatism and metamorphism in southwest Gondwana is presented by Pankhurst et al. (2003). Dating zircons from altered granitoid cobbles from northern Patagonia have given ages of 476 ± 5 and 472 ± 5 Ma. These data are suggestive of mid-Ordovician granite magmatism of the Sierras Pampeanas and orthogneiss formation in northern Patagonia (Pankhurst et al., 2001).

SHRIMP U-Pb data also reveal the importance of the older Neoproterozoic provenance (545-1000 Ma) of sedimentary materials with the dominant age grouping at 545-620 Ma. The Neoproterozoic population represents the third most important group of the investigated formations with 11.2 % of the 107 analysed zircons. These data suggest that the Laingsburg and Tanqua Karoo subbasins were also filled by sediments from readily available Neoproterozoic Pan-African Saldania and Gariep Belts and equivalents, west and south of the subbasins. These successions comprise sedimentary and volcanic rocks, the oldest component of which might have been associated with the break-up of Rodinia and opening of the proto-Atlantic in the inferred time interval 780-750 Ma (Dalziel, 1992; Powell et al., 1993). Deposition of the Gariep Supergroup lasted

from approximately 750 to 580 Ma (Frimmel, 2000). The metavolcanic and metasedimentary rocks of the Bridgetown Formation were dated at approximately 600 Ma by Rozendaal et al. (1999).

Zircon dating also yielded ages of 1000-1300 Ma, corresponding to the metamorphic age of Namaqua-Natal Province (Thomas et al., 1994; Clifford et al., 2004). Mesoproterozoic sources of the investigated upper Ecca Group represent 7.5 % of the 107 analysed zircons.

Less than 7% of the 107 dated zircons show Devonian and Cambrian provenances. A subsidiary Cambrian (495-545 Ma; 5.6%) age grouping with a dominant group between 516 and 542 Ma correlates with the Cape Granite Suite to the south and west, which intruded the Saldania Belt between 550 and 510 Ma (Scheepers and Nortjé, 2000; Scheepers and Poujol, 2002).

No igneous activity which could have provided detritus of Devonian age (354-417 Ma; 6.5 %) in the investigated subbasins is known in South Africa. However, orogenic activity close to the Silurian-Devonian boundary at ca. 400 Ma is recognized in the Deseado Massif in the form of the tonalite at El Laurel (403 ± 29 Ma $^{207}\text{Pb}/^{206}\text{Pb}$ TIMS, 395 ± 4 Ma SHRIMP; Pankhurst et al. 2003). Magmatism in adjacent areas is the most likely source of the Slope deposits and the Laingsburg and Tanqua Karoo submarine fans. Granite of the southernmost Sierras Pampeanas of Argentina shows U-Pb zircon ages of 403 ± 29 Ma, 393 ± 5 Ma, and 382 ± 6 Ma (Stuart-Smith et al., 1999). From the San Rafael block, between the Sierras Pampeanas and Patagonia, Tickj et al. (2001) reported Rb-Sr whole-rock ages on phyllite and mica schists of 371 ± 62 Ma and 379 ± 15 Ma, both of which were interpreted by the authors to relate to low to medium-grade metamorphism. Between the North Patagonia and Deseado Massifs, the Colán Conhue granite was dated at 396 ± 7 Ma (Pankhurst et al., 2003). These U-Pb data, which are within error of the El Laurel tonalite age, indicate that a belt of Devonian granitoid magmatism extended from the Sierra Pampeanas into

southern Patagonia (Pankhurst et al., 2003). In the northern Antarctic Peninsula, U-Pb zircon chronology from the Target Hill orthogneiss, previously regarded as early Paleozoic, has a comparable age (393 ± 1 Ma, TIMS; 399 ± 9 Ma, SHRIMP) and represents a Devonian S-type granitoid (Millar et al., 2002).



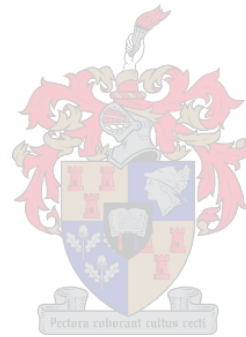
Table 6.5 Inferred provenances of the Permian Laingsburg and Tanqua Karoo sediments, based on 107 U-Pb SHRIMP analyses obtained from 109 detrital zircons.

Age groupings	Provenance of detrital zircons from the Tanqua and Laingsburg subbasins ^a .
Late Carboniferous – Permian (n=58)	Granites and mainly rhyolites of the Choiyoi province of central Chile and Argentina.
Devonian (n=7)	Orogenic activity related magmatism in the Patagonia and north of Patagonia region (El Laurel Tonalites ^b , Colan Conhué Granite ^b , Sierras Pampeanas Granite ^c
Silurian* (n=0)	Not identified
Ordovician (n=15)	Mid-Ordovician intrusive activity reported in northern Patagonia; Arroyo Salado granite ^b (northern Patagonia), Famatinian granite ^d (Argentina, north of Patagonia), Deseado Massif (Argentina) ^b .
Cambrian (n=6)	Cape Granite Suite (South Africa) ^{e, f}
Neoproterozoic (n=12)	Neoproterozoic Pan-African Saldania Belt and Gariiep Group, in the western part of the subbasin (South Africa) ^{g, h}
Mesoproterozoic (n=8)	Namaqua-Natal Province (South Africa) ^{i, j}
Eoproterozoic (n=1)	Kaapvaal Craton (probably recycled from the Cape Fold Belt)

*Zircons of Silurian age were not identified in this study.

(n) Represents the number of dated zircon grains

- ^a Kay et al. (1989)
- ^b Pankhurst et al. (2003)
- ^c Stuart-Smith et al. (1999)
- ^d Pankhurst et al. (2001)
- ^e Scheepers and Nortjé (2000)
- ^f Scheepers and Poujol (2002)
- ^g Frimmel (2000)
- ^h Rozendaal et al. (1999)
- ⁱ Thomas et al. (1994)
- ^j Clifford et al. (2004)

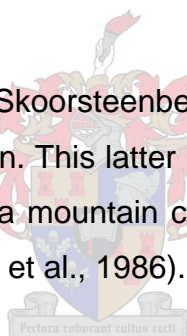


CHAPTER SEVEN

INTERPRETATION

The present study aims to develop a provenance model from source to deposition of the submarine fan complexes of the Skoorsteenberg and Laingsburg Formations with respect to the southern Gondwana geological setting during the Permian. This chapter includes the history of the Laingsburg and Tanqua Karoo subbasins as defined in this investigation and discusses some unresolved problems stated by previous investigators. Basin-fill related factors discussed here include the plate tectonic setting of the subbasins, the source rock lithologies of the detritus and their locations, relief of the source area, the transport history of detritus, climate and effect of weathering on sediments and diagenesis.

It is universally admitted that the Skoorsteenberg and Laingsburg submarine fans were deposited in a foreland basin. This latter is simply defined as a sedimentary basin lying between the front of a mountain chain (the Cape Fold Belt) and the adjacent craton (Kaapvaal) (Allen et al., 1986).



Whole-rock chemistry of the current study indicates that the Laingsburg and Tanqua foreland subbasin sediments originated from a continental island arc (CIA) and an active continental margin (ACM), following the terminology of Bhatia (1983). The distribution of the points in the active continental margin (ACM) and continental island arc (CIA) fields of Bhatia suggests that:

- (1) For the continental island arc, the sediments could have been derived from a wide range of sources but have a dominant contribution from felsic volcanics.
- (2) For the active continental margin, the subbasins were developed on or adjacent to a thick continental crust composed of older fold belt rocks. Igneous

metamorphic materials and sediments related to these terranes are dominantly derived from granite-gneisses and siliceous volcanics of the uplifted basement.

A combination of both a continental island arc and a continental margin revealed by whole-rock major and trace element chemistry of this study is in perfect accordance with the geological setting of southern Gondwana in the Permian. The Tanqua and Laingsburg subbasins resulted from the subduction of the paleo-Pacific plate (i.e. Panthalassa) beneath Gondwana, an active continental margin (ACM) setting. Uplift of the basement and consumption of Panthalassa deep in the mantle below Gondwana, led to the formation of the continental island arc (CIA).

On the Pettijohn et al. (1972) and Herron (1988) sandstones classification diagram the Laingsburg, Slope and Tanqua sandstones plot on the boundary between greywackes and litharenites.

The whole rocks typically have Ca/Na values of 0.3 to 0.5, the plagioclase on the other hand appears to have Ca/Na of 0.1 or less. This suggests that there must be a Ca sink in the rocks other than plagioclase, possibly epidote. The observation that plagioclase is nearly pure albite indicates a low temperature metamorphic, plutonic or authigenic origin. This interpretation is likely because the investigated sandstones contain other detrital grains of undoubted metamorphic and/or plutonic origin such as microcline-perthite and epidote. The lack of chemical zonation shown by these feldspars strongly suggests a metamorphic origin. The origin of these albitic plagioclase crystals as low temperature metamorphic product may have been made possible by the inclusion of volcanic glass in the sediments. Furthermore, the phenomenon of post-depositional albitization indicates that detritus could also be derived from volcanic source. This can be supported by two plagioclase grains ($An_{0.7}Or_{5.8}Ab_{93.5}$ and $An_{4.9}Or_{6.4}Ab_{88.7}$) derived from low temperature rhyolitic rocks.

In general, major and trace element characteristics of the investigated sandstones reveal that the subbasins were mainly filled by intermediate to felsic igneous rocks. The latter include tonalites, granodiorites and adamellites or their volcanic equivalents as suggested by the molar $(\text{CaO}+\text{Na}_2\text{O})-\text{Al}_2\text{O}_3-\text{K}_2\text{O}$ ternary diagram developed by Nesbitt and Young (1984). The present result is reinforced by zircon chemistry which also suggests predominant tonalitic and granodioritic source rocks and also by the zircon morphological study developed by Pupin (1980) which indicates a tonalitic and orogenic calc-alkaline rhyolitic (CAR) provenance.

The very different characteristics of Fan 4 with respect to the other fans are clearly illustrated by its mineralogy and chemistry. Fan 4 is more mature than the other fans, presumably because it occupies a more distal position in the subbasin (Fig. 1.7). Sediments of Fan 4 travelled over longer distances and therefore underwent more recycling. On the $(\text{CaO}+\text{Na}_2\text{O})-\text{Al}_2\text{O}_3-\text{K}_2\text{O}$ ternary diagram, many sandstone samples from the Tanqua deepwater Fan 4 plotted between the weathering trend of tonalite and granodiorite, indicating that this fan was dominantly derived from more intermediate igneous (tonalite-granodiorite) sources whereas other Tanqua Karoo fans investigated are mainly derived from more felsic (granodiorite-adamellite) sources. A similar result is obtained on the discrimination function diagram for provenance signatures of sandstone-mudstone suites using major elements developed by Roser and Korsch (1988). Furthermore, zircons from this fan are inclusion-rich which, according to Pupin (1980), is an indication of a mantle derivation since crustal and migmatite zircons are generally inclusion-poor.

Before locating the aforementioned source rock types by using radiometric dates obtained from detrital zircons from the studied sandstones it is important to bear in mind that three models have been recently proposed to account for the main provenance of the Permian Laingsburg and Tanqua fans. As previously

mentioned, the proposed source areas included: (1) the Cape Supergroup in the Cape Fold Belt (Lock, 1980; Kingsley, 1981; Hälbich, 1983; Cole, 1992; Veevers et al., 1994; Adelman and Fiedler, 1998), (2) a magmatic arc to the south of the present Cape Fold Belt (Elliot and Johnson, 1972; Elliot and Watts, 1974; Martini, 1974; Visser, 1979; Johnson, 1991), and (3) the Northern Patagonian Massif (Van Lente et al., 2003; King et al., 2004). Some interpretations, however, combine these provenance models, but do not give their respective contribution. Andersson et al. (2003) stated that the source area of the Skoorsteenberg Formation is certainly a late Paleozoic thrust belt and a contemporaneous magmatic arc to the south of the Cape Fold Belt whereas Scott et al. (2000) argued that detritus originated from an area between the magmatic arc of the subduction zone and the rising, but submerged, fold-thrust belt, possibly an uplifted area of older, metamorphosed sediments in the paleo-Patagonia region. These differences in opinion with regard to the main provenance of the Tanqua and Laingsburg detritus indicate that the main source area of the investigated formations is poorly defined and must be reconsidered.

The assumption that the adjacent Cape Fold Belt supplied the early foreland Tanqua and Laingsburg subbasin fill would have predicted texturally and mineralogically mature deepwater sands as a result of recycling and breakdown of unstable minerals such as lithic fragments and feldspars, especially plagioclase. In addition, the predominance of almandine garnets with pyrope contents from 10 to 40 mol%, indicative of epidote-amphibolite to granulite facies (Takeuchi, 1994), indicates that the submarine fans were not dominantly derived from the low-grade metasedimentary Cape Fold Belt, thereby confirming the conclusion of Scott (1997). This is reinforced by the paucity of sedimentary zircons which are usually rounded to sub-rounded and show overgrowth and the predominance of pristine juvenile zircons. Furthermore, only one out of 110 dated zircons shows a cratonic derivation ($2,456 \pm 21$ Ma) which may be correlated with the cratonic-derived Cape Supergroup in the Cape Fold Belt (Visser, 1979; Johnson, 1991).

Elliot and Johnson (1972), Martini (1974), Visser (1979), and Johnson (1991) suggested a southern magmatic arc to the south of the Cape Fold Belt as the main source area for the Ecca and Beaufort Groups. This interpretation is relatively close to the results of this investigation. Major element whole-rock chemistry of this study revealed the presence of a continental island arc (CIA) in the source region. The proximity of the Skoorsteenberg and Laingsburg fans to a magmatic arc field is also suggested by abundant plagioclase feldspar (albite) of volcanic origin as well as volcanic quartz which is usually monocrystalline and water clear, with rounded corners and resorption embayments. Moreover, zircon populations in the investigated submarine fans are largely dominated by juvenile zircons with growth discontinuities, vitreous inclusions and sharp edges, suggesting a volcanic origin (Pupin, 1980; Dabard et al., 1996). It is to be noted that a strong similarity exists between zircons identified in this study and juvenile zircons from the Dwyka tuffs described by Bangert et al. (1999). Zircons from the Dwyka tuff horizons are mostly euhedral, show well-developed magmatic zoning, no growth lines and cores. Some are elongated-prismatic to needle-like in shape (equivalent to type P zircon of this study) and some show inclusions. The crystal faces are well-developed and not abraded. The majority of the zircons within the Tanqua and Laingsburg fans are quite small and their size ranges from 80 to 150 μm , with very few grains exceeding 160 μm , while the size of the Dwyka tuff zircons varies between 79 and 250 μm . In addition, the Dwyka zircons dated at 288 ± 3 Ma and 289 ± 3.8 Ma crystallized within dacitic to rhyolitic rocks (Bangert et al. 1999) while the majority of the zircons of this study dated at 270-290 Ma reveal a tonalitic to calc-alkaline rhyolitic source.

U-Pb SHRIMP radiometric dates obtained from 107 detrital zircons indicate that the investigated Slope, Skoorsteenberg and Laingsburg zircon populations are dominated by 260-310 Ma old juvenile zircons (54.2 % of the total analyzed grains). A 260-310 Ma age grouping with a peak at 270-290 Ma, supported by dominant tonalitic and orogenic calc-alkaline rhyolitic source rocks, correlate with volcanic activity in the adjacent northern Patagonian region. Extensive rhyolitic

ignimbrite and consanguineous airborne tuffaceous material, part of the Choiyoi volcanism, erupted here during late Carboniferous-early Permian to Triassic times (Kay et al., 1989).

The insignificant thickness of the Dwyka tuff horizons compared to metre thick fans excludes the possibility of the readily available tuffs being the main source of the investigated fans, but rather that they originated from the same parental magma, i.e. the Choiyoi (290-210 Ma; Kay et al., 1989). Therefore, suggesting that the volcanism continued well after the deposition of the Dwyka tuffs beds (288 ± 3 Ma and 289 ± 3.8 Ma; Bangert et al., 1999) to as late as 253 Ma, which approximately corresponds to both the end of the deposition of the Eccca Group and the second event of the Cape Orogeny as discussed below. The Eccca Group was therefore deposited over a period of approximately 47 Ma. New radiometric dates of this investigation indicate that the Collingham Formation, consisting of turbidites and intercalated ash beds dated at 270 ± 1 Ma by Turner (1999), is no longer the only unit of the Eccca Group that can be related directly to active volcanism to the south and southwest as stated by Wickens (1994), but that turbidites of the Skoorsteenberg and Laingsburg also do.



The absence of zircons younger than 253 Ma in the analyzed population simply suggests that the Choiyoi volcanism, which represents the youngest and main source of the fans (54.2 % of the total analyzed zircons), stopped supplying detritus to the Tanqua and Laingsburg Karoo subbasins after the second event of the Cape Orogeny at 258 ± 2 Ma. The above interpretations are in perfect agreement with the conclusion of Hälbig et al. (1983) who suggested that the subbasins formed and filled during the first two events of the building of the Cape Fold Belt at 278 Ma and 258 Ma. The 258 Ma tectonic event caused the Cape Fold Belt to develop enough to prevent the transport of sediments into the Tanqua and Laingsburg subbasins (Scott, 1997). This explains why the Triassic component of the Choiyoi volcanism is significantly represented in northern

Patagonia while its equivalent (Triassic-age zircons from the Choiyoi province) in southern Africa is poorly represented.

Considering that the Laingsburg Formation is 750m thick along the Buffels River (Sixsmith, 2000) and that the Skoorsteenberg is 400m thick (Wickens, 1994), and accepting that the Skoorsteenberg and Laingsburg formations were deposited over a period of approximately 47 Ma, one can therefore evaluate the sedimentation rate (thickness divided by time) of the two formations. Assuming constant-volume input of detritus and water and a uniform subsidence rate, this study reveals that 8.5 and 14.9 m of sediments were deposited every million year in the Tanqua and Laingsburg subbasins respectively. The tectonic regime in this southern Gondwana region greatly influenced both the sediment input and detritus accommodation space in adjacent subbasins. The more the tectonic compression the larger the sediment input. Less tectonic compressional forces resulted in a shallower, open subbasin in the Tanqua whereas a deeper, narrow subbasin was developed in the Laingsburg as a result of more tectonic compression (Scott, 1997).

The second most important source of the investigated submarine fan and Slope sandstones is of Ordovician age (460-495 Ma). A 460-495 Ma age grouping is correlated with the Arroyo Salado granite of northern Patagonia (476 ± 4 Ma), the Famatinian granite of Argentina, north of Patagonia (470-490 Ma; Pankhurst et al., 2001), and the Deseado Massif of Argentina (476 ± 5 and 472 ± 5 Ma; Pankhurst et al. 2003). These intrusive rocks of the northern Patagonia can be regarded as the most likely supplier of Ordovician-age materials of the Slope, Skoorsteenberg and Laingsburg Formations of the Ecca Group in the retro-arc foreland Karoo Basin, South Africa.

No igneous activity which could have provided detritus of Devonian-age (354-417 Ma) to the investigated subbasins is known in South Africa. However, orogenic activity close to Silurian-Devonian boundary at ca. 400 Ma is recognized in the

Deseado Massif by virtue of the age of the tonalite at El Laurel (403 ± 29 Ma $^{207}\text{Pb}/^{206}\text{Pb}$, TIMS, 395 ± 4 Ma SHRIMP; Pankhurst et al. 2003). Magmatism in adjacent areas is the most likely source of Devonian-age zircons identified in the investigated submarine fan sandstones. Granite of the southernmost Sierras Pampeanas of north of Patagonia shows U-Pb zircon ages of 403 ± 29 Ma, 393 ± 5 Ma, and 382 ± 6 Ma (Stuart-Smith et al., 1999). From the San Rafael block, between the Sierras Pampeanas and Patagonia, Tickj et al. (2001) reported Rb-Sr whole-rock ages on phyllite and mica schists of 371 ± 62 Ma and 379 ± 15 Ma. The Colán Conhue granite, located between the North Patagonia and Deseado Massifs, has given a U-Pb SHRIMP crystallization age of 396 ± 7 Ma (Pankhurst et al., 2003).

The granites of the North Patagonia Massif (NPM) constitute two batholithic series. These are (i) the Somuncura Batholith that lies largely in the northern part of the massif and (ii) the Batholith of Central Patagonia that lies along its southwestern border (Pankhurst et al., 1992). In terms of age and composition, the Somuncura Batholith and the Batholith of Central Patagonia are correlative with the volcano-plutonic Choiyoi Province (Pankhurst et al., 1992), which is identified as the main supplier of detritus that filled the Tanqua and Laingsburg subbasins. This confirms the findings of Van Lente (2004) and King et al. (2004) who suggested a considerable contribution from the North Patagonia Massif. However, abundant fine to very fine angular grains and albitic feldspars of volcanic origin, as well as the predominance of volcanic zircons indicate a dominant contribution from the volcanic component of the transitional arc rather than the plutonic one (North Patagonia Massif) as suggested by King et al. (2004) and Van Lente (2004). This new evidence may solve the ambiguity related to the angularity of grains noticed by King et al. (2004) which was not consistent with a solely plutonic source (the North Patagonian Massif) model proposed by these investigators.

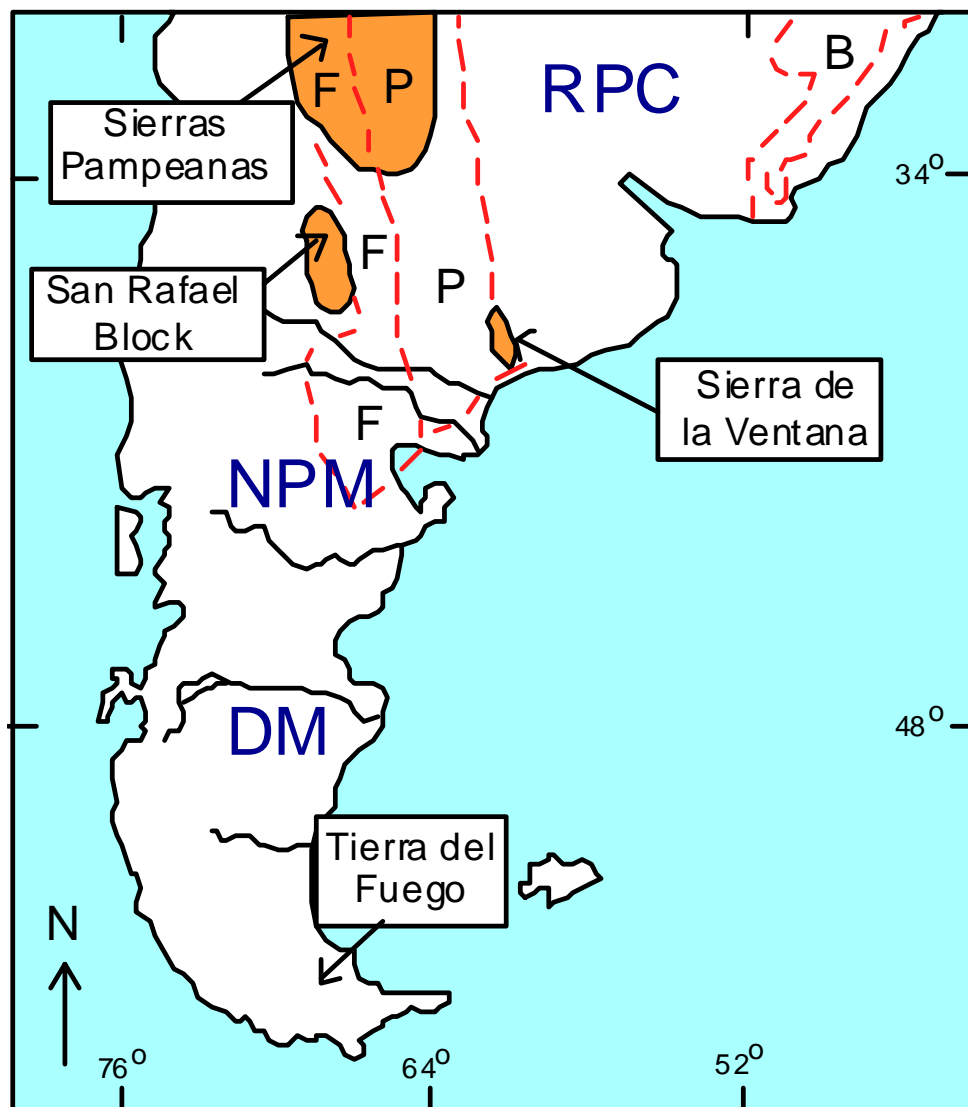


Figure 7.1 Map of the southern South America showing the generalized locations of the Deseado Massif (DM), the North Patagonian Massif (NPM), and the Río de La Plata Craton (RPC). The conjectural extensions of the Dom Feliciano (Bresiliano; B), the Pampean (P) and Famatinian (F) orogenic belts of Neoproterozoic to mid-Ordovician age are also shown (Pankhurst et al., 2003).

The southern African sources of the Tanqua and Laingsburg sediments include the Kaapvaal craton (1 out of 107 dated zircon shows a cratonic derivation), the Mesoproterozoic Namaqua-Natal Metamorphic Complex (7.5% of the 107 analyzed zircons), the Neoproterozoic Pan-African Saldania Belt and Gariep Belt or equivalents in the western part of the subbasins (11.2% of the population), and the Cambrian Cape Granite Suite (5.6% of the 107 dated zircons). These subordinate sedimentary, plutonic and metamorphic rocks were progressively eroded during the infill of the subbasins. The Namaqua-Natal Metamorphic Complex is the probable source of almandine-pyrope, indicative of a medium-to high-grade metamorphic terrane contribution identified in this investigation.

The chemical index of alteration (CIA) developed by Nesbitt and Young (1982), calculated by using whole-rock major element concentrations, shows values which range from 53.3 to 69.3 (average = 64.7, n = 8; Van Lente, 2004) and from 58.7 to 69.1 (the Tanqua sandstones; this study) suggesting low to moderately weathered sources for the Laingsburg and Tanqua submarine fan sandstones respectively. These values indicate lower degrees of weathering than for the average shale (CIA = 70-75; Taylor and McLennan, 1985).



Chemical index of alteration of fresh granite is 45-55 whereas more intense weathering, which results in residual clays such as kaolinite and gibbsite-rich shale, produces chemical index of alteration values close to 100. On the ternary diagram $(CaO^* + Na_2O) - Al_2O_3 - K_2O$ which is the graphic representation of the chemical index of alteration, the Tanqua, Laingsburg and Slope sandstones plot at relatively high alkali values (~5 wt %) and relatively lower Al_2O_3 contents, suggesting a limited breakdown of feldspar and therefore a low to moderate weathering regime or limited transport.

Nesbitt and Young (1982) have shown that Pleistocene tills having chemical index of alteration (CIA) values of around 52, Pleistocene glacial clays having average CIA values of around 65 or Pleistocene varved clays with average CIA

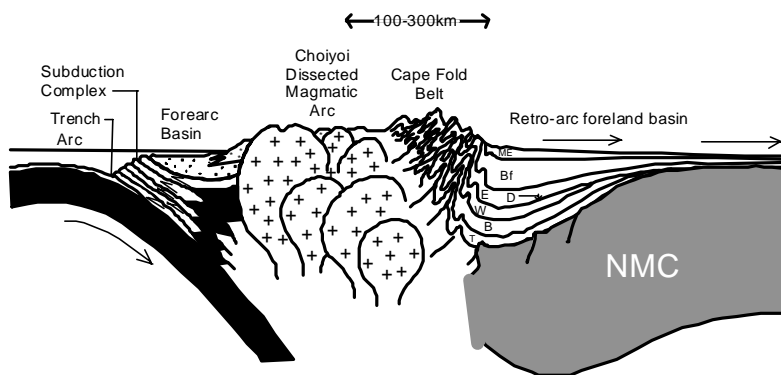
values of around 62 were formed in extreme cold conditions, whereas residual clays with CIA values greater than 90 and Amazon cone muds that have average CIA values between 82 and 86 are likely to have been formed in hot, humid climates. The Tanqua and Slope sandstones with CIA values varying between 58.7 and 69.1, as well as the Laingsburg sandstones showing average CIA of 64.7 are believed to have been deposited in a relatively cold environment which is expected to have prevailed shortly after the Dwyka ice age.

This relatively cold climate may therefore explain the weak chemical weathering and limited breakdown of feldspar observed in this study. The formation of high relief due to rapid uplift of the basement during subduction and associated volcanic activity are typical cases of short-circuiting weathering and also played a major role in the preservation of feldspar.

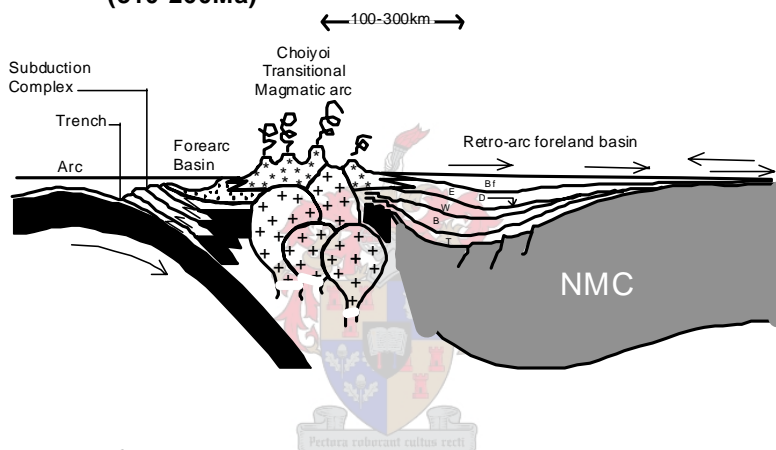
The Laingsburg and Tanqua deepwater fan sandstones comprise very abundant angular quartz and feldspar and abundant unstable lithic fragments. Such immature sedimentary rocks are likely to have formed close to their site of deposition (i.e. limited transport) since long-distance transport of detritus destroys unstable minerals such as albite and rock fragments and favours the formation of well-sorted sandstones with moderately to well-rounded grains. The predominance of zircons with very well preserved crystal faces is another indication of a very short travel distance of the sediments and a nearby source area. Taken together, the angularity of grains, the presence of albitic plagioclase feldspars, abundant matrix and the predominance of pristine zircons strongly indicate that the Skoorsteenbergr and Laingsburg detritus are dominantly first cycle. Mineralogically mature polycyclic sandstones certainly contain subrounded to well rounded zircons and not sphene. The latter is a chemically unstable mineral that usually dissolves at an early stage of diagenesis (Mange and Maurer, 1992). Sphene is rarely found as detrital grains in sandstones.

From the above it is clear that the derivation of the investigated submarine fans from the paleo-Pacific margin of Gondwana, 1500-2000 km south of the subbasins (Lock, 1980), or a 600-km pre-Atlantic Ocean transport proposed by King et al. (2004) is very unlikely. However, Bangert et al. (1999) compared the sizes of the glass shards contained in the Dwyka tuff horizons, which are believed to be consanguineous with the investigated fans, with published grain size versus transport distance relationships (Fisher and Schmincke, 1984) and suggested a maximum transport distance in the order of 100-300 km for the detritus. In addition, Dickinson's (1976) idealized true-scale sections through orogenic basins (e.g., his Figure 30) indicates that a retro-arc foreland basin axis is typically located 150-250 km from the magmatic arc, being separated from it by the width of the intervening fold-thrust belt. The development of a fold-thrust belt between the magmatic arc and the depositional basin (Fig. 7.2c) represents the final stage in the evolution of most retro-arc foreland basins (Dickinson, 1974). Johnson (1991) proposed a similar provenance model for the Karoo Basin. He suggested the development of the Cape Fold Belt while the upper part of the Karoo Sequence was being deposited. The conclusion of Johnson is confirmed in this study by the predominance of the Choiyoi magmatism age zircons (310-260 Ma; 54.2 % of the total dated grains), with a peak at 290-270 Ma, together with an insignificant contribution from the much older metasedimentary orogenic belt and stable craton, indicating that the Choiyoi volcanic activity in the south was prior to the development of the Cape Fold Belt. Zircons from the northern Patagonian area would not dominate the Skoorsteenberg, Laingsburg and Slope zircon populations if the Cape Fold Belt was active and exposed. The latter would have acted as a barrier to the contribution of sediments from the Choiyoi transitional arc.

c. Late Triassic (~200Ma)



b. Late Carboniferous-Permian (310-260Ma)



a. Early Carboniferous

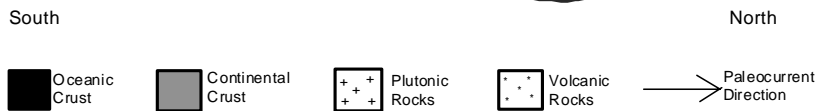
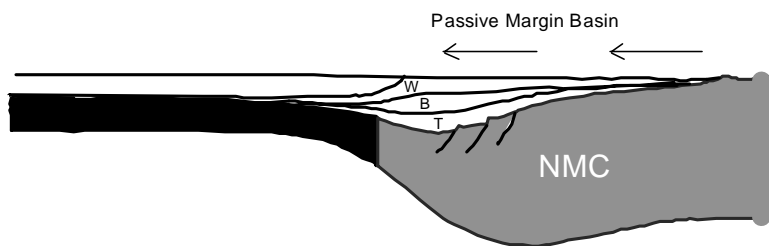


Figure 7.2 Cross section of southern Gondwana showing the three stages in the evolution of the Cape-Karoo Basin. Also shown are the Choiyoi magmatic arc (northern Patagonia) and the subduction zone. ME=Molteno+Elliot Formations, Bf=Beaufort Group, E=Ecca Group, D=Dwyka Group, W=Witteberg Group, B=Bokkeveld Group, T=Table Mountain Group, NMC=Namaqua Metamorphic Complex (Modified after Johnson, 1991).

CHAPTER EIGHT

CONCLUSIONS

The Laingsburg and Tanqua deepwater fan systems were deposited in a retro-arc foreland basin setting in relation to the consumption of the Panthalassa deep in the mantle below Gondwana, an active continental margin setting. Uplift of the basement and subduction of the paleo-Pacific plate beneath Gondwana led to the formation of a continental island arc (i.e. the Choiyoi arc) of intermediate to felsic igneous affinity in the northern Patagonian region.

The Laingsburg and Tanqua Karoo deepwater sandstones show a strong similarity in terms of their provenance. The subbasins were filled by sediments derived from a wide range of igneous rocks dominated by tonalites, granodiorites, adamellites or their volcanic equivalents, as shown by the sandstones whole-rock chemistry and reinforced by zircon morphology and chemistry.

Fan 4 is more mature than other fans, a consequence of its more distal position in the subbasin. Compared to other investigated Tanqua deepwater fans, Fan 4 was dominantly derived from more intermediate igneous rocks, including tonalites and granodiorites.

The Laingsburg, Skoorsteenberg and Slope sandstones may be classified as greywackes and litharenites following the terminology of Pettijohn et al. (1972) and Herron (1988) or quartz-intermediate according to Crook (1974). Both greywackes and litharenites are chemically immature sandstones. This may argue for minimum amount of weathering during erosion, transport and deposition.

Weak chemical weathering and limited breakdown of feldspar observed in this investigation resulted in the competing influence of both a relatively cold climate,

which prevailed shortly after the Dwyka ice age, and high relief due to rapid uplift of the basement during subduction and associated volcanic activity. High relief and volcanic activity are typical causes of rapid deposition, limited transport and short-circuited weathering.

The late Carboniferous-Permian to Triassic Choiyoi arc of northern Patagonia is believed to be the main source of detritus that filled the Tanqua and Laingsburg subbasins.

The Mid-Ordovician Arroyo Salado granite (northern Patagonia), Famatinian granite (Argentina, north of Patagonia), and Deseado Massif (Argentina) of South America represent the second most important sources of the Tanqua and Laingsburg submarine fan complexes of the Karoo Basin, South Africa.

The proximal Neoproterozoic Pan-African Saldania Belt, Gariep Belt and equivalents (South Africa), located in the South and western part of the subbasin, also contributed to a lesser extent to the infill of the western corner of the Karoo Basin.



Subordinate sources include the Mesoproterozoic Namaqua-Natal Province, the magmatism related to Devonian orogenic activity in the Patagonian and northern Patagonian region, the Cambrian Cape Granite Suite and the Kaapvaal Craton, in decreasing order of importance.

The Laingsburg and Tanqua deepwater detritus is dominantly first-cycle. The large abundance of angular quartz and feldspar, together with the predominance of euhedral zircons with very well preserved crystal faces, suggest a very short travel distance of sediments and a nearby source area. Zircon sizes (80-150 μm) together with the ideal location of the orogenic belt and magmatic arc in relation to the adjacent foreland basin in a continental island arc setting, also account for a relatively close provenance. In the Permian times under consideration, the

distance between the Choiyoi transitional arc and the Laingsburg and Tanqua Karoo retro-arc foreland subbasins is believed to have been 100-300 km.

The main eruption phase of the Choiyoi arc (290-270 Ma), from which the investigated submarine fans dominantly originated, predates the main tectonic events associated with the development of the Cape Fold Belt. The infill and formation of the Laingsburg and Tanqua foreland subbasins occurred during the first two events of the Cape Orogeny at 278 Ma and 258 Ma and can be correlated with the late stage of the Choiyoi volcanic activity. The post-258 Ma tectonic events caused a significant tectonic development of the Cape Fold Belt and prevented continued transport of sediments into the Tanqua and Laingsburg subbasins from the south and southwest. The absence of Patagonian zircons younger than 253 Ma indicates that the fold belt did form an impenetrable barrier to the continued contribution of detritus from the arc.

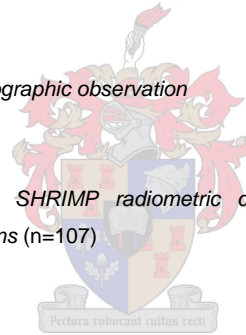
The source rock lithologies, age and morphological similarities existing between the investigated zircons and juvenile zircons of tuff horizons of the Dwyka Group and Prince Albert Formation (Ecca Group) investigated by Bangert et al. (1999) suggest a derivation of these successions from the same parental magma. This indicates that the volcanism continued well after the deposition of the Dwyka tuff beds to as late as 253 Ma, which corresponds to the end of the deposition of the Ecca Group.

A summary of the most important findings together with the methods used during this investigation are shown on Table 8.1.

Table 8.1 Recapitulatory table of the main findings of this study.

Objective	Methods	Results and comments
1. Classification of sandstones and sediment maturity	<ul style="list-style-type: none"> • <i>Whole-rock chemistry</i>: $\log(\text{Na}_2\text{O}/\text{K}_2\text{O})$ vs. $\log(\text{SiO}_2/\text{Al}_2\text{O}_3)$ and Na_2O vs. K_2O. 	Greywackes to litharenites, mineralogically immature, moderately sorted with abundant angular grains.
2. Tectonic setting of the subbasins	<ul style="list-style-type: none"> • <i>Whole-rock chemistry</i>: $(\text{Fe}_2\text{O}_3 + \text{MgO})$ vs. TiO_2, $\text{Al}_2\text{O}_3/\text{SiO}_2$, $\text{K}_2\text{O}/\text{Na}_2\text{O}$, and $\text{Al}_2\text{O}_3/(\text{CaO} + \text{Na}_2\text{O})$, and La/Th vs. Hf 	Active continental margin (ACM) and continental island arc (CIA)
3. Source rock lithologies	<ul style="list-style-type: none"> • <i>Whole-rock chemistry</i>: ternary $(\text{CaO} + \text{Na}_2\text{O})$-$\text{Al}_2\text{O}_3$-$\text{K}_2\text{O}$ diagram, Co/Th vs. La/Sc; Th/Sc vs. Zr/Sc; and La/Th vs. Hf • <i>Zircon chemistry</i>: Y vs. U, Nb/Ta and Yb/Sm, and Nb vs. Ta. • <i>Typological study of zircon</i> 	Tonalites, granodiorites, adamellites or their volcanic equivalents, and orogenic calc-alkaline rhyolites.
4. Effect of chemical weathering on detritus	<ul style="list-style-type: none"> • <i>Whole-rock chemistry</i>: chemical index of alteration (CIA) = $[\text{Al}_2\text{O}_3/(\text{Al}_2\text{O}_3 + \text{CaO} + \text{Na}_2\text{O} + \text{K}_2\text{O})] \times 100$, • <i>Petrographic observation</i> (average degree of alteration of feldspars) 	Low to moderate
5. Climate	<ul style="list-style-type: none"> • <i>Whole-rock chemistry</i>: Chemical index of alteration (CIA) 	Relatively cold

	<ul style="list-style-type: none"> • <i>Petrographic observation</i> (average degree of alteration of feldspars and abundance of other unstable minerals) 	
6. Relief of the source area	<ul style="list-style-type: none"> • <i>Petrographic observation</i> (abundance of rock fragments and feldspars) 	High
7. Transport history of detritus	<ul style="list-style-type: none"> • <i>Petrographic observation</i> (grain roundness and abundance of unstable minerals) • <i>Zircon morphology</i> (crystal faces) 	Dominantly first cycle
8. Diagenesis	<ul style="list-style-type: none"> • <i>Petrographic observation</i> 	Advanced diagenesis due to abundant unstable minerals such as lithic fragments susceptible to diagenesis
9. Geochronology and location of the source rocks	<ul style="list-style-type: none"> • <i>U-Pb SHRIMP radiometric dating of detrital zircons (n=107)</i> 	<p>Relative contribution of each source rock on the basis of 107 zircons, in decreasing order of abundance</p> <ul style="list-style-type: none"> • Choiyoi transitional arc (North Patagonia; n=58) • Arroyo Salado granites, Famatinian granites Deseado Massif, North and northern Patagonia (n=15) • Saldania Belt and equivalents, South Africa (n=12) • Namaqua-Natal Metamorphic Province, South Africa (n=8) • El Laurel tonalites, Colan Conhué granite and Sierras Pampeanas granite, North Patagonia (n=7) • Cape Granite Suite, South Africa (n=6).



10. Relationship between deposition of the Skoorsteenberg and Laingsburg Formations and the development of the Cape Fold Belt (CFB)
- *U-Pb SHRIMP radiometric dating of detrital zircons (n=107)*
 - Kaapvaal Craton, South Africa (n=1)
- The Skoorsteenberg and Laingsburg formations were deposited between 290 and 253 Ma and prior to the development and exposure of the Cape Fold Belt
-



REFERENCES

Adelmann, D. & Fiedler, K. (1998). Origin and characteristics of Late Permian submarine fan and deltaic sediments in the Laingsburg sub-basin, SW Karoo Basin, Cape Province, South Africa. *Z. Deut. Geol. Ges.*, **149**, 27-38.

Allen, P.A., Homewood, P. & Williams, G.D. (1986). Foreland basins: an introduction, 3-12. *In: Allen, P.A., Homewood, P. (Ed.), Foreland Basins*. Blackwell Scientific Publications, Oxford, 453pp.

Andersson, P.O.D., Johansson, A. & Kumpulainen, R. A. (2003). Sm-Nd isotope evidence for the provenance of the Skoorsteenberg Formation, Karoo Supergroup, South Africa. *J. Afr. Earth Sci.*, **36**, 173-183.

Andersson, P.O.D., Worden, R.H., Hodgson, D.M. & Flint, S. (2004). Provenance evolution and chemostratigraphy of a Palaeozoic submarine fan-complex: Tanqua Karoo Basin, South Africa. *Mar. Petrol. Geol.*, (in press).

Asiedu, D.K., Suzuki, S. & Shibata, T. (2000). Provenance of sandstones from the Lower Cretaceous Sasayama Group, Inner Zone of Southwest Japan. *Sediment. Geol.*, **131**, 9-24.

Awwiller, D.N. (1994). Geochronology and mass transfer in Gulf Coast mudrocks (south-central Texas, USA): Rb-Sr, Sm-Nd and REE systematics. *Chem. Geol.*, **116**, 61-84.

Bangert, B., Stollhofen, H., Lorenz, V. & Armstrong, R. (1999). The geochronology and significance of ash-fall tuffs in the glaciogenic Carboniferous-Permian Dwyka Group of Namibia and South Africa. *J. Afr. Earth Sci.*, **29**, 33-49.

Basu, A., Young, S.W., Suttner, L.J., James, W.C. & Mack, G.H. (1975). Re-evaluation of the use of undulatory extinction and polycrystallinity in detrital quartz for provenance interpretation. *J. Sediment. Petrol.*, **45**, 873-882.

Belousova, E.A., Griffin, W.L., O'Reilly, S.Y. & Fisher, N.J. (2002). Igneous zircon: trace element composition as an indicator of source rock type. *Cont. Mineral. Petrol.*, **143**, 602-622.

Beukes, N.J. & Cairncross, B. (1991). A lithostratigraphic-sedimentological reference profile for the Late Mozaan Group, Pongola Sequence: application to sequence stratigraphy and correlation with the Witwatersrand Supergroup. *S. Afr. J. Geol.*, **94**, 44-69.

Bhatia, M.R. (1983). Plate tectonics and geochemical composition of sandstones. *J. Geol.*, **91**, 611-627.

Bhatia, M.R. & Crook, K.A.W. (1986). Trace element characteristics of greywackes and tectonic setting discrimination of sedimentary basins: *Cont. Mineral. Petrol.*, **92**, 181-193.



Boggs, Sam, Jr. (1992). *Petrology of sedimentary rocks*. Macmillan Publishing Company, New York, 707 p.

Bouma, A.H. & Wickens, H. deV. (1991). Permian passive margin submarine fan Complex, Karoo Basin South Africa: possible model to Gulf of Mexico. *Trans. Gulf Coast Assoc. Geol. Soc.*, **XLI**, 30-42.

Bouma, A.H. & Wickens, H. deV. (1994). Tanqua Karoo, ancient analog for fine-grained submarine fans. In: Weimer, P., Bouma, A.H. and Perkins, B.F. (Ed.), *Submarine Fans and Turbidite Systems*, GCSSEPM Fifteen Research Conference, 23-34.

Breitkreuz, C., Bahlburg, H. Delakowitz, B. & Pichowiak, S. (1989). Paleozoic volcanic events in the Central Andes. *J. South Amer. Earth Sci.*, **2** (2), 171-189.

Broquet, C.A.M. (1992). The sedimentary record of the Cape Supergroup: a review. In: de Wit, M.J. and Ransome, I.G.D., (Ed.), *Inversion tectonics of the Cape Fold Belt, Karoo and Cretaceous Basins of Southern Africa*. Balkema, Rotterdam, 159-183.

Camiré, G.E., Laflèche, M.R. & Ludden, J.N. (1993). Archaean metasedimentary rocks from the north-western Pontiac Subprovince of the Canadian Shield: chemical characterization, weathering and modelling of the source areas. *Precamb. Res.*, **62**, 285-305.

Clifford, T.N., Barton, E.S., Stern, R.A. & Duchesne, J.C. (2004). U-Pb Zircon Calendar for Namaquan (Grenville) Crustal Events in the Granulite-facies Terrane of the O'okiep Copper District of South Africa. *J. Petrol.*, **45**, 669-691.

Cole, D.I. (1992). Evolution and development of the Karoo Basin. In: de Wit, M.J. and Ransome, I.G.D., (Ed.), *Inversion tectonics of the Cape Fold Belt, Karoo and Cretaceous Basins of Southern Africa*. Balkema, Rotterdam, 87-100.

Condie, K.C. (1993). Chemical composition and evolution of upper continental crust: contrasting results from surface samples and shales. *Chem. Geol.*, **104**, 1-37.

Condie, K.C. & Wronkiewicz, D.J. (1990). The Cr/Th ratio in Precambrian pelites from the Kaapvaal Craton as an index of craton evolution. *Earth Planet. Sci. Lett.*, **97**, 256-267.

Crook, K.A.W. (1974). Lithogenesis and geotectonics: the significance of compositional variation in flysch arenites (greywackes). In: Dott Jr., R.H. and Shaver, R.H. (Ed.), *Modern and Ancient Geosynclinal Sedimentation*, SEPM Spec. Publ., **19**, 304– 310.

Cullers, R.L. (1994). The controls on the major and trace element variation of shales, siltstones, and sandstones of Pennsylvanian-Permian age from uplifted continental blocks in Colorado to platform sediment in Kansas, U.S.A. *Geochim. Cosmochim. Acta*, **58**, 4955-4972.

Cullers, R.L. (2000). The geochemistry of shales, siltstones, and sandstones of Pennsylvanian-Permian age, Colorado, U.S.A: Implication for provenance and metamorphic studies. *Lithos*, **51**, 181-203.

Cullers, R.L. & Graf, J.L. (1984). Rare earth elements in igneous rocks of the continental crust: intermediate to silicic rocks-ore petrogenesis. In: Henderson, P. (Ed.), *Rare Earth Element Geochemistry*. Amsterdam, Elsevier, 275-316.

Cullers, R.L. & Podkovyrov, V.N. (2000). Geochemistry of the Mesoproterozoic Lakhanda shales in south-eastern Yakutia, Russia: Implication for mineralogical and provenance control, and recycling. *Precamb. Res.*, **104**, 77-93.

Cullers, R.L., Basu, A. & Suttner, L.J. (1988). Geochemical signature of provenance in sand-mixed material in soils and stream sediments near the Tobacco Root batholith, Montana, U.S.A. *Chem. Geol.*, **70**, 335-348.

Cullers, R.L., Barrett, T., Carlson, R. & Robinson, B. (1987). Rare-earth element distributions in size-fractions of Holocene soil and stream sediment, Wet Mountains region, Colorado, U.S.A. *Chem. Geol.*, **63**, 275-297.

Cullers, R.L., Chaudhuri, S., Kilbane, N. & Koch, R. (1979). Rare-earths in size fractions and sedimentary rocks of Pennsylvanian-Permian age from the mid-continent of the U.S.A. *Geochim. Cosmochim. Acta*, **43**, 1285-1301.

Dabard, M.P., Loi, A. & Peucat, J.J. (1996). Zircon typology combined with Sm-Nd whole-rock isotope analysis to study Brioverian sediments from the Armorican Massif. *Sediment. Geol.*, **101**, 243-260.

Dalziel, I.W.D. (1992). Antarctica; a tale of two supercontinents? *Ann. Rev. Earth Planet. Sci.* **20**, 501-526.

De Beer, C.H. (1990). Simultaneous folding in the western and southern branches of the cape fold belt. *S. Afr. J. Geol.*, **93**, 583-591.

De Wit, M.J. & Ransome, I.G.D. (1992). Regional inversion tectonics along the southern margin of Gondwana. In: De Wit, M.J. and Ransome, I.G.D. (Ed.), *Inversion tectonics of the Cape Fold Belt, Karoo and Cretaceous Basins of Southern Africa*. Balkema, Rotterdam, 15-22.

Deer, W.A., Howie, R.A. & Zussman, J. (1966). *An Introduction to the Rock-Forming Minerals*, 2nd ed. Longman, London, 528p.

Deer, W.A., Howie, R.A. & Zussman, J. (1982). *Rock forming minerals, Orthosilicates*, 2nd ed. Longman, New York 919 p.

Deer, W.A., Howie, R.A. & Zussman, J. (1992). *An Introduction to the Rock-Forming Minerals*, 2nd ed. Longman, Essex, 696p.

Di Giulio, A., Tribuzio, R. Ceriani, A. & Riccardi, M.P. (1999) Integrated analyses constraining the provenance of sandstones, a case study: the Section Peak Formation (Beacon Supergroup, Antarctica). *Sediment. Geol.*, **124**, 169-183.

Dickinson, W.R. (1974). Plate Tectonics and Sedimentation, 1-27. In: Dickinson, W.R. (Ed.), *Tectonics and Sedimentation*. SEPM. Spec. Publ., **22**, 204 p.

Dickinson, W.R. (1976). Plate tectonic evolution of sedimentary basins, 1-62. In: Dickinson, W.R. and Yarborough, H. *Plate Tectonics and Hydrocarbon accumulation*. Amer. Assoc. Petrol. Geol. Cont. Educ. Course Note Ser. 1.

Dickinson, W.R. & Suczek, C.R. (1979) Plate tectonics and sandstone compositions. *Amer. Ass. Petrol. Geol. Bull.*, **63**, 2164-2182.

Dickinson, W.R., Beard, L.S., Brakenridge, G.R., Erjavec, J.L., Fergusson, R.C., Inmam, K.F., Knepp, R.A., Lindberg, F.A & Ryberg, P.T. (1983) Provenance of North American Phanerozoic sandstones in relation to tectonic setting. *Bull. Geol. Soc. Amer.*, **4**, 498-499.



Dodson, M.H., Compston, W., Williams, I.S. & Wilson, J.F. (1988). A search for ancient detrital grains in Zimbabwean sediments. *J. Geol. Soc. London.*, **145**, 977-983.

Elliot, D. H. & Johnson, M. (1972). The Gondwanide orogeny: new data from South Africa and the Problem of the Falkland Island. *Abstr. Progm. Geol. Soc. Amer.*, **4**, 498-499.

Elliot, D.H. & Watts, D.R. (1974). The nature and origin of volcanoclastic material in some Karoo and Beacon rocks. *Trans. Geol. Soc. S. Afr.*, **77**, 109-111.

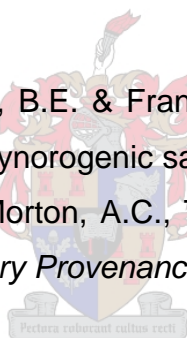
Engel, A.E.J. & Engel, C.G. (1953). Greenville Series in the northwest Adirondack Mountains. *Geol. Surv. Am. Bull.*, **64**, 1013-1097.

Feng, R. & Kerrich, R. (1990). Geochemistry of fine-grained clastic sediments in the Archean Abitibi greenstones belt, Canada: implications for provenance and tectonic setting. *Geochim. Cosmochim. Acta*, **54**, 1061-1081.

Fisher, R.V. & Schmincke, H.U. (1984). *Pyroclastic rocks*. Springer-Verlag, Heidelberg, 472 p.

Fleischer, M. & Altschuler, Z.S. (1969). The relationship of the rare earth composition of minerals to geological environment. *Geochim. Cosmochim. Acta*, **33**, 725-732.

Floyd, P.A., Shail, R., Leveridge, B.E. & Franke, W. (1991). Geochemistry and provenance of Rhenohercynian synorogenic sandstones: implications for tectonic environment discrimination. In: Morton, A.C., Todd, S.P. and Haughton, P.D.W. (Ed.), *Development in Sedimentary Provenance*. Geol. Soc. London, Spec. Publ., **57**, 173-188.



Folk, R.L. (1980). *Petrology of Sedimentary Rocks*. Austins, Texas: Hemphill Publication Company, 182 p.

Frimmel, H.E. (2000). New U-Pb zircon ages for the Kuboos pluton in the Pan-African Gariiep belt, South Africa: Cambrian mantle plume or far field collision effect? *S. Afr. J. Geol.*, **103**, 207-214.

Geel, C.R., Goedbloed, J.W., & Luthi S.M. (2003). Interpretation of the NOMAD Borehole Image Logs in Wells NB-2, -3 and -4. Department of Earth Sciences, Delft University of Technology, Delft The Netherlands.

Geel, C.R., Stefan, M., Luthi, S.M., Goedbloed, J.W., Hodgson, D.M., Hodgetts, D.I. & Flint, S.S. Paleocurrent determination from climbing ripples in the Tanqua-Karoo basin floor fan system (in press).

Geringer, G.J. & Ludick, D.J. (1990). Middle-Proterozoic calc-alkaline, shoshonite volcanism along the eastern margin of the Namaqua Mobile Belt - implications for tectonic evolution in the area. *S. Afr. J. Geol.*, **93**, 389-399.

Gresse, P.G., Theron, J.N., Fitch, F.J. & Miller, J.A. (1992). Tectonic inversion and radiometric resetting of the basement in the Cape Fold Belt. In: De Wit, M.J. and Ransome, I.G.D. (Ed.), *Inversion tectonics of the Cape Fold Belt, Karoo and Cretaceous Basins of Southern Africa*. Balkema, Rotterdam, 217-228.

Gu, X.X., Liu, J.M., Zheng, M.H., Tang, J.X. & Qi, L. (2002). Provenance and tectonic setting of the Proterozoic turbidites in Hunan, South China: Geochemical evidence. *J. sediment. Res.*, **72**, 393-407.

Hälbich, I.W. (1983). Geodynamics of the Cape Fold Belt in the Republic of South Africa, a summary. In: Rast, N. and Delaney, F.M. (Ed.), *Profiles of orogenic belts*. Amer. Geophys. Union, Washington, D.C., Geodynamics series, **10**, 21-29.

Hälbich, I.W. (1992). The Cape Fold Belt-Agulhas bank Transect across the Gondwana Suture in Southern Africa. American Geophysical Union and Interunion Committee on the Lithosphere. Washington, D.C. *Global Geotransect*, **9**, 1-17.

Hälbich, I.W. & Swart, J. (1983). Structural zoning and dynamic history of the cover rocks of the Cape Fold Belt. In: Söhnge, A.P.G. and Hälbich, I.W. (Ed.), *Geodynamics of the Cape Fold Belt*. Geol. Soc. S. Afr. Spec. Publ., **12**, 75-100.

Hällbich, I.W., Fitch, F.J. & Miller, J.A. (1983). Dating the Cape Orogeny, In Söhnge, A.P.G. and Hällbich, I.W. (Ed.), *Geodynamics of the Cape Fold Belt*. Geol. Soc. S. Afr. Spec. Publ., **12**, 165-172.

Hallsworth, C.R., Morton, A.C., Claoué, J. & Fanning, C.M. (2000). Carboniferous sand provenance in the Pennine Basin, U.K: constraints from heavy minerals and detrital zircon age data. *Sediment. Geol.*, **137**, 147-185.

Hanchar, J.M., Finch, R.J., Hoskin, P.W.O., Watson, E.B., Cherniak, D.J. & Mariano, A.N. (2001). Rare earth elements in synthetic zircon: part I. synthesis, and rare earth element and phosphorus doping. *Amer. Mineral.*, **86**, 667-680.

Herron, M.M (1988). Geochemical classification of terrigenous sands and shales from core or log data. *J. Sediment. Petrol.*, **58**, 820-829.

Hodgson, D.M., Hodgetts, D., Flint, S.S., Drinkwater, N.J., Østensen, S., Johannessen, E., Johnson, S.D. & Vik, E. (2003). Outcrop analysis of high continuity, amalgamated sheet turbidites from the Karoo Basin, South Africa: application to reservoir models of Glitne Field, South Viking Graben, North Sea. Petroleum Geology of NW Europe, 6th Conference, Queen Elizabeth II Conference Centre, London, October 2003 (Poster).

Holail, H.M. & Moghazi, A.K.M. (1998). Provenance, tectonic setting and geochemistry of greywackes and siltstones of the Late Precambrian Hammamat Group, Egypt. *Sediment. Geol.*, **116**, 227-250.

Hoskin, P.W.O. & Schaltegger, U. (2003). The composition of zircon and igneous and metamorphic petrogenesis. In: Hanchar, J.M. and Hoskin, P.W.O. (Ed.), *Zircon*. Mineral. Soc. Amer., Rev. Mineral. Geochem., **53**, 27-62.

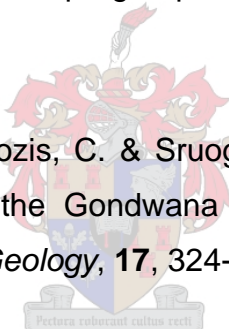
Hower, J., Eslinger, E.V., Hower, M.E. & Perry, E.A. (1976). Mechanism of burial metamorphism of argillaceous sediment. 1: Mineralogical and chemical evidence. *Bull. Geol. Soc. Amer.*, **87**, 725-737.

Hunter, D.R. & Wilson, A.H. (1988). A continuous record of Archaean evolution from 3.5 to 2.6 Ga in Swaziland and northern Natal. *S. Afr. J. Geol.*, **91**, 57-74.

Johnson, M.R. (1991). Sandstone petrography, provenance and plate tectonic setting in Gondwana context of the southeastern Cape-Karoo Basin. *S. Afr. J. Geol.*, **94**, 137-154.

Johnson, M.R., van Vuuren, C.J., Hegenberger, W.F., Key, R. & Shoko, U. (1996). Stratigraphy of the Karoo Supergroup in southern Africa: an overview. *J. Afr. Earth Sci.*, **23**, 3-15.

Kay, S.M., Ramos, V.A., Mpodozis, C. & Sruoga, P. (1989). Late Paleozoic to Jurassic silicic magmatism at the Gondwana margin: analogy to the Middle Proterozoic in North America? *Geology*, **17**, 324-328.



King, R., Van Lente, B., Potts, G., Hodgson, D.M., Andersson, P.O.D., Worden, R.H., Flint, S.S. & Wickens, H. DeV. (2004). Extra-foreland source to turbidites sink in the early Karoo Basin, South Africa. *AAPG Annual meeting 2004: Embrace the Future, Celebrate the Past Technical Program*. (Poster).

Kingsley, C.S. (1977). Stratigraphy and sedimentology of the Eccca Group in the eastern Cape Province, South Africa. *Ph.D. thesis (unpubl.)*, Univ. Port Elizabeth, 290p.

Kingsley, C.S. (1981). A composite submarine fan-delta-fluvial model for the Eccca and Lower Beaufort groups of Permian age in the Eastern Cape Province, South Africa. *Trans. Geol. Soc. S. Afr.*, **84**, 27-40.

Lewis, D.W. (1984). *Practical Sedimentology*. Hutchinson Ross Publishing Company, 229 p.

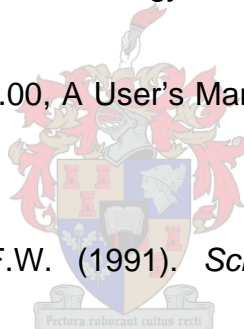
Lock, B.E. (1980). Flat-plate subduction and the Cape Fold Belt of South Africa. *Geology*, **8**, 35-39.

López Gamundí, O.R. & Rosselo, E.A. (1998). Basin fill evolution and paleotectonic patterns along the Samfrau geosyncline: the Sauce Grande basin-Ventana Fold Belt (Argentina) and Karoo basin-Cape Fold Belt (South Africa) revisited. *Geol. Rundsch.*, **86**, 819-834.

Ludwig, K.R. (1999). Using Isoplot/Ex, Version 2.01: a geochronological toolkit for Microsoft Excel. *Berkeley Geochronology Center Spec. Publ.*, **1a**, 47p.

Ludwig, K. R. (2000). SQUID 1.00, A User's Manual. *Berkeley Geochronological Center Spec. Publ.*, **2**, 17p.

Mange, M.A. & Maurer, H.F.W. (1991). *Schwerminerale in Farbe*. Enke, Stuttgart, 148p.



Mange, M.A. & Maurer, H.F.W. (1992). *Heavy Minerals in Colour*. Chapman and Hall, London, 147 p.

Martini, J.E.J. (1974). On the presence of ash beds and volcanic fragments in the greywackes of the Karoo System in the southern Cape Province (South Africa). *Trans. Geol. Soc. S. Afr.*, **77**, 113-116.

McCann, T. (1991). Petrological and geochemical determination of provenance in the southern Welsh Basin. In: Morton, A.C., Todd, S.P. and Haughton, P.D.W. (Ed.), *Development in Sedimentary Provenance*. Geol. Soc. London, Spec. Publ., **57**, 215-230.

McLachlan, I.R. & Jonker, J.P. (1990). Tuff beds in the northwestern part of the Karoo Basin. *S. Afr. J. Geol.*, **93**, 329-338.

McLennan, S.M. (1989). Rare earth elements in sedimentary rocks: influence of provenance and sedimentary processes. In: Lipin, B.R. and McKay, G.A. (Ed.), *Geochemistry and Mineralogy of REE*. Mineral. Soc. Amer., Rev. Mineral., **21**, 169-200.

McLennan, S.M., Taylor, S.R. & Kröner, A. (1983). Geochemical evolution of Archean shales from South Africa, I. The Swaziland and Pongola Supergroups. *Precamb. Res.*, **22**, 93-124.

McLennan, S.M., Hemming, S.R., McDaniel, D.K. & Hanson, G.N. (1993). Geochemical approaches to sedimentation, provenance and tectonics. In: Johnsson, M.J. and Basu, A. (Ed.), *Processes controlling the Composition of Clastic Sediments*. Geol. Soc. Amer. Spec. Pap., **284**, 21-40.

McLennan, S.M., Hemming, S.R., Taylor, S.R. & Eriksson, K.A. (1995). Early Proterozoic crustal evolution: Geochemical and Nd-Pb isotopic evidence from metasedimentary rocks, southwestern North America. *Geochim. Cosmochim. Acta*, **59**, 1153-1177.

McLennan, S.M., Taylor, S.R., McCulloch, M.T. & Maynard, J.B. (1990). Geochemical and Nd-Sr isotopic composition of deep-sea turbidites: Crustal evolution and plate tectonic association. *Geochim. Cosmochim. Acta*, **54**, 2015-2050.

Millar, I.L., Pankhurst, R.J. & Fanning, C.M. (2002). Basement chronology of the Antarctic Peninsula: recurrent magmatism and anatexis in the Palaeozoic Gondwana margin. *J. Geol. Soc. London*, **159**, 145-157.

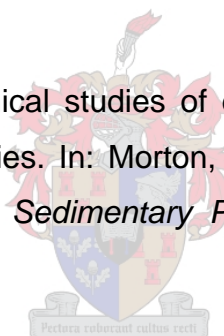
Moen, H.F.G. (1987). The Koras Group and related intrusives north of Upington: a reinvestigation. *Bull. Geol. Surv. S. Afr.*, **85**, 20p.

Moen, H.F.G. (1999). The Kheis Tectonic Subprovince, southern Africa: a lithostratigraphic perspective. *S. Afr. J. Geol.*, **102**, 27-42.

Morton, A.C. (1985). A new approach to provenance studies: electron microprobe analysis of detrital garnets from Middle Jurassic sandstones of the North Sea. *Sedimentology*, **32**, 553-566.

Morton, A.C. (1987). Influences of provenance and diagenesis on detrital garnet suites in the Forties sandstone, Paleocene, central North Sea. *J. Sediment. Petrol.*, **57**, 1027-1032.

Morton, A.C. (1991). Geochemical studies of detrital heavy minerals and their application to provenance studies. In: Morton, A.C., Todd, S.P. and Haughton, P.D.W. (Ed.), *Development in Sedimentary Provenance*. Geol. Soc. London, Spec. Publ., **57**, 31-45.



Morton, A.C. & Hallsworth, C. (1999). Process controlling the composition of heavy mineral assemblages in sandstones. *Sediment. Geol.*, **124**, 3-29.

Nagasawa, H. (1970). Rare earth concentrations in zircon and apatite and their host dacites and granites. *Earth Planet. Sci. Lett.* **9**, 359-364.

Nesbitt, H.W. & Young, G.M. (1982). Early Proterozoic climates and plate motions inferred from major element chemistry of lutites. *Nature*, **299**, 715-17.

Nesbitt, H.W. & Young, G.M. (1984). Prediction of some weathering trends of plutonic and volcanic rocks based on thermodynamic and kinetic considerations. *Geochim. Cosmochim. Acta*, **48**, 1523-1534.

Nesbitt, H.W. & Young, G.M. (1989). Formation and diagenesis of weathering profiles. *J. Geol.*, **97**, 129-147.

Paces, J.B. & Miller, J.D. (1993). Precise U-Pb ages of Duluth Complex and related mafic intrusions, Northeastern Minnesota: Geochronological insights to physical, petrogenic, paleomagnetic and tectonomagmatic processes associated with the 1.1 Ga midcontinent rift system. *J. Geophys. Res.*, **98B**, 13997-14013.

Pankhurst, R.J., Rapela, C.W., Caminos, R., Llambías, E. & Parica, C. (1992). A revised age for the granites of the central Somuncura batholith, North Patagonian Massif. *J. South Amer. Earth Sci.*, **5**, 321-326.

Pankhurst, R.J., Rapela, C.W. & Fanning, C.M. (2001). Age and origin of coeval TTG, I- and S-type granites in the Famatinian belt of NW Argentina. *Trans. Royal Soc. Edinburgh. Earth Sci.*, **91**, 151-168.

Pankhurst, R.J., Rapela, C.W., Loske, W.P., Márquez, M. & Fanning, C.M. (2003). Chronological study of the pre-Permian basement rocks of southern Patagonia. *J. South Amer. Earth Sci.*, **16**, 27-44.

Pettijohn, F.J. (1975). *Sedimentary Rocks*. Harper and Row, New York, 3rd Ed., 628 p.

Pettijohn, F.J., Potter, P.E. & Siever, R. (1972). *Sand and Sandstones*. Springer-Verlag, New York, 618 p.

Pettijohn, F.J., Potter, P.E., & Siever, R. (1987). *Sand and Sandstone*. Springer-Verlag, New York, 553 p.

Pittman, E.D. (1963). Use of zoned plagioclase as an indicator of provenance. *J. Sediment. Petrol.*, **33**, 380-386.

Pittman, E.D. (1970). Plagioclase as an indicator of provenance in sedimentary rocks. *J. Sediment. Petrol.*, **40**, 591-598.

Potter, P.E. (1978). Petrology and chemistry of modern big river sands. *J. Geol.*, **86**, 423-429.

Powell, C.McA., Li, Z.X., McElhinny, M.W., Meert, J.G. & Park, J.K. (1993). Paleomagnetic constraints on timing of the Neoproterozoic break up of Rodinia and the Cambrian formation of Gondwana. *Geology*, **21**, 889-892.

Pupin, J.P. (1980). Zircon and Granite Petrology. *Cont. Mineral. Petrol.*, **73**, 207-220.

Rhodes, R.C. (1974). Discussion on 'A gravity-folding model of the Cape Fold Belt', by A.R. Newton. *Trans. Geol. Soc. S. Afr.*, **11**, 175-182.

Rollinson, H. (1993). *Using geochemical data: evaluation, presentation, interpretation*. Longman, London, 343p.

Roser, B.P. & Korsch, R.J. (1988). Provenance signatures of sandstone-mudstone suites determined using discrimination function analysis of major-element data. *Chem. Geol.*, **67**, 119-139.

Rozendaal, A., Gresse, P.G., Scheepers, R. & Le Roux, J.P. (1999). Neoproterozoic to early Cambrian crustal evolution of the Pan-African Saldania Belt, South Africa. *Precamb. Res.*, **97**, 303-323.

Scheepers, R. & Nortjé, A.N. (2000). Rhyolitic Ignimbrites of the Cape Granite Suite, southwestern Cape Province, South Africa. *J. Afr. Earth Sci.*, **31**, 647-656.

Scheepers, R. & Poujol, M. (2002). U-Pb zircon age of Cape Granite Suite ignimbrites: Characteristics of the last phases of the Saldania magmatism. *S. Afr. J. Geol.*, **105**, 163-178.

Scott, E.D. (1997). Tectonics and sedimentation: the evolution, tectonic influences and correlation of the Tanqua and Laingsburg subbasins, southwest Karoo basin, South Africa. *Ph.D. Thesis*, Louisiana State University, 167p.

Scott, E.D., Bouma, A.H. & Wickens, H. deV. (2000). Influence of tectonics on submarine fan deposition, Tanqua and Laingsburg subbasins, South Africa. In: Bouma, H.A. and Stone C.G. (Ed.), *Fine-grained turbidite systems*. SEPM Spec. Publ. No.68/AAPG Memoir **72**, 47-56.

Shannon, R.D. (1976). Revised effective ionic radii and systematic studies of interatomic distances in halides and chalcogenides. *Acta Crystallogr.*, **A32**, 751-767.

Shnukov, S.E., Cheburkin, A.K. & Andreev, A.V. (1989). Geochemistry of widespread coexisting accessory minerals and their role in investigation of endogenetic and exogenetic processes. *Russ. J. Geol.*, **2**, 107-114.

Sircombe, K.N. (1999). Tracing provenance through the isotope ages of littoral and sedimentary detrital zircon, eastern Australia. *Sediment. Geol.*, **124**, 47-67.

Sixsmith, P.J. (2000). Stratigraphic development of a Permian turbidite system on a deforming basin floor: Laingsburg Formation Karoo Basin, South Africa. *PhD thesis (unpubl.)*, University of Liverpool, 229 p.

Speer, J.A. (1980). Zircon. In: Ribbe, P.H. (Ed.), *Orthosilicates*. Mineral. Soc. Amer. Rev. Mineral., **67**-112.

Sruoga, P. & Llambías, E.J. (1992). Permo-Triassic leucorhyolitic ignimbrites at Sierra de Lihue-Calel, La Pampa province, Argentina. *J. South Amer. Earth Sci.*, **5**, 141-152.

Stuart-Smith, P.G., Miró, R., Camacho, A., Sims, J.P., Skirrow, R.G., Lyons, P., Pieters, P.E. & Black, L.P. (1999). Uranium-Lead dating of felsic magmatic cycles in the southern Sierras Pampeanas, Argentina: implications for the tectonic development of the proto-Andean Gondwana margin in Laurentia-Gondwana connections before Pangea. In: Ramos, V.A. and Keppie, J.D. (Ed.), *Geol. Soc. Amer., Spec. Pap.*, **336**, 87-114.

Takeuchi, M. (1994). Changes in garnet chemistry show a progressive denudation of the source areas for Permian-Jurassic sandstones, Southern Kitakami Terrane, Japan. *Sediment. Geol.*, **93**, 85-105.

Tankard, A.J., Jackson, M.P.A., Eriksson, K.A., Hobday, D.K., Hunter, D.R. & Minter, W.E.L. (1982). *Crustal Evolution of Southern Africa*. Springer-Verlag, New York, 523 p.

Taylor, S.R. & McLennan, S.M. (1985). *The continental crust: its composition and evolution*. Blackwell, Oxford, 312p.

Taylor, S.R., Rudnick, R.L., McLennan, S.M., & Eriksson, K.A. (1986). Rare earth element patterns in Archean high-grade metasediments and their tectonic significance. *Geochim. Cosmochim. Acta*, **50**, 2267-2279.

Theron, J.N. (1969). The Baviaanskloof Range - a South African nappe. *Trans. Geol. Soc. S. Afr.*, **72**, 29-30.

Thomas, R.J. & Eglinton, B.M. (1990). Rb-Sr, Sm-Nd and U-Pb zircon isotopic study of the Mzombe Suite, the oldest intrusive granitoid in southern Natal, South Africa. *S. Afr. J. Geol.*, **93**, 761-765.

Thomas, R.J. Eglinton, B.M. & Bowring, S.A. (1993a). Dating the cessation of Kibaran magmatism in Natal, South Africa. *J. Afr. Earth Sci.*, **28**, 215-238.

Thomas, R.J. Eglinton, B.M., Bowring, S.A., Retief, E.A. & Walraven, F. (1993b). New isotope data from a Late Proterozoic porphyritic granite-charnockite association from Natal, South Africa. *Precamb. Res.*, **61**, 83-101.

Thomas, R.J., Agenbacht, A.L.D., Cornell, D.H., & Moore, J.M. (1994). The Kibaran of southern Africa: tectonic evolution and metallogeny. *Ore Geol. Rev.*, **9**, 131-160.

Tickj, H., Cingolani, C., Varela, R. & Chemale, F.Jr. (2001). Rb-Sr ages from La Horqueta Formation, San Rafael Block, Argentina. *III South American Symposium on Isotope Geology, Pucón, Chile, CD-ROM, Sernageomin, Santiago*, 628-631.

Toulkeridis, T., Clauer, N., Kröner, A., Reimer, T. & Todt, W. (1999). Characterization, provenance, and tectonic setting of the Fig Tree greywackes from the Archaean Barberton Greenstone Belt, South Africa. *Sediment. Geol.*, **124**, 113-129.

Trevena, A.S & Nash, W.P. (1981). An electron microprobe study of detrital feldspar. *J. Sediment. Petrol.*, **51**, 137-150.

Turner, B.R. (1999). Tectonostratigraphical development of the Upper Karoo foreland basin: orogenic unloading versus thermally-induced Gondwana rifting. *J. Afr. Earth Sci.*, **28**, 215-238.

Turner, F.J. & Verhoogen, J. (1960). *Igneous and Metamorphic Petrology*. McGraw-Hill, New York, 694 p.

Ugidos, J.M., Armenteros, I., Barba, P., Valladares, M.I. & Colmenero, J.R. (1997). Geochemistry and Petrology of recycled orogen-derived sediments: a case study from Upper Precambrian siliciclastic rocks of the Central Iberian Zone, Iberian Massif, Spain. *Precamb. Res.*, **84**, 163-180.

Van de Kamp, P.C. & Leake, B.E. (1985). Petrography and geochemistry of feldspathic and mafic sediments of the northeastern Pacific margin. *Trans. Royal Soc. Edinburgh, Earth Sci.*, **76**, 411-419.

Van Lente, B. (2004). Chemostratigraphic trends and Provenance of the Permian Tanqua and Laingsburg depocentres, Southwestern Karoo Basin, South Africa. *PhD thesis (unpubl.)*, University of Stellenbosch, 339p.

Van Lente, B., Wickens, H. DeV., Flint, S.S. & Worden, R.H. (2003). Petrographic evolution of the early S.W. Karoo Basin, South Africa. *British Sedimentological Research Group Annual General Meeting 2003, Leeds*. (Poster).

Veevers, J.J., Cole, D.I. & Cowan, E.J. (1994). Southern Africa: Karoo Basin and Cape Fold Belt. In: Veevers, J. J. and Powell, C. McA., (Ed.), *Permian-Triassic Pangean Basins and Foldbelts along the Panthalassan margin of Gondwana*. *Geol. Soc. Amer. Mem.*, **184**, 223-279.

Visser, J.N.J. (1979). Changes in sediment transport direction in the Cape-Karoo Basin (Silurian-Triassic) in South Africa. *S. Afr. J. Sci.*, **75**, 72-75.

Visser, J.N.J. (1991). Geography and climatology of the Late Carboniferous to Jurassic Karoo Basin in southwestern Gondwana. *Ann. S. Afr. Musea*, **99**, 415-431.

Von Eynatten, H. & Gaupp, R. (1999). Provenance of Cretaceous synorogenic sandstones in the Eastern Alps: constraints from framework petrography, heavy mineral analysis and mineral chemistry. *Sediment. Geol.*, **124**, 81-111.

Von Veh, M.W. (1992). Compressional and extensional tectonics in the southernmost exposures of the Cape Fold Belt. In: De Wit, M.J. and Ransome, I.G.D. (Ed.), *Inversion tectonics of the Cape Fold Belt, Karoo and Cretaceous Basins of Southern Africa*. Balkema, Rotterdam, 185-192.

Watkeys, M.K. (1986). The Achab Gneiss; a "floor" in Bushmanland or a flaw in Namaqualand?. *Trans. Geol. Soc. S. Afr.*, **89**, 103-116.

Weaver, B.L. & Tarney, J. (1984). Empirical approach to estimating the composition of the continental crust. *Nature*, **310**, 575-577.

Wedepohl, K.H. (1991). Chemical composition and fractionation of the continental crust. *Geol. Rundsch.*, **80**, 223.

Wickens, H.deV. (1984). Die stratigrafie en sedimentologie van die Groep Eccawes van Sutherland. *MSc thesis (Unpubl.)*, University of Port Elizabeth.

Wickens, H.deV. (1992). Submarine fans of the Permian Ecca Group in SW Karoo Basin: Their origin and reflection on the tectonic evolution of the basin and its tectonic area. In: de Wit, M. J. and Ransome, I.G.D. (Ed.), *Inversion tectonics of the Cape Fold Belt, Karoo and Cretaceous Basins of Southern Africa*. Balkema, Rotterdam, 117-125.

Wickens, H.deV. (1994). Basin floor fan building turbidites of the southwestern Karoo Basin, Permian Ecca Group, South Africa. *PhD thesis (unpubl.)*, University of Port Elizabeth, 350p.

Wickens, H. deV. & Bouma, H. A. (2000). The Tanqua fan complex, Karoo Basin, South Africa – Outcrop analog for fine-grained, deepwater deposits. In Bouma, A.H. and Stone, C.G. (Ed.), *Fine-grained Turbidite Systems*. SEPM Spec. Publ. 68/AAPG Memoir, **72**, 153-165.

Williams, I.S. (1998). U-Th-Pb geochronology by ion microprobe. In: McKibben, M.A., Shanks III, W.C. and Ridley, W.I. (Ed.), *Applications of microanalytical techniques to understanding mineralizing processes*, Rev. Econ. Geol., **7**, 1-35.

Wronkiewicz, D.J. & Condie, K.C. (1987). Geochemistry of Archean shales from the Witwatersrand Supergroup, South Africa: Source area weathering and provenance. *Geochim. Cosmochim. Acta*, **51**, 2401-2416.

Wronkiewicz, D.J. & Condie, K.C. (1989). Geochemistry and provenance of sediments from the Pongola Supergroup, South Africa: evidence for a 3.0 Ga-old continental craton. *Geochim. Cosmochim. Acta*, **53**, 1537-1549.

APPENDIX A BOREHOLE LOGS WITH SAMPLE POSITIONS

(for location of boreholes see Fig. 1.7)

Abbreviations used:

blk = black

calc. mat. = calcareous material

cc = calcite

gr or Gr = grain

Interlam = interlaminated

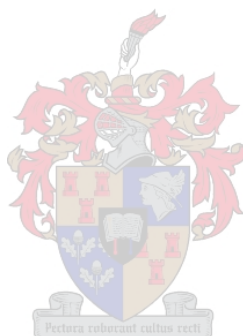
Med. = medium

Q = quartz

sandst or sst = sandstones

sh = shale

siltst. = siltstones

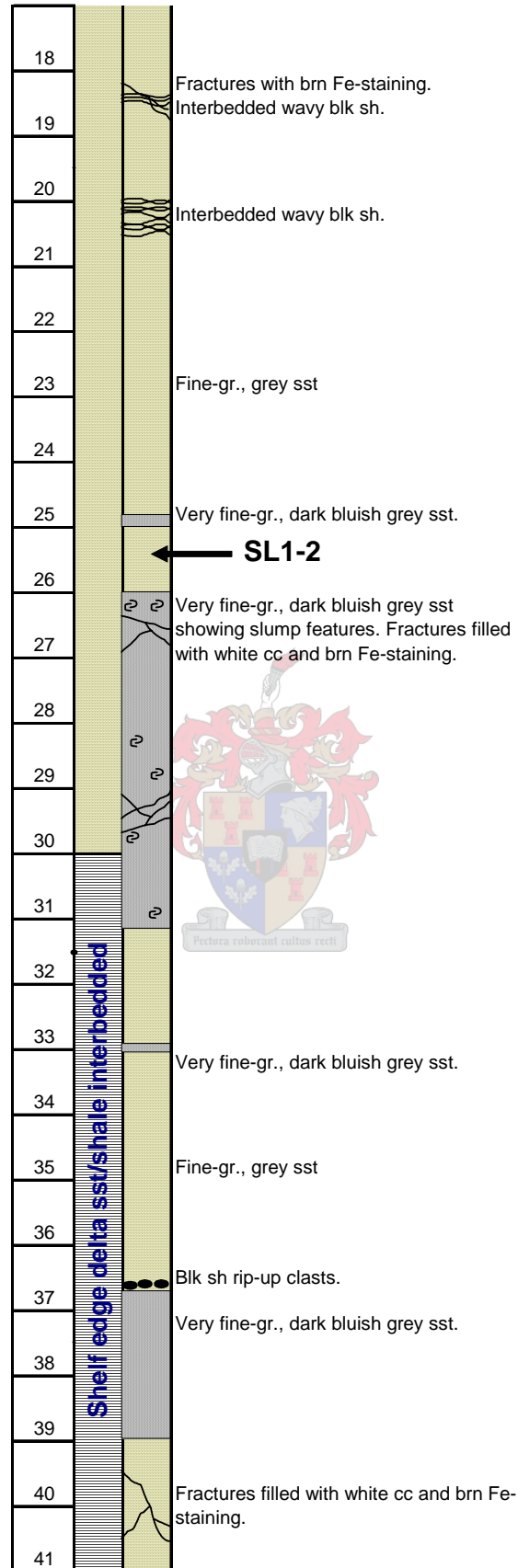


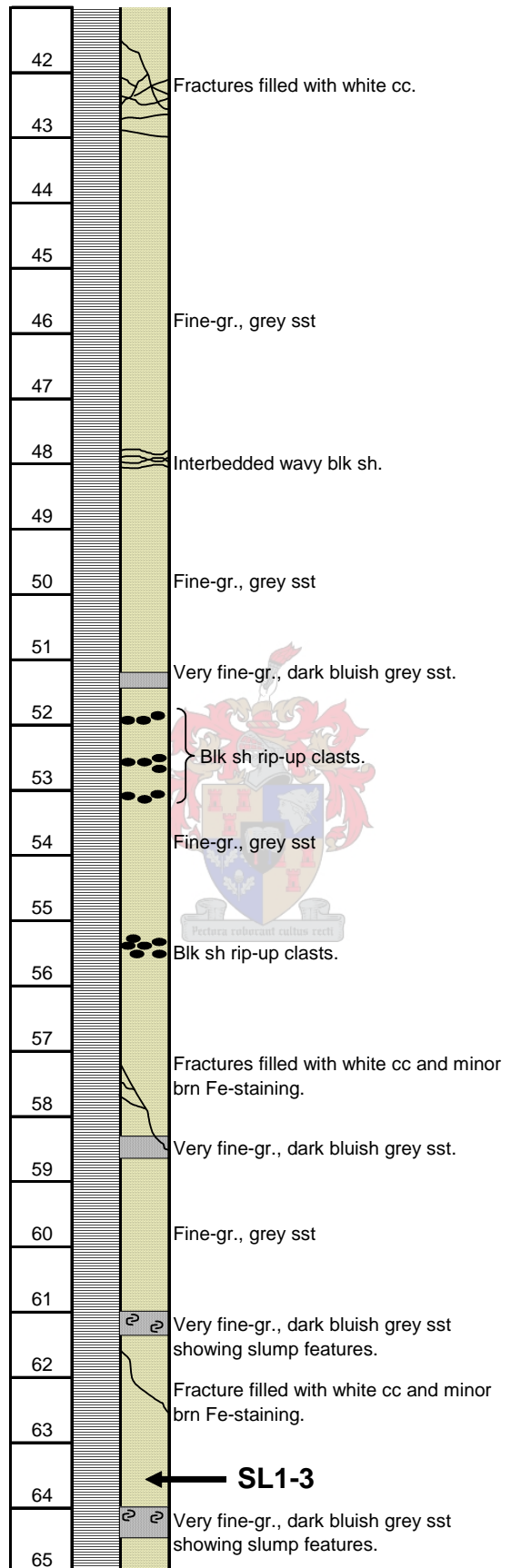
Legend

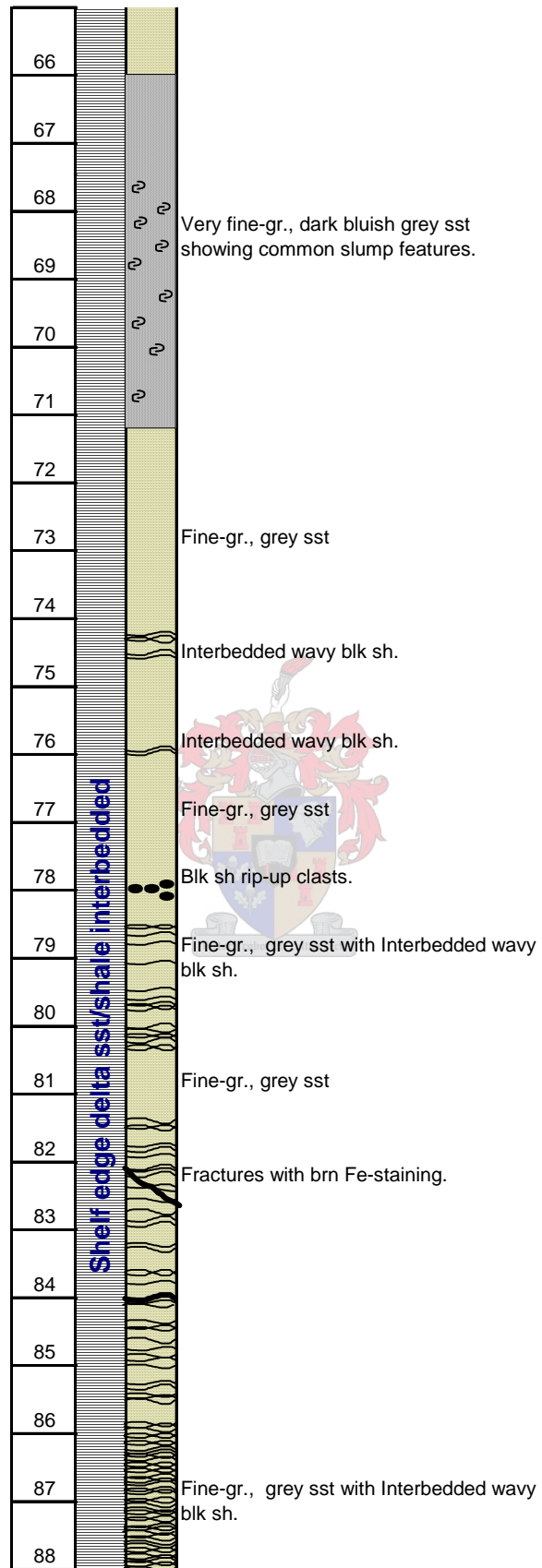
 sandstones	 Sandstones clasts in calcite matrix	 Black shale rip-up clast
 Shale	 interlaminated sandstone and black shale	 Bentonite+ calcite
 sandstone/shale interbedded	 interlaminated siltstone and black shale	 Slump features
 sandstone/siltstone interbedded	 Interlaminated siltstone/fine gr., sst and blk sh	

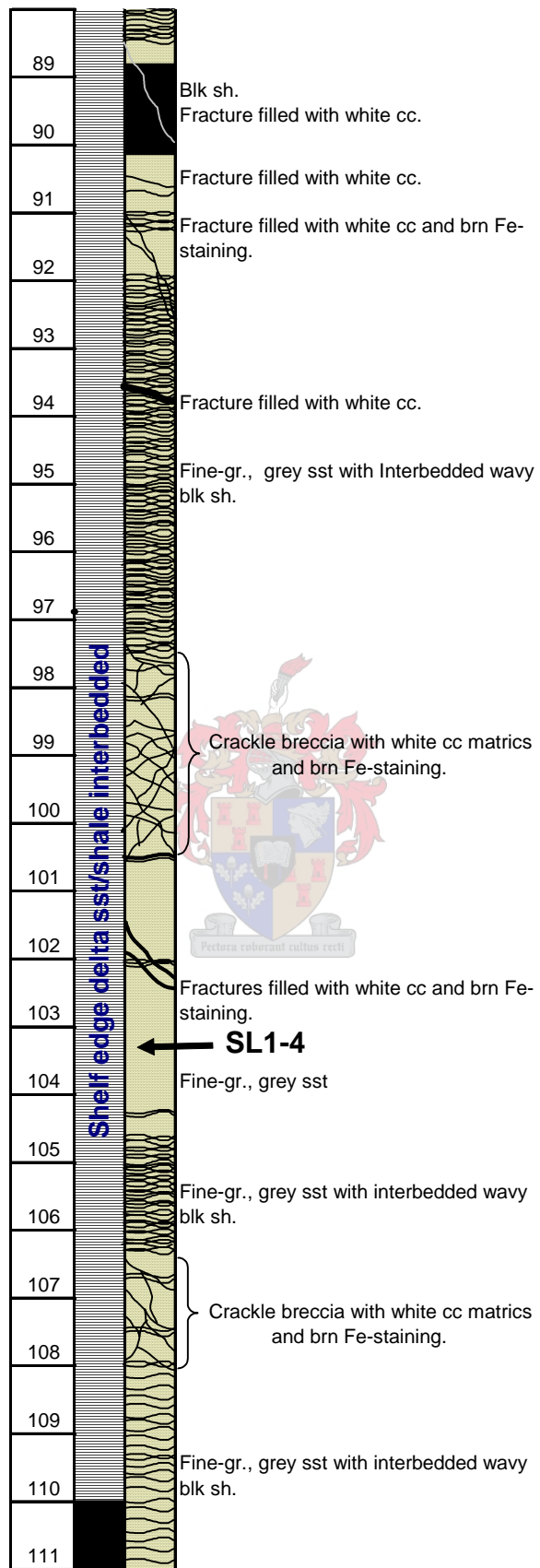
Log SL1
Logged by: S. Kruger (August 2002)
Location: Bitterberg

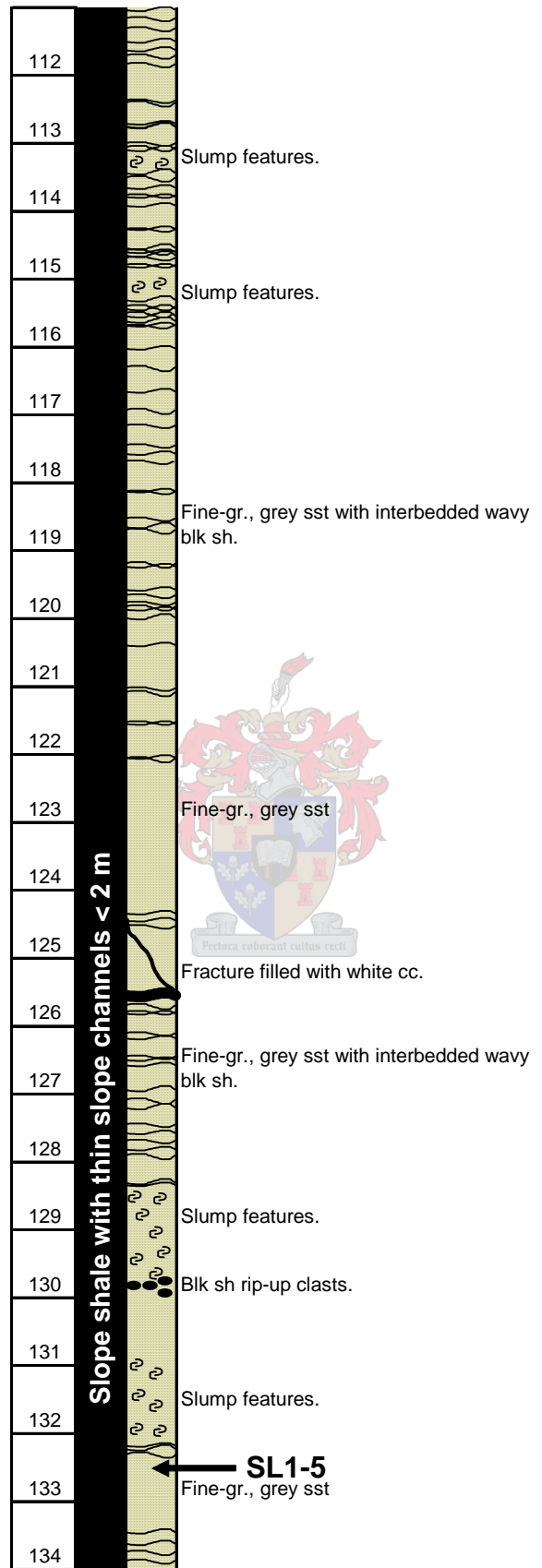
DEPTH (m)	LITHOLOGY	
	Prognose	Log
		Remarks
1		Fine-gr., grey sst
2		Blk sh rip-up clasts.
3		
4		Fine-gr., grey sst
5		
6		
7		Very fine-gr., dark bluish grey sst showing slump features.
8		
9		Fine-gr., grey sst
10		← SL1-1
11		
12		
13		Very fine-gr., dark bluish grey sst showing minor slump features.
14		Very fine-gr., dark bluish grey sst showing minor slump features.
15		
16		Very fine-gr., dark bluish grey sst showing minor slump features.
17		Fracture with brn Fe-staining.

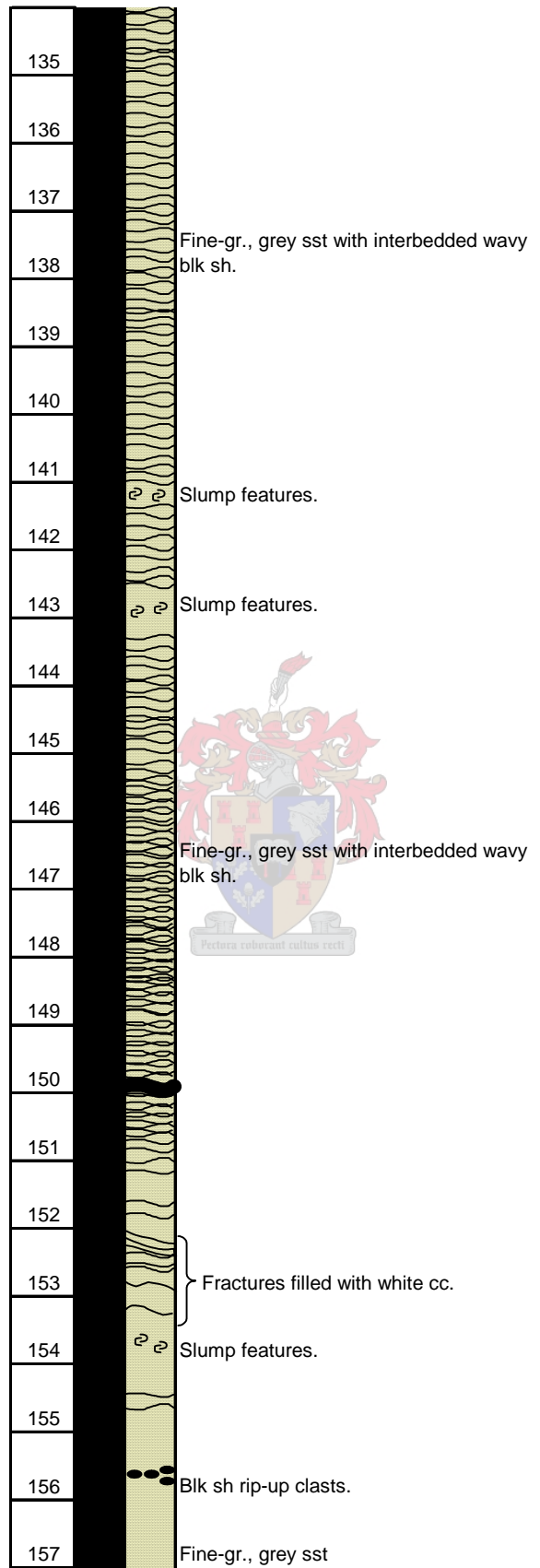


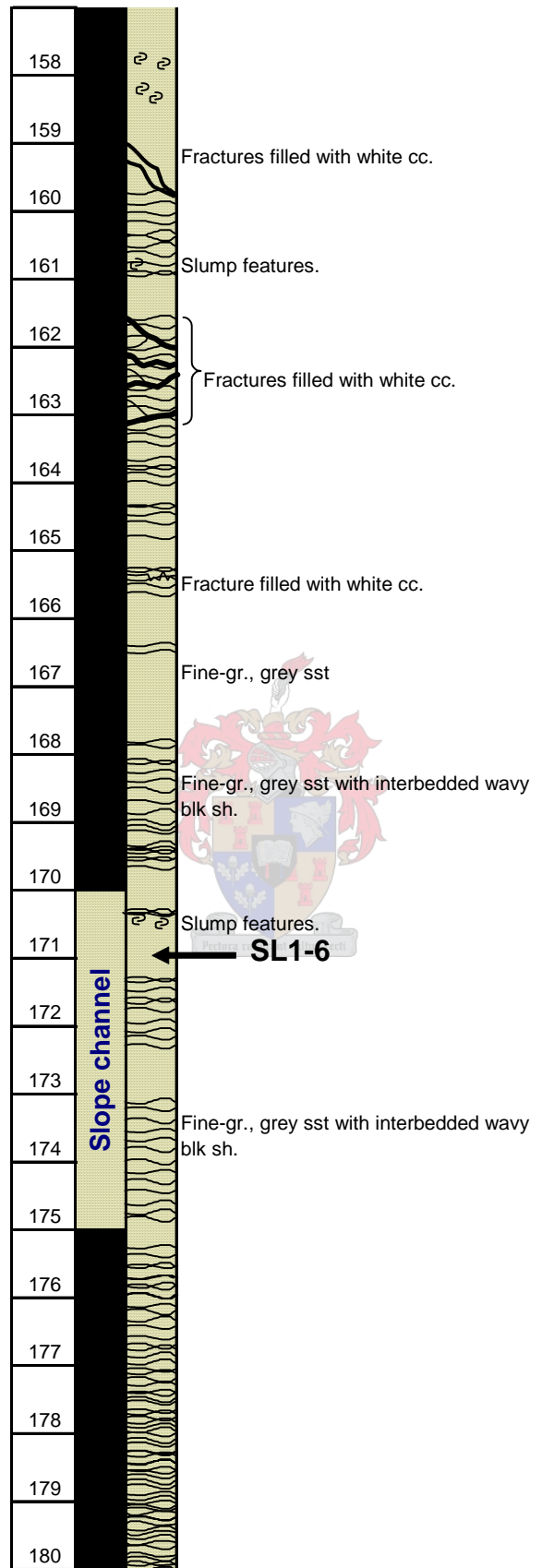


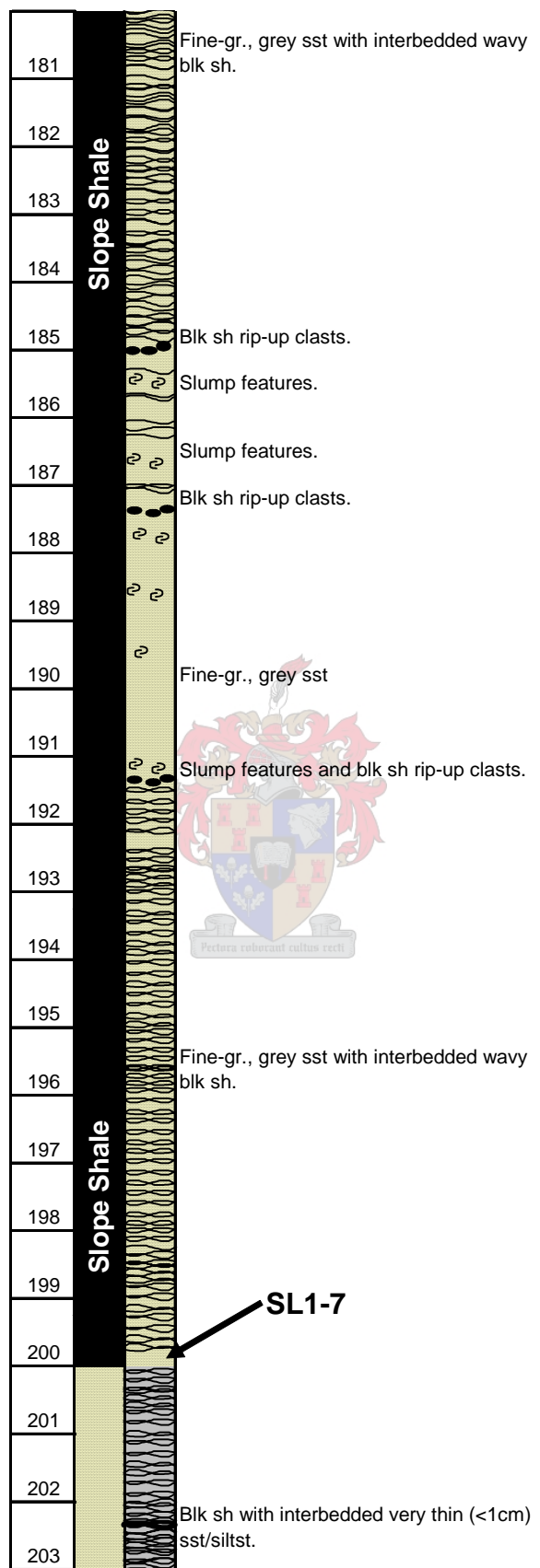


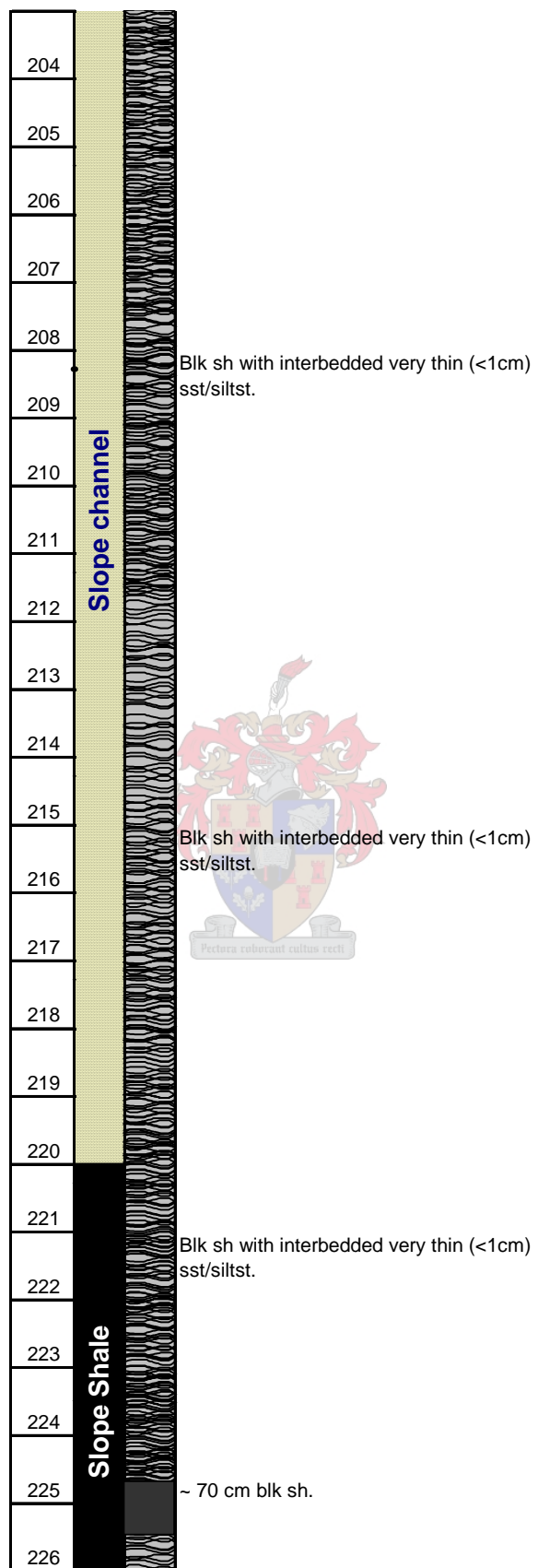


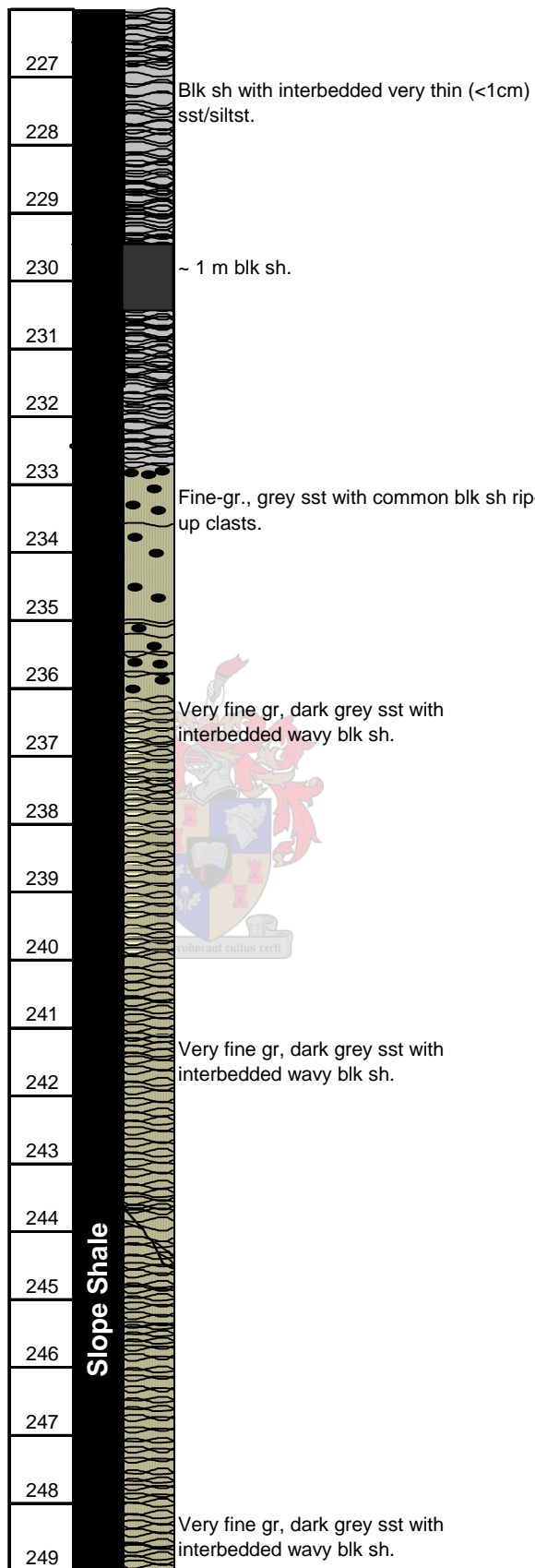


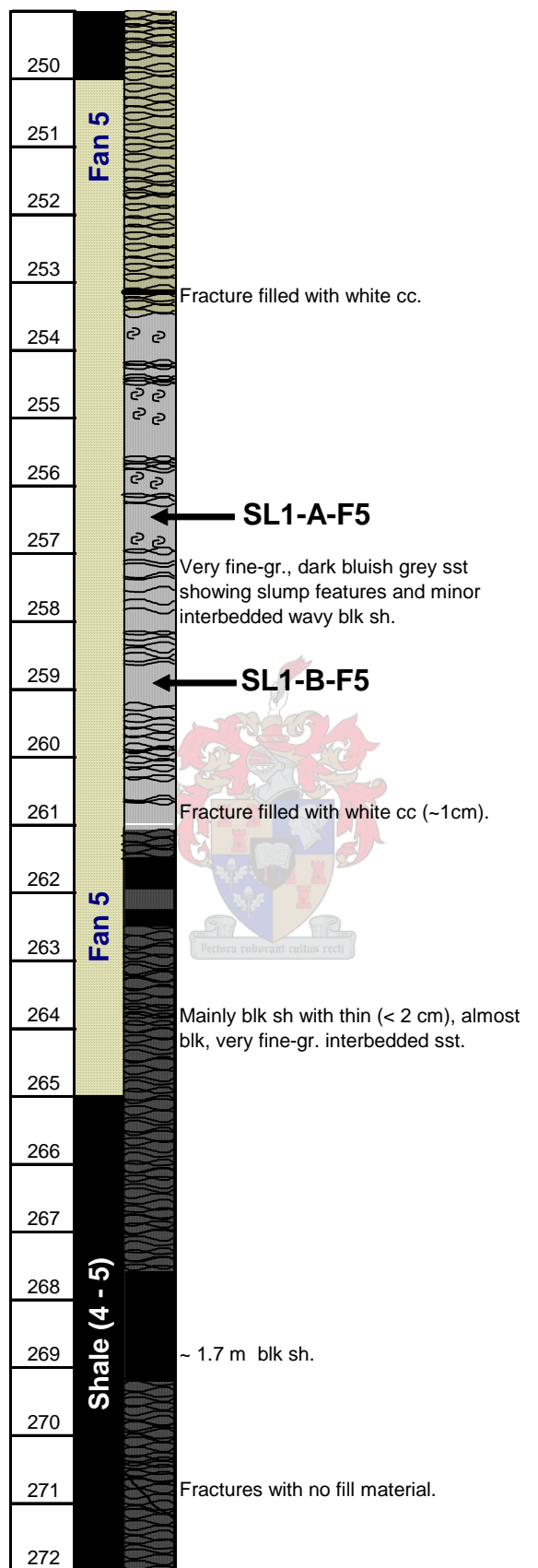


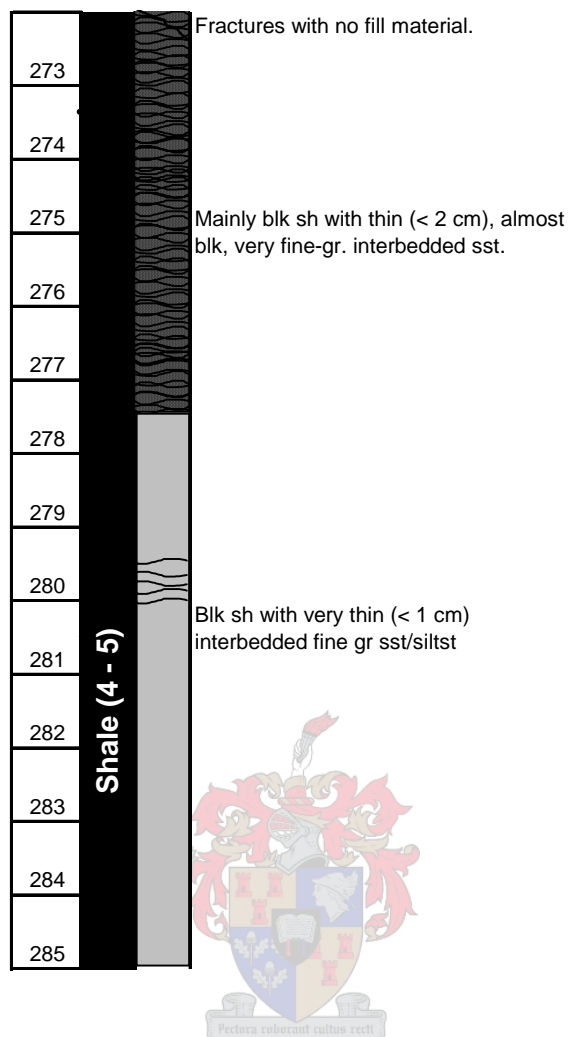






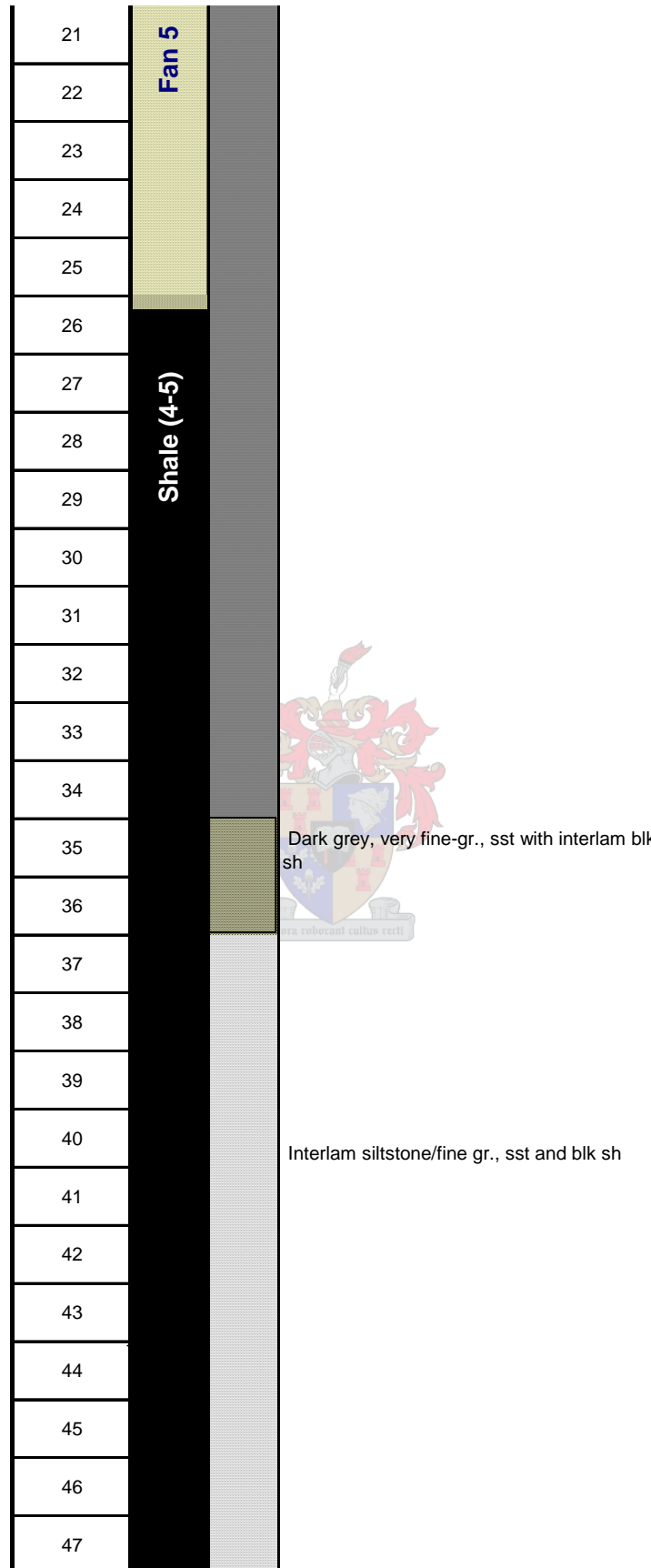






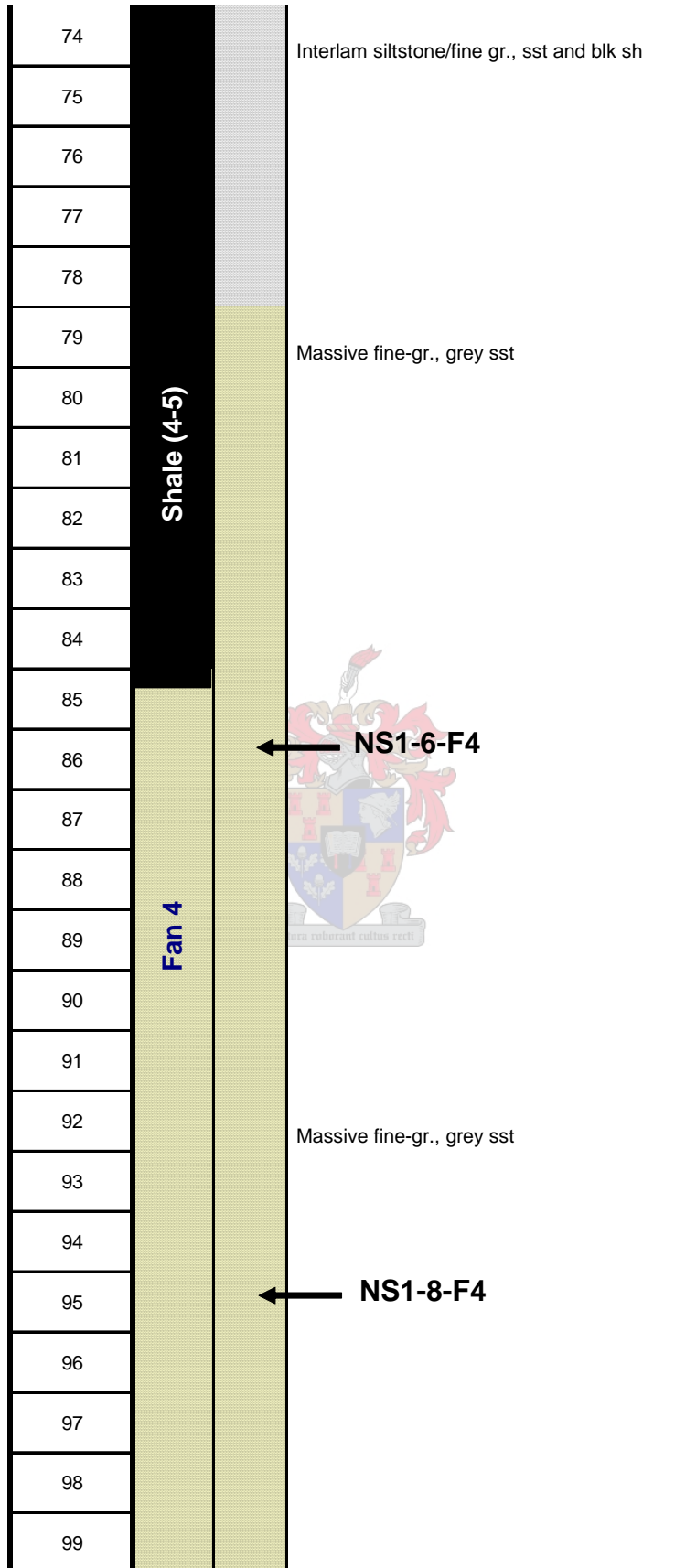
Log NS1
Logged by : Stefan Kruger (April-May 2002)
Location: South of Sout Rivier

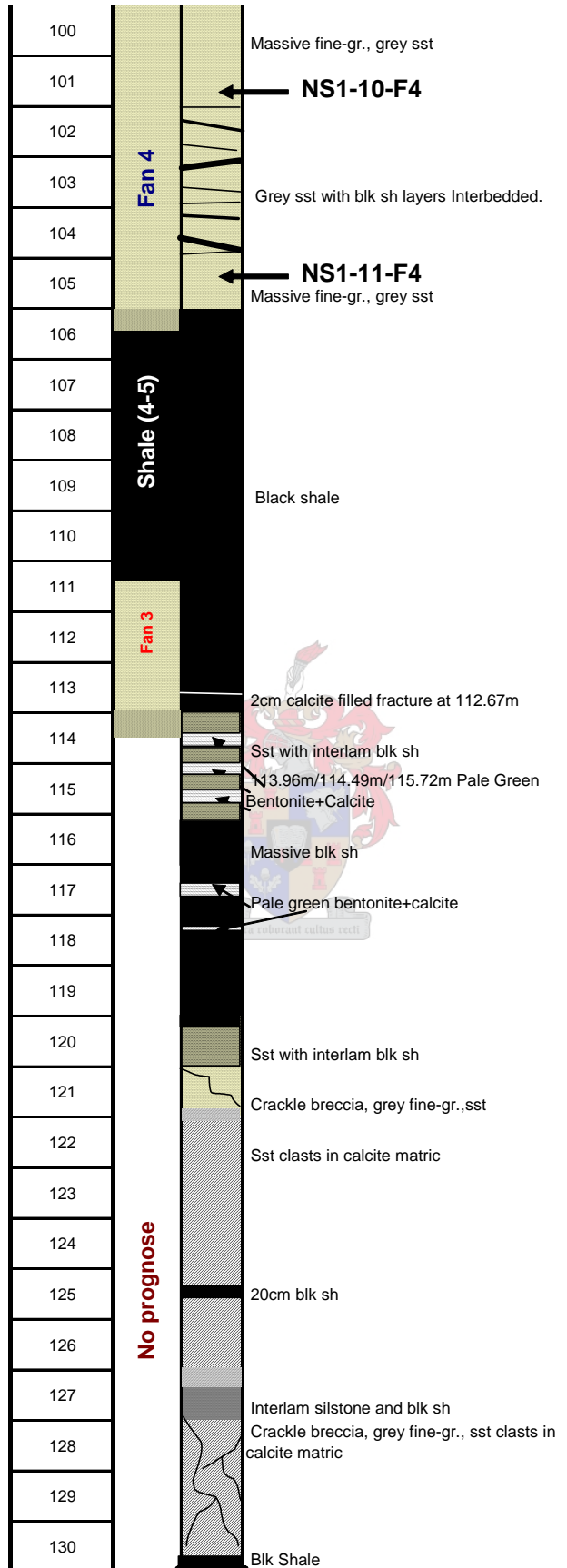
DEPTH (m)	LITHOLOGY			
	Prognose	Log	Remarks	
1	Fan 5			
2				
3			Grey, fine-gr., sst and pale green siltstone	
4				
5				
6			← NS1-1-F5	
7				
8				
9			← Fracture containing pyrite crystals	
10				
11			← NS1-3-F5	
12			Grey, fine-gr., sst and pale green siltstone	
13				
14			← NS1-4-F5	
15				
16				
17				Approx 3cm of dark brown weathered material with minor pyrite
18				
19				Interlam siltstone and blk sh
20				



48	Shale (4-5)	Interlam siltstone/fine gr., sst and blk sh
49		
50		
51		
52		
53		
54		
55		
56		
57		
58		
59		
60		
61		
62		
63		
64		
65		
66		
67		
68		
69		
70		
71		
72		
73		

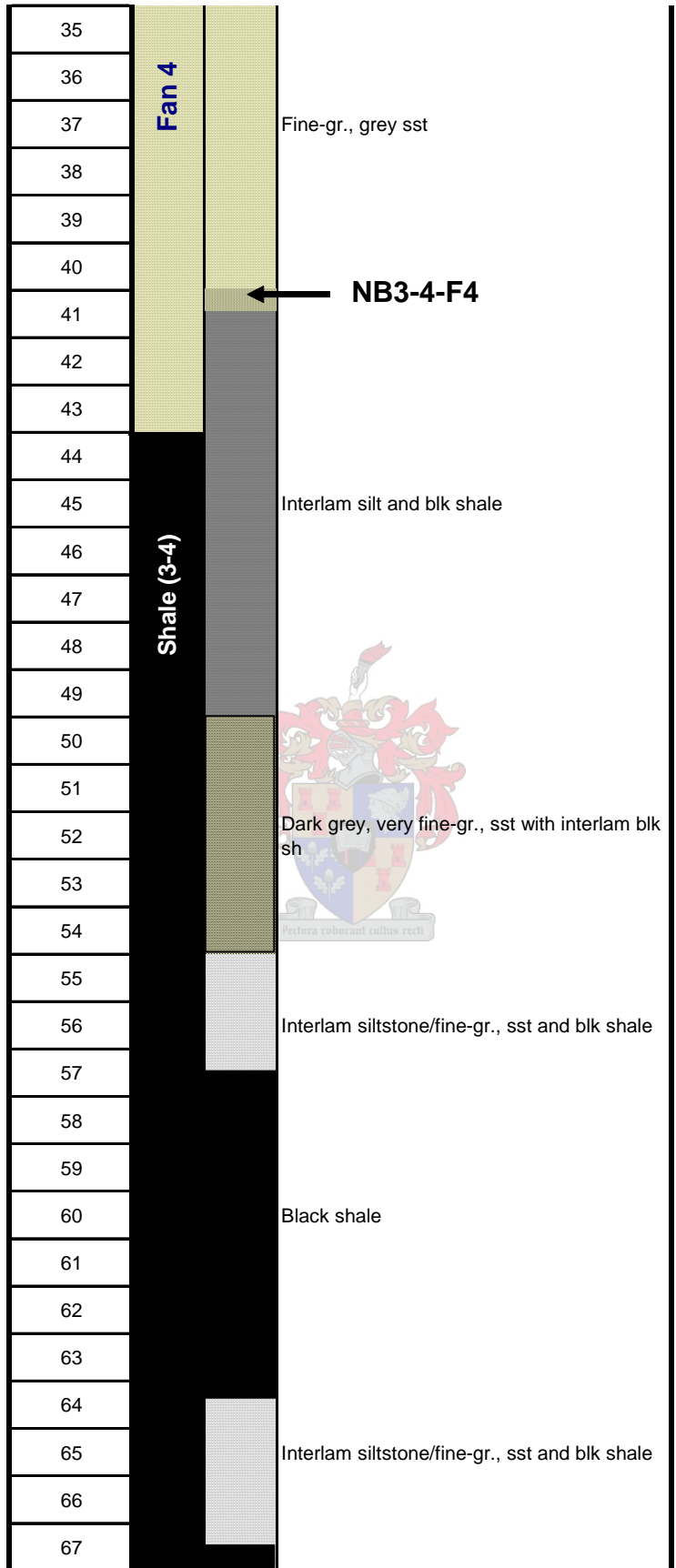


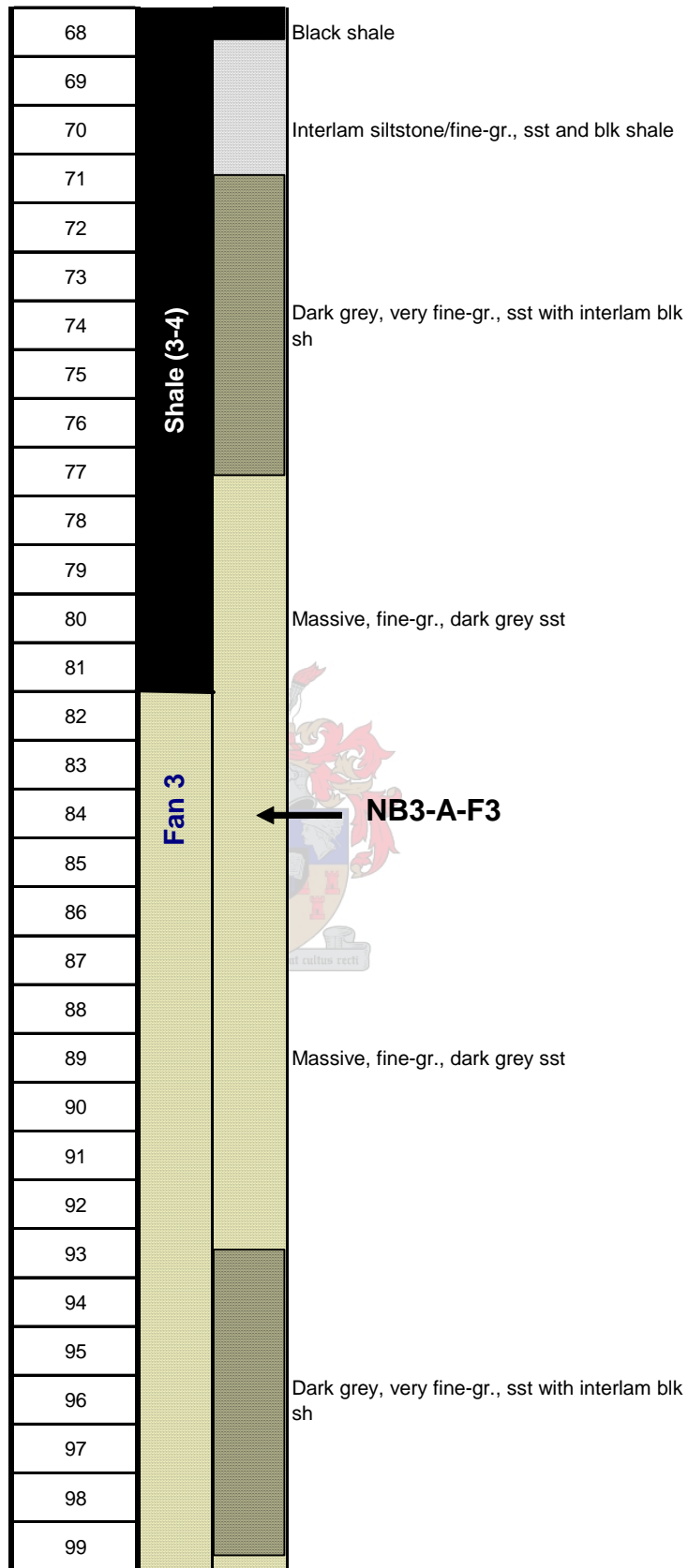


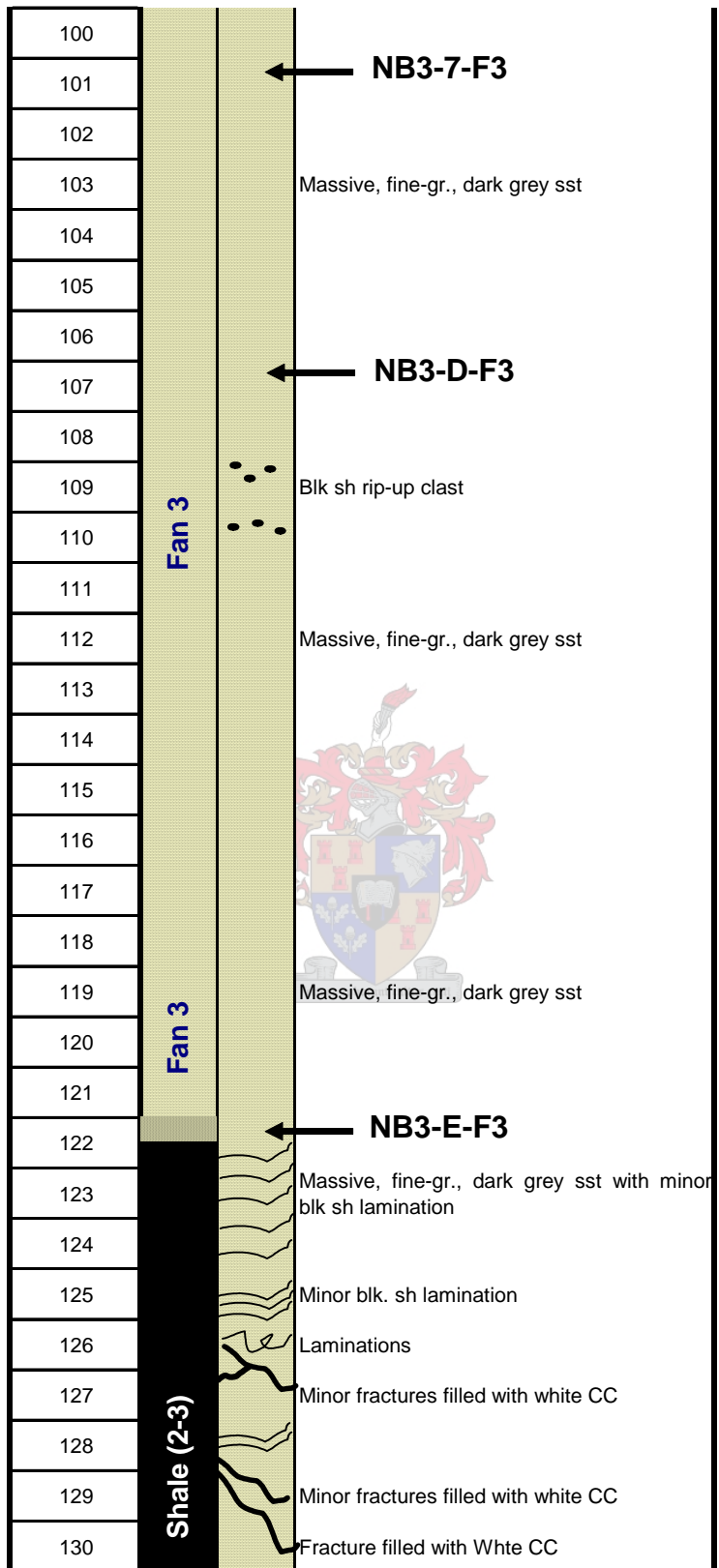


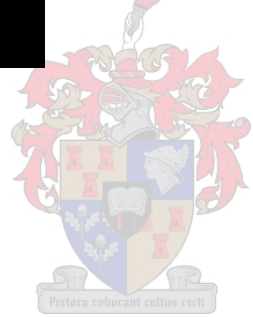
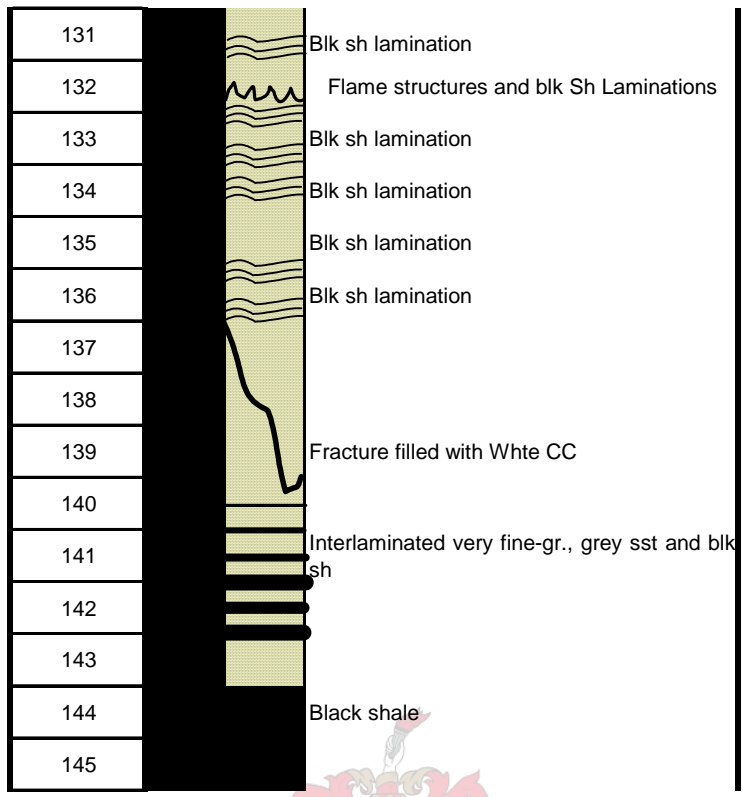
Log NB3
Logged by : Stefan Kruger
Location: Kopjeskraal

DEPTH (m)	LITHOLOGY		
	Prognose	Log	Remarks
13	Fan 4		← NB3-1-F4
14			
15			
16			Fine-gr., grey sst
17			
18			
19			
20			
21			
22			
23			
24			Fine-gr., grey sst
25			
26			
27		← NB3-2-F4	
28		••• Interlam silt and shale rip-up clasts	
29			
30			
31			
32		Massive black shale	
33		← NB3-3-F4	
34			



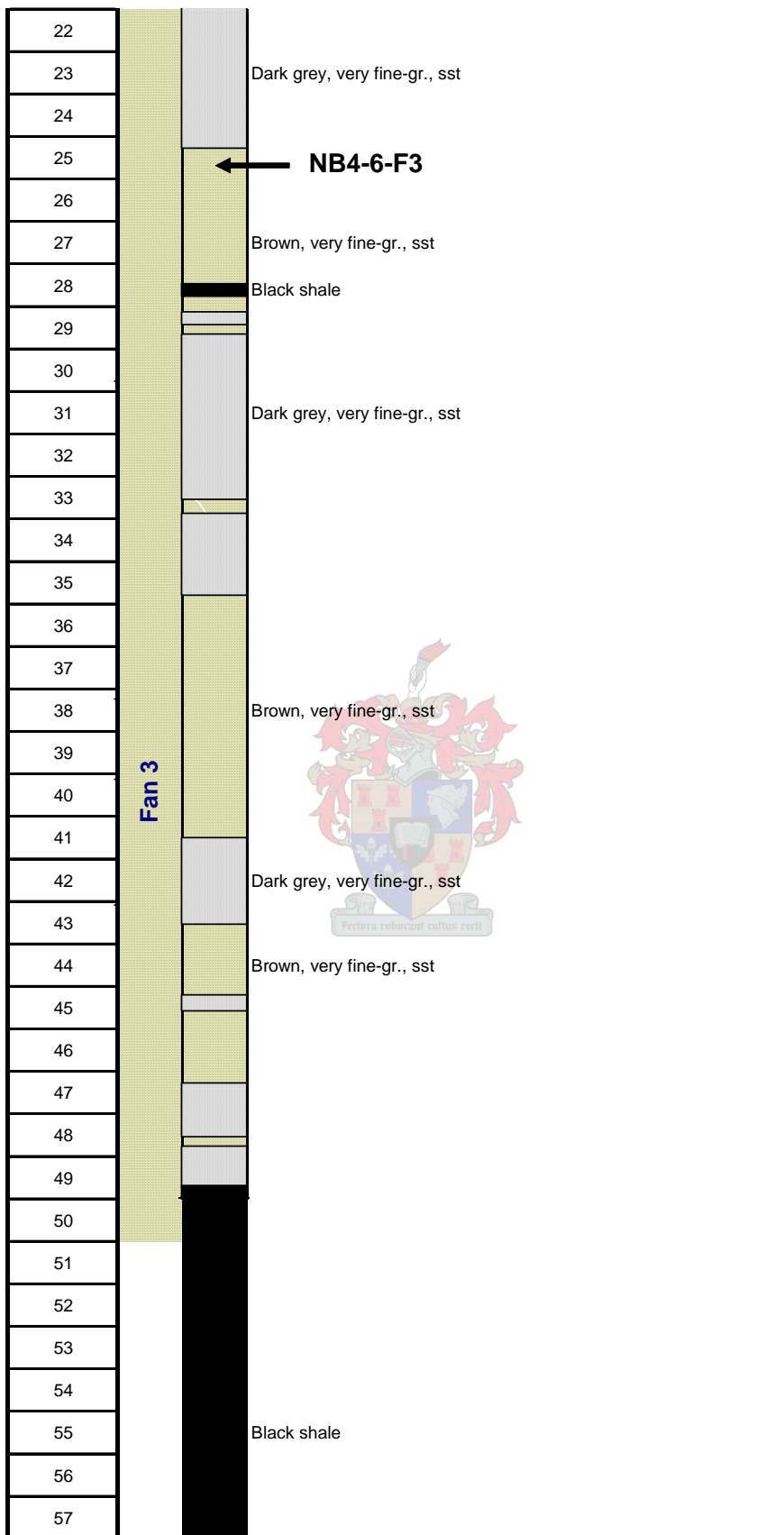






Log NB4
Logged by : Oliver P. Nguema Mve & Ian Derksen (August 2002)

DEPTH (m)	LITHOLOGY		Remarks	
	Prognose	Log		
1	Fan 3			
2			Brown, very fine-gr., sst	
3				
4				
5			Dark grey, very fine-gr., sst	
6			← NB4-1-F3	
7			← NB4-2-F3	
8			Dark grey, very fine-gr., sst	
9			Black shale	
10			← NB4-3-F3 Black shale	
11				
12				
13				
14				
15			← NB4-4-F3	
16			Dark grey, very fine-gr., sst	
17				
18				
19		Fan 3		
20				Shaly sst ← NB4-5-F3
21				Brown, very fine-gr., sst



58
59
60
61
62
63
64
65
66
67
68
69
70
71
72
73
74
75
76
77
78
79
80
81
82
83
84
85
86
87
88
89
90



No prognose

Black shale



APPENDIX B

WHOLE-ROCK CHEMISTRY (XRF & ICP-MS)

B-1 Introduction

Fresh core samples from the NOMAD project boreholes chosen for chemical analyses were crushed, and reduced to powder using a jaw crusher and swing mill. Fused and pressed powder pellets were analyzed for major element contents by standard X-ray fluorescence techniques in the Department of Geology at the University of Stellenbosch while trace element analyses reported here were carried out in the Department of Geological Sciences, University of Cape Town. Details of different analytical techniques are described below.

B-2 Description of the techniques

B-2.1 X-Ray Fluorescence Spectrometry

Whole-rock major element chemical analyses for Si, Ti, Al, Fe, Mn, Mg, Ca, Na, K, P, Ni and Cr were done by XRFS on a Philips 1404 Wavelength Dispersive spectrometer, at the University of Stellenbosch.



The spectrometer is fitted with a Rh tube and six analyzing crystals, namely: LIF200, LIF220, LIF420, PE, TLAP and PX1; the detectors are a gas-flow proportional counter, scintillation detector or a combination of the two. The gas-flow proportional counter uses P10 gas, which is a mixture of 90% Argon and 10% Methane. Major elements were analyzed on a fused glass bead at 50 kV and 50 mA tube operating conditions and trace elements were analyzed on a powder briquette at 60 kV and 40 mA tube operating conditions. Matrix effects in the samples were corrected for by applying theoretical alpha factors and measured line overlap factors to the raw intensities measured with the SuperQ Philips software. Standards that were used in the calibration procedures for both major element analyses are as follows: AGV-1 (Andesite from USGS), BHVO-1 (Basalt from USGS), JG-1 (Granodiorite from GSJ), JB-1 (Granodiorite from

GSJ), GSP-1 (Granodiorite from USGS), SY-2 (Syenite from CCRMP), SY-3 (Syenite from CCRMP), STM-1 (Syenite from USGS), NIM-G (Granite from MINTEK), NIM-S (Syenite from MINTEK), NIM-N (Norite from MINTEK), NIM-P (Pyroxenite from MINTEK), NIM-D (Dunite from MINTEK), BCR (Basalt from USGS), GA (Granite from CRPG), GH (Granite from CRPG), DRN (Diorite from ANRT), and BR (Basalt from CRPG). Replicate analyses of samples and standards indicate that the accuracy of major element analysis is within 5%.

Abbreviations used:

ANRT: Association Nationale de la Recherche Technique, Paris

CCRMP: Canadian certified Reference Materials Project

CRPG: Centre de Recherches Petrographiques et Geochimiques

GSJ: Geological Survey of Japan

MINTEK: Council for Mineral Technology, South Africa

NIM: National Institute of Metallurgy, South Africa

USGS: United States Geological Survey, Reston

B-2.2 inductively coupled plasma emission mass spectroscopy (ICP-MS)

Trace elements of the same sandstones samples were measured by inductively coupled plasma emission mass spectroscopy (ICP-MS) in the Department of Geological Sciences, University of Cape Town. Bulk rock sample powders (50 mg) were dissolved using a HF/HNO₃ digestion procedure in Teflon beakers. The digested samples were analyzed using a Perkin Elmer/Sciex Elan 6000 ICP-MS. For the operating conditions, nebuliser gas flow (0.78 L/min), auxillary gas flow (0.75 L/min), main gas flow (15 L/min), and a ICP-RF power of 1150W, were used. The instrument was used in the “autolens mode” and operating conditions were optimized to minimize oxide and double-charged ion formation (both Ce/CeO and Ba⁺/Ba⁺⁺ <0.03). Instrument drift was corrected by internal standardization using Rh, In, Re and Bi. Calibration was achieved by external standardization using standards made from multi-element standard solutions.

Table B1 Major element analyses of the Slope (SL 1) and Skoorsteenberg Fan 5 (F5) sandstones

Sample	Slope Sandstones							Skoorsteenberg Fan 5 sandstones				
	SL1-1	SL1-2	SL1-3	SL1-4	SL1-5	SL1-6	SL1-7	SL1-A-F5	SL1-B-F5	NS1-1-F5	NS1-3-F5	NS1-4-F5
SiO ₂	73.43	68.24	67.65	70.46	73.32	66.76	68.33	67.84	71.47	74.39	71.94	69.05
TiO ₂	0.54	0.52	0.68	0.63	0.50	0.61	0.50	0.71	0.62	0.49	0.56	0.66
Al ₂ O ₃	11.93	13.41	13.81	13.05	12.15	14.20	12.40	15.08	13.65	12.30	11.74	13.13
Cr ₂ O ₃	0.06	0.03	0.02	0.02	0.04	0.02	0.05	0.01	0.00	0.00	0.03	0.02
Fe ₂ O ₃	3.53	4.21	4.48	4.08	2.94	4.22	3.94	4.85	3.81	3.00	3.28	4.35
MnO	0.07	0.08	0.08	0.08	0.07	0.08	0.11	0.10	0.09	0.07	0.08	0.10
NiO	0.00	0.00	0.00	0.00	0.00	0.00	0.01	0.01	0.01	0.01	0.00	0.00
MgO	1.50	2.27	2.27	1.83	1.44	2.54	1.99	2.53	1.95	1.70	1.64	2.36
CaO	1.20	1.79	2.02	1.13	2.28	1.27	2.96	1.36	1.85	1.09	1.11	1.30
Na ₂ O	2.38	2.50	1.96	2.30	2.66	2.13	2.59	2.00	2.44	3.24	3.90	2.65
K ₂ O	2.92	2.99	3.10	3.37	1.94	3.90	2.87	3.44	2.67	2.16	2.09	2.84
P ₂ O ₅	0.14	0.16	0.20	0.18	0.15	0.18	0.20	0.24	0.24	0.19	0.17	0.18
L.O.I	1.93	2.04	2.09	1.91	1.97	2.11	2.14	1.99	1.92	1.88	1.85	2.01
Total	99.61	98.24	98.36	99.04	99.46	98.01	98.08	100.16	100.72	100.52	98.37	98.64
Al ₂ O ₃ /(CaO+Na ₂ O)	3.34	3.13	3.47	3.81	2.46	4.18	2.24	4.48	3.18	2.84	2.35	3.33
Al ₂ O ₃ /SiO ₂	0.16	0.20	0.20	0.19	0.17	0.21	0.18	0.22	0.19	0.17	0.16	0.19
K ₂ O/Na ₂ O	1.23	1.20	1.59	1.47	0.73	1.83	1.11	1.72	1.09	0.67	0.54	1.07
Al ₂ O ₃ /TiO ₂	22.17	25.69	20.43	20.61	24.34	23.13	24.96	21.32	21.98	25.20	20.96	19.86
log(Na ₂ O/K ₂ O)	-0.09	-0.08	-0.20	-0.17	0.14	-0.26	-0.04	-0.24	-0.04	0.18	0.27	-0.03
log(SiO ₂ /Al ₂ O ₃)	0.79	0.71	0.69	0.73	0.78	0.67	0.74	0.65	0.72	0.78	0.79	0.72
Fe ₂ O ₃ +MgO	5.03	6.47	6.75	5.91	4.38	6.75	5.93	7.38	5.76	4.70	4.92	6.70
CIA	64.74	64.82	66.12	65.76	63.83	66.07	59.59	68.91	66.23	65.47	62.33	65.93
D1	-3.99	-3.36	-3.47	-4.20	-2.13	-5.06	-2.80	-3.65	-2.83	-3.09	-2.81	-3.85
D2	-0.18	-0.60	-1.11	-0.09	-0.48	-0.30	0.17	-1.15	-0.59	-0.14	0.73	-0.91
D3	3.33	2.30	1.97	3.52	1.04	4.10	2.78	1.97	1.70	2.23	2.95	2.46
D4	0.96	1.59	2.16	1.70	0.03	3.08	1.31	2.26	1.27	0.50	0.25	2.21

Oxides are in wt%; chemical index of alteration (CIA) =100 X [(Al₂O₃)/(Al₂O₃+CaO+Na₂O+K₂O)] from Nesbitt and Young (1982); D1, D2, D3 and D4 are discrimination functions used in the provenance discrimination diagram of Roser and Korsch (1988).

Table B1 (continued) Major element analyses of the Skoorsteenberg Fan 4 (F4) and Fan 3 (F3) sandstones

Sample	Skoorsteenberg Fan 4 sandstones								Skoorsteenberg Fan 3 sandstones									
	NS1-6-F4	NS1-8-F4	NS1-10-F4	NS1-11-F4	NB3-1-F4	NB3-2-F4	NB3-3-F4	NB3-4-F4	NB3-A-F3	NB3-7-F3	NB3-D-F3	NB3-E-F3	NB4-1-F3	NB4-2-F3	NB4-3-F3	NB4-4-F3	NB4-5-F3	NB4-6-F3
SiO ₂	75.40	76.04	74.42	73.97	71.91	75.74	75.75	74.43	74.67	69.79	70.29	72.70	74.76	73.01	70.21	72.49	71.17	74.52
TiO ₂	0.45	0.52	0.50	0.47	0.54	0.48	0.64	0.45	0.52	0.65	0.62	0.53	0.49	0.51	0.62	0.61	0.61	0.45
Al ₂ O ₃	11.61	11.36	12.15	11.41	12.28	11.86	11.35	11.32	12.23	13.19	13.99	12.40	10.98	12.14	12.76	12.37	12.51	12.65
Cr ₂ O ₃	0.02	0.06	0.00	0.04	0.10	0.00	0.05	0.06	0.03	0.03	0.00	0.05	0.03	0.06	0.03	0.02	0.03	0.01
Fe ₂ O ₃	2.92	3.05	3.65	3.10	3.85	2.89	3.17	3.36	3.02	4.21	4.18	3.93	3.18	4.01	4.22	3.79	3.89	3.22
MnO	0.07	0.07	0.09	0.09	0.08	0.08	0.06	0.08	0.08	0.08	0.09	0.08	0.06	0.07	0.09	0.08	0.07	0.07
NiO	0.00	0.00	0.01	0.00	0.00	0.02	0.00	0.00	0.01	0.00	0.01	0.02	0.00	0.00	0.01	0.00	0.00	0.01
MgO	1.41	1.44	1.73	1.41	1.71	1.34	1.22	1.55	1.47	2.12	2.27	1.90	1.45	1.68	2.14	2.04	2.13	1.62
CaO	0.99	0.85	1.37	1.45	1.21	1.11	1.15	1.08	1.11	1.01	1.18	1.29	1.11	1.57	1.22	1.05	1.00	0.98
Na ₂ O	2.79	2.74	3.10	2.95	2.32	2.57	2.41	2.52	2.86	2.66	2.77	2.55	2.37	2.70	3.28	2.63	2.86	2.75
K ₂ O	1.54	1.49	1.64	1.40	2.74	2.33	2.26	2.25	2.35	2.73	2.82	2.43	2.10	2.44	2.76	2.62	2.74	2.28
P ₂ O ₅	0.11	0.13	0.19	0.13	0.12	0.15	0.13	0.11	0.19	0.18	0.20	0.17	0.11	0.12	0.20	0.17	0.16	0.16
L.O.I	1.89	1.88	1.85	1.96	2.04	1.81	1.94	1.93	1.79	1.92	1.78	1.81	1.87	2.04	1.97	1.96	1.95	1.87
Total	99.19	99.61	100.69	98.39	98.90	100.36	100.12	99.14	100.32	98.55	100.19	99.84	98.50	100.35	99.50	99.82	99.12	100.57
Al ₂ O ₃ /(CaO+Na ₂ O)	3.07	3.17	2.72	2.59	3.48	3.22	3.19	3.14	3.08	3.60	3.54	3.23	3.16	2.84	2.83	3.36	3.24	3.39
Al ₂ O ₃ /SiO ₂	0.15	0.15	0.16	0.15	0.17	0.16	0.15	0.15	0.16	0.19	0.20	0.17	0.15	0.17	0.18	0.17	0.18	0.17
K ₂ O/Na ₂ O	0.55	0.54	0.53	0.47	1.18	0.91	0.94	0.89	0.82	1.03	1.02	0.95	0.88	0.90	0.84	1.00	0.96	0.83
Al ₂ O ₃ /Na ₂ O	4.16	4.15	3.92	3.87	5.29	4.61	4.72	4.48	4.28	4.96	5.06	4.86	4.64	4.50	3.89	4.71	4.38	4.61
Al ₂ O ₃ /TiO ₂	25.79	21.67	24.29	24.18	22.79	24.85	17.85	25.21	23.57	20.25	22.59	23.52	22.59	23.76	20.52	20.18	20.55	28.36
log(Na ₂ O/K ₂ O)	0.26	0.26	0.28	0.33	-0.07	0.04	0.03	0.05	0.08	-0.01	-0.01	0.02	0.05	0.04	0.07	0.00	0.02	0.08
log(SiO ₂ /Al ₂ O ₃)	0.81	0.83	0.79	0.81	0.77	0.81	0.82	0.82	0.79	0.72	0.70	0.77	0.83	0.78	0.74	0.77	0.75	0.77
Fe ₂ O ₃ +MgO	4.33	4.49	5.38	4.52	5.56	4.24	4.38	4.91	4.49	6.33	6.45	5.83	4.63	5.69	6.36	5.83	6.02	4.83
CIA	68.57	69.12	66.57	66.32	66.20	66.36	66.12	65.91	65.92	67.36	67.39	66.44	66.35	64.42	63.72	66.27	65.47	67.81
D1	-2.59	-2.86	-2.01	-2.08	-3.66	-3.42	-3.58	-3.59	-3.23	-3.58	-3.24	-3.25	-3.72	-2.74	-3.41	-4.06	-4.09	-2.97
D2	-1.44	-1.70	-1.18	-1.26	-0.82	-0.48	-0.68	-1.08	-0.14	-0.87	-0.62	-1.13	-1.36	-0.56	0.12	-0.93	-0.55	-0.70
D3	0.19	0.18	0.04	-0.12	2.28	2.24	2.28	1.89	2.38	2.10	1.99	1.53	1.72	1.62	3.00	2.60	3.01	1.48
D4	-0.52	-0.15	-0.32	-0.73	0.94	0.24	0.61	0.36	0.40	1.59	1.54	0.86	0.49	0.20	1.47	1.86	1.93	0.11

Oxides are in wt%; chemical index of alteration (CIA) = 100 X [(Al₂O₃/(Al₂O₃+CaO+Na₂O+K₂O))] from Nesbitt and Young (1982); D1, D2, D3 and D4 are discrimination functions used in the provenance discrimination diagram of Roser and Korsch (1988).

Table B1 (continued) Major element analyses of the Skoorsteenberg undifferentiated Fan (FX) and Laingsburg fan (LGSB) sandstones

Sample	Skoorsteenberg fan sandstones with interstitial calcite cement									Laingsburg fan sandstones							
	NB-FX	NB-FX	NB-FX	NB-FX	NB-FX	NB-FX	NB-FX	NB-FX	NB-FX	LGSB 1	LGSB 2	LGSB 3	LGSB 4	LGSB 5	LGSB 6	LGSB 7	LGSB 8
SiO ₂	69.25	74.98	74.29	71.96	73.81	73.07	73.01	74.95	66.28	73.77	72.48	71.39	73.88	72.25	67.45	70.41	69.80
TiO ₂	0.59	0.44	0.48	0.56	0.56	0.48	0.51	0.43	0.68	0.52	0.50	0.56	0.51	0.58	0.51	0.67	0.51
Al ₂ O ₃	13.31	10.87	10.05	12.93	12.45	10.67	12.14	11.10	14.03	12.59	12.75	13.09	12.17	12.47	12.78	12.81	12.23
Cr ₂ O ₃	0.00	0.00	0.01	0.14	0.02	0.03	0.06	0.03	0.03	0.01	0.02	0.02	0.02	0.02	0.03	0.02	0.02
Fe ₂ O ₃	3.53	2.70	3.30	4.39	3.71	3.59	4.01	2.81	4.19	3.34	3.32	3.62	3.35	3.70	2.92	3.97	3.20
MnO	0.11	0.08	0.10	0.10	0.09	0.10	0.07	0.10	0.11	0.06	0.06	0.08	0.08	0.08	0.19	0.08	0.07
NiO	0.01	0.02	0.01	0.01	0.01	0.00	0.00	0.00	0.00	0.00	0.00	0.00	0.00	0.01	0.01	0.00	0.01
MgO	1.85	1.45	1.46	1.88	1.79	1.52	1.68	1.21	1.95	1.33	1.59	1.74	1.54	1.95	1.42	1.91	1.51
CaO	3.63	2.50	3.28	1.44	0.92	3.34	1.57	2.74	3.56	0.68	0.66	1.02	1.24	1.06	6.55	1.99	4.78
Na ₂ O	2.21	2.39	2.35	2.93	2.83	2.12	2.70	2.24	2.12	2.41	3.18	2.66	2.31	2.30	2.40	2.29	2.16
K ₂ O	2.48	1.57	1.44	2.41	2.22	1.54	2.44	1.80	2.96	2.49	2.01	2.66	2.05	2.50	2.26	2.41	2.33
P ₂ O ₅	0.18	0.13	0.16	0.20	0.18	0.12	0.12	0.11	0.15	0.13	0.15	0.15	0.14	0.17	0.13	0.19	0.15
L.O.I	2.19	1.99	2.09	1.81	1.82	2.19	2.04	2.14	2.36	1.34	1.16	1.34	1.18	1.15	1.86	1.65	1.75
Total	99.32	99.12	99.02	100.74	100.39	98.79	100.35	99.66	98.41	98.67	97.88	98.33	98.47	98.24	98.51	98.40	98.52
Al ₂ O ₃ /(CaO+Na ₂ O)	2.28	2.23	1.79	2.96	3.32	1.96	2.84	2.23	2.47	4.07	3.32	3.56	3.43	3.71	1.43	2.99	1.76
Al ₂ O ₃ /SiO ₂	0.19	0.14	0.14	0.18	0.17	0.15	0.17	0.15	0.21	0.17	0.18	0.18	0.16	0.17	0.19	0.18	0.18
K ₂ O/Na ₂ O	1.12	0.66	0.61	0.82	0.79	0.73	0.90	0.80	1.40	1.03	0.63	1.00	0.89	1.09	0.94	1.05	1.08
Al ₂ O ₃ /TiO ₂	22.67	24.54	21.07	23.04	22.39	22.05	23.76	25.64	20.63	24.21	25.50	23.38	23.86	21.50	25.06	19.12	23.98
log(Na ₂ O/K ₂ O)	-0.05	0.18	0.21	0.09	0.10	0.14	0.04	0.10	-0.15	-0.01	0.20	0.00	0.05	-0.04	0.03	-0.02	-0.03
log(SiO ₂ /Al ₂ O ₃)	0.72	0.84	0.87	0.75	0.77	0.84	0.78	0.83	0.67	0.77	0.75	0.74	0.78	0.76	0.72	0.74	0.76
Fe ₂ O ₃ +MgO	5.38	4.15	4.76	6.26	5.50	5.12	5.69	4.02	6.14	4.67	4.91	5.36	4.89	5.65	4.34	5.88	4.71
CIA	61.53	62.75	58.72	65.59	67.60	60.40	64.42	62.08	61.89	69.29	68.55	67.37	68.49	68.03	53.27	65.69	56.88
D1	-1.81	-2.57	-2.07	-2.29	-3.09	-1.77	-2.74	-2.18	-1.89	-3.23	-2.53	-3.27	-2.94	-3.90	0.34	-2.91	-1.21
D2	-0.27	-1.38	-1.49	-0.55	-0.97	-1.76	-0.56	-0.90	0.05	-0.70	-0.55	-0.42	-1.50	-1.46	1.54	-1.15	0.30
D3	1.31	0.53	-0.05	1.14	1.40	-0.62	1.62	0.67	1.73	1.69	1.10	2.13	0.68	1.84	1.36	1.29	1.44
D4	1.17	0.25	0.05	0.20	0.57	-0.05	0.20	-0.36	1.43	-0.02	-0.25	0.78	0.24	1.57	0.26	1.42	0.59

Oxides are in wt%; chemical index of alteration (CIA) = $100 \times [(Al_2O_3)/(Al_2O_3+CaO+Na_2O+K_2O)]$ from Nesbitt and Young (1982); D1, D2, D3 and D4 are discrimination functions used in the provenance discrimination diagram of Roser and Korsch (1988). Major element data of the Laingsburg fan sandstones are from Van Lente (2004).

Table B2 Trace elements of the Slope and Tanqua Karoo submarine fan sandstones determined by ICP-MS

Sample	Slope sandstones					Tanqua Fan 5 (F5) sandstones				
	SL1-1	SL1-2	SL1-4	SL1-6	SL1-7	SL1-A-F5	SL1-B-F5	NS1-1-F5	NS1-3-F5	NS1-4-F5
Sc	8.33	9.32	10.2	9.72	8.42	12.4	9.49	6.12	6.93	10.9
V	66.2	62.6	71.4	67.3	58.9	83.9	65.0	45.7	55.9	77.4
Cr	249	57.0	49.9	35.8	197	108	43.0	42.0	34.6	61.0
Co	74.2	50.0	49.6	38.6	62.5	27.8	38.2	89.1	61.6	48.1
Ni	14.9	13.8	16.1	14.7	14.6	20.0	15.2	15.8	16.8	19.6
Cu	13.5	13.8	18.3	20.7	17.1	26.5	25.5	13.8	17.4	24.4
Rb	86.1	92.7	110	131	104	129	96.0	73.1	77.0	102
Sr	168	276	208	271	331	168	158	125	125	116
Y	20.8	21.3	27.1	23.5	22.1	29.6	24.6	21.0	25.0	28.7
Zr	102	96.9	114	103	93.7	129	120	78.3	108	113
Nb	9.97	11.0	12.8	11.9	10.8	14.4	12.2	8.71	11.5	13.7
Cs	3.07	3.63	5.52	7.48	6.20	9.19	6.46	3.28	3.94	6.11
Ba	512	651	590	786	707	542	376	487	481	584
La	31.2	31.0	28.7	32.2	36.0	38.1	33.5	23.3	30.0	34.5
Ce	67.3	66.0	73.1	65.8	75.0	81.2	72.1	48.2	65.1	75.6
Pr	7.58	7.65	7.97	7.93	8.34	9.11	8.11	5.87	7.48	8.69
Nd	29.7	30.0	32.3	31.5	32.1	35.7	31.8	23.8	30.1	34.6
Sm	5.44	5.58	6.36	5.87	5.66	6.83	6.03	4.64	5.80	6.68
Eu	1.07	1.11	1.27	1.09	1.10	1.31	1.17	0.89	1.07	1.30
Gd	4.62	4.81	5.80	5.22	4.87	6.28	5.37	4.15	5.04	6.16
Tb	0.67	0.69	0.86	0.75	0.69	0.92	0.78	0.62	0.76	0.90
Dy	4.18	4.32	5.29	4.67	4.22	5.82	4.94	3.89	4.72	5.67
Ho	0.81	0.82	1.04	0.91	0.82	1.14	0.96	0.77	0.93	1.09
Er	2.24	2.28	2.92	2.55	2.28	3.23	2.71	2.20	2.64	3.07
Tm	0.33	0.33	0.42	0.37	0.33	0.47	0.40	0.32	0.38	0.45
Yb	2.15	2.16	2.74	2.42	2.17	3.10	2.58	2.08	2.49	2.89
Lu	0.31	0.31	0.38	0.35	0.31	0.44	0.38	0.30	0.35	0.41
Hf	2.89	2.77	3.10	2.93	2.73	3.53	3.42	2.21	2.94	3.17
Ta	0.80	0.85	0.99	0.93	0.88	1.08	0.94	0.69	0.87	1.23
Pb	16.2	20.1	18.4	21.5	21.4	23.7	20.8	12.6	16.0	20.1
Th	9.92	10.8	12.0	11.9	12.1	13.5	11.6	9.14	10.7	12.5
U	2.45	3.88	3.04	3.56	3.49	3.42	3.24	2.32	2.89	3.29
La/Th	3.14	2.88	2.40	2.70	2.98	2.83	2.88	2.55	2.81	2.76
Co/Ni	4.97	3.63	3.08	2.62	4.28	1.39	2.52	5.64	3.67	2.45
Th/U	4.06	2.78	3.93	3.34	3.46	3.95	3.58	3.93	3.69	3.80
Ce/Sm	12.4	11.8	11.5	11.2	13.3	11.9	12.0	10.4	11.2	11.3
K/Rb	282	268	254	246	229	222	231	246	225	232
K/Ba	47.4	38.1	47.3	41.2	33.7	52.7	59.0	36.9	36.1	40.3
La/Sc	3.74	3.33	2.82	3.31	4.27	3.08	3.53	3.81	4.32	3.16
Co/Th	7.5	4.6	4.2	3.2	5.2	2.1	3.3	9.7	5.8	3.9
Zr/Sc	12.2	10.4	11.2	10.6	11.1	10.4	12.7	12.8	15.6	10.3
Th/Sc	1.19	1.16	1.17	1.22	1.43	1.09	1.22	1.49	1.54	1.15
Cr/Th	25.08	5.28	4.17	3.01	16.26	7.99	3.70	4.59	3.24	4.88
Th/Co	0.13	0.22	0.24	0.31	0.19	0.49	0.30	0.10	0.17	0.26
La/Co	0.42	0.62	0.58	0.83	0.58	1.37	0.88	0.26	0.49	0.72
(La/Lu) _N	10.42	10.35	7.74	9.45	11.90	8.93	9.19	8.05	8.87	8.69

Eu/Eu*	0.65	0.65	0.64	0.60	0.64	0.61	0.63	0.62	0.60	0.62
La _N /Sm _N	3.61	3.50	2.84	3.45	4.01	3.51	3.50	3.17	3.25	3.25
Gd _N /Yb _N	1.74	1.81	1.72	1.75	1.82	1.64	1.69	1.62	1.64	1.73
La _N /Yb _N	9.79	9.74	7.08	8.98	11.20	8.32	8.79	7.59	8.14	8.05

Concentrations are in ppm.

Note that Eu* is calculated using the equation $Eu/Eu^* = Eu_N / (Sm_N \cdot Gd_N)^{1/2}$ (Rollinson, 1993), where the subscript N represents the chondrite-normalized value.

Table B2 (continued)

Sample	Tanqua Fan 4 (F4) sandstones					Tanqua Fan 3 (F3) sandstones				
	NB3-1-F4	NB3-4-F4	NS1-6-F4	NS1-8-F4	NS1-10-F4	NB3-7-F3	NB3-E-F3	NB4-1-F3	NB4-5-F3	NB4-10-F3
Sc	6.60	5.55	6.40	7.82	6.56	9.43	8.48	6.15	5.55	5.86
V	58.7	43.6	48.1	55.9	54.3	70.2	66.9	53.5	40.5	44.2
Cr	477	185	62.1	269	175	57.5	409	79.4	107	185
Co	83.3	97.5	91.4	76.6	84.1	51.0	63.2	101	89.7	88.5
Ni	19.1	16.3	12.8	15.4	14.7	17.0	19.5	12.8	11.4	14.1
Cu	20.8	15.5	12.1	15.2	12.8	18.5	15.8	11.7	12.3	10.9
Rb	74.5	80.4	51.8	51.2	45.4	91.2	76.4	67.0	68.4	53.5
Sr	143	159	154	152	165	166	152	133	136	215
Y	17.6	21.2	17.2	19.3	18.0	27.0	20.9	19.2	17.5	18.6
Zr	102	79.0	95.2	98.9	103	122	108	115	75.2	96.2
Nb	9.90	8.65	8.57	9.52	8.96	12.6	9.69	9.19	6.95	8.29
Cs	3.13	4.01	2.62	2.65	2.48	4.37	3.32	2.91	2.59	2.86
Ba	480	526	281	321	230	689	661	565	647	231
La	21.7	25.7	26.8	30.8	29.4	34.7	30.2	21.2	24.5	26.9
Ce	49.8	56.2	56.0	65.2	61.0	72.7	61.3	54.3	49.9	56.7
Pr	5.33	6.67	6.29	7.24	6.95	8.44	7.03	5.61	5.85	6.44
Nd	21.3	27.6	24.3	28.3	27.1	33.7	27.6	22.8	23.3	25.9
Sm	4.09	5.39	4.43	5.22	5.00	6.33	5.08	4.43	4.25	4.81
Eu	0.80	1.13	0.86	1.04	0.96	1.25	0.99	0.85	0.90	0.98
Gd	3.55	4.66	3.82	4.47	4.16	5.59	4.33	3.80	3.61	4.10
Tb	0.53	0.66	0.55	0.63	0.59	0.84	0.65	0.58	0.53	0.59
Dy	3.33	4.06	3.41	3.84	3.66	5.19	3.98	3.66	3.36	3.51
Ho	0.65	0.76	0.66	0.74	0.70	1.01	0.79	0.72	0.65	0.69
Er	1.86	2.12	1.88	2.05	1.98	2.87	2.28	2.01	1.83	1.90
Tm	0.27	0.31	0.28	0.29	0.29	0.42	0.33	0.30	0.27	0.28
Yb	1.80	1.97	1.84	1.99	1.93	2.75	2.12	2.00	1.77	1.84
Lu	0.25	0.28	0.26	0.28	0.28	0.39	0.32	0.29	0.25	0.26
Hf	2.86	2.19	2.42	2.62	2.85	3.49	2.93	3.14	1.95	2.51
Ta	0.77	0.68	0.67	0.73	0.69	0.95	0.74	0.84	0.55	0.74
Pb	16.3	16.8	15.3	15.2	14.6	18.8	17.0	14.0	13.2	13.6
Th	7.83	8.95	8.50	9.78	9.25	12.1	10.1	9.06	8.59	8.90
U	2.59	2.55	2.18	2.29	2.20	3.21	2.55	2.40	1.98	2.27
La/Th	2.76	2.87	3.16	3.15	3.17	2.87	2.97	2.34	2.85	3.02
Co/Ni	4.35	5.98	7.13	4.97	5.73	3.01	3.24	7.92	7.87	6.28
Th/U	3.02	3.51	3.90	4.28	4.20	3.76	3.98	3.78	4.34	3.93
Ce/Sm	12.2	10.4	12.6	12.5	12.2	11.5	12.1	12.2	11.7	11.8
K/Rb	305	232	247	241	299	248	263	259	333	223
K/Ba	47.4	35.5	45.6	38.5	58.9	32.9	30.4	30.8	35.2	51.7

La/Sc	3.28	4.64	4.19	3.95	4.48	3.68	3.56	3.45	4.42	4.58
Co/Th	10.6	10.9	10.8	7.83	9.09	4.22	6.23	11.2	10.4	9.95
Zr/Sc	15.5	14.2	14.9	12.7	15.7	13.0	12.8	18.7	13.5	16.4
Th/Sc	1.19	1.61	1.33	1.25	1.41	1.28	1.20	1.47	1.55	1.52
Cr/Th	60.9	20.7	7.31	27.5	18.9	4.76	40.4	8.76	12.4	20.8
Th/Co	0.09	0.09	0.09	0.13	0.11	0.24	0.16	0.09	0.10	0.10
La/Co	0.26	0.26	0.29	0.40	0.35	0.68	0.48	0.21	0.27	0.30
(La/Lu)N	8.82	9.57	10.8	11.4	11.1	9.23	9.85	7.65	10.2	10.6
Eu/Eu*	0.64	0.69	0.64	0.66	0.65	0.64	0.65	0.64	0.70	0.67
LaN/SmN	3.33	3.00	3.81	3.72	3.70	3.45	3.74	3.01	3.63	3.52
GdN/YbN	1.60	1.92	1.69	1.82	1.75	1.65	1.65	1.54	1.66	1.81
LaN/YbN	8.13	8.83	9.88	10.5	10.3	8.54	9.60	7.18	9.38	9.87

Concentrations are in ppm.

Note that Eu* is calculated using the equation $Eu/Eu^* = Eu_N / (Sm_N \cdot Gd_N)^{1/2}$ (Rollinson, 1993), where the subscript N represents the chondrite-normalized value.



APPENDIX C

ZIRCON CHEMISTRY (LA-ICP-MS)

Mineral separates were prepared from sandstone samples in the Geology Department at the University of Stellenbosch. Samples were crushed and ground and put through a sieve of 500 μm . The fine part of the sample was washed in water to extract the lighter and ultra-fine content of the sample. After washing, samples were put in an oven to dry thoroughly.

The dry, washed samples with a grain size less than 500 μm were then separated into a light and a heavy mineral part by the method of density separation using bromoform (specific gravity 2.89). A hand magnet was applied to the samples to remove iron flakes coming from the grinding machines. Zircons were handpicked. The Tanqua sample included detrital zircons from Fans 3, 4, and 5. The Laingsburg sample comprised zircons from Fan A (lower fan) and Fan F (upper fan).

The source rock lithologies of the Tanqua and Laingsburg submarine sandstones have been investigated using trace element abundances in detrital zircons obtained after separation. Zircon grains were mounted on double-sided sticky tape. Two batches of individual zircons were analyzed. The first analysis was mainly focused on some rare earth and trace elements used in the discrimination diagrams of source rock lithologies of Belousova et al. (2002), whereas the second analysis comprised the majority of rare earth elements and some important trace elements of zircons also useful for provenance studies. It is noteworthy that only the second batch included zircons from the Laingsburg Formation.

The elements were analyzed using a Perkin Elmer/Sciex Elan 6000 ICP-MS and a Cetac LSX-200 laser ablation module in the Geology Department, University of Cape Town. Analyses were done with a pulse rate of 5Hz (pulse per second) and

beam energy of 5 mJ per pulse. A 50-micron-diameter beam was used for the trace element analyses reported here.

The ICP-MS operated with a nebuliser gas flow (0.95 L/min), a main gas flow (15 L/min), an auxillary gas flow (0.75 L/min), and a ICP RF power of 1150 W respectively. Oxide formation was minimized by adjusting the operating conditions to keep Th/ThO less than 0.005. Sensitivity during optimization (scanning across Nist-612 and 10 microns/s with a laser energy ~5 mJ/pulse, pulse repetition rate equal to 20 Hz, beam diameter equal 200 microns) was 6732 cps/ppm. The detection limits for all the elements under these operating conditions was less than 100 ppb.

The geochemical data obtained are reported in the following tables.

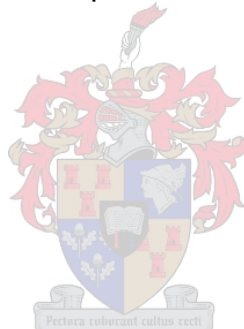


Table C1. Trace element contents (in ppm) of zircons (second batch) from the Laingsburg submarine Fan A sandstones.

Zircon Number	FAZ1	FAZ2	FAZ3	FAZ4	FAZ5	FAZ6	FAZ7	FAZ8	FAZ9	FAZ10
La	1.08	12.5	5.47	3.28	62.4	27.4	656	33.5	43.0	3.91
Ce	36.5	47.9	49.8	19.7	235	325	943	501	469	45.0
Pr	0.39	5.34	2.29	1.47	25.2	15.7	102	33.2	36.1	3.59
Nd	3.09	29.5	12.1	5.98	123	89.9	354	171	202	24.0
Sm	4.40	33.9	8.20	4.39	55.6	48.8	46.3	97.5	93.0	19.9
Eu	1.08	14.5	2.08	0.99	9.11	10.4	6.93	20.3	17.9	4.01
Gd	19.8	129	22.0	14.1	107	106	77.2	150	140	69.3
Dy	93.4	265	72.3	61.7	256	307	227	376	295	234
Ho	39.3	74.7	29.0	22.8	83.2	104	81.3	122	92.6	84.0
Er	191	254	139	106	348	433	351	509	387	357
Yb	433	343	318	219	543	742	675	959	771	641
Lu	94.0	60.2	76.7	45.1	106	156	133	198	147	132
Y	1259	2012	927	676	2494	3086	2411	3742	2787	2477
Nb	2.47	2.83	2.78	3.42	4.00	4.98	5.80	9.31	6.76	1.87
Hf	13234	11111	13719	5541	15130	17304	17310	18271	15255	12015
Ta	1.10	0.87	0.73	1.02	0.70	1.27	1.26	2.46	1.21	0.66
Th	295	249	311	151	415	843	746	979	602	568
U	417	450	428	228	637	529	1104	1729	1133	525
ΣREE	917	1270	737	504	1954	2365	3652	3171	2693	1618
Yb/Sm	98.4	10.1	38.8	50.0	9.77	15.2	14.6	9.83	8.29	32.2
Nb/Ta	2.25	3.24	3.83	3.35	5.71	3.93	4.60	3.78	5.58	2.82
Eu/Eu*	0.35	0.67	0.47	0.39	0.36	0.44	0.35	0.51	0.48	0.33
Ce/Ce*	13.2	1.37	3.29	2.10	1.39	3.67	0.85	3.52	2.79	2.81

Table C1 (continued) Fan A

Zircon Number	FAZ11	FAZ12	FAZ13	FAZ14	FAZ15	FAZ16	FAZ17	FAZ18	FAZ19	FAZ20	FAZ21
La	7.47	49.4	9.91	1.11	19.8	1.06	1.13	466	1.69	45.7	19.1
Ce	37.5	111	93.2	20.3	79.5	41.0	32.3	1032	29.8	122	112
Pr	3.06	12.8	5.24	1.00	5.83	0.78	0.98	93.3	0.85	13.5	7.14
Nd	19.4	49.3	27.4	8.40	27.9	10.2	6.03	409	6.06	70.2	39.0
Sm	15.3	19.1	15.0	9.61	12.4	14.3	6.47	97.6	12.5	28.1	20.8
Eu	1.56	2.78	3.15	0.66	1.41	3.20	1.17	15.0	2.12	5.09	3.66
Gd	54.5	46.7	55.2	43.0	34.7	57.1	32.0	134	77.5	61.1	59.0
Dy	193	140	226	160	118	212	161	335	371	219	221
Ho	67.4	54.0	84.9	58.8	45.0	77.5	63.9	107	139	64.9	80.4
Er	267	231	400	258	195	346	302	460	627	231	366
Yb	438	408	693	451	364	683	614	831	1236	366	648
Lu	82.2	78.7	180	85.9	74.8	137	119	153	241	66.1	136
Y	1883	1526	2624	1718	1310	2334	1883	3067	4124	2007	2422
Nb	3.21	5.91	5.15	5.88	2.17	2.71	3.15	9.25	7.29	2.37	8.68
Hf	16880	14736	19718	14243	16587	13700	17384	18485	15177	20909	15145
Ta	0.77	1.11	1.68	1.63	1.01	1.18	1.48	2.05	2.32	0.80	2.42
Th	341	147	550	130	311	447	246	638	343	210	468
U	579	267	728	147	330	610	493	1196	779	1161	556
ΣREE	1186	1203	1793	1097	978	1584	1341	4133	2744	1293	1713
Yb/Sm	28.6	21.4	46.2	46.9	29.4	47.9	94.9	8.51	98.5	13.0	31.1
Nb/Ta	4.19	5.31	3.07	3.60	2.15	2.30	2.13	4.52	3.14	2.95	3.58
Eu/Eu*	0.17	0.28	0.33	0.10	0.21	0.34	0.25	0.40	0.21	0.38	0.32
Ce/Ce*	1.83	1.03	3.03	4.51	1.73	10.6	7.20	1.16	5.83	1.15	2.26

Note: $Eu/Eu^* = Eu_N / (Sm_N + Gd_N)^{1/2}$, $Ce/Ce^* = Ce_N / (La_N + Pr_N)^{1/2}$ (Hoskin and Schaltegger, 2003) and $\Sigma REE = \Sigma(La-Lu)$. The subscript N represents the chondrite-normalized value.

Table C2. Trace element contents (in ppm) of zircons (second batch) from the Laingsburg submarine Fan F sandstones.

Zircon Number	FFZ1	FFZ2	FFZ3	FFZ4	FFZ5	FFZ6	FFZ7	FFZ8	FFZ9	FFZ10
La	6.69	5.95	5.56	6.42	96.6	10.0	6.32	10.4	17.3	11.6
Ce	24.8	26.3	22.4	32.2	379	78.5	74.7	49.6	130	164
Pr	3.15	2.84	2.70	2.33	50.2	4.05	2.71	3.16	7.36	4.09
Nd	18.3	16.5	16.4	13.9	249	20.2	14.8	15.4	46.1	18.5
Sm	12.6	8.69	12.0	6.66	96.9	12.6	12.1	5.64	23.8	12.2
Eu	1.41	1.02	1.78	0.74	14.8	2.63	2.29	1.37	5.21	3.17
Gd	58.8	22.8	70.2	22.3	131	45.8	51.4	19.0	59.9	48.3
Dy	258	96.0	321	79.2	224	194	214	69.6	205	208
Ho	97.5	35.2	123	26.4	68.7	81.3	83.8	26.4	74.8	83.8
Er	434	158	561	114	266	376	405	122	333	389
Yb	772	278	920	225	474	809	809	252	644	808
Lu	153	55.8	210	45.6	101	179	192	50.5	134	172
Y	3000	1049	3740	826	2150	2485	2684	830	2296	2626
Nb	3.61	5.21	4.31	1.25	6.60	9.24	10.11	2.78	6.44	9.07
Hf	13826	13051	18847	6519	13261	15995	20097	11448	14649	18651
Ta	1.00	2.15	1.82	0.21	1.56	3.47	2.93	0.85	1.72	2.41
Th	278	206	311	88	820	637	673	210	798	941
U	449	441	716	302	826	768	1200	230	714	1326
ΣREE	1839	707	2265	575	2151	1814	1869	625	1681	1922
Yb/Sm	61.5	32.0	76.9	33.8	4.89	64.4	66.8	44.6	27.0	66.1
Nb/Ta	3.61	2.42	2.36	5.98	4.23	2.66	3.46	3.26	3.75	3.77
Eu/Eu*	0.16	0.22	0.19	0.19	0.40	0.33	0.28	0.40	0.42	0.40
Ce/Ce*	1.26	1.50	1.35	1.95	1.28	2.88	4.22	2.03	2.69	5.58

Note: $Eu/Eu^* = Eu_N / (Sm_N \cdot Gd_N)^{1/2}$, $Ce/Ce^* = Ce_N / (La_N \cdot Pr_N)^{1/2}$ (Hoskin and Schaltegger, 2003) and $\Sigma REE = \Sigma (La-Lu)$. The subscript N represents the chondrite-normalized value.

Table C3 Trace element contents (in ppm) of zircons (second batch) from the Tanqua submarine Fan 3 sandstones.

Zircon Number	F3G2Z1	F3G2Z2	F3G2Z3	F3G2Z4	F3G2Z5	F3G2Z6	F3G2Z7	F3G2Z8	F3G2Z9	F3G2Z10
La	0.29	0.72	126	1.00	2.94	8.01	7.66	1.62	0.15	1.81
Ce	12.9	10.2	434	58.4	41.2	54.8	61.7	39.3	16.9	70.5
Pr	0.41	0.59	51.7	1.42	2.12	4.68	2.89	2.15	0.34	1.74
Nd	3.15	5.80	448	14.9	14.8	24.6	13.2	11.0	1.85	11.1
Sm	6.55	10.1	93.7	16.6	9.50	25.2	9.34	13.3	2.59	7.38
Eu	1.36	0.72	13.2	6.07	2.83	5.69	2.42	4.83	0.45	2.26
Gd	33.3	62.8	160	68.8	30.2	114	40.5	49.1	17.5	24.9
Dy	118	348	334	228	137	403	160	176	73.0	85.0
Ho	43.6	137	120	89.5	54.4	154	64.9	57.9	30.7	35.7
Er	195	675	545	391	304	667	316	244	142	184
Yb	331	1304	916	690	733	1145	578	478	271	431
Lu	63.3	240	220	147	180	219	146	107	56.9	112
Y	1271	4193	3677	2608	1741	4398	2077	1786	915	1150
Nb	1.77	2.71	5.27	3.25	4.77	3.57	3.94	2.29	2.69	9.14
Hf	12790	16851	18118	12440	18632	12745	16228	16356	15308	15765
Ta	0.60	1.58	2.57	0.74	2.14	1.33	1.79	1.63	1.78	3.12
Th	37	219	492	428	270	474	404	451	168	567
U	53	854	627	296	1536	617	775	799	447	1065
ΣREE	810	2794	3462	1712	1512	2825	1402	1184	613	968
Yb/Sm	50.6	129	9.78	41.6	77.2	45.4	61.9	36.0	105	58.5
Nb/Ta	2.97	1.72	2.05	4.39	2.23	2.68	2.19	1.40	1.52	2.93
Eu/Eu*	0.28	0.09	0.33	0.55	0.51	0.32	0.38	0.58	0.21	0.51
Ce/Ce*	8.77	3.66	1.26	11.5	3.86	2.10	3.07	4.92	17.7	9.31

Note: $Eu/Eu^* = Eu_N / (Sm_N \cdot Gd_N)^{1/2}$, $Ce/Ce^* = Ce_N / (La_N \cdot Pr_N)^{1/2}$ (Hoskin and Schaltegger, 2003) and $\Sigma REE = \Sigma (La-Lu)$. The subscript N represents the chondrite-normalized value.

Table C3 (continued) Fan 3

Zircon Number	F3G2Z11	F3G2Z12	F3G2Z13	F3G2Z14	F3G2Z15
La	22.0	1.49	1.81	0.63	0.91
Ce	88.3	29.6	34.3	6.3	11.1
Pr	6.35	1.00	0.69	1.31	1.45
Nd	44.0	7.20	6.05	7.19	10.5
Sm	9.89	6.48	5.03	10.9	13.8
Eu	1.95	1.18	1.12	0.84	4.14
Gd	25.6	29.6	20.5	48.6	56.6
Dy	92.2	112	69.2	207	174
Ho	36.1	44.9	29.1	70.0	60.9
Er	176	211	141	282	259
Yb	385	415	337	522	439
Lu	81.9	95.4	74.7	95.4	83.3
Y	1159	1354	924	2149	1677
Nb	2.07	6.50	1.70	1.16	0.93
Hf	14884	19157	15042	16898	10244
Ta	1.22	3.30	0.82	0.73	0.31
Th	256	336	253	125	115
U	280	639	317	767	304
ΣREE	969	955	721	1252	1115
Yb/Sm	38.9	64.0	67.0	48.1	31.8
Nb/Ta	1.70	1.97	2.06	1.60	3.01
Eu/Eu*	0.37	0.26	0.34	0.11	0.45
Ce/Ce*	1.75	5.70	7.17	1.62	2.26

Table C3 (continued) Trace element abundances (in ppm) of zircons (first batch) from the Tanqua submarine Fan 3 sandstones.

Zircon Number	F3 Z1	F3 Z2	F3 Z3	F3 Z4	F3 Z5	F3 Z6	F3 Z7	F3 Z8	F3 Z9	F3 Z10	F3 Z11	F3 Z12	F3 Z13
Y	3902	2330	2001	1611	2839	5047	2907	2175	1730	1967	7020	742	1773
Nb	9.79	9.58	2.27	2.75	4.37	10.7	12.0	5.65	2.22	3.62	11.0	1.48	7.76
Ce	51.4	58.3	67.7	377	45.4	312	76.1	63.3	173	60.9	320	118	183
Sm	17.4	9.49	15.6	40.1	6.49	101	37.9	6.34	40.5	16.2	171	9.18	38.5
Eu	3.85	2.22	2.60	5.50	2.00	17.1	8.43	2.10	11.5	3.92	37.8	2.40	3.90
Yb	1135	783	673	539	1225	1568	1026	710	510	580	1799	294	530
Lu	222	152	123	105	228	299	201	154	94.3	123	331	62.5	102
Hf	14466	17351	16526	15035	20234	17211	19835	14704	12833	12489	10805	12084	13444
Ta	2.31	2.74	0.95	1.24	1.75	2.50	6.60	1.55	0.82	1.21	4.86	0.63	2.57
Th	462	412	368	262	250	1086	195	425	568	467	1732	241	550
U	495	635	573	303	763	982	962	677	446	368	1727	308	592
Yb/Sm	65.2	82.5	43.3	13.4	189	15.6	27.1	112	12.6	35.9	10.5	32.1	13.8
Nb/Ta	4.24	3.50	2.38	2.23	2.50	4.27	1.82	3.65	2.70	2.98	2.25	2.33	3.02

Zircon Number	F3 Z14	F3 Z15	F3 Z16	F3 Z17	F3 Z18	F3 Z19	F3 Z20	F3 Z21	F3 Z22	F3 Z23	F3 Z24	F3 Z25	F3 Z26	F3 Z27
Y	2054	5147	3592	2511	2049	1378	1894	1088	896	4253	1067	4005	719	2220
Nb	6.46	5.20	3.79	6.84	2.79	1.42	1.69	8.97	7.41	4.80	1.48	4.44	1.18	5.15
Ce	147	22.0	23.3	113	22.1	24.2	34.1	15.2	33.0	63.3	22.8	99.7	4.74	117
Sm	28.2	10.2	9.05	38.8	8.83	12.0	9.51	21.7	12.5	22.5	6.11	49.8	6.81	54.8
Eu	2.51	1.08	1.13	7.59	1.83	2.91	2.10	10.2	6.21	1.90	1.18	7.69	0.47	8.60
Yb	573	1659	1274	969	759	466	644	406	336	1164	310	1370	131	764
Lu	106	356	238	160	150	97.7	133	89.1	72.0	229	57.4	268	23.4	176
Hf	14321	14158	15937	10718	12278	12991	15112	10708	11432	12533	13209	16622	18224	15798
Ta	3.13	2.40	1.59	2.26	1.16	0.55	0.52	5.99	4.68	1.89	0.85	1.40	0.76	1.44
Th	155	302	317	456	382	94.0	206	167	158	877	208	236	96.8	412
U	266	1136	834	698	584	374	393	283	257	1051	262	526	507	772
Yb/Sm	20.3	162	141	25.0	86.0	38.9	67.8	18.7	26.8	51.8	50.7	27.5	19.3	13.9
Nb/Ta	2.06	2.17	2.39	3.03	2.39	2.58	3.23	1.50	1.59	2.54	1.74	3.18	1.56	3.57

Table C4 Trace element contents (in ppm) of zircons (second batch) from the Tanqua submarine Fan 4 sandstones.

Zircon Number	F4G2Z1	F4G2Z2	F4G2Z3	F4G2Z4	F4G2Z5	F4G2Z6	F4G2Z7	F4G2Z8	F4G2Z9	F4G2Z10	F4G2Z11
La	1.05	8.19	13.1	0.38	25.5	90.4	0.57	0.37	1.24	35.5	4.60
Ce	43.6	70.3	102	47.5	136	232	38.9	12.5	13.1	144	31.7
Pr	1.59	8.19	6.04	0.51	27.4	28.0	0.52	0.14	1.60	20.2	3.63
Nd	13.5	59.3	42.3	4.04	192	138	3.81	1.93	12.9	113	15.9
Sm	14.0	24.0	19.8	5.81	65.8	48.9	6.68	2.71	7.82	42.5	8.86
Eu	3.12	3.31	4.19	1.87	7.33	4.71	2.24	1.14	0.51	6.63	1.78
Gd	57.7	37.3	50.1	30.1	106	127	38.9	16.1	35.5	79.1	25.6
Dy	202	91.6	149	123	355	360	154	68.7	202	261	110
Ho	77.8	36.0	57.6	53.0	149	129	64.7	28.5	89.0	109	47.8
Er	363	174	274	255	694	545	297	143	427	523	230
Yb	665	411	583	561	1399	948	642	343	827	1047	564
Lu	148	102	127	114	277	169	129	77.2	157	219	122
Y	2370	1095	1832	1625	4448	3691	1878	922	2619	3202	1484
Nb	4.59	3.44	3.74	4.69	4.16	4.28	4.26	2.00	2.83	8.86	3.38
Hf	14345	18781	15924	15674	16907	12444	13778	13110	16129	16228	13702
Ta	1.42	0.67	1.97	1.76	2.43	1.19	1.67	1.03	1.87	3.86	1.24
Th	403	284	631	295	299	733	298	131	173	523	297
U	526	1113	723	491	891	942	391	367	766	702	573
ΣREE	1590	1026	1429	1196	3433	2821	1378	695	1775	2599	1166
Yb/Sm	47.6	17.1	29.4	96.6	21.3	19.4	96.1	126	106	24.6	63.7
Nb/Ta	3.22	5.13	1.90	2.67	1.71	3.60	2.56	1.94	1.51	2.30	2.72
Eu/Eu*	0.34	0.34	0.41	0.43	0.27	0.18	0.43	0.53	0.09	0.35	0.36
Ce/Ce*	7.93	2.01	2.70	25.3	1.20	1.08	16.8	12.9	2.18	1.26	1.82

Note: $Eu/Eu^* = Eu_N / (Sm_N + Gd_N)^{1/2}$, $Ce/Ce^* = Ce_N / (La_N + Pr_N)^{1/2}$ (Hoskin and Schaltegger, 2003) and $\Sigma REE = \Sigma (La-Lu)$. The subscript N represents the chondrite-normalized value.

Table C4 (continued) Trace element abundances (in ppm) of zircons (first batch) from the Tanqua submarine Fan 4 sandstones.

Zircon Number	F4 Z1	F4 Z2	F4 Z3	F4 Z4	F4 Z5	F4 Z6	F4 Z7	F4 Z8	F4 Z9	F4 Z10	F4 Z11	F4 Z12
Y	904	2164	2707	2257	2550	2087	7952	8477	1689	3036	2116	3983
Nb	1.55	3.30	7.85	4.24	5.82	2.12	2.11	6.68	2.25	8.62	5.41	7.87
Ce	24.8	39.6	85.6	32.9	37.6	209	4.95	41.1	79.4	179	48.5	24.2
Sm	2.30	10.2	25.9	9.10	8.60	28.5	15.3	36.8	16.0	57.5	22.4	17.6
Eu	0.61	2.67	7.19	2.69	2.03	4.38	0.84	3.96	3.59	12.4	3.97	3.78
Yb	340	654	808	606	963	701	2179	2519	512	1016	856	1330
Lu	72.5	138	151	142	188	143	442	464	106	212	186	261
Hf	17032	18494	15499	15412	16673	22173	22848	27699	18336	24701	20989	19382
Ta	0.83	1.15	3.06	2.87	2.29	1.37	0.96	2.81	0.83	2.03	1.94	2.69
Th	244	533	615	301	342	473	148	293	232	987	329	218
U	321	688	674	896	460	827	681	989	281	1335	586	468
Yb/Sm	148	64.3	31.3	66.6	112	24.6	142	68.5	32.0	17.7	38.2	75.4
Nb/Ta	1.86	2.88	2.56	1.48	2.55	1.55	2.19	2.38	2.72	4.25	2.79	2.92

Zircon Number	F4 Z13	F4 Z14	F4 Z15	F4 Z16	F4 Z17	F4 Z18	F4 Z19	F4 Z20	F4 Z21	F4 Z22	F4 Z23	F4 Z24	F4 Z25
Y	2693	2807	4340	5108	1177	2916	1752	1653	5275	3298	3129	7591	5293
Nb	7.85	6.55	7.84	17.6	3.03	9.48	3.81	5.97	4.17	9.86	3.86	7.44	10.0
Ce	205	90.8	87.1	543	16.3	148	138	75.2	3.15	160	29.9	112	400
Sm	107	16.2	37.1	54.8	14.3	25.0	13.1	9.92	12.7	85.9	28.9	121	103
Eu	15.9	3.04	4.65	9.96	3.38	5.45	3.88	1.78	2.53	15.0	2.78	6.82	29.1
Yb	1053	996	1209	1652	291	873	735	569	1588	922	865	2135	1448
Lu	210	210	256	324	45.4	163	169	115	298	176	155	371	278
Hf	22722	20765	27077	23452	16242	23470	24665	20944	21536	19133	19315	21913	18242
Ta	2.42	2.36	1.76	4.01	1.00	3.11	1.93	2.80	2.20	6.15	1.20	3.63	2.91
Th	922	893	470	1286	79.2	824	650	683	92.9	390	228	442	821
U	1007	1047	493	1069	209	485	874	1094	539	776	320	975	1399
Yb/Sm	9.86	61.4	32.6	30.1	20.3	34.9	55.9	57.4	125	10.7	30.0	17.7	14.1
Nb/Ta	3.25	2.78	4.45	4.38	3.01	3.05	1.97	2.13	1.89	1.60	3.21	2.05	3.44

Table C5 Trace element contents (in ppm) of zircons (second batch) from the Tanqua submarine Fan 5 sandstones.

Zircon Number	F5G2Z1	F5G2Z2	F5G2Z3	F5G2Z4	F5G2Z5	F5G2Z6	F5G2Z7	F5G2Z8	F5G2Z9	F5G2Z10	F5G2Z11
La	0.66	31.0	62.6	4.00	4.70	8.01	19.7	0.35	24.4	11.0	24.2
Ce	35.7	160	392	38.3	43.7	61.5	148	10.0	118	86.7	116
Pr	0.42	30.6	57.6	4.65	1.67	4.99	20.2	0.20	21.3	3.99	6.68
Nd	6.24	174	368	33.5	14.2	31.6	137	3.53	162	23.9	22.3
Sm	11.5	98.7	179	23.9	10.4	17.2	56.0	7.55	47.4	11.1	14.9
Eu	2.44	11.1	20.7	2.57	1.86	2.63	7.15	1.18	5.19	2.89	2.23
Gd	72.8	129	277	67.1	44.8	54.5	96.8	56.3	90.2	45.1	51.4
Dy	324	346	606	249	175	204	272	272	211	153	197
Ho	134	136	213	101	66.2	83.0	111	112	79.9	59.5	79.1
Er	647	636	904	439	310	407	546	514	344	267	357
Yb	1002	1330	1356	771	557	750	974	976	558	519	681
Lu	248	249	306	153	121	199	236	189	124	115	152
Y	4131	4190	6473	2952	2075	2742	3569	3354	2508	1883	2434
Nb	6.78	7.69	7.01	1.74	5.54	5.76	11.15	1.18	6.04	4.60	3.92
Hf	20785	15118	18415	13748	14492	18292	20309	14181	12436	16749	17288
Ta	2.47	3.70	2.41	0.78	1.53	2.24	4.66	0.99	1.38	1.04	2.12
Th	333	462	1204	252	285	670	1035	156	663	378	660
U	564	1184	887	379	387	1110	1364	317	730	515	787
ΣREE	2484	3332	4742	1888	1350	1822	2622	2142	1787	1298	1703
Yb/Sm	87.4	13.5	7.58	32.2	53.7	43.6	17.4	129	11.8	46.6	45.7
Nb/Ta	2.75	2.08	2.91	2.22	3.62	2.57	2.39	1.19	4.36	4.43	1.85
Eu/Eu*	0.26	0.30	0.28	0.20	0.26	0.26	0.30	0.17	0.24	0.39	0.25
Ce/Ce*	15.9	1.22	1.53	2.08	3.65	2.28	1.73	8.93	1.21	3.07	2.14

Note: $Eu/Eu^* = Eu_N / (Sm_N \cdot Gd_N)^{1/2}$, $Ce/Ce^* = Ce_N / (La_N \cdot Pr_N)^{1/2}$ (Hoskin and Schaltegger, 2003) and $\Sigma REE = \Sigma (La-Lu)$. The subscript N represents the chondrite-normalized value.

Table C5 (continued) Trace element abundances (in ppm) of zircons (first batch) from the Tanqua submarine Fan 5 sandstones.

Zircon Number	F5 Z1	F5 Z2	F5 Z3	F5 Z4	F5 Z5	F5 Z6	F5 Z7	F5 Z8	F5 Z9	F5 Z10	F5 Z11	F5 Z12
Y	2063	4000	1454	1685	1174	1347	1423	5304	1403	2420	1170	2322
Nb	2.99	7.12	1.46	19.1	22.3	25.2	3.65	17.9	2.10	2.56	1.52	8.10
Ce	37.2	99.9	12.0	43.1	65.7	62.3	18.9	913	78.8	24.7	13.7	277
Sm	6.94	28.7	10.8	56.4	49.5	63.4	2.70	518	32.9	17.5	4.37	40.6
Eu	1.77	5.51	0.62	20.3	24.7	25.9	0.44	71.3	4.63	2.06	1.11	3.30
Yb	734	1402	428	481	475	461	541	1520	431	820	470	952
Lu	154	318	81.3	99.3	108	97.7	112	298	85.5	160	104	216
Hf	14426	18307	19964	14981	13961	13834	18379	19499	15916	18625	16768	18429
Ta	1.66	3.72	0.71	13.42	15.93	17.38	1.45	5.06	0.82	0.97	0.78	2.90
Th	312	1306	237	428	149	339	195	3097	338	211	146	420
U	328	1274	411	655	234	430	331	2220	313	272	231	597
Yb/Sm	106	48.9	39.8	8.53	9.61	7.28	200	2.93	13.1	46.9	108	23.5
Nb/Ta	1.80	1.92	2.06	1.43	1.40	1.45	2.51	3.53	2.58	2.63	1.93	2.79

Zircon Number	F5 Z13	F5 Z14	F5 Z15	F5 Z16	F5 Z17	F5 Z18	F5 Z19	F5 Z20	F5 Z21	F5 Z22	F5 Z23	F5 Z24	F5 Z25
Y	3953	2817	1033	1447	1479	2484	1658	989	814	1932	2100	3133	4508
Nb	6.63	5.88	2.76	2.41	3.22	4.18	4.21	3.63	2.07	3.11	4.23	5.17	1.31
Ce	360	39.5	84.0	41.1	34.8	43.3	88.9	12.4	39.4	150	55.8	33.2	7.29
Sm	213	17.1	13.1	6.45	4.90	7.60	20.8	10.9	10.0	21.9	16.6	11.6	12.8
Eu	27.2	2.54	0.55	2.07	2.10	2.43	1.62	1.31	1.85	2.83	3.39	2.67	1.60
Yb	1176	950	269	521	656	838	499	238	282	702	718	1029	1325
Lu	224	175	50.5	110	147	163	98.3	45.2	68.1	137	146	211	257
Hf	21298	16729	19454	17781	14369	16159	16015	16397	20703	17533	15384	19136	20014
Ta	2.03	2.30	1.23	1.11	0.95	1.47	1.55	1.41	0.73	1.67	1.78	2.49	0.95
Th	1299	375	170	283	330	405	187	82	312	712	761	298	124
U	964	526	318	306	452	553	436	237	419	724	988	385	306
Yb/Sm	5.53	55.4	20.6	80.8	134	110	23.9	21.8	28.1	32.0	43.4	88.6	103
Nb/Ta	3.27	2.56	2.25	2.17	3.38	2.84	2.72	2.58	2.84	1.87	2.37	2.08	1.37

Table C6 Provenance of the Tanqua and Laingsburg submarine fan sandstones based on the CART tree (Belousova et al., 2002).

Zircon number	Zircons from the Tanqua Fan 3		Zircon number	Zircons from the Tanqua Fan 4		Zircon number	Zircons from the Tanqua Fan 5	
	Zircon number	Source rock		Zircon number	Source rock		Zircon number	Source rock
F3 Z1		granitoid (70-75 % SiO ₂)	F4 Z1		granitoid (< 65% SiO ₂)	F5 Z1		granitoid (70-75 % SiO ₂)
F3 Z2		granitoid (70-75 % SiO ₂)	F4 Z2		granitoid (70-75 % SiO ₂)	F5 Z2		granitoid (70-75 % SiO ₂)
F3 Z3		granitoid (70-75 % SiO ₂)	F4 Z3		granitoid (70-75 % SiO ₂)	F5 Z3		granitoid (< 65% SiO ₂)
F3 Z4		granitoid (70-75 % SiO ₂)	F4 Z4		granitoid (70-75 % SiO ₂)	F5 Z4		granitoid (< 65% SiO ₂)
F3 Z5		granitoid (70-75 % SiO ₂)	F4 Z5		granitoid (70-75 % SiO ₂)	F5 Z5		granitoid (< 65% SiO ₂)
F3 Z6		syenite/monzonite	F4 Z6		granitoid (70-75 % SiO ₂)	F5 Z6		granitoid (< 65% SiO ₂)
F3 Z7		granitoid (70-75 % SiO ₂)	F4 Z7		syenite/monzonite	F5 Z7		granitoid (70-75 % SiO ₂)
F3 Z8		granitoid (70-75 % SiO ₂)	F4 Z8		syenite/monzonite	F5 Z8		granitoid (> 75 % SiO ₂)
F3 Z9		granitoid (70-75 % SiO ₂)	F4 Z9		granitoid (70-75 % SiO ₂)	F5 Z9		granitoid (< 65% SiO ₂)
F3 Z10		granitoid (70-75 % SiO ₂)	F4 Z10		granitoid (70-75 % SiO ₂)	F5 Z10		granitoid (70-75 % SiO ₂)
F3 Z11		granitoid (> 75 % SiO ₂)	F4 Z11		granitoid (70-75 % SiO ₂)	F5 Z11		granitoid (< 65% SiO ₂)
F3 Z12		granitoid (< 65% SiO ₂)	F4 Z12		granitoid (70-75 % SiO ₂)	F5 Z12		granitoid (70-75 % SiO ₂)
F3 Z13		granitoid (70-75 % SiO ₂)	F4 Z13		granitoid (70-75 % SiO ₂)	F5 Z13		granitoid (70-75 % SiO ₂)
F3 Z14		granitoid (70-75 % SiO ₂)	F4 Z14		granitoid (70-75 % SiO ₂)	F5 Z14		granitoid (70-75 % SiO ₂)
F3 Z15		syenite/monzonite	F4 Z15		granitoid (70-75 % SiO ₂)	F5 Z15		granitoid (< 65% SiO ₂)
F3 Z16		granitoid (70-75 % SiO ₂)	F4 Z16		syenite/monzonite	F5 Z16		granitoid (70-75 % SiO ₂)
F3 Z17		granitoid (70-75 % SiO ₂)	F4 Z17		granitoid (< 65% SiO ₂)	F5 Z17		granitoid (70-75 % SiO ₂)
F3 Z18		granitoid (70-75 % SiO ₂)	F4 Z18		granitoid (70-75 % SiO ₂)	F5 Z18		granitoid (70-75 % SiO ₂)
F3 Z19		granitoid (< 65% SiO ₂)	F4 Z19		granitoid (70-75 % SiO ₂)	F5 Z19		granitoid (< 65% SiO ₂)
F3 Z20		granitoid (70-75 % SiO ₂)	F4 Z20		granitoid (70-75 % SiO ₂)	F5 Z20		granitoid (< 65% SiO ₂)
F3 Z21		granitoid (< 65% SiO ₂)	F4 Z21		syenite/monzonite	F5 Z21		granitoid (< 65% SiO ₂)
F3 Z22		granitoid (< 65% SiO ₂)	F4 Z22		granitoid (70-75 % SiO ₂)	F5 Z22		granitoid (70-75 % SiO ₂)
F3 Z23		granitoid (70-75 % SiO ₂)	F4 Z23		granitoid (70-75 % SiO ₂)	F5 Z23		granitoid (70-75 % SiO ₂)
F3 Z24		granitoid (< 65% SiO ₂)	F4 Z24		syenite/monzonite	F5 Z24		granitoid (70-75 % SiO ₂)
F3 Z25		granitoid (70-75 % SiO ₂)	F4 Z25		granitoid (> 75 % SiO ₂)	F5 Z25		syenite/monzonite
F3 Z26		granitoid (< 65% SiO ₂)	F4G2Z1		granitoid (70-75 % SiO ₂)	F5G2Z1		granitoid (70-75 % SiO ₂)
F3 Z27		granitoid (70-75 % SiO ₂)	F4G2Z2		granitoid (< 65% SiO ₂)	F5G2Z2		granitoid (70-75 % SiO ₂)
F3G2Z1		granitoid (< 65% SiO ₂)	F4G2Z3		granitoid (70-75 % SiO ₂)	F5G2Z3		syenite/monzonite
F3G2Z2		granitoid (70-75 % SiO ₂)	F4G2Z4		granitoid (70-75 % SiO ₂)	F5G2Z4		granitoid (70-75 % SiO ₂)
F3G2Z3		granitoid (70-75 % SiO ₂)	F4G2Z5		syenite/monzonite	F5G2Z5		granitoid (70-75 % SiO ₂)
F3G2Z4		granitoid (70-75 % SiO ₂)	F4G2Z6		granitoid (70-75 % SiO ₂)	F5G2Z6		granitoid (70-75 % SiO ₂)
F3G2Z5		granitoid (70-75 % SiO ₂)	F4G2Z7		granitoid (70-75 % SiO ₂)	F5G2Z7		granitoid (70-75 % SiO ₂)
F3G2Z6		granitoid (70-75 % SiO ₂)	F4G2Z8		granitoid (< 65% SiO ₂)	F5G2Z8		granitoid (70-75 % SiO ₂)
F3G2Z7		granitoid (70-75 % SiO ₂)	F4G2Z9		granitoid (70-75 % SiO ₂)	F5G2Z9		granitoid (70-75 % SiO ₂)
F3G2Z8		granitoid (< 65% SiO ₂)	F4G2Z10		granitoid (70-75 % SiO ₂)	F5G2Z10		granitoid (70-75 % SiO ₂)

F3G2Z9	granitoid (< 65% SiO ₂)	F4G2Z11	granitoid (70-75 % SiO ₂)	F5G2Z11	granitoid (70-75 % SiO ₂)
F3G2Z10	granitoid (< 65% SiO ₂)				
F3G2Z11	granitoid (< 65% SiO ₂)				
F3G2Z12	granitoid (< 65% SiO ₂)				
F3G2Z13	granitoid (< 65% SiO ₂)				
F3G2Z14	granitoid (70-75 % SiO ₂)				
F3G2Z15	granitoid (< 65% SiO ₂)				

Note that the CART was developed for the recognition of zircon from different rock types based on single grain trace element geochemistry.

Table C6 (Continued)

Zircons from the Laingsburg Fan A		Zircons from the Laingsburg Fan F	
Zircon number	Source rock	Zircon number	Source rock
FAZ1	granitoid (< 65% SiO ₂)	FFZ1	granitoid (70-75 % SiO ₂)
FAZ2	granitoid (< 65% SiO ₂)	FFZ2	granitoid (< 65% SiO ₂)
FAZ3	granitoid (< 65% SiO ₂)	FFZ3	granitoid (70-75 % SiO ₂)
FAZ4	basalt	FFZ4	basalt
FAZ5	granitoid (70-75 % SiO ₂)	FFZ5	granitoid (< 65% SiO ₂)
FAZ6	granitoid (70-75 % SiO ₂)	FFZ6	granitoid (70-75 % SiO ₂)
FAZ7	granitoid (70-75 % SiO ₂)	FFZ7	granitoid (70-75 % SiO ₂)
FAZ8	granitoid (70-75 % SiO ₂)	FFZ8	granitoid (< 65% SiO ₂)
FAZ9	granitoid (70-75 % SiO ₂)	FFZ9	granitoid (70-75 % SiO ₂)
FAZ10	granitoid (70-75 % SiO ₂)	FFZ10	granitoid (70-75 % SiO ₂)
FAZ11	granitoid (< 65% SiO ₂)		
FAZ12	granitoid (< 65% SiO ₂)		
FAZ13	granitoid (70-75 % SiO ₂)		
FAZ14	granitoid (< 65% SiO ₂)		
FAZ15	granitoid (< 65% SiO ₂)		
FAZ16	granitoid (70-75 % SiO ₂)		
FAZ17	granitoid (70-75 % SiO ₂)		
FAZ18	granitoid (70-75 % SiO ₂)		
FAZ19	granitoid (70-75 % SiO ₂)		
FAZ20	granitoid (< 65% SiO ₂)		
FAZ21	granitoid (70-75 % SiO ₂)		

Note that the CART was developed for the recognition of zircon from different rock types based on single grain trace element geochemistry.

APPENDIX D

ZIRCON GEOCHRONOLOGY (SHRIMP)

D.1 Introduction

For the identification and categorization of different zircon varieties, another zircon split fraction was mounted on a double-sided sticky tape, and later in epoxy on a glass petrographic slide. More than one hundred individual zircons from the Tanqua Karoo Fans 3, 4 and 5 and from the Laingsburg Fans A and F were then evaluated for morphology and inclusions using optical microscopes and numerous scanning electron microscope (SEM) images used in the typological study were taken. Some of these images are shown in the text but the majority is available on CD (Appendix E).

A split fraction of zircon was sent for Sensitive High Resolution Ion Microprobe (SHRIMP) analysis at the Australian National University (ANU) in Canberra, Australia. The sent fraction includes zircons from the Slope, Tanqua and Laingsburg deepwater sandstones. The Tanqua samples include detrital zircons from Fans 3, 4, and 5. The Laingsburg sample comprises zircons from Fan A and Fan F.



D.2 Methodology, procedures and philosophy related to the SHRIMP analysis done by Dr. R. Armstrong at the Australian National University

D.2.1 Analytical procedures

The zircon concentrates were mounted in epoxy using a binocular microscope, together with the Research School for Earth Sciences (RSES) reference zircons FC1 and SL13. All zircons were photographed in transmitted and reflected light and these, together with SEM cathodoluminescence (CL) images, were used to decipher the internal structures of the sectioned grains and to target specific areas within the zircons for spot analysis. The cathodoluminescence (CL) and

photographic imaging is very important in identifying possible cores, rims or different growth zones, or to avoid possible metamict zones or inclusions. Complex or structured zircons are extremely common in detrital populations and a mixed analysis of two or more different growth zones in a single crystal produces a meaningless age. With the unique spatial resolution of the SHRIMP technique this can be avoided. The non-destructive nature of the SHRIMP *in situ* technique also allows the analyst to conduct post-analysis examination of the exact spot excavated during the U-Pb analysis to confirm no mixed ages were measured. It is also possible to perform further analyses - on the same spot - which might be of interest in further characterising the source of the zircons (e.g. Hf or O isotopes, or REE profiles).

U-Pb analyses were done using both the SHRIMP I and the SHRIMP RG instruments at the RSES. The data have been reduced in a manner similar to that described by Williams (1998), using the SQUID Excel Macro of Ludwig (2000). For the zircon calibration the Pb/U ratios have been normalized relative to a value of 0.1859 for the $^{206}\text{Pb}/^{238}\text{U}$ ratio of the FC1 reference zircons, equivalent to an age of 1099 Ma (Paces and Miller, 1993). Uranium and thorium concentrations were determined relative to the SL13 standard.

Uncertainties given for individual U-Pb zircon analyses (ratios and ages) are at the 1σ level. Concordia plots and weighted mean age calculations were carried out using Isoplot/Ex (Ludwig, 1999).

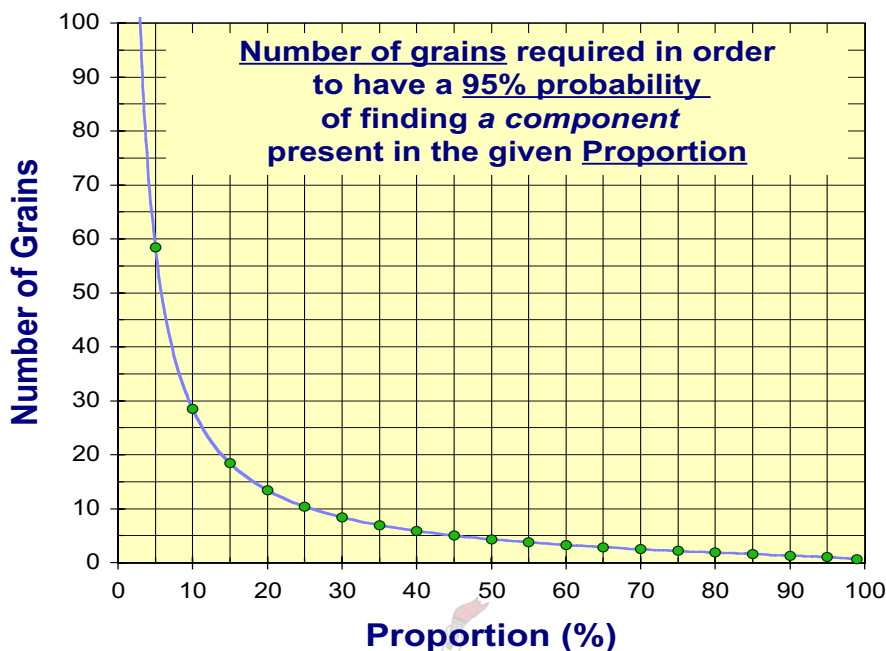
D.2.2 Notes on the analytical philosophy followed during this study

The way in which U-Pb analysis of detrital zircons is conducted is critically dependent on the aims of the project. Careful sample/grain selection is obviously always crucial in any analysis, but meaningful outcomes can only be achieved if the appropriate analytical technique - combined with the correct emphasis and

philosophy in sample selection - is followed. These should be fully explained when presenting or analyzing such data. The methodology and philosophy of the current research is described below.

Because of their resilient character, detrital zircons are very useful recorders of sediment provenance and can be used to identify particular sources or terranes which were eroded, some of which might not have been preserved to the present day. Detrital zircons can also provide *maximum* ages of sedimentation (through dating the youngest detrital grain), and here the aim would be to identify this youngest population, rather than analyze all representative components. For provenance studies it is crucial that all possible contributions are represented in the analyzed sample. The various approaches and methodologies employed during this project are outlined below.

- ◆ Zircon selection is made as *random* as possible. This to avoid misleading age patterns in which important populations fail to appear, or minor populations acquire undue emphasis.
- ◆ The number of analyses done per sample is also important in ensuring that one has the best chance of sampling all representative age components. A minimum of 58 analyses is usually considered the optimum number of analyses. This means that one would have a 95% probability of finding a component that would be present in a proportion of 5% (Dodson et al., 1988) as illustrated below.



- ◆ Pb-loss and resultant discordance are ever-present problems in interpreting individual data points in detrital studies. If the Pb-loss is severe and the timing of Pb-loss is unconstrained the only "age" one can use is the $^{207}\text{Pb}/^{206}\text{Pb}$ age. This assumes recent Pb-loss and is a *minimum* age estimate only. For this reason it is preferable to ignore severely discordant analyses. In this study we have excluded as few analyses as possible. These discarded analyses are shown in the relevant concordia plots, but are excluded from the cumulative probability plots. In some cases - especially for the younger zircons - it is difficult to decide whether an analysis is highly discordant or not, and the decision can be somewhat subjective. We have used other criteria, such as very high U or Th contents (where Pb-loss is more probable), or high common Pb contents (indicating possible alteration) to help make these decisions.
- ◆ Selecting the site of the analysis is critical, and it is only with the SHRIMP's unique spatial resolution that this can be achieved. During this study the average spot size was approximately 20-25 μm in diameter, and this was

sufficiently small to access most internal zones of interest and to avoid overlapping onto more than one domain. Again, this is critical, as *a mixed analysis provides no geochronological information*. Some zircons from these samples are complicated by core/rim internal structures, cracks or inclusions. All these have to be avoided in three dimensions to achieve a meaningful analysis. Selecting the site to analyse is done using the combined aids of transmitted, reflected light microphotography and SEM cathodoluminescence imaging. As the SHRIMP spot is only 1-2 μm deep, it will be possible to perform any further analyses (such as REE, Hf or O isotope analyses) on exactly the same zone of zircon on which the age information was gathered, if required.

- ◆ Detrital provenance studies rely on obtaining large numbers of relatively low-precision analyses. For younger zircons ($\sim < 800$ Ma) most of the geochronological information is contained in the $^{206}\text{Pb}/^{238}\text{U}$ geochronometer, as the ^{207}Pb peak is very small. For this study a "Preferred Age" refers to the way in which individual ages for grains are calculated. If the zircon is younger than 700 Ma (based on the $^{206}\text{Pb}/^{238}\text{U}$ date) then the $^{206}\text{Pb}/^{238}\text{U}$ age is used. For older zircons the $^{207}\text{Pb}/^{206}\text{Pb}$ date is used. Obviously highly discordant data points with no constraints on the timing of Pb-loss are discarded.
- ◆ In complex, multi-age zircons, the youngest identified zone was analyzed with the view to obtaining the age of the source rock (rather than the age of the xenocrystic cores). In a few rare cases both cores and rims were analysed as this might provide interesting and characteristic age signatures. In some cases zircons are just too metamict or altered and these were not analyzed. This might have the potential for biasing the final result if all these zircons come from a particular source, but is unavoidable as the data from such zone/zircons would be compromised and too difficult to interpret.